THE VISCOSITY OF WATER AT HIGH PRESSURE.

A thesis submitted for the degree of

DOCTOR OF PHILOSOPHY

in the

UNIVERSITY OF LONDON

by

JAMES BRIAN CAPPI, B.Sc.(Eng)., A.C.G.I.

Department of Chemical Engineering
and Chemical Technology,
Imperial College of Science and Technology,
London, S.W.7.

June 1964.

C7 23JUN1964

ABSTRACT.

A liquid phase relative viscometer has been constructed and operated at pressures up to 10,000kg/cm^2, over the temperature range 2 - 100°C. The falling body viscometer consists of a stainless steel tube containing two cylindrical bodies, one of high and the other of low density, and is housed in a pressure vessel. Measurements are made by inverting the vessel and timing the fall of the 'sinkers' by means of an electrical inductance system within the vessel, arrangements being made for only one sinker to fall at a time. The use of two sinkers allows density as well as viscosity to be calculated.

The pressure in the system is generated by a small multi-stroke intensifier, and measured by means of a manganin coil gauge, all of which rotates with the vessel.

The viscosity of n-pentane has been determined at 30°C up to 10,000kg/cm^2, to an estimated accuracy of $\pm$ 1.2%, and found to be in good agreement with Bridgman's work under the same conditions. Similar measurements have been made on water at nine temperatures between 2 and 100°C, and on heavy water at 25°C, to an estimated accuracy of $\pm$ .8%, and the water viscosity data of Bridgman have been found to be in error.

The viscosity of water at high pressure is interpreted in terms of a two species structure of the liquid, (hydrogen bonded and unbonded), one of which tends to disappear on raising temperature and pressure, and the heavy water data provide evidence of a large and constant rotational contribution to momentum transport in water at high pressure.

The viscosities of several liquids, including that of water modified to a single species structure, have been found to fit, over all or part of the 10,000kg/cm^2 pressure range, a semi-empirical expression of the form:-

$$\eta_p/\eta_o = (V_p/V_o)^{-C}\exp(PB).$$

Acknowledgements.

I am indebted to Dr. K.E. Bett for the supervision of this work, and for his valuable guidance and advice.

I wish to express my gratitude to Mr. A.M. Alger, and the departmental workshop staff, for their helpful co-operation and workmanship in making possible the fabrication of the apparatus, and to Mr. Tyley, of the departmental electronics workshop, for his assistance in constructing and developing the instrumentation.

I am grateful to my wife for her encouragement and endless patience during the course of the research, and for her invaluable assistance, together with that of Mrs. E. Williams, of Barry, Glamorgan, in preparing this thesis.

Thanks are due to the Department of Scientific and Industrial Research and the Esso Petroleum Company for financial assistance, and to the National Engineering Laboratory for the sponsoring of the work.

CONTENTS.

			Page.
		ABSTRACT.	1
		ACKNOWLEDGEMENTS.	2
		CONTENTS.	3
		NOMENCLATURE.	8
CHAPTER 1.		INTRODUCTION.	11
CHAPTER 2.		METHODS OF HIGH PRESSURE VISCOMETRY.	18
	(i)	Flow through a capillary.	19
	(ii)	Falling body viscometers.	22
	(iii)	Rolling ball viscometers.	24
	(iv)	Rotating cylinder viscometers.	24
	(v)	Oscillating disc, cylinder or sphere viscometers.	25
	(vi)	High frequency methods.	25
CHAPTER 3.		DESIGN AND DEVELOPMENT OF VISCOMETER.	
	(i)	Type of viscometer chosen.	26
	(ii)	Method of timing.	28
	(iii)	Density measurement.	31
	(iv)	Design of viscometer.	32
	(v)	Description of timing system.	36
	(vi)	Development and performance of timing system.	40
	(vii)	Development of viscometer.	44
CHAPTER 4.		THEORIES OF VISCOMETER.	51

			Page.
CHAPTER 5.		DESIGN AND DEVELOPMENT OF PRESSURE SYSTEM.	
	(i)	General requirements of system.	65
	(ii)	Intensifier.	67
	(iii)	Valve and gauge block.	72
	(iv)	Pressure vessel.	75
	(v)	Pressure pipe.	79
	(vi)	Auxiliary pressure system.	80
	(vii)	Autofrettage.	82
	(viii)	Operation of the high pressure system.	83
CHAPTER 6.		HIGH PRESSURE SEALS.	
	(i)	Development and theories.	91
	(ii)	Application.	103
CHAPTER 7.		DESIGN AND CALIBRATION OF PRESSURE MEASURING SYSTEM.	
	(i)	Design and construction.	107
	(ii)	Calibration requirements.	115
	(iii)	Bridge Calibration.	115
	(iv)	Gauge temperature calibration.	118
	(v)	Gauge pressure calibration.	121
CHAPTER 8.		ANCILLARY EQUIPMENT.	
	(i)	Main structure.	134
	(ii)	Mounting of high pressure system.	138

		Page.
(iii)	Vessel stop.	139
(iv)	Temperature control.	141
CHAPTER 9.	CALIBRATION AND PERFORMANCE OF VISCOMETER.	
(i)	Timer.	144
(ii)	Viscometer.	147
(iii)	Performance at high pressure.	161
CHAPTER 10.	DENSITY MEASUREMENT.	165
CHAPTER 11.	EXPERIMENTAL PROCEDURE.	
(i)	Filling the viscometer.	174
(ii)	Viscosity determinations.	176
CHAPTER 12.	RESULTS.	179
(i)	Water.	179
(ii)	Deuterium oxide.	192
(iii)	Normal Pentane.	192
(iv)	Pressure transmitting fluid.	195
(v)	Accuracy of results.	195
(vi)	Accuracy of smoothed results.	198
CHAPTER 13.	DISCUSSION A.	
(i)	Comparison of results.	200
(ii)	Improvement of apparatus.	213
CHAPTER 14.	DISCUSSION B.	

			Page.
	(i)	Anomalous behaviour of water.	224
	(ii)	Isotopic substitution.	229
	(iii)	The structure of water.	230
	(iv)	Momentum transport in water.	234
	(v)	Viscosity of H_2O_{II}	239
	(vi)	The pressure dependence of viscosity.	245
	(vii)	Viscosity of water at constant volume.	250
CHAPTER 15.		CONCLUSIONS.	253
APPENDIX 1.		TRIGGERING CIRCUIT.	255
APPENDIX 2.		DERIVATION OF VISCOMETER RELATIONSHIPS.	
	(i)	Concentric conditions.	256
	(ii)	Eccentric conditions.	259
APPENDIX 3.		STRESS CALCULATIONS.	
	(i)	Radius ratio of high pressure cylinder.	265
	(ii)	Strains in the high pressure cylinder.	267
	(iii)	Bursting pressure.	268
	(iv)	Radius ratio of low pressure cylinder.	269
	(v)	Design of vessel top closure.	269
APPENDIX 4.		RESULTS.	
	(i)	Specimen calculation.	271
	(ii)	Summary of experimental results.	275
	(iii)	Smoothed viscosity data.	286

Page.

(iv) Pressure transmitting fluid. 289

APPENDIX 5. PRESSURE DEPENDENCE OF VISCOSITY. 290

REFERENCES. 294

NOMENCLATURE.

List of principal symbols used.

a	Intermolecular distance.
A	Empirical constant.
B	Empirical constant.
c	Radial clearance of annulus, or Poisson's ratio.
C	Slope in Fig. 69.
Cp	Specific heat at constant pressure.
Cv	Specific heat at constant volume.
d	Diameter.
2d	Displacement of sinker axis.
D	Intercept, in Fig. 69.
E	Young's Modulus, bond energy, or activation energy.
E_A	Energy required by molecule changing its position relative to its neighbours, to overcome intermolecular forces.
E_p	Activation energy at constant pressure.
E_v	Activation energy at constant volume.
F	Viscous drag on a falling sphere.
g	Acceleration of gravity.
H	Helmholtz free energy.
I	Moment of inertia.
k	Experimental viscometer constant.
k'	Theoretical ideal viscometer constant.
K	Integration constant.
l	Length of sinker or capillary.
L	Length of viscometer tube.

m	Mass
M	Molecular weight
N	Avogadro's number
N_{RE}	Modified Reynolds number
Suffix o	At atmospheric pressure
Suffix p	At pressure P
P_y	Yield pressure
P	Pressure
ΔP	Pressure difference
Q	Volume flow rate
r	Radius
r_1	Radius of sinker
r_2	Radius of viscometer tube
R	Fixed arm of Smith's bridge, or gas constant.
R_1, R_2	Ratio arms of Smith's bridge.
s	Radius of incremental annulus
S	Resistance of manganin pressure gauge, or entropy.
t	Temperature ^{o}C, or dimension of time.
t^*	Uncorrected fall time
t^*_p, t^*_o	Fall times, corrected except for buoyancy.
T	Absolute temperature
T^*	Corrected fall time, or transpiration time
u_s	Velocity at radius s.
U	Internal energy.
ΔU_v	Molar heat of evaporation.
v	Terminal velocity, or specific volume.
V	Volume of sinker, or molar volume.
w	Buoyancy corrected weight of sinker.
X	Resistance of variable arm of Smith's bridge.
Z	Co-ordination number.

β	Coefficient of isothermal compressibility
γ	Radius ratio
δ	Increment
ε	Depth of intermolecular potential
ε_t	Tangential strain
η	Absolute viscosity
θ	Angle
κ	Coefficient of adiabatic compressibility
λ	Shear force
ν	Frequency
ρ_s	Density of sinker or solid
ρ_f	Density of fluid.
Σ	Sum of
τ	Shear Stress
σ	Molecular diameter
σ_y	Tensile yield stress
Ω	Ohms.

CHAPTER 1.

INTRODUCTION.

The theory of the liquid state has not yet been developed as successfully as the theories of the gas and solid states, and advancement of the subject is dependent, on the one hand, on the development and elaboration of theories, and on the other, on the measurement of liquid state properties in order to discover the pattern of behaviour of liquid systems, and to provide accurate data for the application of theories to real systems.

The study of liquid state properties at high pressure has long been recognised as being of equal importance to the variation of these properties with temperature, but the availability of data at high pressure is restricted by the inconvenience and difficulty of experimenting under these conditions. A liquid state property which yields useful information on the nature and magnitude of intermolecular forces, and their variation with intermolecular distances, is the coefficient of viscosity.

Although the dependence of viscosity on temperature has been extensively studied, no completely satisfactory theory of viscous flow has yet been advanced. Changing temperature alone produces large simultaneous changes in volume, internal energy and its distribution between the various degrees of freedom, and possibly the degree of association and the structure of a liquid. All of these factors influence viscosity, and the complex changes which occur on variation of temperature alone complicate the derivation and application of viscous and liquid state theories. The variation of pressure as well as temperature, enables large volume changes to be made with only small changes in internal energy, and allows the data to be analysed at constant pressure, temperature, volume, internal energy or viscosity.

The measurement of viscosity under pressure, therefore, provides an important contribution to the understanding of the process of viscous flow and the development of liquid state theories. Such measurements are also of great importance in engineering applications, particularly in bearing lubrication, high pressure pump or compressor lubrication and high pressure hydraulics and pressure transmission.

The availability of high pressure liquid viscosity data varies with the pressure range considered. At pressures up to 1,000 kg/cm^2, there is little difficulty in making measurements, and data is fairly abundant; for further information on this pressure range, the reader is referred to the reviews by Bridgman [22] and Bradley [16]. An extensive bibliography on the viscosity of lubricants under pressure is contained in an A.S.M.E. report of 1954 [62].

The first measurements above 1,000kg/cm^2 on pure liquids were those by Faust,[45] in 1914, who determined the viscosities of carbon disulphide, ether and ethyl alcohol up to 3,000kg/cm^2. Cohen & Bruins [26] reported the viscosity of mercury up to 1,500kg/cm^2 in 1925, and the range on mercury was extended shortly afterwards to 12,000kg/cm^2 by Bridgman [20]. In 1925 Bridgman [19] reported his investigation of the viscosity of 43 pure compounds, including mostly organic compounds and water, at pressures up to 12,000kg/cm^2. Dow, [38, 41] employing Bridgman's apparatus, measured the viscosity up to 12,000kg/cm^2 of 7 binary mixtures of liquids selected from Bridgman's studies, and included some measurements on n-decane. Dow also studied the effect of pressure up to 4,000kg/cm^2 on several monosubstituted toluenes [40].

The only measurements to exceed 12,000kg/cm^2, and the highest so far reported, are those made by Bridgman [23] in 1949, on i-pentane, n-butyl bromide, and a few alcohols, up to 30,000kg/cm^2.

Bridgman's original 12,000kg/cm^2 apparatus was employed once more in a modified form in a comprehensive investigation on lubricants up to 10,000kg/cm^2 by the A.S.M.E. [5], in 1953, and included in this work are results on 5 high hydrocarbons up to 3,700kg/cm^2. High hydrocarbons (C_{25} and C_{26}) have also been investigated extensively up to 3,400 kg/cm^2, by Webb et al [54, 139, 140], and Lowitz [88]; and Kuss [74, 75, 76, 77], has reported the viscosity of a large number and variety of organic compounds up to 2,000kg/cm^2. Three high hydrocarbons were investigated up to 1,400kg/cm^2 in 1957 by Boelhouwer & Toneman [14], together with some oils and silicones, and Zolotykh [148] in 1960 measured the viscosity of glycerol and some oils up to 3,600kg/cm^2.

The effect of pressure on the viscosity of liquids is very different from other pressure effects. Most liquid properties change by a factor which is usually less than 10 as the pressure rises; furthermore, the effect of pressure on liquid properties does not vary greatly from compound to compound, and the temperature effect on properties at high pressure is usually less than that at atmospheric pressure. Viscosity, on the other hand, normally shows a roughly exponential increase with pressure, and different compounds show widely different pressure effects. Water and mercury, for example, approximately double their viscosity at 10,000kg/cm^2, whereas eugenol, were it not to freeze at just over 3,000kg/cm^2 at 30°C, would have, by extrapolation, a viscosity increase of 10^6 fold at 10,000kg/cm^2.

The temperature effect on viscosity, too, shows rather unusual pressure dependence, as compared with other properties. Bridgman's measurements at 30°C and 75°C on viscosity, show that the temperature effect at 10,000kg/cm^2 can be as much as four times greater than that at atmospheric pressure.

The magnitude of the viscosity-pressure effect appears to depend to a large extent on the complexity of the molecule. Although this term is difficult to define qualitatively, the pressure effect increases

as one goes to higher members of a structural series, and isomers tend to have larger pressure coefficients than their normal counterparts.

Numerous empirical and semi-empirical attempts have been made to relate viscosity to the pressure or volume of the system, the simplest, proposed by de Guzman [55] and Arrhenius [4], being of the form:

$$\eta = A\exp(PB).$$

$$\text{or,} \quad \eta = A\exp(P\,\Delta V/RT).$$

It is thought that PB, or $P\,\Delta V/RT$, refers to work that a molecule must do in order to flow, and the exponent of this term represents the ~~distribution~~ proportion of molecules possessing the requisite energy. Equations of this form are not completely satisfactory for describing the pressure dependence of viscosity, for, although a roughly exponential behaviour is usually exhibited, a more detailed inspection of viscosity behaviour shows that the first 2,000 or 4,000kg/cm^2 produces a greater than exponential increase in viscosity, followed by a near exponential rise. At very high pressures, the viscosity behaviour again shows a greater than exponential rise, as shown in Fig. 1.

Batschinsky [10] proposed a very simple relationship, depending only on specific volume:-

$$\eta = c/(v - w)$$

where c and w are constants.

However, the expression predicts that viscosity would be independent of temperature at constant volume, which is not so.

More elaborate expressions have been proposed by Andrade[2], [3], Eyring [52], and Panchenkov [109].

Andrade gives, $\eta v^{1/3} = A\exp\left\{(P - r/v^2)S/T\right\}$,

and $\eta_p/\eta_o = (v_o/v_p)^{1/6}(\mathcal{K}_o/\mathcal{K}_p)^{\frac{1}{2}}\exp\left\{c/T(1/v_p - 1/v_o)\right\}$

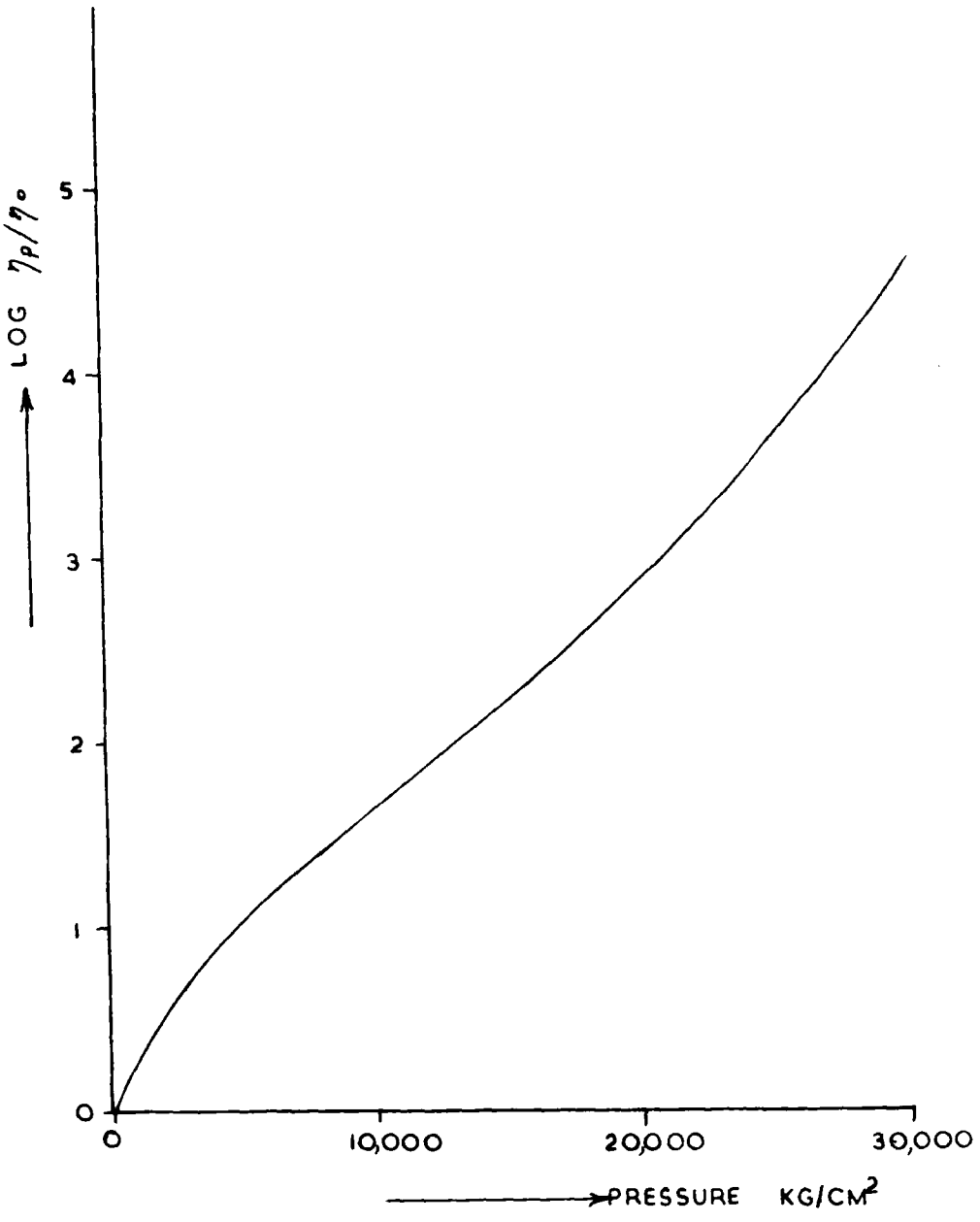

FIG. 1. TYPICAL PRESSURE EFFECT ON VISCOSITY.

where A, r, S, and c are constants, v is specific volume, and β is adiabatic compressibility. The first expression of Andrade's is an elaboration of the simpler exponential relationships, but the second expression includes in its pre-exponential term an estimate of the dependence of molecular collision frequency on volume. However, neither expression is satisfactory above 3,000kg/cm^2.

Eyring, whose theory of viscous flow suggests that the rate determining process is the distribution of molecules with sufficient energy to form a 'hole' in the liquid structure into which a neighbouring molecule might diffuse, proposed the expression,

$$\eta = \frac{1.09 \times 10^{-3} M^{\frac{1}{2}} T^{3/2} \exp(E/RT)}{V^{2/3} \Delta U_v}$$

where η is the viscosity in poise, M the molecular weight, V the molar volume in cc., ΔU_v the molar energy of evaporation, (cal.), and E the activation energy associated with the formation of a 'hole'. The change in activation energy with pressure is the principle cause of viscosity increase in this theory, but the expression can be fitted to experimental data only if E is adjusted empirically.

Panchenkov proposes,

$$\eta = 3(6R)^{\frac{1}{2}}(w^2/N)^{1/3}(\rho^{4/3}/M^{5/6})T^{\frac{1}{2}}\exp(E/RT).\left\{1 - \exp(-E/RT)\right\}^2,$$

where w = total volume of molecules, N = Avogadro's number, ρ = density, and E = bond energy. Agreement with experimental data relies on suitable choices of E and w.

Many attempts have been made to relate viscosity to pressure, temperature and liquid and molecular properties, on the basis of the theories of statistical mechanics and quantum mechanics, reviewed by ~~Lawrence~~ Brush (79). Unfortunately, insufficient progress has so far been made to calculate from first principles the viscosity of even the simplest liquids.

It is evident that in the pressure range above 1,000kg/cm^2, and particularly above 2,000kg/cm^2, a great deal of work is needed to accumulate viscosity data of theoretical and practical significance. The data that exist above 3,500kg/cm^2 have all been obtained from the same instrument, and it is important that some of these values be checked independently. Viscosity data at high pressure are required on a greater range of compounds, and the behaviour of mixtures at high pressure remains practically unexplored. Data on gases above 3,000 kg/cm^2 are non existant, and results on pure gases dissolved in pure liquids are not available at any pressure.

It is the principal object of this work, therefore, to construct and develop a high pressure viscometer suitable for working in a pressure range well above that achieved by existing modern instruments. The operating pressure limit is set at 10,000kg/cm^2, as few compounds can be taken above this pressure at normal temperatures, without freezing. The temperature range is set, in the first instance, at 0 - 100°C, but the possible extension of this range is allowed for in the design. Although the instrument is designed to measure the viscosity of liquids, provision is made for modifying it, so as to make it possible to handle also gases and liquid-gas mixtures up to 10,000 kg/cm^2.

There are indications that the existing data on water at 10,000kg/cm^2 are in error, and a study of water is made, therefore, as an example of the application of the instrument.

CHAPTER 2.

METHODS OF HIGH PRESSURE VISCOMETRY.

Introduction.

Many viscometers for use at pressures greater than one atmosphere have been constructed since the first attempts to measure the pressure effects on viscosity in 1882 by Babo [8] and Roentgen [120]. However, the various instruments can be classified according to a number of operating principles which depend on the method of shearing the fluid under investigation.

The basic methods of shearing the fluid, the order of shear rates obtainable and the suitability of the methods for absolute or relative measurements, are set out in table 1.

Table 1.

Mode of shearing	Order of shear rate	Type of result
1. Flow through a capillary with known pressure gradient.	Low or high, for low viscosities. Low, for high viscosities.	Absolute or relative.
2. Solid body falling in fluid.	Low.	Absolute or relative.
3. Ball rolling in an inclined tube.	Low.	Relative.
4. Continuous relative motion of two surfaces, or rotating cylinders.	Low or high, for low viscosities. Low, for high viscosities.	Absolute.
5. Oscillation of a disc, cylinder or sphere.	Low.	Absolute.
6. Crystal oscillating in the fluid.	High and variable.	Relative.

The suitability of the various methods for this project will now be examined.

(i) Flow through a capillary.

The earliest instruments utilised flow through a capillary, (8, 26, 27, 45, 57, 120, 138) with a column of mercury providing the driving force, but they were very inconvenient to operate, as only one reading was obtainable for each setting up of the instrument. Capill-

ary instruments have since been developed for pressure purposes which facilitate repetitive measurements, and they differ mainly in the manner in which the driving force through the capillary is generated. All the capillary viscometers are based on Poiseuilles Law for laminar flow through a tube:-

$$Q = \frac{\pi d^4 \Delta P}{128 \eta l}$$

The various classes of capillary instrument are typified by the following examples.

(a) Pipette Type.

This consists essentially of a reservoir delivering a known volume of fluid through a capillary, as in the instrument of Swearingen & Redding[133], for use with oils at 270 kg/cm^2. The equipment consisted of a vertical glass capillary surmounted by a reservoir, and a glass cock at the discharge, all housed in a pressure chamber. The vessel was partly filled with test liquid, and pressurised with gas. The viscometer reservoir was filled by inverting the vessel, and the flow through the capillary started by opening the cock with a shaft through the vessel wall. The discharge of the reservoir was observed through viewing ports. Other examples are the experiments on mercury, by Cohen & Bruins[26], and by Bridgman[19].

The shaft and viewing ports would present difficulties at 10,000kg/cm^2, and the direct contact between pressure transmitting fluid and test fluid would severely limit the scope of the instrument.

(b) Mercury Column.

In this type of instrument, a column of mercury is used to drive the fluid through a capillary. The mercury column can be arranged in a number of ways:-

Example (1).

Michels & Gibson[98] measured the viscosity of nitrogen to 1,000kg/cm^2, in an instrument similar to an inverted Oswald viscometer, with the open ends of the limbs joined to a single tube immersed in

mercury. It was made of glass, and contained in a pressure vessel. The two limbs of the viscometer were filled with gas, and a rapid pressure increase caused mercury to rise in the largest limb of the inverted U. This column was then utilised to drive the gas through the capillary. The instrument is difficult to operate, and relies on large volume changes of the test fluid, and is therefore unsuitable for liquids.

Example (2).

Hyde[68] devised an ingenious closed circuit system of driving fluids through a capillary with a mercury U tube, by tilting the whole instrument. The capillary and U tube contained the pressure (1,000kg/cm^2), and were mounted on a knife edge balance system to detect the transfer of the mercury from one side of the U tube to the other. This was the first instrument produced, suitable for repetitive measurements. Its application to 10,000kg/cm^2 would necessitate a cumbersome instrument, which would result in a loss of sensitivity. Also, the viscosity range of each instrument is limited.

More recent instruments, which bear a resemblance to Hyde's in the form of the mercury column, are those of Eakin & Ellington[43], and Parisot & Johnson[110].

Example (3).

Rankine[116] proposed an instrument consisting of a vertical capillary as part of a closed loop of tubing. The second vertical limb of the loop contained a slug of mercury, and the rest of the system was filled with test fluid, the whole unit being enclosed in a pressure vessel. A measurement was made by inverting the vessel, so that the falling slug of mercury drove fluid around the loop and through the capillary, the passage of the mercury being detected by electrical contacts.

The system has been used by Phillips[112] for gases to 110kg/cm^2, and by Boyd[15], Nassini & Pastonesi[105], and Comings[28, 29, 30]. It is simple in construction, but the viscosity range of each instrument is restricted, and with liquids, there is the possibility of seepage of the liquid past the mercury slug, as is found

with mercury gas compressors [118].

(c) Continuous discharge capillaries.

Fluid is discharged through a capillary from a reservoir at pressure P_1 to a lower pressure P_2, usually with gas cylinders or compressors maintaining the pressure P_1. This method has been employed by Dane & Birch[33], and by several other workers[34, 95, 104, 144]. Its application to 10,000kg/cm^2 would severely complicate the maintenance of the two reservoirs at their appropriate pressures, and furthermore, the flow measurement would present great difficulties.

(ii) Falling body viscometers.

With this type of instrument, a spherical or cylindrical body falls vertically in a tube. When the diameter of the tube is large compared with that of the falling body, the fluid flow approximates to the condition of a sphere falling in an infinite medium. Under these conditions, the application of Stokes law, $F = 6\pi\eta vr$, with appropriate wall effect corrections, results in absolute measurements, case (1). When the two diameters are similar, the flow is essentially that through an annulus, case (2).

Case (1).

This is represented by the viscometer of Suge[131], which was used for viscous fluids to 2,000kg/cm^2. It consisted of a pressure tube containing a magazine of identical balls at the top. The balls were released one by one, by means of a key extending through the vessel wall, and their time of fall was measured between two stations by an electrical capacity method.

More recently, Zolotykh[148] has extended the use of this type of instrument to 3,600kg/cm^2, and made repetitive observations by inversion of the pressure chamber. Unfortunately, the method is suitable only for viscous fluids, and a system based on a large (tube/ball diameter) ratio, which is desirable, presents considerable difficulty in tracking the ball by non-optical methods.

Case (2).

When flow through an annulus of finite length is complicated by relative movement of the annular surfaces, the flow conditions become mathematically complex. For this reason, falling body instruments of this type are normally utilised for relative measurements. A difficulty encountered in this system is maintaining the falling body on the axis of the tube, and in one case, Bridgman[19] provided guides on the body in order to achieve a coaxial fall. Bridgman's instrument is the only one to have operated up to and beyond, (12,000kg/cm^2), the proposed range of this work, and was also used by Kleinschmidt[72], and Dow[38, 41], and again in a slightly modified form by the A.S.M.E.[5]. The instrument consisted of a tube within a pressure vessel, and a cylindrical body falling in the tube. Measurements were made by inversion, and observation of the passage of the falling body was made by means of electrical contacts. A similar system was used by Heiks & Orban[59] to 200kg/cm^2, but timing was achieved by the inclusion of a cobalt 60 source in the falling body. The disadvantage of the system is the high precision of the components required.

An unguided, needle shaped body, falling in a pressurised capillary, has been used by Van Wijk & Van der Veen[143] to 1,500 kg/cm^2, and by Boelhouwer & Toneman[14] to 1,400kg/cm^2, and a similar system using a steel ball by Schroer & Becker[124]. In all these instruments, the body was raised by means of an external magnetic field, and timing by various electrical methods was employed. Application of this method to 10,000kg/cm^2 would necessitate placing the capillary inside a pressure vessel, so as to keep deformations (and hence, changes in the viscometer constant), low, with consequential complications in the magnetic raising of the body.

Hawkins, Solberg & Potter[58], and Scott[125], used inversion type falling body instruments to 230kg/cm^2 and 600kg/cm^2 respectively, with unguided sinkers, and Jobling & Lawrence[69] em-

ployed a similar instrument to 440kg/cm^2, but guided the sinker over the initial part of its fall.

Bridgman[23] extended his pressure range to 30,000kg/cm^2 by using a vane falling between two stops, and timing electrically. This instrument is small and simple, but the accuracy is poor.

(iii) Rolling ball viscometers.

In these instruments a ball rolling down an inclined pressure tube (usually 15° to the horizontal) is timed from end to end by electrical means. This system was proposed by Flowers[48] and utilised by many workers[12, 25, 42, 51, 60, 61, 66, 71, 73, 75, 87, 89, 92, 94, 121, 122, 123, 130, 139, 141]. The complex flow conditions have necessitated its use as a relative instrument, and the pressure limit to which it has been employed is 5,000kg/cm^2. At these pressures, deformation of the pressure tube introduces a considerable error (Fritz & Weber[51]), which could be overcome by using a tube within a pressure vessel, but this expedient detracts from the simplicity of the system.

Kuss[73] and Fritz & Weber[51] have used the rolling ball system at inclinations to the horizontal of the order of 80°.

(iv) Rotating cylinder viscometers.

Although this system has had extensive application at atmospheric pressure, its utilisation under pressure has been limited to the instruments of Thomas[135] for operation at 3,000kg/cm^2, and those of others[117, 126, 127], at pressures up to 400kg/cm^2. These consisted of two coaxial cylinders housed in a pressure vessel, one cylinder being driven by a motor inside or outside the vessel, and the torque transmitted to the other cylinder being measured by a spring and potentiometer device. Its bulk, and the necessity of either a heat producing motor within the vessel, or of introducing a shaft through the vessel wall, precludes it from use at 10,000kg/cm^2.

(v) Oscillating disc, cylinder or sphere viscometers.

These consist of a disc, cylinder or sphere, suspended on a fine wire in a pressure vessel, and oscillating either freely in the test fluid, or oscillating within adjacent guard surfaces. Measurement of the period and of its decrement enables viscosity to be computed absolutely. It has been used mainly for gases, up to 1,000 kg/cm^2, by Maass[93, 103], Felsing & Blankenship[47], and Gonikberg & Vereshchagin[53]. The method has also been used on water and steam up to 340kg/cm^2, by Moszyinski[102]. Although the precision of this type of instrument is claimed to be high, the value of the viscosity of water at 20°C given by Moszyinski, differs by 2% from the National Bureau of Standards value.

The adaptation of this technique to 10,000kg/cm^2 is discouraged by the unknown variation in the properties of the suspension under pressure, the considerable bulk of the system, and the very long periods encountered with low viscosity materials.

(vi) High frequency methods.

If a crystal immersed in the test fluid is oscillated electrically, a measure of the viscosity of the fluid can be obtained either from the attenuation of the sound wave produced [44, 64, 83, 119, 129, 132, 134] or from measurements of the electrical properties and resonant frequency of the crystal itself [9]. The former method has been used up to 9,000kg/cm^2 [64, 129], but agreement with established data is very poor [119]. The latter method has been used up to 1,000kg/cm^2, and comparisons with Bridgman's data [19] are quite good. Although this method is convenient to use under pressure, the results are difficult to interpret, as the shear rates are high and variable; furthermore, the method is difficult to apply to polar liquids.

CHAPTER 3.

DESIGN AND DEVELOPMENT OF VISCOMETER.

(i) Type of viscometer chosen.

A viscometer which possesses the versatility of being able to handle any liquid, must comply with the following conditions:-

(a) One phase only must be maintained throughout the instrument, so as to eliminate the possibilities of chemical reaction, contamination, partial miscibility or saturation of liquids with gases, i.e. contact between the test fluid and mercury, gases, or any pressure transmitting fluid, must be avoided.

(b) No electrical conductor must be in contact with the test fluid in the viscometer, so as to allow the application of the instrument to polar and conducting liquids.

The only instruments discussed in the previous chapter which possess these characteristics, and are, at the same time, easily adaptable for use at 10,000kg/cm^2, are the rolling ball viscometer, and the falling body viscometer.

The falling ball type of instruments of Suge[131] and Zolotykh[148] have already been eliminated for reasons previously discussed, and the capillary and unguided needle type of falling body instrument, (Boelhouwer & Toneman[14]), has shortcomings in addition to those already mentioned. With any falling body instrument, based on a small tube/body diameter ratio, it is imperative for the tube diameter to be highly uniform. The bore of a metal capillary cannot be produced as uniformly as a tube large enough to allow internal working of the bore, and both the bore variations and the quality and uniformity of the surface finish of a capillary are difficult to inspect. Also, it has not been established whether a guided or an unguided falling body is preferable, and the former type would be extremely difficult to produce accurately for use in a capillary.

In the absence of an entirely novel system, the choice of instrument lies between a rolling ball, a guided falling body, hereafter called the sinker, and an unguided sinker. At 10,000kg/cm^2, all these systems must employ a self contained viscometer within a pressure vessel, and all require either inversion or an internal magnetic retrieving system to facilitate repetitive measurements. Inversion complicates the high pressure system, but on the other hand, magnetic retrieving introduces problems of temperature equilibrium, and calls for a large number of conductors entering the pressure vessel. The case against magnetic retrieving is further weighted by two design features which are dealt with in subsequent sections. Firstly, the electro-magnetic timing system (next section) might be upset by residual magnetic fields, which could be set up by the strong fields of a retrieving system, and these same residual fields might affect the terminal velocity of the sinker. Secondly, the use of two sinkers in the viscometer tube (Section iii) would make magnetic retrieval particularly difficult to apply. An inversion system is therefore used for this work.

In the case of an inversion system, an unguided sinker must be guided over the first part of its travel to maintain an axial fall as the viscometer is brought to rest in the vertical position, as in the viscometer of Jobling & Lawrence[69]. The unguided sinker, guided sinker, and rolling ball are all mathematically complex systems, and increasingly so in this order. The following design is based on the guided sinker, without there being a clear indication of which system, under similar conditions, will give the most accurate and reproducible results. The rolling ball method is the most difficult to correct for ball and tube compressibilities, is prone to setting up turbulence, and can introduce uncertainties due to the ball slipping instead of rolling down the tube. The unguided sinker gives the closest approach to ideal flow conditions if falling axially, but the

eccentricity, and hence fall time, can depart from the ideal to an unknown extent. The guided sinker produces more turbulence than the unguided one, but the eccentricity is always within known limits. Although designed for a guided sinker, the instrument developed as a result of this study is readily adaptable to the other two systems, and its use and comparison under all three conditions would in itself provide a valuable contribution to high pressure viscometry.

(ii) Method of timing.

The methods of timing which have been used in the past with high pressure falling body or rolling ball viscometers may be enumerated as follows:-

(a) Direct visual observation e.g. Zolotykh[148]. (3,600kg/cm^2).

(b) Falling body making and breaking electrical circuits within the viscometer e.g. Bridgman[19]. (12,000kg/cm^2).
Hersey & Shore[61]. (4,000kg/cm^2).

(c) Detection of the falling body by capacity measurements within the viscometer e.g. Suge[131]. (2,000kg/cm^2).

(d) Detection of the falling body by monitoring a radioactive source in the body from outside the pressure vessel e.g. Heiks & Orban[59]. (260kg/cm^2).

(e) Detection of a magnetically soft sinker by coils wound on the outside of the pressurised viscometer tube e.g. Roelhouwer & Toneman[14]. (1,400kg/cm^2).

System (a) is difficult to apply at 10,000kg/cm^2, since windows would be required in the viscometer tube as well as in the pressure vessel, and visual access to the sides of the pressure vessel complicates the thermostating arrangements.

Systems (b) and (c) are eliminated by the requirements of the exclusion of all conductors from within the viscometer.

System (d) would prove insensitive when applied to the very thick pressure vessel required for 10,000kg/cm^2, since the usual form of radiation counter could not be placed inside the vessel.

System (e) would be satisfactory if the coils were placed in the pressure chamber, and it is this system which is used. Coils wound on the viscometer tube will perform as required, only if the tube itself is not magnetic, and compressibility corrections for the tube and sinker are considerably simplified if these two components are of the same material, which results in a non magnetic sinker also. Since section (iii) provides for the use of aluminium alloy sinkers, which are also non magnetic, small pellets of soft iron are set inside the sinkers to provide adequate ferromagnetic detection sensitivity. The basis of the detection system is illustrated in Fig. 2.

A pair of coils, (1) and (2) are wound on the viscometer tube and arranged as part of an a.c. bridge, as shown. The resistive arms, together with all the necessary balancing arrangements, are remote from the pressure vessel. The output is observed on an oscilloscope, and is zero at balance. As the soft iron enters coil (1), its inductance is increased, the bridge is unbalanced, and the output rises. When the pellet is midway between the coils, the inductance of each is increased by the same amount, and the bridge is rebalanced. On passing through coil (2), the pellet unbalances the bridge once more, but in the opposite phase to the first unbalance. Fig. 3 represents the bridge peak voltage output, and the phase angle relative to the input signal, as the pellet passes through the coils. A number of pairs of coils were made with different dimensions and wire gauges, to find the most suitable proportions, and Fig. 4 shows the dimensions which gave the best performance for a tube bore approximately $\frac{3}{8}$ inch. The criterion of performance was

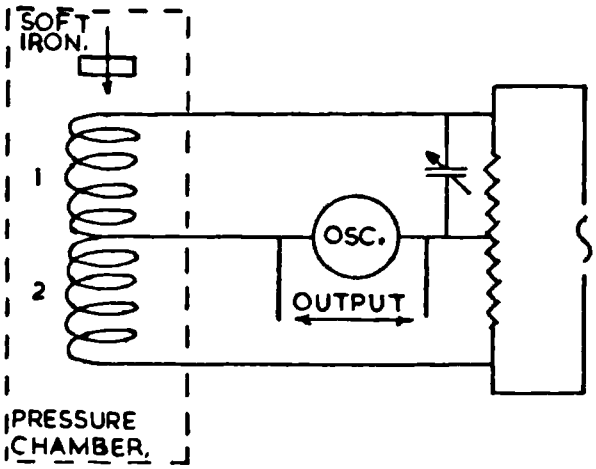

FIG. 2. VISCOMETER TIMING SYSTEM.

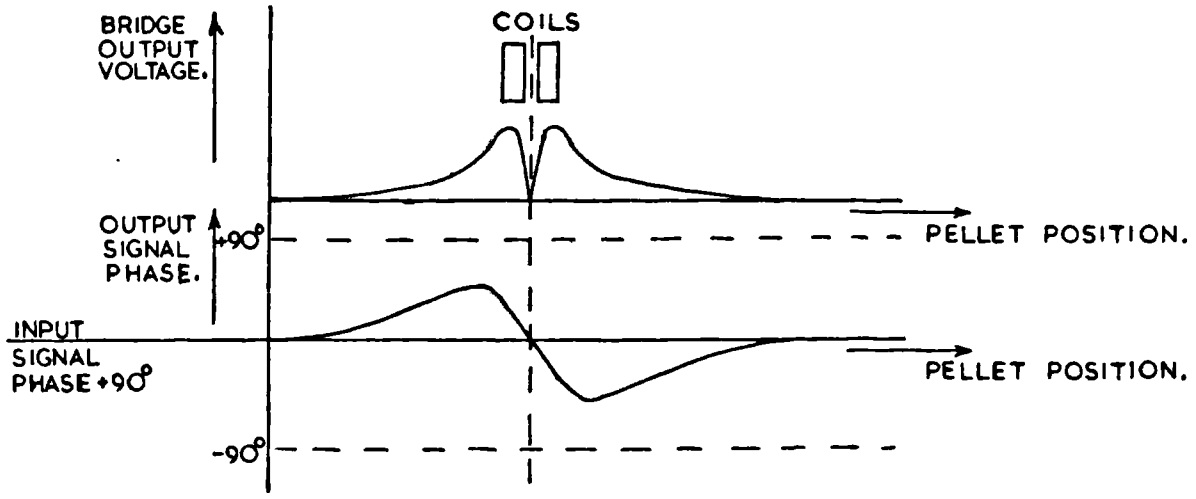

FIG. 3. TIMING CIRCUIT SIGNALS.

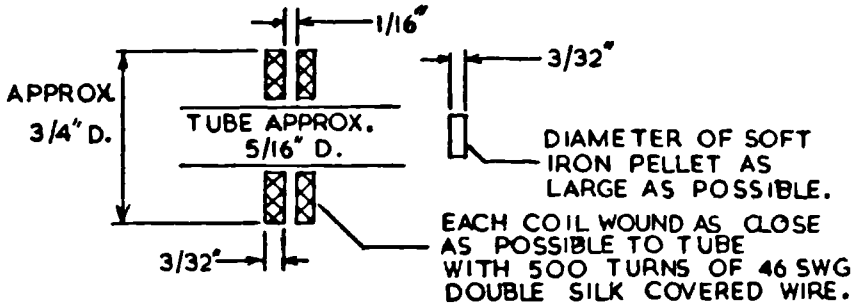

FIG. 4. TIMING TRANSDUCER DIMENSIONS.

chosen as the rate of change of output voltage with pellet position at the central balance point, for a constant number of ampere turns. Pairs of coils, each set up as an independent bridge circuit, are wound near each end of the viscometer tube to serve as timing stations. The detection of the balance point when the pellet is central in the coils, is dealt with in section (v).

(iii) Density measurement.

The first order theory of a falling body viscometer given in Chapter 4 shows that:-

$$\eta = \frac{wgT^*k}{lL}$$

If subscript 1 refers to a particular sinker, then

$$\eta = V_1 g(\rho_{s1} - \rho_f)(T_1^*/l_1 L)k_1.$$

Application of 10,000kg/cm^2 pressure can change ρ_f by as much as 28%, and it is therefore necessary to know ρ_f under pressure in order to compute viscosity. When employing a stainless steel sinker (see section iv.), ρ_{s1} is about 7.9 g/cm^3. If ρ_f is approximately 1 g/cm^3, a 28% change in ρ_f will change $(\rho_{s1} - \rho_f)$ by only 4.1%. A knowledge of ρ_f to 5% will, therefore, allow computation of viscosity to 0.2%.

If a second sinker, of density ρ_{s2} is allowed to fall in the same fluid as the first sinker, then:-

$$\eta = V_2 g(\rho_{s2} - \rho_f)(T_2^*/l_2 L)k_2.$$

All the factors except η and ρ_f are known, and solution of these two simultaneous equations give ρ_f approximately, enabling η to be corrected for buoyancy effects. For greater accuracy, ρ_{s2} must be as small as possible. Such a system employing two sinkers was proposed by Jobling & Lawrence[69], but as far as is known, has never been utilised. The present viscometer allows the use of two sinkers, and the accuracy of density that the system gives, is dealt with in Chapter 10.

(iv) Design of viscometer.

The viscometer design is based on the assumption of the availability of a pressure vessel, capable of maintaining constant pressure up to 10,000kg/cm^2, and constant temperature over the desired range. It is also assumed that the vessel is able to rotate in either direction on an axis precisely at 90° to the bore axis, and that the vessel can be locked in an exactly vertical position with either end uppermost. It is further assumed that any necessary electrical conductors entering the pressure chamber are available at one end of the bore, and that the opposite end of the vessel is fitted with a removable closure. This arrangement of closures is chosen to allow the possible further development of the instrument for use with gases and gas/liquid solutions, which could be admitted under pressure through the free end of the vessel.

The general arrangement of the viscometer is shown in Fig. 5. The actual measurements are carried out in a stainless steel tube (1). This was produced from a solid bar of EN58JM steel, which is an easy machining grade of an extremely good corrosion resisting austenitic stainless steel. This material was chosen for its combination of corrosion resistance, machinability and non-magnetic characteristics. The bore of the tube was produced by drilling, reaming, and then honing, and the manufacturer claims the hole to be round and parallel to within .0003 inches. The surface finish in the bore is about 5 micro-inches. Its diameter is .302 inches and the tube is about 8 inches long. A pair of grooves are machined half an inch from each end of the tube at (2), allowing a falling sinker to achieve terminal velocity before timing commences. The walls of these grooves are provided with radial slots, as shown in the coil detail Fig 5a to ventilate the coils during volume changes of the pressure transmitting fluid. To each end of the tube is attached a stainless steel pocket,

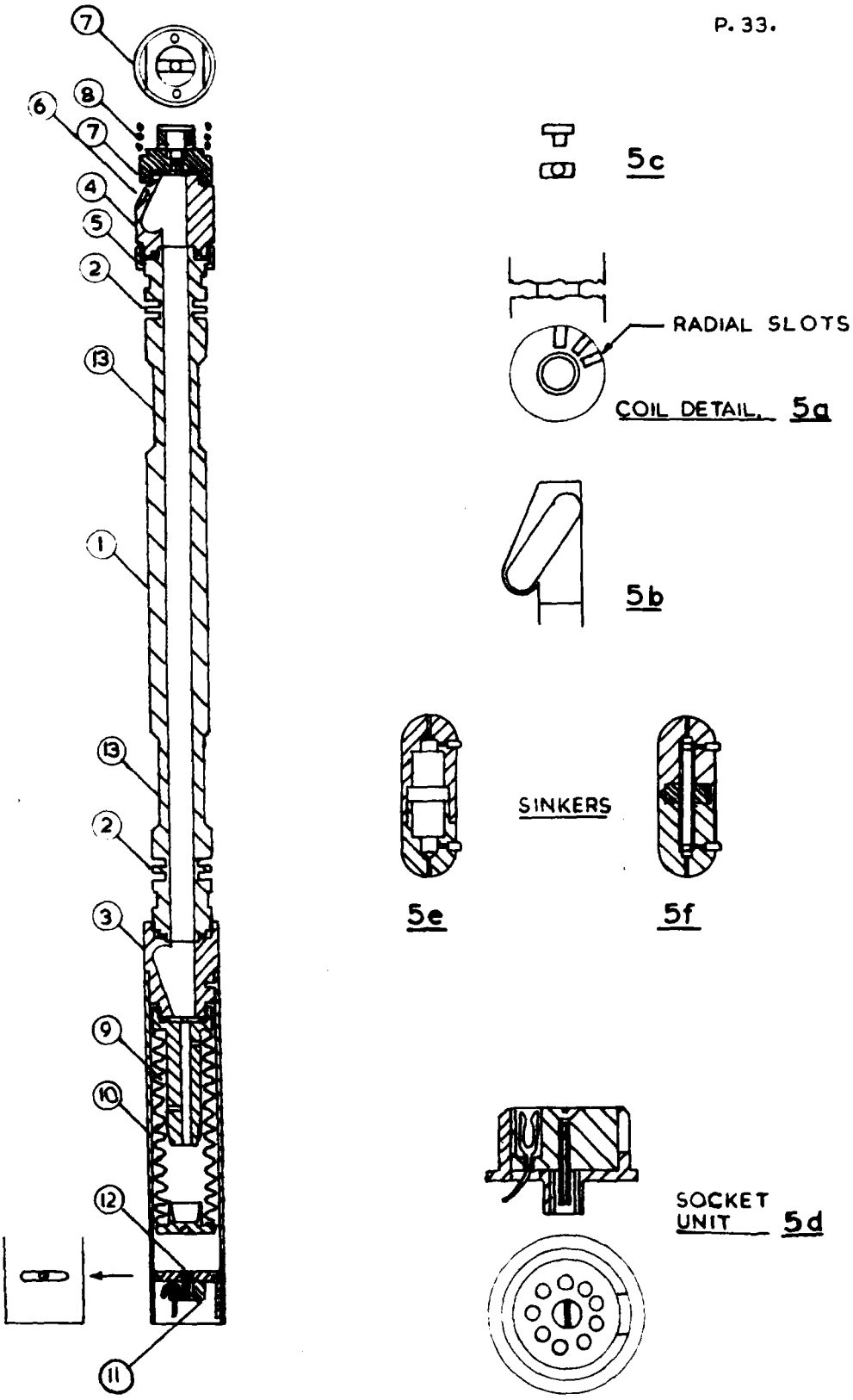

FIG. 5. THE HIGH PRESSURE VISCOMETER

(3) and (4), each pocket being accurately located on the end of the tube, and the joints are sealed with O rings. End (4) is secured with a collar, (5), so that it can be correctly orientated with end (3). The pockets in (3) and (4) are formed by internal grinding so as to hold a sinker as shown in Fig. 5b, whilst a second sinker is falling, and by turning the vessel containing the viscometer in appropriate directions, two sinkers can be manoeuvred individually up and down the tube at will.

End (4) is fitted with a .0005 inch thick silver bursting disc, (6), which provides some relief inside the viscometer in the event of a sudden failure of the pressure system. End (4) is closed with the stainless steel component (7) and an O ring, and this end of the viscometer is located on the axis of the pressure vessel by means of the socket and flats in the end of (7) engaging the vessel closure detail shown in Fig. 5c. The spigot on 5c locates the axis of the viscometer, and the flats maintain the pockets in (3) and (4) in the correct plane. A filling hole, sealed with an O ring and grub screw is included in component (7), and there are also screwed holes provided for withdrawing the viscometer from the vessel. The top end of the viscometer is free to move longitudinally, relative to the vessel closure, to accommodate strains arising from changes in temperature and pressure. The instrument is completed, at the top end, by a spring (8), which bears against the vessel closure, and forces the viscometer firmly against its bottom location.

End (3) is closed with a bellows unit, (9), and sealed with an O ring. The bellows unit consists of a stainless steel bellows, soft soldered at each end to two stainless steel components which are designed to leave the minimum of free volume in the bellows when it is fully collapsed. This whole unit is screwed onto the end of (3), and its function is to accommodate volume changes in the test fluid during pressure and temperature changes. There is a screwed

hole in the bottom of the bellows unit where a rod may be attached to expand or collapse the bellows manually.

A brass tube, (10), accurately located on (3), extends over the bellows unit to the electrical connections plug unit, (11). The plug unit consists of pins, as shown, cast into a moulded 'Araldite' block, and set out so as to fit a standard 9 hole miniature valve base socket. The plug is secured by a screw to a brass carrier, (12), which is free to rotate relative to tube (10). Part (12) also has a tongue which polarises the whole unit before the plug engages the socket shown at Fig. 5d. This socket is fixed to the bottom closure of the vessel, and consists of a brass holder containing a 9 pin valve base. The brass holder maintains the bottom end of the viscometer on the vessel axis, and also provides the longitudinal location. Once the plug is polarised and engaged, the whole viscometer may be turned about the plug unit by a limited amount, so as to set the pockets in (3) and (4) in the correct plane.

The overall diameter of the viscometer is 15/16 inch, and is $14\frac{1}{2}$ inches long. It is intended for use in a 1 inch bore vessel, to allow adequate ventilation space, and numerous holes are drilled wherever cavities exist, so that damage will be kept to a minimum in the event of a sudden decompression. The coil windings are terminated at miniature sockets attached at (13), and P.T.F.E. insulated wires connect miniature plugs at (13) to the plug unit at (11).

Two sinker designs are shown in Fig. 5e and Fig. 5f. 5e is for a sinker of the same material as the viscometer tube, and is designed to keep weight to a minimum. The two halves are a push fit together, and the soft iron pellet is a free fit in its locating cavity. The interior of the sinker is ventilated at each end by a 1/64 inch diameter hole. Three guiding pins at each end are produced by forcing stainless steel wire into radial holes, drilled right through for ventilation of the inner end of the pin. The second sinker de-

sign, 5f, is for aluminium alloy, and produces the maximum ratio of aluminium to iron, and hence a low density. The two halves are located on the soft iron pellet, and are held together with an aluminium stud. The arrangements for ventilation, and for aluminium wire pins, are similar to those described for the first sinker.

(v) Description of timing system.

The actual sinker detection transducer has already been described in section (ii). For long times of fall, the transducer bridge would pass through its central balance point so slowly, that hand starting and stopping of a timer, by observing the output signal on an oscilloscope, would be perfectly adequate. However, the viscosity changes under pressure are very large, and to maintain fall times within manageable limits at high pressures, the fall times at atmospheric pressure must be the minimum that accuracy will allow. Under such conditions, hand starting and stopping for fall times of, say, 10 seconds, would introduce a large human error. To obviate this, detection of the bridge balance points, and triggering of the timer must be automatic. The system used is represented in the block diagram in Fig. 6. The supply for the system is by an 'Advance' audio frequency signal generator, type J2, having outputs matched for 600ohm and 5ohm loads. The two a.c. bridge transducers are supplied via stepdown transformers from the 5ohm source, and the whole system between bridge output and the timer is transistorised and battery powered to eliminate 'noise' from mains supply.

The bridge output is amplified by two, two-stage transistor amplifiers, adjusted to give a total gain of 5000. The amplified signal is then limited to voltages a little above those produced when the soft iron pellet is close to its central position in the transducer, and the limited signals are displayed on a double beam oscilloscope so that the correct functioning of the

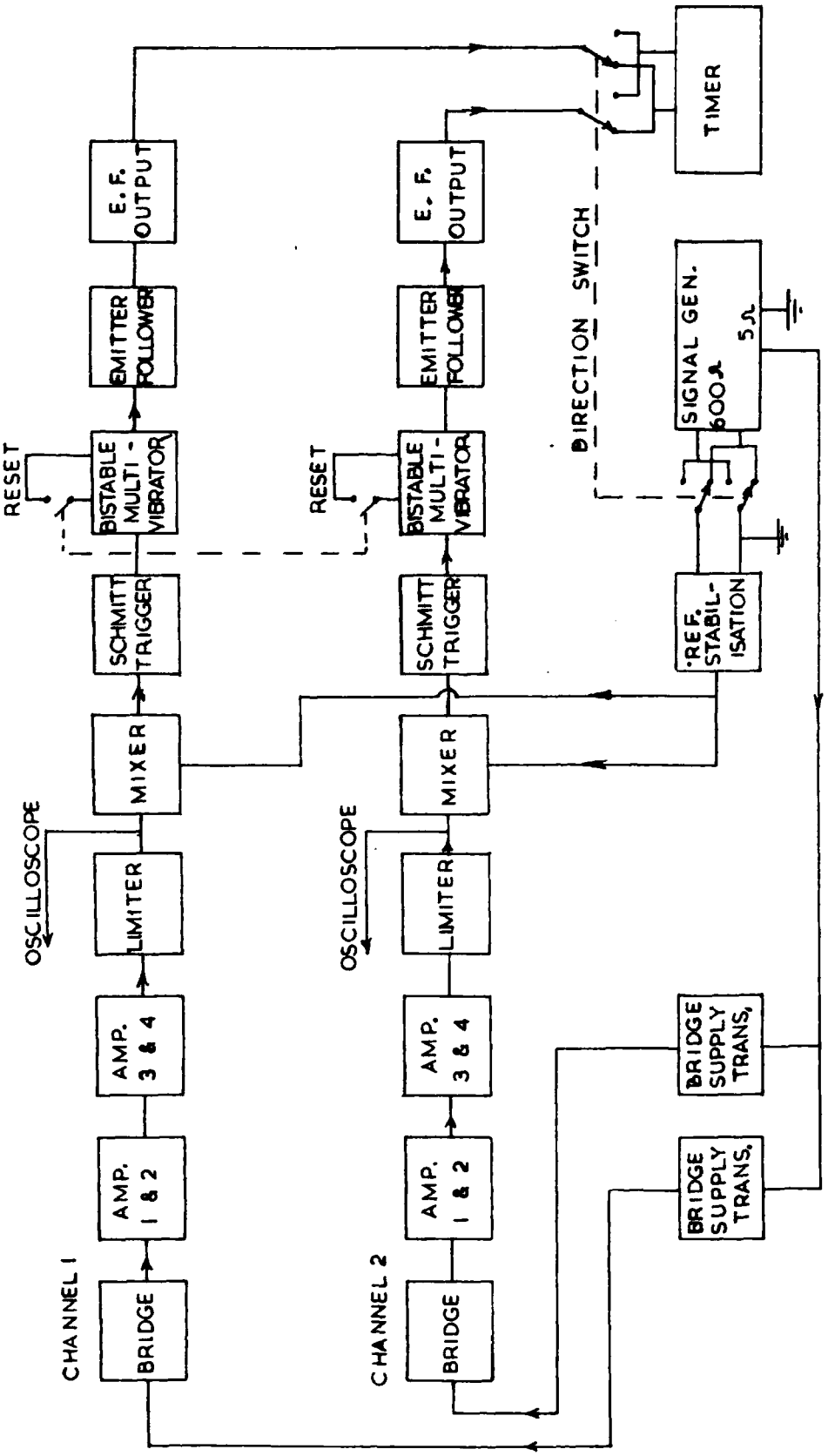

FIG. 6. TIMER TRIGGER CIRCUIT

system may be observed. The peak voltage output from the limiter is shown in Fig. 7a. The 600 ohm output from the signal generator is utilised as a phase and voltage reference signal. The phase of this output is switched according to the direction of travel of the sinker, and the sine wave signal is chopped to produce an approximate square wave. The chopped reference signal is shown in Fig. 7c, and the phase angle of the bridge signal, relative to the reference signal, is shown in Fig. 7b. The bridge and reference signals are mixed, and the resultant signals are illustrated in Figs. 7d and 7e. When the sinker is at position (1), just before the bridge balance point, the bridge signal subtracts from the reference signal peak voltage as in Fig. 7d. With the sinker at position (2), immediately after balance point, the peak voltage of the mixed signal is just above the reference signal peak voltage, as in Fig. 7e. The mixed signal is fed to a Schmitt trigger, and the reference peak voltage is adjusted to a value slightly below the voltage at which the Schmitt trigger will function. As soon as the sinker has passed the bridge balance position, the mixed signal peak voltage rises above the reference signal peak voltage, and the Schmitt trigger emits a pulse.

The pulse is fed to a bistable multivibrator, which, on receiving a pulse, itself emits a pulse. However, whereas the Schmitt trigger will pass an indefinite number of pulses, the bistable multivibrator will emit one pulse only, until it is manually reset. This facility allows the circuit to function only when set ready by resetting of the bistable multivibrator. The pulse is matched, by an emitter follower, to the required impedance, and is utilised to start or stop a Labgear type D4108 time period counter, coupled to a Labgear type D4109 register, to increase the timing range. This combination gives a time range of 10^{-4} sec. to 10 secs. on decatron counters, and 10 secs. to 10,000 secs. on a mechanical register. The timer stability is claimed by the manufacturer to be .02% over the temperature range -10 to $+70^{\circ}C$.

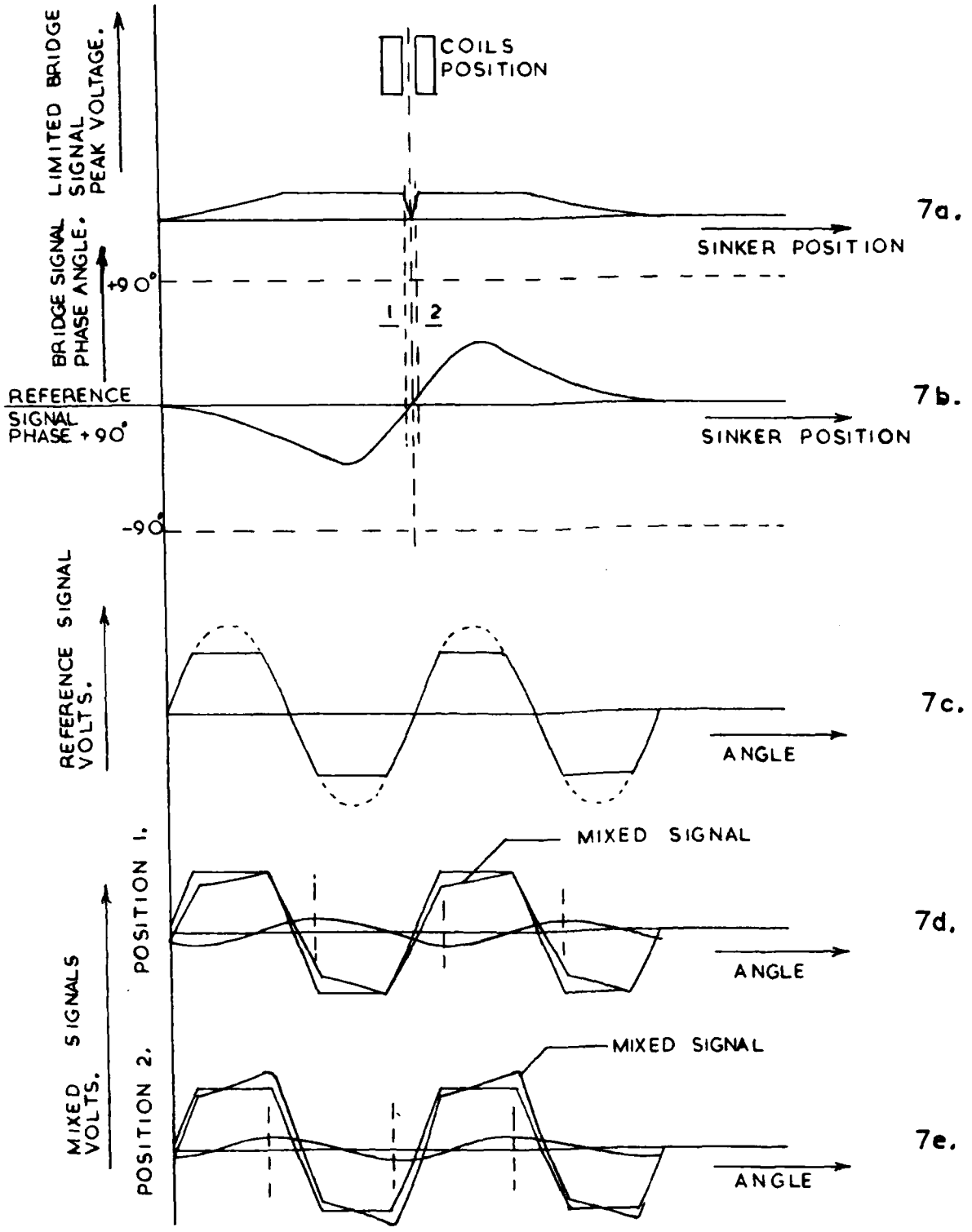

FIG.7. TRIGGER CIRCUIT SIGNALS.

There are two independent triggering circuits, and the pulse from each can be directed to either the start or stop facility on the timer. When a sinker is to be timed for a particular direction of fall, the triggering channels must be connected to the timer appropriately, and the reference signal phase must also be set according to direction. The switches which perform these two functions are ganged together, so that setting one switch at the chosen direction of fall orientates the whole system. Because the pulse supply is a one shot system, the trigger circuits have to be reset after each triggering. The actual circuit for one transducer and triggering channel is set out in Appendix 1.

(vi) Development and Performance of Timing System.

(a) Development.

The triggering circuits were built by the departmental electronics workshop, and the correct functioning of the channels was checked during assembly by passing a soft iron pellet through the transducers. However, when the system was applied to the actual viscometer and sinkers, it was found that triggering occurred at B instead of the designed position, A, in Fig. 8. The trouble was traced to eddy currents induced in the non-magnetic shell of the sinker. When only soft iron approaches the first coil of the transducer, the inductance of that coil increases, and unbalances the bridge in the phase that does not trigger the system. However, when the first coil is approached, instead, by soft iron contained in a long shell of non-magnetic conductor, the eddy currents in the shell, which reaches the coil first, are accompanied by a magnetic field in opposition to the coil field, and the resultant coil field is reduced. This condition unbalances the bridge in the opposite

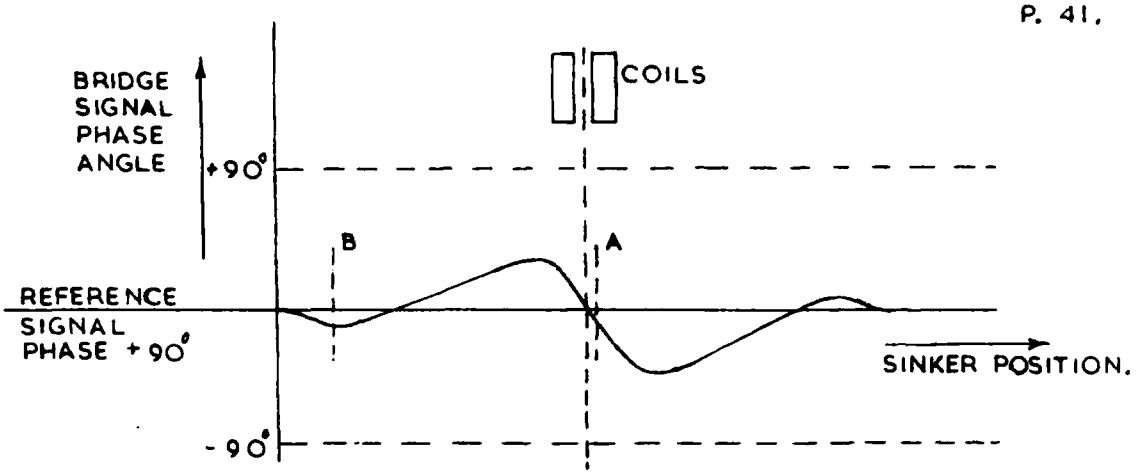

FIG. 8. SIGNAL CAUSING PREMATURE TRIGGERING

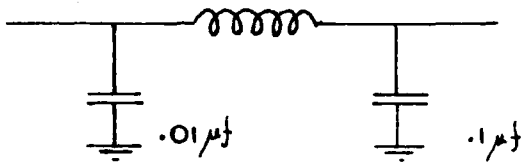

FIG. 9. TRIGGER CIRCUIT FILTER

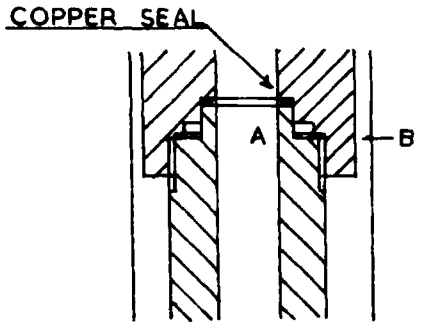

FIG. 10. VISCOMETER SEAL

phase to that desired, and the timer is triggered prematurely. When the sinker approaches closer to the coil, the effect of the soft iron exceeds that of the eddy currents, and the resulting signal phase, as the sinker passes right through the transducer, is as shown in Fig. 8.

The difficulty was overcome by reducing the operating frequency from 6,000c.p.s., for which the system was designed, to 500c.p.s. At this frequency, the magnitude of the eddy currents is so small as to no longer disturb the proper functioning of the system. At 500c.p.s., the smallest unit of time that the system will resolve at each timing station, is .002 sec., and with a fall time of 10 secs. this leads to a maximum error from this source of $\pm$ .02%.

When the viscometer was installed in its pressure vessel, remote from the triggering channels and balancing system, it was found that good bridge balancing could be obtained only by very careful screening of the connecting leads between the transducer half of the bridge on the viscometer, and the balancing half of the bridge. It was also found that a complete avoidance of all earth loops was necessary. Once these conditions were achieved, the system behaved as well in its working position as it did with the whole system close together on the bench, with short connecting leads.

However, even though the connecting leads were well screened (coaxial cables in an earthed conduit), a great deal of trouble was caused by the leads picking up stray high frequency electromagnetic radiation from equipment in the surrounding building. If this occurred when a triggering channel was set for operation, the circuit would sometimes trigger of its own accord. On some days, electromagnetic activity was so bad as to make the timing system almost unusable. A tuned circuit for passing only the desired

frequency to the amplifiers would have a prohibitively large resistive component at 500c.p.s., and would therefore be unsatisfactory. The difficulty was overcome by filtering out as much high frequency signal as possible, without losing much of the low frequency signal, with filters of the type shown in Fig. 9, placed before and after the triggering channel amplifiers. By this means, the frequency with which the timer was prematurely triggered by stray signals was considerably reduced, and by resetting the pulse circuit only a few seconds before it was due to function, the wastage of results was reduced to only a few per cent.

(b) Performance of timing system.

This section describes the behaviour of the timing system at atmospheric pressure and temperature, and its performance under pressure and at other temperatures is discussed in Chapter 9.

As the present instrument measures only relative viscosity, the distance between the 'electromagnetic' centres of the timing transducers is immaterial. The criterion of performance is the reproducibility of the position at which the sinker triggers the timer in either direction, and this reproducibility was checked by mounting a sinker on a brass rod, which in turn was mounted at its opposite end on the moving base of a cathetometer. The vernier scale on the cathetometer base could be read to the nearest .0002 inch.

The procedure of this experiment was to move the sinker clear of the transducer coils and balance the bridge. The reference signal voltage was also adjusted, by resetting the trigger circuit, and raising the reference signal voltage until the system triggered of its own accord. The reference signal voltage was then reduced slightly and the trigger circuit reset, to check that the

reference voltage was not too high. A final check on the reference voltage was achieved by putting the bridge out of balance in the appropriate phase by adjusting the resistive arms of the bridge, and observing the height of the signal on the oscilloscope when the unbalance was sufficient to trigger the timer.

With adjustments completed, the cathetometer slide was moved so as to advance the sinker into the coils, and the slide position on the vernier scale was noted when triggering occurred. This procedure was carried out several times in each direction to check both the reproducibility of the triggering position, and also the reproducibility of carrying out the adjustments.

It was found that the triggering position for each direction, in each transducer, was reproducible to within $\pm$.0005 inch. The separation of the two triggering positions for each transducer is .008 inch, and the distance separating the mean triggering positions of the two transducers is approximately 7 inches. The maximum error caused by the transducers, under these test conditions, is therefore $\pm$.015%.

(vii) Development of Viscometer.

(a) General.

The stainless steel viscometer described, in section (iv) is, in fact, the second instrument produced. The first was of similar design, but was constructed of an aluminium alloy to specification RR77. This latter alloy was selected for a number of reasons, as follows:-

(1) The material is non-magnetic.

(2) As mentioned before, it is preferable to construct the viscometer tube and the sinker shell of the same material. An alu-

minium alloy tube allows the use of an aluminium alloy sinker of low density, and an aluminium alloy sinker shell with inserts of a high density metal, such as gold, to give a high density sinker. The reverse procedure of employing, say, a stainless steel tube, presents no problem of achieving a high density stainless steel sinker, but a stainless steel shelled sinker of low density is extremely difficult to produce.

(3) RR77 is amongst the hardest of aluminium alloys, has good machining properties, and exhibits particularly good isotropy.

During some development trials, the aluminium viscometer was filled with methanol, which was slightly wet, and within twenty minutes, severe corrosion resulted in a badly pitted surface inside the tube. However, this viscometer, damaged though it was, did provide another lesson. The aluminium viscometer was assembled in the pressure vessel, and 10,000kg/cm^2 applied. During this test, one of the vessel seals failed suddenly at full pressure, and the viscometer was subjected to a rapid decompression. The test fluid inside the viscometer was unable to expand quickly enough, with the result that the thin walls of the viscometer tube at the root of the coil grooves suffered a slight permanent expansion, and the top end of the viscometer, (Fig.5 part 7), was forced off, stripping the threads. All other components, including the coils, were undamaged. The aluminium viscometer differed from the stainless steel one in two respects. Firstly, the long hole in the bellows assembly, (Fig.5 part 9), was 1/16 inch diameter, in the aluminium viscometer, compared with 3/16 inch diameter in the stainless steel viscometer. Secondly, part 4, in Fig. 5, was not fitted with a bursting disc in the case of the aluminium viscometer. The rapidly expanding fluid had only a long 1/16 inch diameter hole at one end of the tube to escape through, accounting for the large pressure difference between the inside and outside of the viscometer. The provision of the enlarged hole, and the 10kg/cm^2 bursting disc as a result of this experience, is to obviate a similar failure.

The pressure relief modifications are the only ones that have had to be made to the structure of the viscometer. The transducer coils, and the pocket system for holding a second sinker, have proved trouble free. The bellows and the silver bursting disc occasionally fail from fatigue, but these are regarded as expendable items.

(b) Contamination.

The most important factor affecting the proper functioning of the viscometer, is the assembling and filling of the instrument with the complete exclusion of all forms of dirt from the interior. The presence of any dirt is reflected in either sticking of the sinker in the viscometer tube, or in erratic and inconsistenttimes of fall, and it was found that great care was necessary to eliminate this source of trouble.

The procedure followed for assembling the viscometer in the dust free condition is as follows:-

The pockets, (parts 3. and 4., Fig 5), are assembled on the tube, (part 1), and this assembly is cleaned as a unit. Preliminary cleaning of this unit is by filling and emptying a few times with clean recrystallisable benzene, following by drying in a vacuum oven at 60°C.

The tube and pockets are then inspected, and any remaining dirt is removed by forcing plugs of cotton wool down the tube and by probing the pockets with cotton wool and tweezers. The interior surfaces of these components are sufficiently smooth to prevent catching up of the cotton wool. The final stage of cleaning is by thoroughly flushing the tube and pockets with a jet of distilled, de-ionised and filtered water, from a glass wash bottle, and vacuum drying. All other components are washed and flushed with benzene, dried, and stored under clean glass covers or in clean aluminium foil

until required for assembly. The vacuum oven in which all parts are dried is provided with a filtered air supply.

The various components are protected from atmospheric dust until immediately before assembly, and assembly is carried out as quickly as possible. During assembly, the threads are coated with a molybdenum disulphide based grease.

All liquids entering the assembled viscometer are first filtered before transfer to the filling vessel, and then filtered again on being transferred from the filling vessel to the viscometer.

(c) Seals.

The viscometer was designed for use with O ring seals, and these were employed during initial work. The O ring materials used were the same as those employed in the rest of the high pressure section, and for reasons described in Chapter 6, the O ring materials, of necessity, possessed good low temperature properties. These O rings sealed the viscometer satisfactorily over the whole temperature and pressure range when at steady pressures, but it was found that leaks occurred during pressure changes. Two mechanisms of leakage were found, each occurring under different conditions, as follows:-

(1) The elastomers which were suitable for sealing 10,000kg/cm^2, were found to have incomplete solvent resistance. In any case, complete solvent resistance in an elastomer is rare, and improved low temperature properties usually involve a deterioration in solvent resistance.

An O ring in its working position in the viscometer assembly is surrounded by the pressure transmitting fluid, petroleum ether, on one side, and test fluid on the other side, of the seal. At atmospheric pressure, the O ring elastomer is swelled by petroleum ether, and possibly by the test fluid too, and this involves the absorption of fluid molecules into the macromolecular structure of

the elastomer. Application of hydrostatic pressure to the elastomer reduces the amount of fluid that the elastomer is able to absorb, and so petroleum ether, and possibly test fluid, is ejected from the O ring in all directions. By this means, raising the pressure transfers a very small quantity of petroleum ether into the test fluid region, and vice versa.

When the test fluid and pressure transmitting fluid are miscible, the effect of this transfer is quite unnoticeable, because the quantities involved are so small. However, when experiments were carried out with water in the viscometer, the introduction of a trace of a second phase (the petroleum ether) caused a considerable change in the sinker fall time. The order of magnitude of the change is something like a 1% change in time for a .01% concentration of petroleum ether. (Both water and the petroleum ether are of similar viscosity). It was the use of water which led to the detection of this mechanism of leakage, and the realisation that O rings could be made to work as a pump, by raising and lowering the pressure. The quantity of petroleum ether in the water, as shown by the time of fall of the sinker, increases with each pressure cycle.
(2) When the viscometer is operating at 10,000kg/cm^2, and 20-30°C, the O ring materials are quite close to a condition in which they are too rigid to function as seals. A rapid drop in pressure of about 2,000kg/cm^2 can lower the temperature of the O ring sufficiently for it to temporarily lose its sealing properties, and a leak occurs and continues until the temperature recovers. Again, the quantities involved are small, and this mechanism of leakage, too, was detected by the use of water in the viscometer.

Leakage by mechanism (2) can be guarded against by careful operation, but the lack of a suitable elastomer, which is completely solvent resistant, excludes the use of O rings in the viscometer if contamination is to be avoided.

The O rings were replaced by compression seals, cut from annealed copper foil, .002 inch thick. These were found perfectly satisfactory for rising and steady pressures over the full range of pressure , but leaks occurred during rapid pressure falls. The probable cause of these leaks is illustrated in Fig.10. The mass of fluid, in relation to the mass of surrounding metal, is large in region A, compared with region B. A sudden pressure fall would therefore reduce the temperature of the metal at A by a greater amount than at B. The resulting differential contraction unloads the seal at A, causing a temporary leak. Gradual reduction of the pressure, taking about 3 hours for 10,000kg/cm^2, allows the satisfactory use of this seal. A system specifically designed for compression seals, with heavier threads, and with seal and threads closer together, would permit faster pressure reductions.

The assembled stainless steel viscometer, with the plug unit removed, together with a stainless steel sinker and an aluminium alloy sinker, is shown in Plate 1.

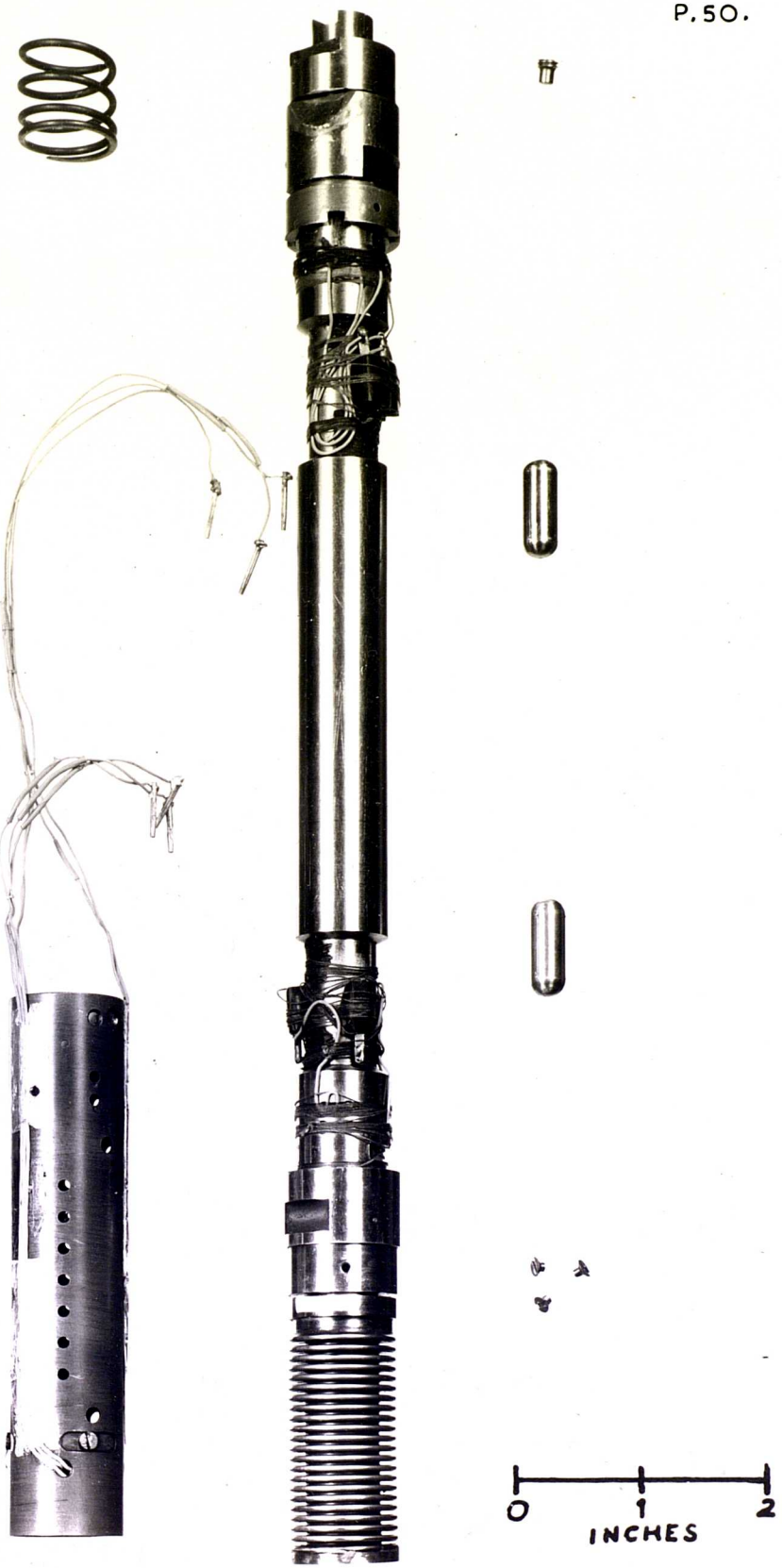

PLATE 1. VISCOMETER

CHAPTER 4.

THEORIES OF THE VISCOMETER.

The ideal falling body viscometer would consist of a perfectly round and parallel vertical tube, and a perfectly round and parallel sinker, with no guiding pins. The shape of the ends of the sinker would be immaterial, provided the sinker was perfectly symmetrical. The sinker would fall at its terminal velocity exactly on the axis of the tube, and flow conditions would be laminar throughout.

Under these conditions, the buoyancy corrected weight of the sinker would be balanced by:-

(a) A pressure difference across the ends of the sinker, associated with the flow of fluid through the annulus.

(b) A shear stress on the cylindrical portion of the sinker, resulting from the flow of fluid through the annulus and the relative motion of sinker and tube.

(c) A shear and pressure force at each end of the sinker, resulting from the flow of fluid into and out of the annulus.

If each of these forces could be accurately determined from the dimensions of the viscometer and the properties of the fluid, the ideal viscometer could be employed as an absolute instrument. However, even in this ideal case, it would be difficult to determine the viscometer dimensions with sufficient accuracy, and the computation of force (c) is very complex.

In practice, forces (a) and (c) are small compared with force (b).

In Appendix 2, a theory relating viscosity to the dimensions of the viscometer is derived for the ideal case, neglecting force (c). Equation 10.A2. gives:-

$$\eta = \frac{wgT^*}{2\pi lL} \cdot \frac{\left\{(r_2^2 + r_1^2)\ln.(r_2/r_1) - (r_2^2 - r_1^2)\right\}}{(3r_2^2 - r_1^2)} \qquad 1.$$

Lohrenz, Swift & Kurata [84] derived a relationship for similar conditions to those applying to equation 1. Rearrangement of their expression gives:-

$$\eta = \frac{wgT^*}{4\pi 1L} \cdot \frac{\left\{(r_2^2 + r_1^2)\ln.(r_2/r_1) - (r_2^2 - r_1^2)\right\}}{(r_2^2 + r_1^2)} \qquad 2.$$

which was restated in a later paper by Lohrenz & Kurata [85], on rearrangement as:-

$$\eta = \frac{wgT^*}{2\pi 1L} \cdot \frac{\left\{(r_2^2 + r_1^2)\ln.(r_2/r_1) - (r_2^2 - r_1^2)\right\}}{(r_2^2 + r_1^2)} \qquad 3.$$

The difference between 3 and 1 is accounted for by Lohrenz et al's incorrect expression for flow rate past the sinker, i.e.

$Q = \pi r_1^2 v$,

which should be $Q = \pi r_2^2 v$ from Appendix 2, equation 9.A2.

However, as (r_2/r_1) tends to 1, the difference between the two expressions becomes small.

Equation 1 may be rewritten as:-

$\eta = \frac{wgT^*}{1L}.k'$, where k' is the theoretical ideal viscometer constant. 4.

In a real viscometer, employing guiding pins on the sinker, the relationship,

$$\eta = \frac{wgT^*}{1L}.k \qquad 5.$$

may be applied, where k is the experimentally determined viscometer constant. Lohrenz, Swift & Kurata [84] found by careful measurement of viscometer dimensions that k is 5 to 20% less than k', depending on the radius ratio and length of the sinker. The difference between k and k' is accounted for by force (c) and by the additional viscous drag caused by the guiding pins, which are located in the region of high velocity fluid flow in the annulus. It was also found [84], that

k is not always independent of the time of fall of the sinker. Fig. 11 represents a typical variation of k/k' with Reynold's number, N_{Re}, N_{Re} being defined by Lohrenz, Swift & Kurata as:-

$$N_{Re} = \frac{2v\rho r_1}{\eta} .D \qquad 6.$$

$$\text{where} \quad D = \sqrt{2\left\{\ln.(r_2/r_2 - \frac{(r_2^2 - r_1^2)}{(r_2^2 + r_1^2)}\right\}} \qquad 6A.$$

Lohrenz, Swift & Kurata found that up to $N_{Re} = .2$, k/k' was a constant, corresponding to laminar flow conditions around the sinker. At Reynold's numbers greater than this, k/k' decreases, because of energy losses through turbulence at the entry to the annulus and/or at the annulus exit. Turbulence may occur also around the guiding pins. Lohrenz & Kurata [85] found that flow in an uninterrupted annulus remains laminar at least up to $N_{Re} = 10$. They also determined a friction factor f_{ee}, corresponding to force (c), as a function of N_{Re}, and their correlation is reproduced in Fig. 12. The friction factor f_{ee}, is for use in the relationship, [85]:-

$$f = f_c + \frac{2f_{ee}r_1}{1} .D + (\text{a factor due to viscous drag on the guiding pins}). \qquad 7.$$

f_c is a factor for viscous drag on the cylindrical portion of the sinker, and f is an overall friction factor. Lohrenz & Kurata found that f_c could be correlated with N_{Re} as:-

$$f_c = 16/N_{Re} \qquad 8.$$

Equation 7, together with Fig. 12 is useful in determining the approximate proportion of the total drag on the sinker which is due to force (c). However, Fig. 12 was compiled from experiments on square

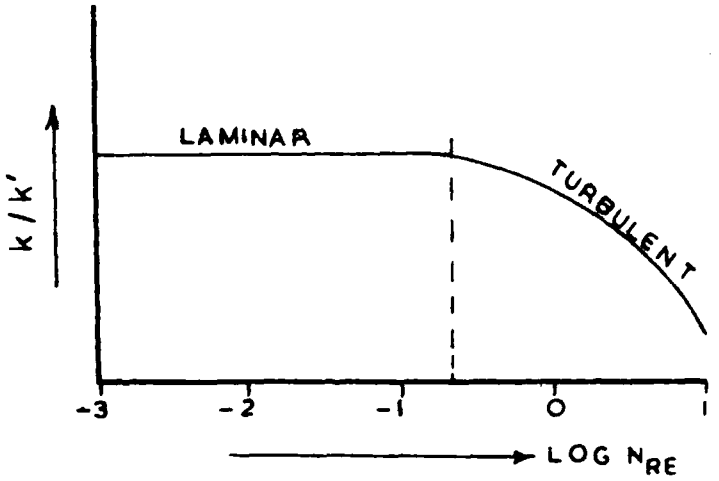

FIG. 11, NON-LINEARITY OF FALLING BODY VISCOMETER

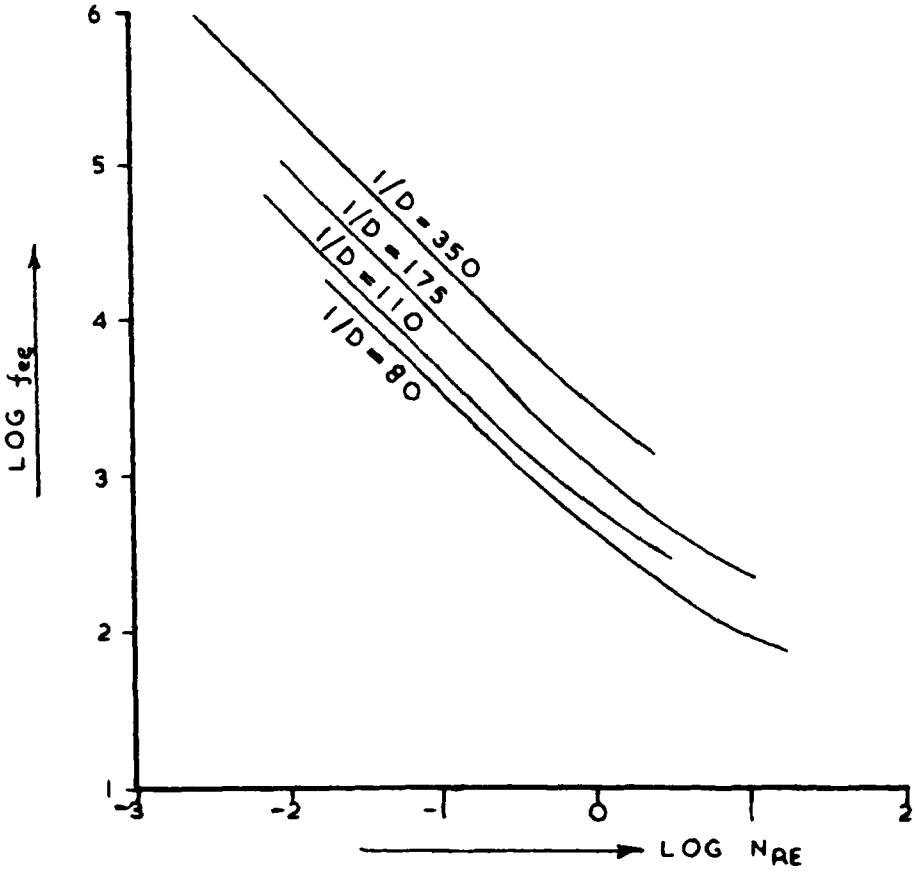

FIG. 12. DEPENDENCE OF ANNULUS ENTRANCE & EXIT DRAG ON N_{RE}.

ended sinkers, and therefore applies precisely only to sinkers of that geometry. Lohrenz & Kurata's experiments do not enable the viscous drag due to guiding pins in the annular section to be determined.

The factor k, in equation 5, must be determined experimentally, since, even if it were possible to measure the dimensions of the viscometer accurately, it would still be necessary to calibrate, owing to the uncertainties in the relative magnitude of force (c), the viscous drag on the guiding pins, and the viscous drag on the cylindrical section of the sinker.

However, a theoretical analysis of k is important from the point of view of predicting the effects of a change of temperature and pressure on the value of k. Employing a steel tube and a magnesium sinker, Lohrenz & Kurata [85] found that equation 3, together with the known properties of the tube and sinker materials, could be used to predict the temperature coefficient of k to 5%, for actual changes of k up to 60%. In experiments where changes in k are much less, equation 3, or similar relationships, could, therefore, be safely applied to predict the temperature coefficient of k with considerable accuracy.

As the calculation of the temperature coefficient of k involves only a consideration of dimensional changes caused by temperature, it follows that the pressure coefficient of k may be computed in a similar manner.

It has been assumed, so far, that the sinker always falls concentrically. Even a sinker fitted with guiding pins is able to take up a degree of eccentricity, which depends on the clearance between the pins and the tube, and it is desirable to be able to predict what effect the possible eccentricity could have on the terminal velocity of the sinker. Equation 24.A2., Appendix 2, allows an approximate calculation of the terminal velocity under eccentric conditions, and the use of this relationship is described in the appendix. The expression for eccentric fall is:-

$$v = \frac{wg}{6\pi l\eta} \cdot \frac{\sum_n \left(\frac{c_1^3}{\sum_n (r_1^2 + r_2 c_1)} \right)}{\left\{ r_2 + \frac{1}{3n} \cdot \sum_n \left(\frac{3r_1^2 c_1 + 4r_2 c_1^2}{r_1^2 + r_2 c_1} \right) + \frac{r_2}{3n} \cdot \sum_n \left(\frac{c_1^3 \cdot \sum_n (1/c_1)}{\sum_n (r_1^2 + r_2 c_1)} \right) - \frac{r_2}{3n} \cdot \sum_n \left(\frac{c_1^2}{r_1^2 + r_2 c_1} \right) \right\}} \qquad 9.$$

From 9 is derived an expression for terminal velocity of a concentric sinker, where the flow in the annular gap between the tube and sinker is assumed to be the same as that through a gap between parallel surfaces. i.e.

$$v = \frac{wg}{2\pi l\eta} \cdot \frac{c^3}{(3r_1^2 r_2 + 3cr_2^2 + 3cr_1^2 + 4c^2 r_2)} \qquad 10.$$

Equation 10 is similar to that derived by Lawaczeck [78], which rearranges to:-

$$v = \frac{wg}{2\pi l\eta} \cdot \frac{c^3}{(3r_1^3 + 6r_1^2 c + 4c^2 r_1)} \qquad 11.$$

Lawaczeck also applied the parallel surfaces approach, but did a stepwise calculation, firstly on simple flow between stationary parallel surfaces, and then on relative movement of parallel surfaces with no fluid flow.

A similar expression was also presented in the A.S.M.E. Pressure-Viscosity Report [5] as:-

$$v = \frac{wg}{6\pi l\eta} \cdot (r_2/r_1)^2 \cdot (c/r_2)^3 \cdot \{1 - \tfrac{1}{2} \cdot (c/r_2) - 13/20 \cdot (c/r_2)^2 - 13/40 \cdot (c/r_2)^3 + \ldots\} \qquad 12.$$

but the derivation was not indicated.

In a comprehensive theoretical and practical study of the falling body viscometer by Scott [125], the relationship,

$$\eta = A(\rho_s - \rho_f)T^* - Bf'\rho_f/T^* \qquad 13.$$

was derived for square ended cylinders without guiding pins. The derivation assumes that all of the kinetic energy contained in the fluid stream leaving the annulus is lost in turbulence, and an allowance is made for the finite length of sinker over which annular flow develops. The constant A is given by:-

$$A = \frac{c^3 g}{6Lr_1 F}$$

where $F = (1 + 3c/2r_1 + 7c^2/5r_1^2 + 4c^3/5r_1^3 + ...)$, and the first term is therefore similar to equation 10. The second term gives the correction for kinetic energy losses, and the factor f' is a small correction, close to unity, for the effects of the development of fluid flow. The values of B and f' are dependent on the dimensions of the viscometer, and are given by:-

$$B = \frac{9Lcr_1}{280Fl}\ (1 - c/3r_1 + 353/540c^2/r_1^2 + \ldots)$$

and $f' = 1.056(1 - .11c/r_1 + \ldots)$.

Equation 13, which is similar to that applying to a capillary viscometer, was tested by a set of falling body viscometers of carefully determined dimensions, and the experimental results were found to agree with equation 13 to within 2%. The kinetic energy correction term in equation 13 is not as sensitive as the first term to small dimensional changes, and as the second term is small, its inclusion in corrections to fall times for temperature or pressure changes would be insignificant.

Terminal velocities for the eccentric condition may be

calculated from equation 9, and compared with terminal velocities for the concentric condition calculated from equation 10, to determine the order of the effect of a given eccentricity. Provided there is no contact between the tube wall and any guiding pins, the forces which maintain the sinker concentric with the tube are provided partly by the radial pressure effects of fluid entering and leaving the annulus. Sinker end shapes which are radiused or conical, make the best use of this pressure effect, though Scott found that such end shapes produce little noticeable effect on the general behaviour of the sinker. However, only included cone angles of 90° were considered. Self centering is also provided by flow along the length of the sinker. If the sinker becomes eccentric, a couple is produced by asymmetrical shear drag on the sinker, which tilts it. The fluid flow past a tilted sinker produces pressures which form a couple opposite that tending to tilt the sinker, and the net result is that the sinker tends to fall centrally. The self centring nature of sinkers depends on the velocity, and eccentricity is therefore most likely to occur during the longest times of fall. It is impossible to produce a sinker which is perfectly symmetrical, and departures from symmetry are probably the largest contributing factors to eccentric fall of the sinker. Eccentricity may be caused, too, by a non-vertical viscometer tube. A high sinker velocity may also result in eccentricity and snaking of the sinker, due to a high degree of turbulence in the fluid. Scott observed that at high sinker velocities, an unguided sinker would oscillate about an axis perpendicular to the axis of fall, accompanied by lateral oscillations also. At even higher velocities, the oscillations became so severe that the sinker collided with the tube as it veered from side to side. The dissipation of energy by this means increases the fall time.

A numerical comparison of some of the relationships considered may be made by inserting experimental conditions. For this purpose, the following example is selected:-

	Fluid	Water
η	Viscosity ($25^{\circ}C$)	.0087poise.
T^*	Time of fall of sinker	40.3 seconds.
L	Distance of fall	17.8cms.
w	Buoyancy corrected weight of sinker	3.61g.
l	Length of sinker	1.5cms.
r_1	Radius of sinker	.3738cm.
r_2	Radius of tube	.3840cm.
c	Radial clearance	.0102cm.

The figures for r_1 and r_2 are not sufficiently precise for a proper comparison of k and k', but consistent use of the data will afford a comparison between the proposed relationships.

(a). Comparison of Equations 1 and 10.

Insertion of the above conditions in equation 1 gives:-

$$\eta = .0052481,$$

and in equation 10, $\eta = .0052687$

The approximation of the annulus to parallel surfaces is therefore very close to the more rigorous analysis leading to equation 1, for radius ratios of the order of this example. ($r_2/r_1 = 1.0273$).

(b). Comparison of temperature and pressure coefficients of k, from equations 1 and 10.

When the sinker and tube are of the same material, r_1, r_2

and c all change by the same ratio for a given change in temperature and pressure.

From equations 1 and 5, k will vary as the ratio:-

$$\frac{1}{lL} \cdot \frac{\left\{(r_2^2 + r_1^2)\ln.(r_2/r_1) - (r_2^2 - r_1^2)\right\}}{(3r_2^2 - r_1^2)}$$

When (r_2/r_1) is constant, the term:-

$$\frac{\left\{(r_2^2 + r_1^2)\ln.(r_2/r_1) - (r_2^2 - r_1^2)\right\}}{(3r_2^2 - r_1^2)}$$

is constant. Then,

$$k \propto \frac{1}{lL} \propto \frac{1}{(1 + \delta l)(L + \delta L)}$$

When is very small,

$$k \propto \frac{1}{lL(1 + 2\delta)} \qquad 14.$$

Similarly, from equations 10 and 5,

$$k \propto \frac{1}{lL(1 + 2\delta)} \qquad 14.$$

Thus, for a sinker-tube assembly of a common material, only corrections for changes in length of the tube and of the sinker need to be made for changes in temperature and pressure.

When tube and sinker are of dissimilar materials, a numerical comparison must be made to check how closely equation 10 will predict a change in k to that predicted by the more rigorous relationship 1. Only the terms

$$\frac{\left\{(r_2^2 + r_1^2)\ln.(r_2/r_1) - (r_2^2 - r_1^2)\right\}}{(3r_2^2 - r_1^2)}$$

from equation 1, and

$$\frac{c^3}{(3r_1^2r_2 + 3cr_2^2 + 3cr_1^2 + 4c^2r_2)}$$

from equation 10, need be considered. In the example taken in (a),

$$\frac{\left\{(r_2^2 + r_1^2)\ln.(r_2/r_1) - (r_2^2 - r_1^2)\right\}}{(3r_2^2 - r_1^2)} = .000,006,169,136 \quad 1_1$$

and $$\frac{c^3}{(3r_1^2r_2 + 3cr_2^2 + 3cr_1^2 + 4c^2r_2)} = .000,006,193,218 \quad 10_1$$

As an example, decrease r_1 by .2%, keeping r_2 constant. Then r_2 = .3840cm., r_1 = .3731cm., and c = .0109cm. Under these conditions,

$$\frac{\left\{(r_2^2 + r_1^2)\ln.(r_2/r_1) - (r_2^2 - r_1^2)\right\}}{(3r_2^2 - r_1^2)} = .000,007,522,311 \quad 1_2$$

and $$\frac{c^3}{(3r_1^2r_2 + 3cr_1^2 + 3cr_2^2 + 4c^2r_2)} = .000,007,548,460 \quad 10_2$$

$$\frac{1_2}{1_1} = 1.219,346 \quad \text{and} \quad \frac{10_2}{10_1} = 1.218,826$$

Equation 10, therefore, predicts a 22% change in k to within $\frac{1}{4}$% of that predicted by equation 1. As the error in equation 3, similar to equation 1, in predicting large changes in k, is up to 5% [85], there is no advantage in employing the rigorous equation 1, and the simpler expression, equation 10, is adequate for the purpose of calculating temperature and pressure coefficients of k.

(c). Comparison of concentric and eccentric terminal velocities, from equations 9 and 10.

Inserting η = .0052,687, from (a), in equation 10, the terminal velocity for concentric fall is 17.8/40.3 cm/sec. i.e. .441,687 cm/sec.

Inserting these same conditions in equation 9, and putting n = 12, the corresponding terminal velocity is:-

.466,221 cm/sec., when d = .0009cm.,
and .528,630 cm/sec., when d = .0018cm.

i.e. when axis of sinker is displaced .0018cm., (17.6% of c), terminal velocity increases by 5%,
and, when sinker axis is displaced by .0036cm., (35.2% of c), terminal velocity increases by 19.7%.

Over the range of displacement covered by the calculations, the percentage velocity increase follows an approximate square law, as shown in Fig.13. From Fig.13, for this particular sinker, a 1% increase in terminal velocity would be caused by a displacement of the sinker axis of .0008cm., and a .1% change would be produced by a .00024cm. displacement.

In equation 9, the r_2 term is much larger than the other terms in the denominator at moderate eccentricities. However, $\sum_n c_1^3$ rises considerably with increasing eccentricity, causing an increased terminal velocity, as shown in Fig. 13. If an unguided sinker were able to approach maximum eccentricity, the term $\sum_n (1/c_1)$ in the denominator tends to infinity, and reduces the terminal velocity. The effects of the full range of eccentricity are illustrated qualitatively in Fig. 14.

(d). Application of equation 7.

From equations 7 and 8, the relative magnitudes of the

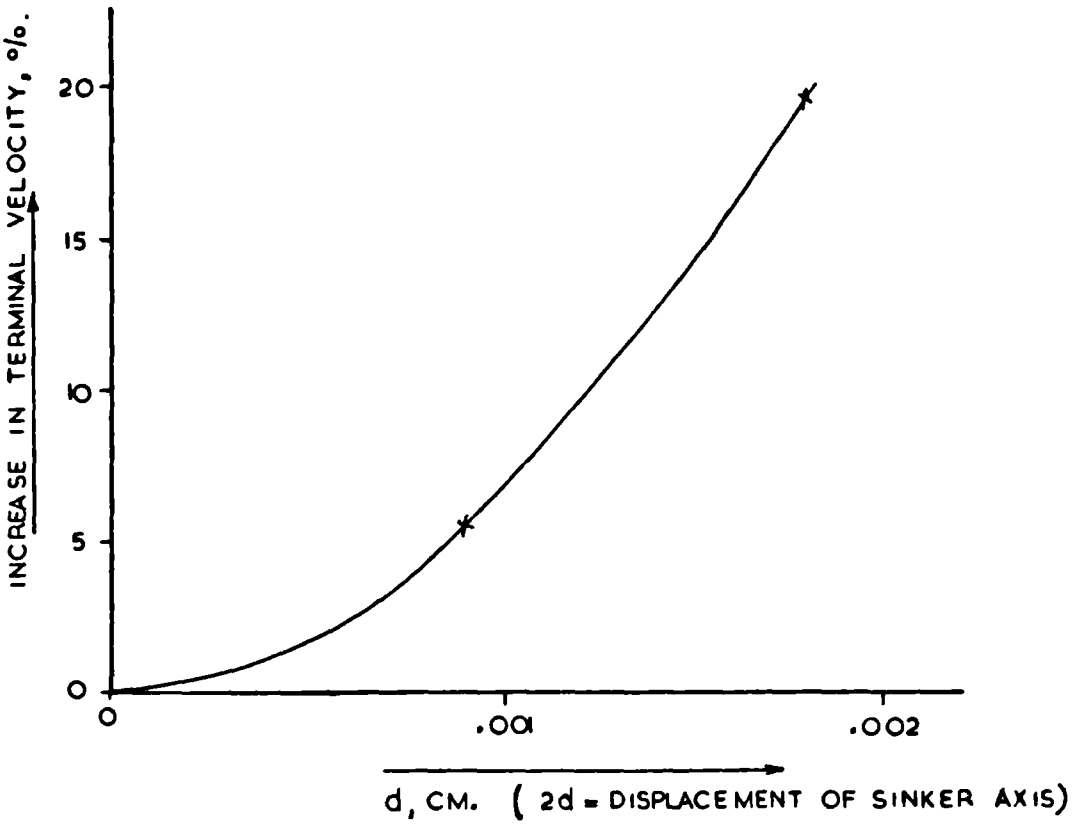

FIG. 13, EFFECT OF ECCENTRICITY ON TERMINAL VELOCITY.

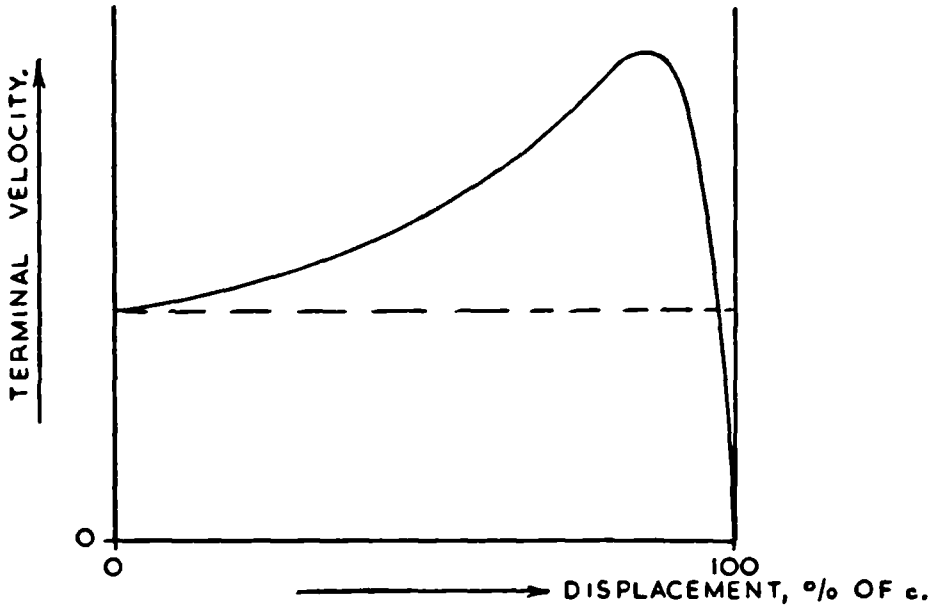

FIG. 14. EFFECT OF ECCENTRICITY ON TERMINAL VELOCITY.

viscous drag on the cylindrical part of the sinker, and on the ends of the sinker, are:-

$16/N_{Re}$ for the cylindrical section,

and $\frac{2f_{ee}r_1}{l}.D$ for the ends.

Taking the same sinker example as used in (a), (b) and (c),

$D = .003,606$ (from equation 6A), $1/D = 280$,

$N_{Re} = .23$ (from equation 6), and $16/N_{Re} = 69.5$

Then from Fig. 12, $f_{ee} = 4 \times 10^3$

$$\therefore \quad \frac{2f_{ee}r_1}{l}.D = 7.2$$

Thus, the viscous drag on the cylindrical section of the sinker is 69.5/7.2, or 9.7 times greater than the drag on the ends of the sinker. The neglect of the drag on the ends of the sinker is reasonable, therefore, in calculating temperature and pressure coefficients of k for small changes in k.

CHAPTER 5.

DESIGN AND DEVELOPMENT OF PRESSURE SYSTEM.

(i) General Requirements of System.

The high pressure system must include a pressure vessel, for which the basic requirements have already been outlined. These requirements are:-

1. The vessel must be capable of holding 10,000kg/cm^2 pressure for long periods, at temperatures up to 100°C.
2. Closures must be provided each end, one of which carries six electrical connections.
3. The vessel must be capable of rotation about an axis at 90° to the bore, and of being locked either end up in a vertical position.
4. To accommodate the viscometer, the bore dimensions must be 1 inch diameter x 15 inches long.

The rest of the pressure system must consist of a means of raising and holding the vessel pressure, a means of reducing the pressure, and a means of measuring pressure. These facilities may be arranged in three ways as follows:-

(1) By providing a rotatable vessel, connected to the rest of the system through a rotating coupling.

(2) By providing a rotating vessel, pressure gauge and valve, which may be disconnected from the pressure raising facility after the required pressure has been achieved.

(3) By arranging for the whole high pressure system to rotate.

It was decided to adopt method (3) and the layout of the high pressure system is illustrated in Drawing 1. There are three basic units; an intensifier, for generating the pressure, the valve and pressure gauge block, and the vessel itself. The whole

system is carried on five $2\frac{1}{2}$ inch bore, double row, self aligning ball bearings, at A, B, C, D, and E. As brittle construction materials must be avoided in the high pressure system, suitable steels have a yield stress which is below 10,000kg/cm^2, and a method of construction which maintains elastic conditions substantially above 10,000kg/cm^2 must be employed. All the available methods are based on cylinders which have the bore in compression and the outside in tension at atmospheric pressure, which is achieved with concentric cylinders with interference fits, wire or tape winding, or autofrettage, which is simply raising the pressure in the cylinder until its bore is overstrained.

The latter method is used throughout, because it is simpler, and gives a more favourable stress pattern at the various cross bores and discontinuities.

The large volume of the pressure vessel would require an extremely large single stroke intensifier to produce the required pressure, and in order to minimise the rotating mass, a multistroke intensifier, with suction and delivery valves, was built.

A manganin coil resistance pressure gauge is employed for measuring the high pressure. This is convenient in that adequate accuracy is available, and it is easily applied to a rotating system. The coil, not shown in Drawing 1, is situated in the cavity (32), in the valve and gauge block.

The sole function of the hand valve is to hold or reduce the pressure in the system, as required. Almost all of the seals in the system are O rings; they being selected for the sake of simplicity in the design. Wherever possible in the design of the high pressure system, discontinuities have been provided with the largest convenient radius to reduce stress raising tendencies.

All of the large diameter threads in the pressure system are of Whitworth form, and are either 6, 8, or 10 threads per inch.

The threads taking high loads are truncated, and are hand chased to provide a slight taper and a sloppy fit. These measures have been applied to reduce the risk of seizure in the event of scuffing. A design shear stress of $3\frac{1}{2}$ tons/in^2 on the superficial area was employed on all the threads.

All numbers in the following descriptions refer to Drawing 1.

(ii) Intensifier.

(a) Low pressure cylinder.

The low pressure cylinder, (1), together with the piston, (3), provide the force for driving the high pressure piston, (4), into its cylinder, (2). Cylinders (1) and (2) are coupled together by a screw thread, and their axes are accurately aligned by spigot (5), and faces (6).

The bore of the cylinder is 1.75 inches, and has a ground finish. Oil pressure up to 10,000 p.s.i. may be supplied to the low pressure cylinder through a Blackhawk flexible hose, (7), which is connected by a Blackhawk hand coupling, (8), sealed into the cylinder by O ring (a). The 1.68 radius ratio of the low pressure cylinder is derived in Appendix 3.

At its blind end, the cylinder is undercut with a smooth radius, allowing the piston to 'bottom' freely, and the blind face is countersunk to prevent the piston plugging the fluid entry hole.

The cylinder is carried in bearing A, and adjacent to the bearing is a pair of spanner flats. A separate supply of fluid is employed for filling, or priming the high pressure cylinder, and this enters the system through a steel tube, (9), at pressures up to 40,000 p.s.i. This tube terminates in a head, secured by screwing and soldering, and is sealed by O ring (b) against plug (10). This in turn is sealed into the low pressure cylinder by

O ring (c). The system is arranged so that when the cylinder is stationary, the tube, (9), is sealed and locked in place by pressure, so that fluid at 40,000 p.s.i. may be transferred from tube (9) to tube (11). When the pressure is released, the cylinder is free to rotate about the stationary tube (9). The coupling enables priming fluid to be supplied to the intensifier when stationary, and the cylinder may be rotated without the inconvenience of uncoupling the priming line, when the pressure is released.

The low pressure cylinder is manufactured from Hadfields Hecla 306 3% chrome molybdenum steel, normalised and tempered to 50 tons/in^2. The tubing, (9) and (11), is $\frac{1}{4}$ x 1/16 inch chrome molybdenum 100,000 p.s.i. material, and other components are in annealed EN26 steel.

(b) High pressure cylinder and collar.

The high pressure cylinder, (2), is machined from a specially forged and inspected bar of Hadfield's Hecla 138H 2$\frac{1}{2}$% nickel chrome molybdenum steel, heat treated to 80 tons/in^2 maximum stress. This gives a hardness of 370 B.H.N., and an elongation of 16%. The radius ratio of 7.6 for the high pressure cylinder is derived in Appendix 3, and permits an autofrettage pressure of 19,500kg/cm^2, and a working pressure of 12,000kg/cm^2. The cylinder bore is true with the coupling arrangements between the two cylinders, and, except for the small taper at (12), is of uniform diameter from end to end. The delivery end of the cylinder is fitted with a pair of valves, (13) and (14), in tandem, and one of the valves, (13), together with the O ring (d), provides the closure for the cylinder. The delivery valve bodies are secured by the screwed spigot, (15), on the valve and gauge block. The high pressure cylinder is carried on bearing, B, and spanner flats are machined alongside. A pair of diametrically opposed spy holes, for observing the position and con-

dition of the pistons, are shown at (16).

Two high pressure inlet valves, (17 and 18), are housed in the collar, (19). The collar, machined from a forging of Hecla 138H steel, is forced onto the cylinder, (2), on a .004 inch per inch taper, as far as the location at (20). At this position, the interference is .003 inch, resulting in a radial stress of 4 tons/in^2 between the cylinder and the collar. Valve body (17) is sealed against the high pressure cylinder by O ring (g), and fluid enters the high pressure cylinder through a 1/16 inch diameter cross bore.

Diametrically opposite the inlet valves, an identical housing is machined in the collar and cylinder, so that an additional set of valves may be fitted, to provide an alternative source of high pressure fluid. However, in the form shown, this facility is sealed with an EN26 blanking plug, and O ring (i).

After assembly of the collar on the high pressure cylinder, the faces (22) were lapped square with the collar threads, and face (23) was ground square with the thread at the delivery end of the unit at the machining stage. Face (24) is square with the cylinder bore, and provides a positive stop for the low pressure piston, (3).

The high pressure cylinder was first bored and honed to .360 inch diameter, and a short piston for autofrettaging made to suit. After application of the autofrettaging pressure of 19,500kg/cm^2, described later, the bore was honed out to .375 inch to produce a uniform diameter. The bore variations are within .0002 inch and the surface finish 5 microinches.

(c) Pistons.

The low pressure piston, (3), is manufactured from Hecla 108 1% carbon chrome steel, hardened to 600 D.P.H. Its running clearance in its cylinder is .001 inch. It is fitted with a moving Bridgman type seal, consisting of a Hecla 152 head, (25), and a

neoprene seal,(26).

The high pressure piston bears directly on the low pressure piston, a.002 inch thick disc of hard copper foil being placed between the two, and the counterbore in which the high pressure piston sits has a very large radius remote from the region of high stress concentration, to prevent the type of failure which is common with thrust blocks in this region of stress.

The high pressure piston is a simple cylinder, ground and honed from a bar of Hecla 108 1% carbon chrome steel, hardened to 600/650 D.P.H. Surface finish is 10 microinches, and the clearance at atmospheric pressure is .0013 inch, but this is reduced to about .0008 inch at 10,000kg/cm^2 by the compressive stress in the piston increasing its diameter. The piston is sealed by a pair of O rings on a moving carrier, (27), described in Chapter 6. The two pistons are aligned by pumping to the top of their stroke with little load between the two. This allows both pistons to lie naturally in their cylinders. The relative position of the two pistons is then maintained on subsequent strokes by the load which always exists between them, due to friction in the seals. The pistons are aligned approximately by the brass ring, (28).

(d) Valves.

The intensifier valves, which work on the principle of a hard steel ball plugging a hole by virtue of the pressure difference across the ball, have operated satisfactorily at pressures up to 13,000kg/cm^2 without failure. The valve bodies are machined from EN26 steel, in the annealed condition, and standard high carbon steel balls are employed. A $\frac{1}{8}$ inch diameter ball is used to plug a 1/16 inch diameter hole. Before use, a freshly cut square edged seat has a new ball impressed on it to provide an initial seal, the ball

afterwards being discarded. A second ball is used for the first application of full pressure difference across the valve, and this condition deforms the seat permanently, producing a spherical band (about 1/64 inch wide), on which the ball sits. The second ball is discarded, and a third ball is employed in the valve for working conditions.

As the ball must be properly presented to its seat under all conditions of rotation of the intensifier, a brass guide, (29), loaded by a spring, (29a), is provided for each ball. The valve bodies are sealed by O rings (d), (e), (f), (g), and (h). In each of these five seals, the O ring is trapped between two components, which, ideally, should properly mate together on a full circle adjacent to the O ring, to minimise extrusion under pressure. If any component were slightly out of true, the required condition would not be produced. To allow for the inevitable imperfections in these valve components, where there are two nominally flat surfaces together, one face is machined flat, and the other is machined with a $\frac{1}{4}^{\circ}$ 'convex' taper. By this means, all the valve components were made to mate properly, adjacent to the seal rather than remote from it.

O ring (d) forms a piston type seal of $\frac{3}{8}$ inch diameter. If the seal at this position had been made a gasket type, the seal diameter would be $\frac{1}{2}$ inch, almost doubling the end load, and also requiring a step in the bore in an inaccessible area. Assembly of O ring (d) is aided by component (30). This brass sleeve is first inserted in the bore and supported, in the position shown, by the piston, so that the O ring may be placed in position, and supported by the brass sleeve. The valve body, (13), is then pushed home. The O ring slides up the taper on the valve body, and the brass sleeve is thereafter held in place behind the O ring by friction.

Each valve body has two small threaded holes near its outer diameter for extraction purposes.

(iii) Valve and Gauge Block.

(a) Block and gauge chamber.

The valve and pressure gauge block is machined from a forging of Hecla 138H steel in the annealed condition.

Pressurised fluid from the intensifier enters at the spigot, (15), and passes right through the block along a $\frac{1}{8}$ inch diameter gallery to the pressure pipe, (31). The gallery also directs fluid via cross drillings, to the pressure gauge chamber, (32), and to the let down valve opposite. Bearing C supports one end of the block, and the whole system on bearings A, B, and C rotates as a rigid unit.

A hole, .010 inch diameter, $\frac{3}{8}$ inch long, produced by spark erosion, connects the main gallery with the pressure gauge chamber, which is 1 inch long by $\frac{3}{4}$ inch diameter. The small size of the connecting hole serves as a throttle to protect the delicate pressure gauge from rapid decompression elsewhere in the system. An O ring, (j), and the electrical connections closure, (33), seals the gauge chamber.

The let down valve is screwed into the block as a self contained unit, and is sealed by O ring (k). A 1/16 inch diameter hole connects the valve to the main gallery, and the O ring seat at (k), is countersunk for the connection of 100,000 p.s.i. $\frac{1}{4}$ inch O.D. tubing.

Spanner flats are provided adjacent to the let down valve and the pressure gauge plug.

(b) Pressure gauge closure.

As well as sealing the gauge chamber, closure (33) must provide four electrical connections into the chamber for the manganin coil. One of these may be 'ground', leaving only three connections to be insulated, and for each of these, a ceramic cone, (35), is employed. Three such cones surround a central spigot on which the manganin coil is mounted. The cones are 14° included angle, and are about 3/16 inch long and 3/16 inch at their largest diameter. A solid invar cone, set inside the ceramic cone, completes the seal, and connecting leads are soft soldered to each end of the invar. The invar, ceramic, and closure (33) are all lapped together with diamond dust, so that they take up the relative positions shown. After the lapping operation, the outer corner of the narrow end of the ceramic cone is ground away. Application of pressure forces ceramic and invar cones down the pressure gradient, and the precautions taken prevent either component from fouling any ridges arising from the lapping, which would otherwise crack the ceramic.

Initial pressurisation of the electrical seals was aided by the use of a heavy grease to give the inital seal. After one application of full pressure, the pressure ends of the seals were filled with 'Araldite' as an additional precaution against leakage.

Component (33) was machined from EN26 steel, and hardened to 90 tons/inch^2 before the lapping operation. The closure is designed so that the ceramic cones are surrounded by a large radius ratio of metal, to withstand the high stresses associated with this type of seal. The conical holes in the metal terminate in 1/16 inch diameter holes, and each is inclined so that it connects with a central collecting well, $\frac{1}{4}$ inch in diameter. This method allows the use of a heavy plug behind the closure, and the

plug supports the pressure load on the closure over most of its area. A $\frac{1}{4}^{o}$ taper on the face of closure (33) adjacent to the O ring seal, provides for proper mating of the extrusion gap.

A copper-constantan thermocouple is inserted in one of the 1/16 inch diameter holes in closure (33), immediately behind a ceramic seal. The thermocouple leads, the three insulated connecting leads, and a lead to ground, are all gathered at the collecting well, and are channelled up a $\frac{1}{4}$ inch diameter tube, (37), and terminate in a 'Plessy' six pin socket, (38).

The pressure plug, (34), is made from EN26 steel in the annealed condition, and care was taken to produce the loaded face square with the thread.

(c) Let down valve.

A replaceable seat, (39), is provided for the valve, and is made from annealed EN26 steel. It is sealed by an O ring, (k), and is held in place by the valve body, (40). O ring (l) prevents fluid from the low pressure side of the valve escaping into the thread region, so that appearance of fluid from the thread then indicated a leakage from seal (k) only. A valve bonnet, (41), carries a 26-threads per inch spindle, (42), EN26 steel being the material of construction for (40), (41), and (42). The valve spindle, (43), is controlled by a piston, (44), which is constrained from all rotational motion by socket set screws, (45). A steel ball, (46), transmits thrust from the piston to the valve spindle, and the spindle is free to move within a cone of a few degrees angle, about the ball centre. This allows the tip of the spindle to guide itself without constraint into its seat. The collar, (47), extracts the spindle in the event of it sticking in its seat, and backlash in the ball thrust unit is reduced to a minimum by tightening collar (47) against shims.

Valve spindle (43) is manufactured from Hecla 174 5% chrome

molybdenum vanadium steel, hardened to 550 D.P.H. Two such spindles may be used in the valve, one with a 30° and the other a 60° included angle at the tip. The spindle sits initially on a square edged seat, but the relatively soft EN26 deforms to a work hardened conical seat on tightening the spindle. The linear motion of the spindle, relative to its seat, tends to prevent scuffing which frequently occurs with a rotating spindle when employed at high pressure.

Thrust between the rotating spindle, (42), and the non rotating piston, (44), is transmitted by a ball thrust race, (48). Spindle (42) bears against a collar, (49), for extraction purposes, the latter being screwed into the piston on a left hand thread, and its position adjusted by shimming to control backlash. Parts (44), (47), and (49), are constructed of stainless steel.

An O ring (m) prevents pressure transmitting fluid entering the lubricant of the thrust race unit. Fluid passing the valve from the pressure system escapes through a hole in the valve body, and runs to waste.

(iv) Pressure Vessel.

(a) Vessel.

The vessel was machined from an ultrasonically inspected forging of Hecla 138H steel, hardened to 80 tons/inch^2. Its 1 inch diameter x 15 inches long bore is contained in outside dimensions of $7\frac{1}{2}$ inches diameter x $22\frac{1}{2}$ inches long, employing a similar radius ratio as the high pressure cylinder. Accurate locations are provided for mounting bearing trunnions on the sides of the vessel.

The principle aims in machining the vessel, were to produce two parallel coaxial trunnion mountings exactly at 90° to the bore axis. The bore itself was first completed in the rough machined forging. It was produced firstly by drilling a $\frac{1}{2}$ inch pilot hole, followed by a core drill 1/64 inch under size. A short shell reamer was employed for finishing to size, and during this operation, a very large quantity of cutting fluid was pumped down the bore for swarf clearance,

resulting in a high standard of surface finish. A close fitting mandrel was inserted in the finished bore, and the external turning was carried out by setting the work up on the machines with the mandrel running true. By this means, the ends of the vessel were produced square with the bore to within .0002 inch per 12 inches. Trunnion location faces (50) were then ground square with the ends, and parallel with each other. The trunnion axis locations, (51), were produced coaxially by means of a jig.

Each of the bearing trunnions (52) and (53) is secured to the vessel by 8 cap screws and two studs and countersunk nuts. The latter ensure torque transmission without backlash or slippage. Bearings D and E support the vessel, and longitudinal adjustment and location of the vessel, and of the rest of the pressure system, is provided by the two screwed rings, (54). A shaft, (55), and handwheel is bolted to trunnion (53) for manual rotation of the pressure system.

Fluid from the pressure pipe, (31), enters the vessel through a 1/16 inch diameter cross drilling. The atmospheric pressure cavities formed by the closures at each end of the vessel are ventilated by cross drillings, which serve to relieve leaking pressure transmitting fluid, and to drain the cavities of thermostating fluid prior to removing a closure. Each end of the vessel is provided with a facility, (56), for attaching a means of locking the vessel in the vertical plane, and spanner flats also are provided.

(b) Electrical connections closure.

The basic construction of the electrical connections closure to the vessel is similar to that for the pressure gauge closure, but it differs in the manner in which the electrical connections enter the pressure chamber. In the vessel closure, the electrical conductors consist of mineral insulated wires, commercially known as 'Thermocoax'

wires, consisting of one or two conductors embedded in highly compressed magnesium oxide powder, contained in a stainless steel sheath. The sheathed wires utilised in this application are of 1.5 mm. outside diameter, and contain two conductors, one of them chromel, and the other alumel. Three 'Thermocoax' wires are sealed into a block of EN26 steel, (57), providing six conductors in all. This method was chosen in preference to the ceramic cone type of seal, because it requires less space, is less laborious to manufacture, and is less liable to fail when subjected to large temperature changes. Use of these wires for pressure connections was first described by Simon [128], and tested by Cornish & Ruoff[31] to 30 K.bars.

Hard soldering was employed to seal the Thermocoax wires into the closure, and great care had to be taken to ensure that the solder flowed along the whole length of the joint (1 inch) to provide mechanical strength, and right round the joint to eliminate leakage paths. The soldering operation was carried out in the following manner.

Immediately after drilling the 1/16 inch diameter holes in closure (57), the unit was cleaned chemically with trichlorethylene, and the mechanically and chemically cleaned wires assembled in the holes. A stainless steel hard soldering flux was applied, and particles of hard solder were placed in small wells made at the ends of the holes, at the high pressure side of the closure. The assembly was placed, with the wells uppermost, in an oven at 750°C, purged with nitrogen to maintain an inert atmosphere. Twenty minutes were allowed for the soldering operation, and after this time, the oven was cooled rapidly with nitrogen to 600°C, and the work then removed. Inspection showed that solder had run the length of the joint, and pressure testing proved the joints to be satisfactory.

Most of the finish machining on closure (57) was completed after soldering, and careful designing was necessary to avoid soldering flux running onto surfaces requiring a good finish, as this was found to

produce deep corrosion pits. The closure is sealed with an O ring, (n), and the fit of the spiggot in the end of the vessel bore is important, as this determines the location of the viscometer. The brass valve holder, (58), which is described in Chapter 3, screws onto closure(57). Correct alignment of these two components was achieved by assembling the finished brass component on the unfinished closure, and the work set up so that part (58) ran true. This allowed the important locating diameter on the closure to be machined truly concentric with the viscometer location on part (58). The face of the closure adjacent to the O ring seal is tapered by $\frac{1}{4}^{o}$ in the interests of proper seating against the vessel.

The principle of collecting the wires in a central tube is similar to the methods applied in the pressure gauge closure. Plug (59) is made of annealed EN26 steel.

(c) Top closure.

The top closure, sealed by O ring (p), is designed specifically so that it may be coupled and uncoupled frequently and easily. It consists of the plug, (60), a screwed ring, (61), and eleven $\frac{3}{4}$ inch diameter cap screws, (62), which transmit the compression load between (60) and (61). The cap screws also permit a considerable degree of preloading of the seal. A large expendable washer, (63), prevents the cap screws from damaging the plug. Parts (60), (61), and (63) are all manufactured from EN26 steel in the annealed condition.

Plug (60) has an unobstructed centre of large diameter, which is available for high pressure pipe connections, should the need for gas or gas/liquid solution transfer into the viscometer under pressure, arise. The spiggot engaging the vessel bore is machined concentric with the viscometer locating pin, (69). By setting the closure in the desired angular position before tightening the coupling, the viscometer is maintained in the correct plane for its working.

Some calculations, relevant to the design of the screwed ring, (61), are given in Appendix 3.

(v) Pressure Pipe.

When the pressure system is inverted for viscosity measurements, the vessel is rapidly brought to rest and locked in the vertical position. As well as transmitting pressure from the intensifier to the vessel, the pressure pipe must also transfer torque from the vessel to the rest of the pressure system. The moment of inertia of the intensifier - block unit, and typical angular retardations, leads to torque transmissions in the pipe of the order of 60 to 80 lbs.ft. The coupling between the pipe and the vessel at one end, and the block at the other end, must be capable of transmitting this torque without disturbing the pressure seals.

The pipe is manufactured from Harwood Engineering Company's 200,000 p.s.i. tubing, and is a compound tube with an inner stainless steel core of $\frac{3}{8}$ inch diameter, and an outer chrome molybdenum steel shell of $\frac{3}{4}$ inch diameter. The tube bore is 1/16 inch diameter. Each end of the tube is drilled for a short length to $\frac{1}{8}$ inch diameter, and countersunk to 90°. Seats in the vessel and block are treated similarly, and an EN26 steel olive, (64), is employed to provide the seal at each end of the pipe. Each olive is $\frac{3}{8}$ inch diameter, and has a bore of .015 inch, which acts as a throttle between the two halves of the pressure system in the event of failures.

Stainless steel flanges, (65), are splined onto each end of the pipe, the splines being cut as an interference fit, so that torque transmission may take place between flange and pipe without any backlash. The flanges transmit thrust to the pipe through collars, (66), screwed onto the ends of the pipe, and at the vessel end of the pipe, a spacer, (67), is placed between the flange and collar. Spigots, (68), on the flanges, maintain proper alignment of the pipe, and

these were machined with the pipe unit assembled and running on centres.

Coupling of the seal is provided by six 7/16 inch diameter high tensile steel studs, and countersunk nuts which transmit torque without backlash.

(vi) Auxiliary Pressure System.

The complete pressure system is illustrated in Fig. 15, the system within the dashed enclosure having already been described. The intensifier has two independent fluid supplies as follows:-

1. Low pressure supply.

Full working pressure in the vessel may be achieved with about 8,000 p.s.i. in the low pressure cylinder of the intensifier. This pressure is supplied through the flexible hose by D.T.D. 585 hydraulic fluid pumped by a 'Blackhawk' 10,000 p.s.i. hand pump. The pump is fitted with ball check valves, and a hand valve for pressure release. Pressure in this circuit is registered on a Budenberg 0-1000 atmosphere steel tube gauge. The flexible hose is a 'Blackhawk' product and the tubing and fittings which complete the circuit are American Instrument Company 100,000 p.s.i. products.

2. Priming supply.

The priming supply fills the high pressure cylinder of the intensifier, and it is this fluid which pressurises the system to 10,000kg/cm^2 or more. In view of the delicate nature of the viscometer and manganin coil pressure gauge, it is preferable for the pressure transmitting fluid to possess a low viscosity under pressure, in order to minimise damage should an instantaneous decompression occur. Such a pressure transmitting fluid has the disadvantage that it is difficult to seal, and is devoid of lubrication properties. Bridgman[19] reported the viscosity of petroleum ether up to 12,000kg/cm^2, and his results indicate an adequately low viscosity for the range of

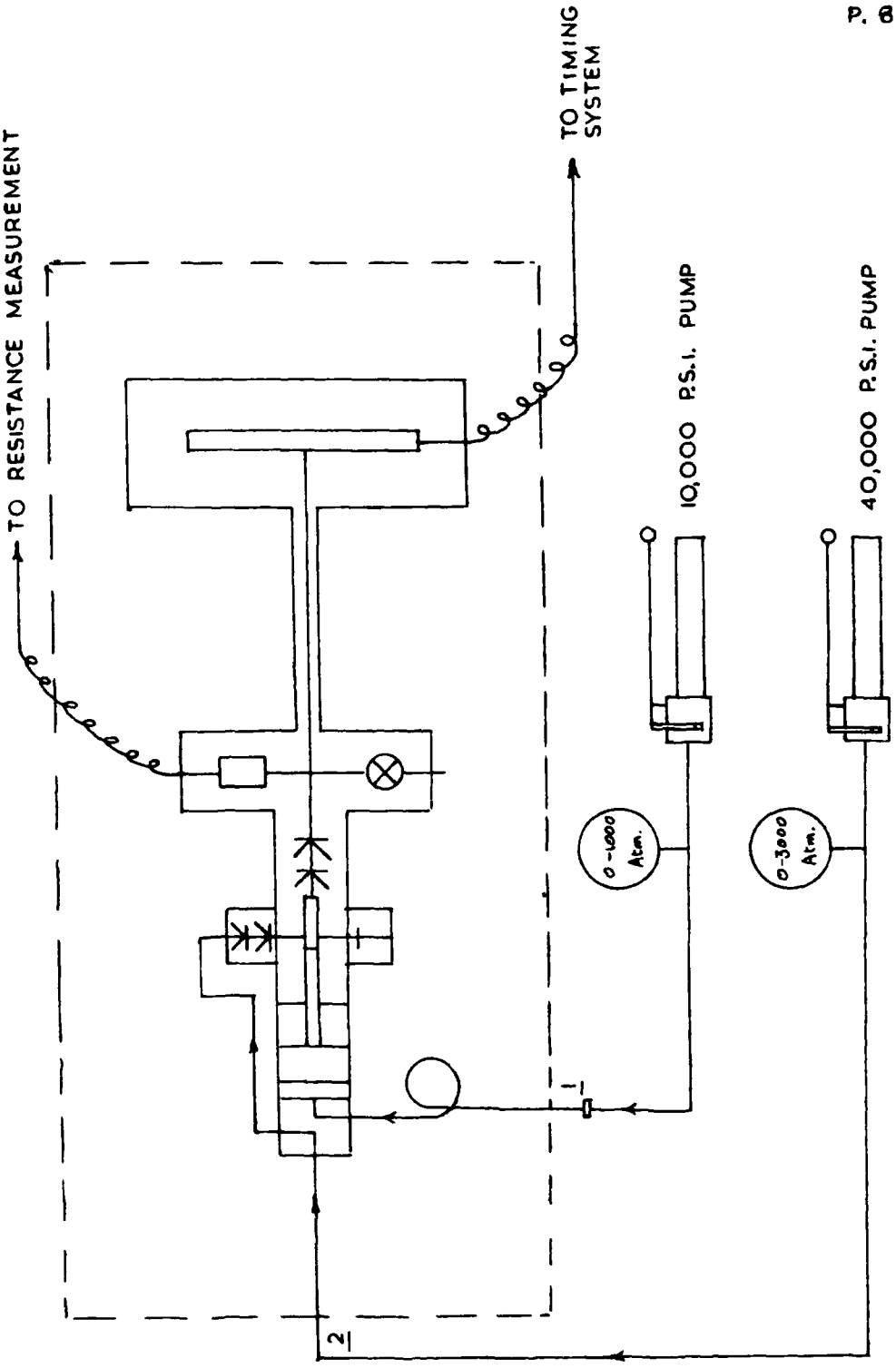

FIG. 15. COMPLETE PRESSURE SYSTEM

the present work. The boiling range of the petroleum ether studied in Bridgman's work is unknown. Petroleum ether of boiling range 100-120°C is employed as the pressure transmitting fluid in the high pressure system, and 10% of D.T.D. 585 hydraulic fluid is added to improve lubrication properties. The latter fluid was selected as it is thought to possess a low pressure - viscosity coefficient. The viscosity of the mixture is about .7 c.p. at room temperature, and some results for measurements of the pressure effects on its viscosity are given in Appendix 4.

A 40,000 p.s.i. Blackhawk hand pump is utilised for filling the high pressure cylinder with petroleum ether mixture, and standard American Instrument Company 100,000 p.s.i. tubing and fittings are employed. The pressure supplied by the hand pump is indicated on a 0-3,000 atmosphere Budenberg steel tube gauge.

(vii) Autofrettage.

The main components of the high pressure system were designed for a working pressure of 12,000kg/cm^2 and autofrettage pressure of 19,500kg/cm^2, as set out in Appendix 3. Overstraining of the various components was carried out as follows:-

1. Intensifier.

The intensifier is self autofrettaging, as the low pressure cylinder is sufficiently robust to provide the necessary thrust on the high pressure piston to produce 19,500kg/cm^2. For this purpose, the low pressure was supplied by a 40,000 p.s.i. hand pump instead of its 10,000 p.s.i. pump.

The application of 19,500 kg/cm^2 was confined to the high pressure cylinder and the 1/16 inch diameter cross-bores. The three openings to the cylinder were sealed by O rings and blanking plugs similar to part (21) in Drawing 1. A short piston was employed for improved rigidity, and a brass filler was used in the cylinder, so as to keep the piston stroke to a minimum for producing the required

pressure. In this way, a greater length of cylinder was overstrained than is normally subject to maximum working pressure.

2. The rest of the system.

As no equipment was available for autofrettaging the remainder of the high pressure system, the intensifier had to be used for this purpose. After two enlargements of the high pressure cylinder bore since overstraining (see Chapter 6), it is estimated that the cylinder would behave elastically up to 16,500kg/cm^2. To avoid any possibility of further overstrain in the cylinder, its maximum pressure has been limited to 13,000kg/cm^2. The whole of the high pressure system has been subjected to this pressure, except the following components:-

The let down valve.

The electrical connections plug (33).

The electrical connections plug (57).

Blanks were fitted in place of these during autofrettage, and they have been used up to 11,000kg/cm^2 only.

As the fit of the bore locating spigots on closures (57) and (60) is important, the machining of these components was left until after the overstraining of the vessel bore.

(viii) Operation of the High Pressure System.

(a) Assembly.

Great care is always taken during assembly to maintain a high standard of cleanliness, and freedom from blemishes on metal sealing surfaces. Any scratches or other blemishes on the important O ring housings are removed either by polishing in a lathe with polishing paper, if this is possible, or by working the surface in-situ with diamond dust paste. O rings are always inspected for dust which could cause a leak, and threads cleaned and inspected for damage. The threads are lubricated with a molybdenum disulphide grease, and

O rings coated with a light oil to reduce the risk of pinching a ring during assembly.

Most of the high pressure seals can be assembled with the main pressure units in place on their bearings. However, seals (d), (e), and (f) require the removal and separation of the intensifier and block for their assembly, as the intensifier, block and delivery valves are all assembled in one operation, and mounted as a unit in relation to the vessel and pressure pipe. The comparative inaccessibility of seals (d), (e), and (f), is of no inconvenience, as they have never failed or been replaced, and have had only one inspection.

The high pressure piston seal may be assembled or replaced without disturbing the high pressure cylinder. This is achieved by supporting the high pressure cylinder and removing the low pressure cylinder. The use of a specially bent tube connected to the inlet valves allows the piston and seal to be pumped out of the cylinder.

The low pressure piston and seal, and the 40,000 p.s.i. rotating coupling were assembled on the bench, and have never required any attention other than lubrication of the piston.

The eleven cap screws on the top closure of the vessel are always tightened in a set pattern to maintain a uniformly distributed load around the closure.

All fluids entering the hand pump reservoir are filtered to maintain the check valves free of dirt.

(b) Operation.

The most important feature of operation, apart from producing the required pressure, is to ensure that the high pressure piston and cylinder remain free of damage. The piston was inspected frequently, and every three strokes it was sprayed with a liberal quantity of penetrating oil carrying colloidal graphite. This form of lubricant was employed as it stood the best chance of

reaching the regions at the end of the piston where lubrication is most needed. At the conclusion of the work, both piston and cylinder were still highly polished and unscratched.

The method of raising the pressure in the vessel was governed mainly by the characteristics of the suction and delivery valves in the intensifier. It was found that these ball valves sealed perfectly once they had 'seated', but some difficulty was experienced occasionally in making the balls seat. The main factors contributing to this difficulty were the very low viscosity of the petroleum ether, and the fact that the valve seats had deformed to a profile suitable for withstanding 13,000kg/cm^2, and were, therefore, not ideal for seating at low pressures. Best results were produced by the suction valves, possibly because these never had to withstand high pressures for the long periods that applied to the delivery valves. The suction valves would seal perfectly once the pressure had reached about 600kg/cm^2, and would then continue to seal down to 200kg/cm^2 if left undisturbed.

2,000kg/cm^2 was usually necessary to seat the delivery valves, and only then would they seal by letting the low pressure down in the low pressure cylinder very quickly. Towards the end of the work, the minimum sealing pressure had risen to 3,000kg/cm^2, indicating that renewal of the delivery valve balls was necessary. Once the balls had seated, they would always seat without fail on subsequent strokes of the intensifier which produced a higher pressure. At times, when the delivery valves were particularly temperamental, a small quantity of neat DTD 585 hydraulic fluid was pumped into the system in such a way that at, say, 2,500kg/cm^2, the viscous fluid would be in the ball valves. A viscous fluid would always seat the valves, and once seated, they would seal down to 200kg/cm^2, but when disturbed, they would again need re-seating at 2,000kg/cm^2 or more.

Pressures of about 1,600kg/cm^2 were produced directly by the 40,000 p.s.i. hand pump. With petroleum ether, this pump would produce pressures higher than 1,600kg/cm^2 only with great difficulty, because of leakage losses in its check valves. Pumping started with the let down valve open and the piston at the top of its stroke. Fluid was pumped into the system until it appeared at the let down valve, which was then closed with a key. When the pressure reached 600kg/cm^2 the pistons moved to the bottom of their stroke on further pumping. Continued pumping would produce 1,600kg/cm^2, or if really necessary, 2,000kg/cm^2 could be obtained. For working up to this pressure, the suction valves and piston seal were relied upon to hold the vessel pressure.

Working of the 10,000 p.s.i. pump transferred the pistons to the top of their stroke and raised the pressure from 1,600kg/cm^2 to about 2,500kg/cm^2 with the viscometer in the vessel. The delivery valves were seated at this point by one of the methods previously described, and the success of this operation was judged by the movement of the pistons on letting down the low pressure. The pistons returned to the bottom of their stroke if the valve did not seat.

Once the delivery valves had seated, the production of any higher pressure was relatively straightforward. The high pressure cylinder was primed to 1,600kg/cm^2, and the charge transferred past the delivery valves by pumping the pistons to the top of their stroke. This cycle was repeated until the required pressure was produced.

Pressure reductions were made by very slight opening of the let down valve. The minimum pressure reduction that the valve would handle was about 40kg/cm^2 at 10,000kg/cm^2. It was found convenient to disconnect the low pressure flexible hose by the hand coupling for rotation of the pressure system, but no attention was required by the coupling on the priming line.

All leaks were traced by the appearance of petroleum ether,

and the detection of this was helped by the molybdenum disulphide carried out of the threads by the leak.

The overall behaviour of the pressure system was very satisfactory, the only troubles remaining being the inadequacies of the 40,000 p.s.i. pump, and the behaviour of seal (j), discussed in Chapter 6.

A view of the assembled intensifier, and valve and gauge block units is shown in Plate 2. The pressure vessel is shown in Plate 3, and Plate 4 is of the assembled manganin coil and plug unit, and the viscometer electrical connections unit.

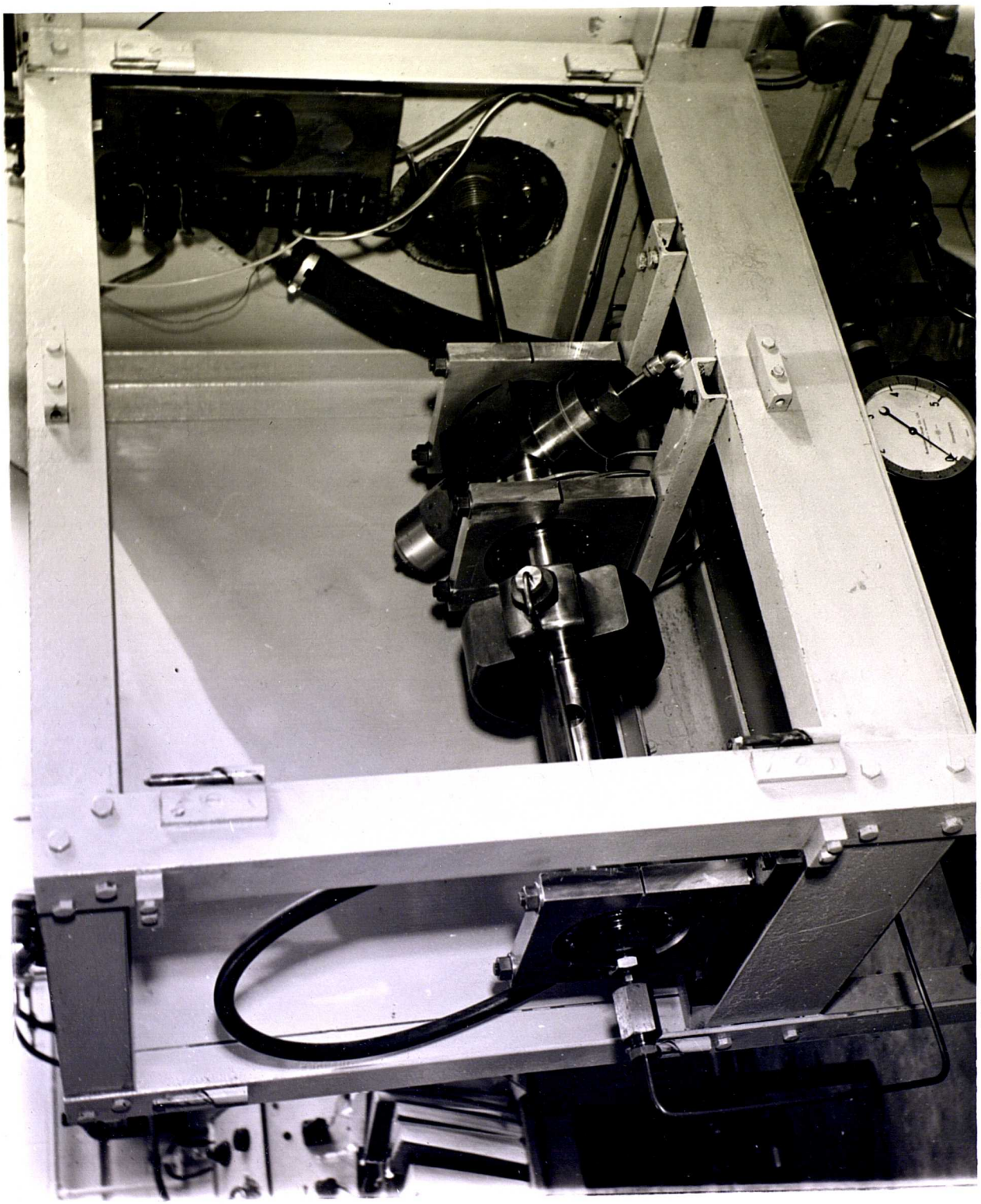

PLATE 2. HIGH PRESSURE SYSTEM

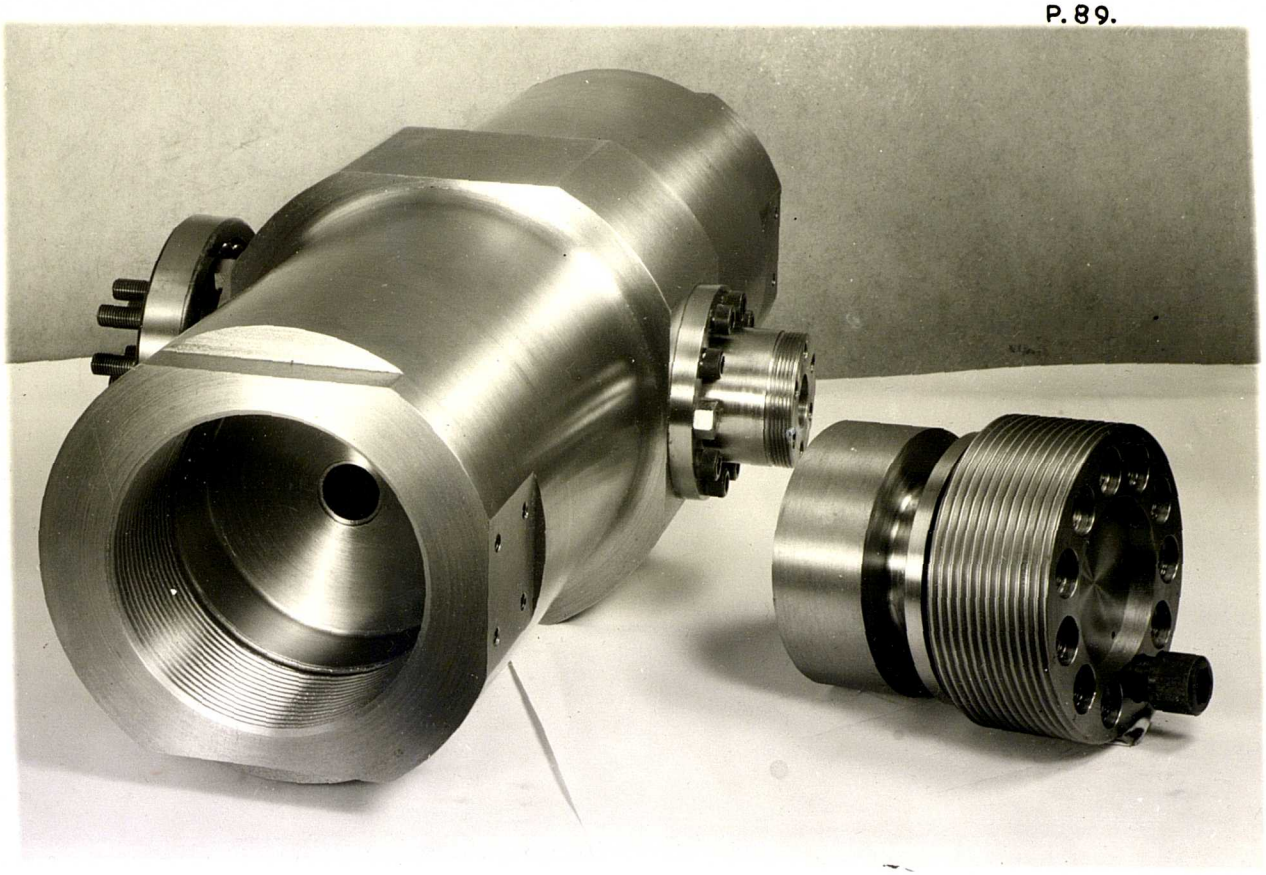

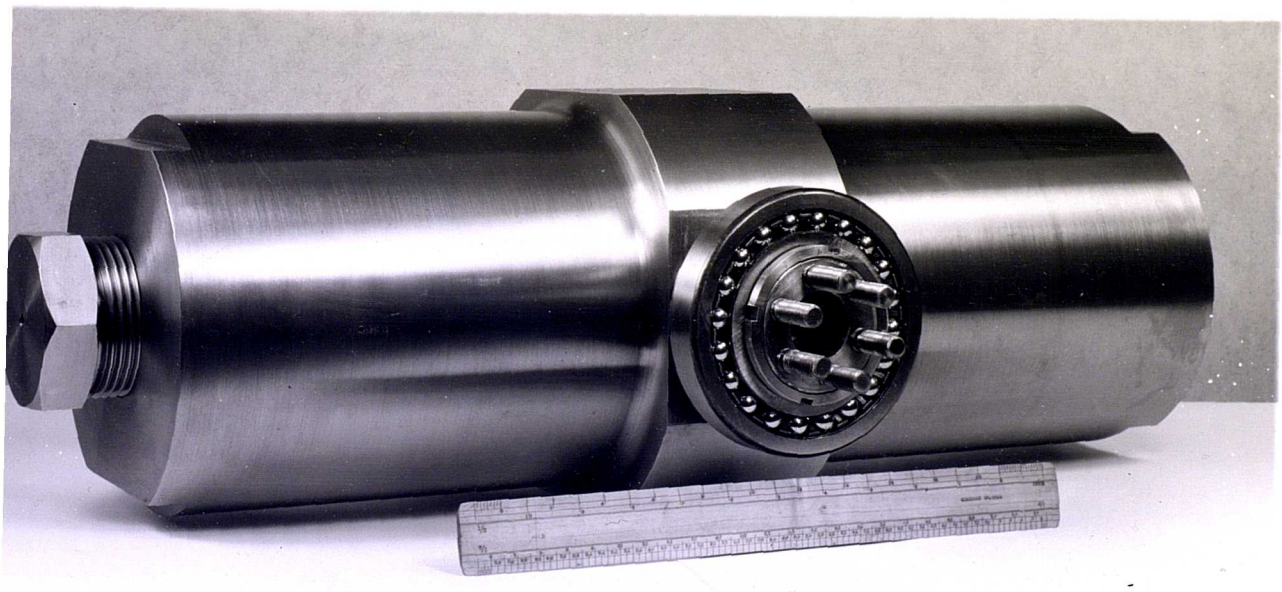

PLATE 3. PRESSURE VESSEL

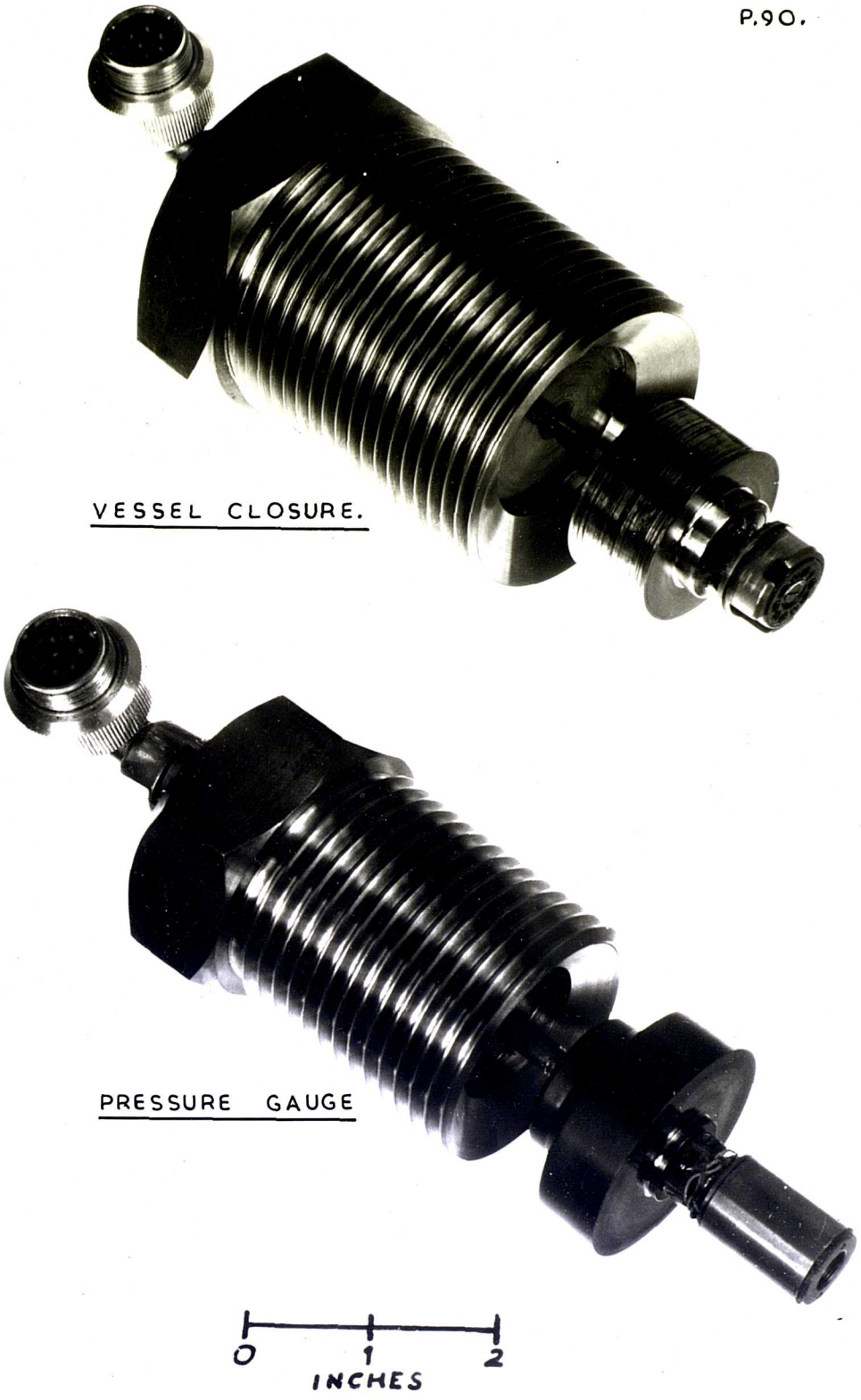

PLATE 4. H.P. ELECTRODE CLOSURES

CHAPTER 6.

HIGH PRESSURE SEALS.

(i) Development and Theories.

As a large number of seals were required for the high pressure system, O rings were selected for this duty because of their great simplicity. A number of workers [35, 67, 80, 142] had previously sealed pressures up to 12,000kg/cm^2 successfully with standard O rings, but, none of these workers had handled such low viscosity fluids as petroleum ether, and considerable development of the seal was required before it gave satisfactory service.

All of the high pressure seals are, with the exception of those at each end of the pressure pipe, based on the O ring principle. In addition to O rings, a Poulter packing [114] was used on the high pressure piston during initial development work. Both O ring and Poulter packing are self sealing, and work on identical principles. Their self energising nature relies on the stress derived from the initial compression, superimposed on the prevailing hydrostatic pressure, to maintain the stress between the sealing surfaces in excess of the hydrostatic pressure.

Sealing difficulties were first experienced during the autofrettaging of the intensifier. During this process, only O rings, (d), (g), and (i) (Drawing 1), were in use, each with a blanking plug, and a Poulter packing was used on the piston, backed up by a brass anti-extrusion disc. All the seals were of conventional 80 Shore hardness acrilonitrile-butadiene oil resisting elastomers, the Poulter packing being of high nitrile content, and the O rings of medium nitrile content. It was found that the Poulter packing leaked consistently and rapidly at 3,000kg/cm^2, although it sealed the petroleum ether perfectly below this pressure, behaving very much like a pressure relief valve, and several Poulter bungs from the same batch of elastomer produced

the same results. The pressure was sealed eventually by a bung comprising a layer of soft silicone rubber, sandwiched between two layers of the ordinary rubber packing, illustrated in Fig.16. This combination, together with the standard O rings, sealed the intensifier satisfactorily up to the autofrettage pressure of 19,500kg/cm^2.

After autofrettage and honing of the high pressure cylinder, the whole high pressure system was assembled with standard O rings, and the high pressure piston again fitted with a Poulter packing, from a batch of larger diameter than the first, but of similar material. Again, leakage occurred at the moving Poulter packing at 3,000 kg/cm^2, in a similar manner to the failure of the first batch of Poulter bungs. The technique of employing a pad of silicone rubber was once again employed in order to raise the pressure sufficiently to pressure test the whole high pressure system, but no brass backing was used, and on achieving 5,500kg/cm^2, various standard O rings leaked in the manner already characterised by the Poulter packing. After a few strokes of the intensifier, whilst investigating the new sources of leakage, the high pressure piston seized in its cylinder, and the full pressure of the 40,000 p.s.i. priming pump was required to remove the damaged piston. Examination of the piston and cylinder showed them both to be deeply scored on the one side. However, the scoring on the piston stopped about 1/16 inch short of the end, indicating that the corner of the piston had not dug into the cylinder metal. Almost all of the silicone rubber pad had escaped past the nitrile rubber pad, and appeared as a paste down the side of the piston. Presumably, an uneven build up of this silicone rubber had forced the piston hard over to one side, and this, combined with a small leak of petroleum ether having washed all the lubricant away, was the probable cause of the seizure. Clearly, a more systematic study of the sealing problems was called for.

The high pressure cylinder was honed out from .375 inch to .395 inch diameter, to remove the damage, and new pistons made to suit.

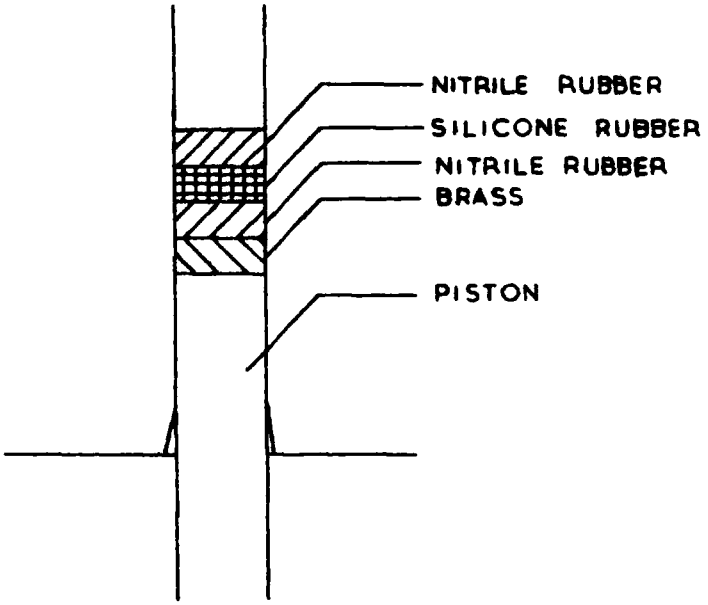

FIG. 16. H.P. PISTON SEAL.

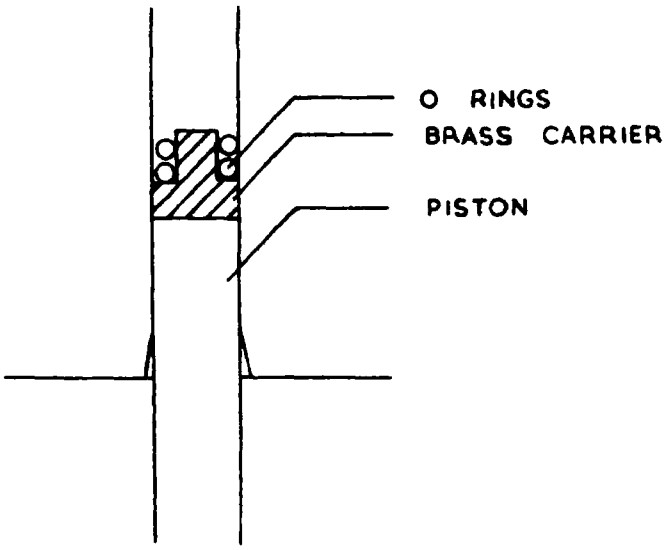

FIG. 17. H.P. PISTON SEAL.

The equipment was reassembled with nitrile rubber O rings and a Poulter packing, producing, once more, a leak at the piston at 3,000 kg/cm^2. The following tests were carried out as attempts to raise the pressure which could be sealed:-

1. The single Poulter packing was replaced by two bungs, doubling the length of the seal.

Result. No change in leakage pressure.

2. A Poulter packing bung was ground to improve the surface finish.

Result. No change in leakage pressure.

3. A bung was modified, by the insertion of a steel core, so that the interference between cylinder-diameter and bung diameter was increased by a factor of three.

Result. No change in leakage pressure.

4. The Poulter packing was replaced by two Shore hardness medium nitrile rubber O rings on a brass carrier, as shown in Fig. 17.

Result. Leakage pressure at piston raised to 5,000kg/cm^2.

5. The O rings on the carrier were replaced by O rings of 50 Shore hardness medium nitrile rubber.

Result. Leakage pressure at piston raised to 5,500kg/cm^2.

Leakage also occurred in some of the static O ring seals.

The conclusions drawn from these experiments are:-

1. The leakage pressure is independent of the leakage path length and of surface finish. (Assuming there are no obvious flaws in the surface).

2. The leakage pressure is substantially independent of the initial stress between the rubber and steel surfaces.

3. A radical change in the initial hardness of the seal makes little difference to the leakage pressure.

4. Under the conditions that prevail in the intensifier, a static seal will leak at a slightly higher pressure than a similar dynamic seal.

5. The leakage pressure of a seal is probably a property of the

seal material rather than of the geometry of the seal.

The theory postulated to account for the last conclusion is as follows:-

Any elastomer-to-metal seal must maintain the normal stress across the seal at a higher value than the prevailing hydrostatic pressure. Ideally, the elastomer composing an O ring or Poulter seal must behave as a fluid, so that the full hydrostatic pressure, acting on the unsupported areas of the seal, is transmitted, without loss through rigidity, to the supported sealing areas of the elastomer. The typical stress caused by compressing an O ring to 80% ofits normal thickness is 20kg/cm^2; thus, if the hydrostatic pressure behind the ring is raised to 5,000kg/cm^2, at least 99.6% of the prevailing pressure must be transmitted through the rubber to maintain the stress across the seal at 5,000kg/cm^2. If, through any reason, the sealing stress drops to the value of the hydrostatic pressure, leakage will occur.

It is postulated that the rigidity modulus of an elastomer rises under the application of hydrostatic pressure, in a manner similar to the increased rigidity modulus caused by a drop in temperature.

A typical O ring elastomer transmits very nearly 100% of the hydrostatic pressure to the sealing faces, but if a rise in pressure should increase the rigidity of the material, there will come a point where the loss in transmitted stress is so great that the seal leaks. A similar form of leakage occurs with O ring seals at low temperatures. It is thought that the high nitrile rubber Poulter packing leaked at 3,000kg/cm^2, because at this pressure, the material was too stiff to maintain the self energising nature of the seal. The following experiment indicates the correctness of this assumption:-

A high nitrile rubber Poulter packing was assembled in the high pressure cylinder of the intensifier, and the pressure of the petroleum ether in the system was raised, by means of the high pressure

piston, until the Poulter seal leaked in the characteristic manner. The temperature of the whole intensifier was raised, whilst still under pressure, and it was found that leakage at the Poulter seal now occurred at a higher pressure. This procedure was repeated a number of times, and successively higher temperatures produced successively higher leakage pressures. The temperature was then reduced, and the reverse effect was observed, showing that the leakage pressure was a function of the seal temperature only. The results of this investigation are given in Table 2, together with the results of similar experiments carried out using soft and hard medium nitrile rubber O rings to seal the piston. The temperature was measured on the outside of the intensifier, and is probably within 2 or 3°C of the actual seal temperature.

TABLE 2.

Material	Shore hardness.	Stiffening point.	Leakage pressure kg/cm^2 and temperature.
High nitrile rubber	80.	-12°C	3000. 4000. 6000. 8000. 9500. 17°C. 30°C. 45°C. 55°C. 70°C.
Medium nitrile rubber.	50.	-19.5°C.	5500. 7500. 8000. 9000. 10000. 19°C. 26°C. 31°C. 37°C. 43°C.
Medium nitrile rubber.	80.	-19.5°C	5000. 19°C.

If application of pressure to an elastomer increases its rigidity modulus, it is very likely that raising the temperature reduces

the stiffness. The vastly improved performances of the seals in Table 2 at the higher temperatures indicates a close connection between stiffening under pressure and leakage pressure.

It was clear that a material was required whose rigidity modulus did not rise under pressure as rapidly as in the materials already tested, and it was thought that elastomers with good low temperature properties might possess the desired characteristics. Three low temperature elastomers were submitted for trial by Dowty Seals Ltd. They were:-

Material	Stiffening point.
AM90 low nitrile rubber.	-57.5°C.
Polyurethane.	-35°C.
LS53 silicone rubber.	Approx. -55°C.

The stiffening point is defined as the temperature at which the rigidity modulus rises to 10,000 p.s.i. For comparison, the stiffening points of the materials previously tested are given in Table 2.

The low temperature materials were supplied as sheet, approximately .070 inch thick, and square section O rings were cut from the sheet with cork borers to make a seal for the piston. These new materials behaved with petroleum ether at room temperature as follows:-

(1) LS53 silicone rubber.

This failed completely at 7,500kg/cm^2, through inadequate mechanical strength, and so its sealing properties could not be properly assessed.

(2) AM90 low nitrile rubber.

This leaked at 9,500kg/cm^2 at 19°C.

(3) Polyurethane.

No leaks occurred up to 13,000kg/cm^2.

The low temperature behaviour of all the materials tested, except the silicone rubber, is shown in Fig. 18, compiled from data supplied by the manufacturers. The four nitrile rubbers appear to

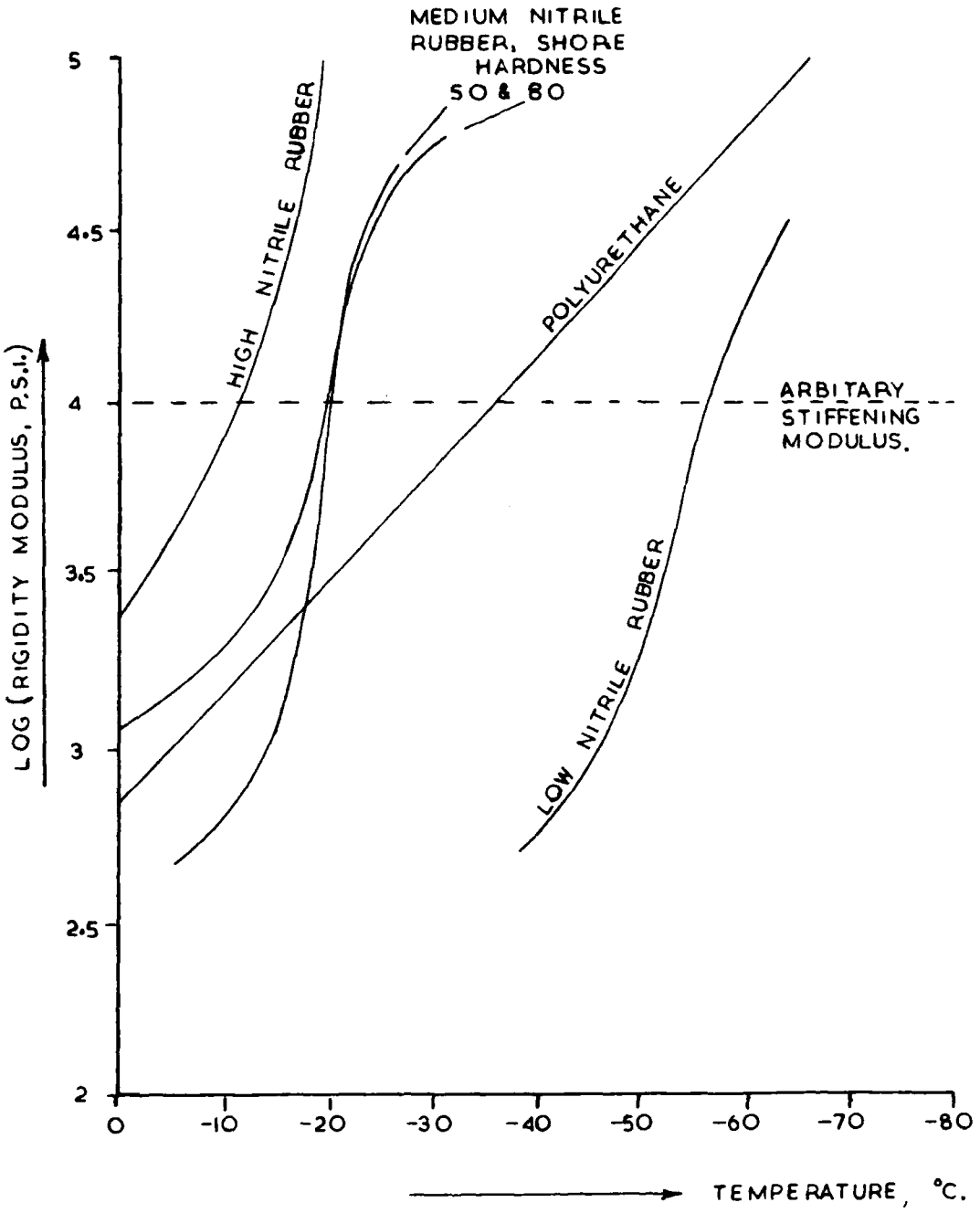

FIG. 18. LOW TEMPERATURE PROPERTIES OF ELASTOMERS.

show a distinct correlation between stiffening point and the leakage pressure at room temperature, but the polyurethane, which has a higher stiffening point than the low nitrile rubber, has the highest leakage pressure of all. The experience of O ring manufacturers is that a seal will leak at about 5 or 10°C below the stiffening point, but the rigidity modulus to which this corresponds is not known. The rigidity of the low nitrile rubber rises very sharply at its stiffening point, whereas that of the polyurethane rises comparatively slowly. This anomalous behaviour of polyurethane goes some way to explain its superior sealing properties at high pressure.

In spite of the apparent inadequacy of standard O ring materials, other workers have nevertheless employed them with success at very high pressure. The simple picture already drawn of an O ring leaking when it reaches a certain stiffness is complicated by a number of factors, and the successful performance of an O ring elastomer above its normal leakage pressure depends on circumstances in which its self energising nature becomes less dependent on the maintainance of fluid-like properties in the material. Some of these factors are:-

(1) Fluid viscosity.

Most of the successful users of O rings at high pressures (7, 35, 67, 80, 142) state the use of a pressure transmitting fluid which is highly viscous at high pressures, and none of them mention the use of low viscosity fluids. To check if fluid viscosity is a factor in sealing, medium nitrile rubber O rings were assembled on the piston seal, and the system pressurised with petroleum ether. Leakage occurred at 5,000kg/cm^2. The seal was left undisturbed whilst the petroleum ether was replaced with the very much more viscous DTD585 hydraulic fluid, and pressurisati n to 10,000kg/cm^2 produced no leakage under these conditions. On reverting to petroleum ether, leakage again took place at 5,000kg/cm^2. The pressure at which the

O ring will seal is therefore dependent on fluid viscosity.

When the normal stress across an O ring seal drops to the value of the prevailing hydrostatic pressure, a momentary leak occurs and the leaking fluid exerts a shear stress on the sealing face of the O ring. This shear stress acts in the same direction as the hydrostatic pressure on the O ring, and will therefore tend to raise the normal stress across the seal above the value at which leakage occurs. The greater the shear stress derived from leakage, the stiffer may be the elastomer before failure. The much greater shear stresses which could be associated with the leakage of a highly viscous liquid might account for the anomalous sealing capabilities of an O ring under these conditions.

(2) <u>O ring housing strains.</u>

If the dimensions and shape of an O ring change under pressure, the effect of rigidity in the elastomer would be greater than if none of these changes took place. The necessary force for deforming a stiffened elastomer must be supplied by the hydrostatic pressure, and the greater the deformation for a given stiffness, the smaller will be the proportion of hydrostatic pressure transmitted through the elastomer to the sealing face.

An O ring is made to change its dimensions or shape by the application of pressure through three causes:-

1. At atmospheric pressure an O ring takes up the configuration illustrated in Fig. 19a. Application of pressure makes the configuration tend towards the condition shown in 19b. According to Fawcett [46], this condition is achieved with typical O rings by 1,000 to 4,500 p.s.i., above which pressure there is no further deformation of the ring into the housing corners. This behaviour, therefore, is not a factor in the sealing characteristics of an O ring.
2. Application of 10,000kg/cm^2 pressure to an elastomer increases

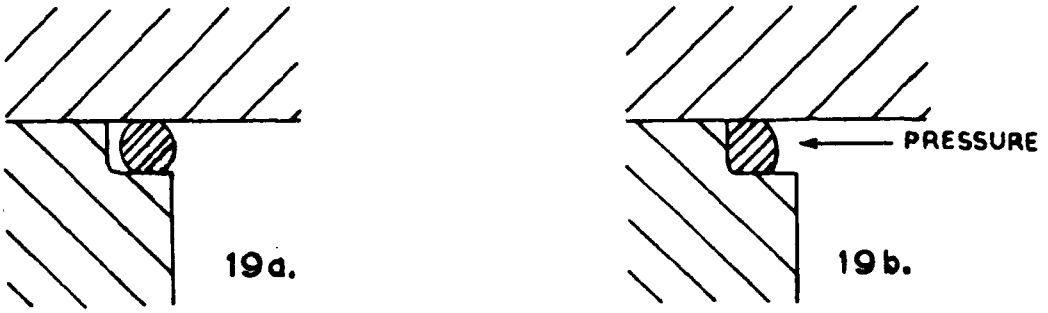

FIG. 19. O RING CONFIGURATIONS.

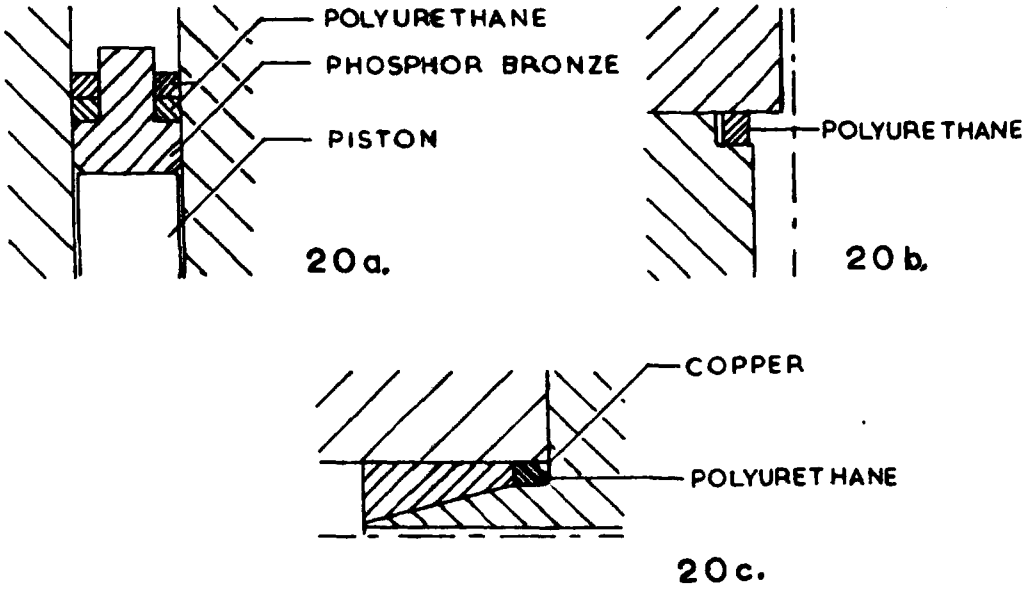

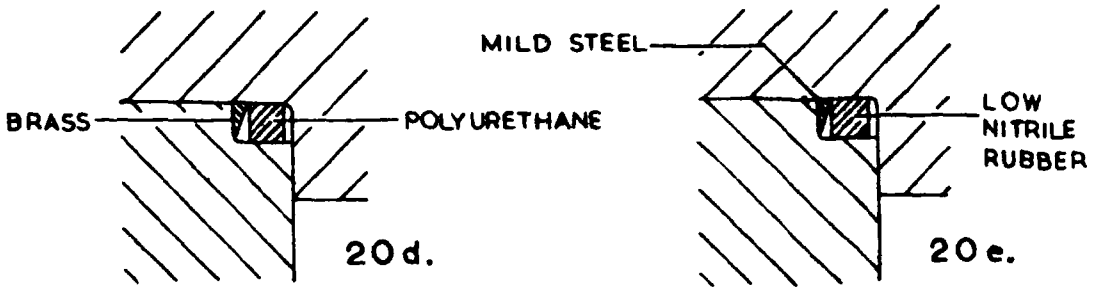

FIG. 20. HIGH PRESSURE SEALS.

its density by 10 to 15%. This density change must be accommodated by a change in shape and dimensions of the O ring, and will therefore contribute to a loss in pressure transmission through the elastomer. The density change is, however, a fixed property of the material, and its contribution as a cause of leakage is therefore fixed for any seal configuration.

3. The application of pressure to a seal of the type illustrated in Fig. 19, will change the O ring housing dimensions in two respects. Its diameter will increase, according to the radius ratio of the cylinder at that point and the properties of the steel, and the gap confining the O ring will increase, according to the rigidity and preloading of the closure. The housing strains must be accommodated by dimension changes in the O ring, and these strains will therefore influence the degree of pressure transmission through the elastomer. This contribution to the tendency for an O ring to leak, depends entirely on the construction of the closure. A very rigid closure which has had a considerable preloading before pressurising, should leak at a considerably higher pressure than a less rigid closure, merely hand tightened. The seal described by Whalley [142] was of a very rigid nature, and this could explain the success of his seal to 10,000kg/cm^2. Also, O rings (d), (g), and (i), in a material which normally leaked at 5,500kg/cm^2, were able to seal the full autofrettage pressure of 19,500kg/cm^2 when the closures were impact tightened, giving a high degree of preloading.

(3) Secondary sealing effects.

A seal which forms a substantial extrusion gap under pressure is often provided with a metal antiextrusion ring [35,67]. It is possible that the O ring provides the seal at lower pressures, and that the metal ring, sitting across the gap, provides the seal at high pressures on the unsupported area principle. An O ring antiextrusion ring

seal, working on exactly these principles, is described by Babb,[7]. Also, it was found that O ring (i), which leaked consistently at 5,500kg/cm^2 with normal tightening, would sometimes seal to 10,000 kg/cm^2 when backed up with an antiextrusion ring. An unsupported area secondary seal, by an antiextrusion ring, or even by the O ring itself, might explain the anomalous performance of some seals.

(ii) Application.

Of the materials tested, polyurethane and low nitrile rubber are clearly the most suitable for sealing the pressures covered in this work. The limit of the former material is not reached, and at room temperature, a static seal in low nitrile rubber would certainly seal 10,000kg/cm^2. All of the high pressure seals, except the two in the vessel, are manufactured in polyurethane, this being selected for its superior abrasion resistance, swell resistance and mechancial properties. The vessel seals are in Dowty AM90 low nitrile rubber for the temperature range 25 -100°C, and below 25°C, polyurethane is used. AM90 for the upper temperature range is selected for its better temperature resistance. Some of the seals have been found to require antiextrusion rings, and the details of each seal are as follows:-

1. High pressure piston seal.

The seal illustrated in Fig. 20a, has given good service in the high pressure cylinder, stroking frequently up to 10,000kg/cm^2. A phosphor-bronze carrier is employed, as a brass one was found to extrude to an undesirable extent. After one application of pressure, the carrier becomes an interference fit in the cylinder at low pressures. The bevel on the lower face of the carrier allows work hardening at that point before extrusion can take place. Two polyurethane rings provide the seal, and these are cut from sheet. The rough cut sealing

faces seem to have no effect on their sealing efficiency. The upper ring provides the main seal, and the lower ring is the only one subject to extrusion.

Ring dimensions are :-

Thickness .070 inch.

Width, approx. 1/16 inch.

Interference on diameter .025 inch.

The seal is usually dismantled after ten complete full pressure cycles in the vessel, which involves about 100 pressure cycles between 2,000 and 10,000kg/cm^2 in the intensifier. The lower ring is replaced with the upper ring, and a new upper ring fitted.

2. Static seals (e), (f), (g), (h), (i), (k).

These seals consist of a square section ring of polyurethane, as shown in Fig. 20b. Compression on the .070 inch thick ring is .016 inch. The maximum diameter of these seals is 5/16 inch, and they give very long service without the use of antiextrusion rings. The closures are hand tightened with standard spanners.

Seals (e) and (f) are exceptional in that they never suffer from extrusion, and therefore have an indefinite life. This effect is derived from the fact that seal (d) is of larger diameter, and the hydraulic load at (d) is greater than the loads at (e) and (f), preventing any extrusion gap ever appearing at the latter two seals.

3. Seal (d).

Seal (d) is illustrated in Fig. 20c. A single polyurethane ring is employed, of the same dimensions as in the piston seal. A copper antiextrusion ring is used, formed by fusing the ends of copper wire together in a bunsen flame. Both seal and antiextrusion ring have indefinite lives.

4. Seal (j).

A polyurethane ring is used as illustrated in Fig. 20d, employing ring dimensions of .070 inch thickness, .016 inch compression and $\frac{7}{8}$ inch diameter. The housing was machined large enough for an O ring only, but a brass antiextrusion ring was found necessary, and is fitted as shown. Because of space limitations, the width of the sealing ring has to be cut considerably, and consequently, this seal is rather temperamental. The housing needs to be widened, and this would solve all the problems associated with this particular seal. It is, in fact, the only troublesome seal on the equipment.

5. Seal (n).

This seal is illustrated in Fig. 20e, with a moulded, low nitrile rubber seal, and a mild steel antiextrusion ring. There is room in this housing for only a small section mild steel ring, and it was found that with the hand tightening that could be applied to this closure, the antiextrusion ring itself extrudes rapidly at full pressure, with the result that the seal fails completely and suddenly. The closure could not be sledged because of the bearings carrying the vessel, and it was not convenient to re-machine the seal housing to take a more substantial antiextrusion ring. The problem was solved by use of a specially designed hydraulic spanner, which fits on the plug (59) and on the flats on the vessel. The closure is preloaded by this tool to about 30 - 35 tons thrust, which is about half of the hydraulic load on the closure at 10,000kg/cm^2. The life of the antiextrusion ring is very long under these conditions, and that of the rubber seal is indefinite.

6. Seal (p).

This is identical to seal (n), except that adequate preloading is supplied by the set screws (62). The rubber seal has an indefinite life, but because this closure is removed frequently, the antiextrusion

ring must be extracted occasionally to remove an extrusion lip which builds up progressively.

CHAPTER 7.

DESIGN AND CALIBRATION OF PRESSURE MEASURING SYSTEM.

(i) Design and Construction.

As the means of measuring pressure must be incorporated in a rotating high pressure system, an electrical method of measurement is the most convenient. Electrical alternatives available are the measurement of resistance change of an electrical conductor subject to hydrostatic pressure, and the measurement of strain on the outside of a tube containing the pressure, employing a resistance strain gauge. Of these, the former is the more accurate. A resistance pressure gauge should possess a high pressure coefficient, a linear resistance-pressure relationship, and a zero temperature coefficient; but, in a practical case, the choice of resistance material must be a compromise between these requirements. Manganin wire has been the material most frequently used in resistance gauges since Lisell [82] first suggested its use in 1903. It has a good coefficient, and does not deviate greatly from linearity. At temperatures removed from room temperature, its temperature coefficient is high. However, most samples of manganin exhibit a maximum in their resistance between 20 and 40°C, and provided one is near to the temperature at which the maximum occurs, the temperature corrections applying to a pressure measurement are relatively small.

Darling and Newhall [36] proposed the use of a gold chromium alloy, which has a very low temperature coefficient, but its pressure coefficient is about 1/3 that of manganin. At room temperature, there is no advantage of the gold chrome alloy over manganin.

Manganin is known to exhibit a drift in its calibration with time, and this characteristic is its greatest disadvantage.

However, in the absence of a systematic study of the suitability of other materials, manganin was selected, in spite of its lack of stability, as being capable of sufficient accuracy for the present work.

The work of Adams et al [1] indicates that the winding of a manganin coil with large, loose turns, produces a higher and more stable pressure coefficient than small, tightly wound coils. The resistance stability of the coil is all important, and its manufacture, in such a way that it is never subject to any mechanical strain or constraint, once wound, is the first requirement of the design. This condition must apply at high pressure, as well as at atmospheric pressure, and preferably during rapid pressure changes also.

In the interests of resistance stability, in both the manganin wire and its insulation, it is advantageous for the coil to be exposed to dry media only, and the requirement of the coil remaining undamaged during rapid pressure changes, suggests that the medium transmitting pressure to the coil should also be of low viscosity.

As the resistance change of a 100ohm manganin coil is only 2.2ohm for a 10,000kg/cm^2 pressure change, a resistance measuring system of high sensitivity is required. This is best achieved by a four wire system of connecting the coil to the resistance measuring instrument, two wires being attached to each end of the coil.

The manganin coil constructed for the present work, is illustrated in Fig.21. The gauge occupies a cavity $\frac{3}{4}$ inch diameter and $1\frac{3}{8}$ inches long, leaving adequate space for ventilation.

The manganin is wound as a simple single layer coil in a 50 t.p.i. thread, machined on a hollow brass former (1). The thread detail is shown in Fig.22, and the groove provided for the .007 inch diameter insulated wire leaves ample room for its free movement.

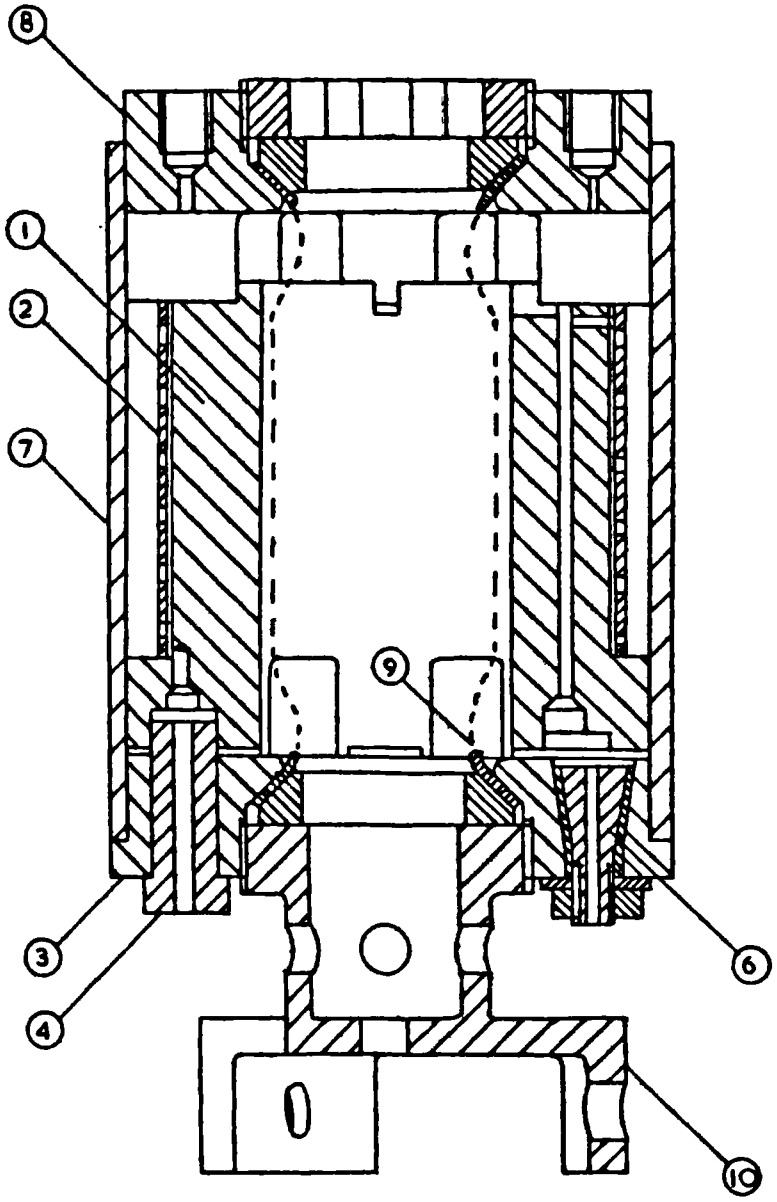

FIG. 21. MANGANIN COIL PRESSURE GAUGE.

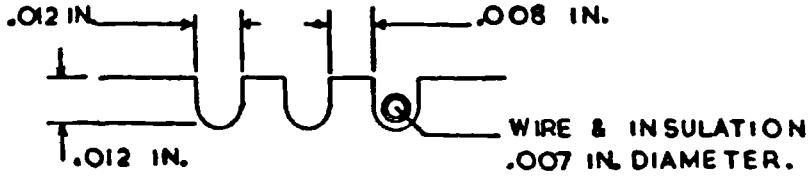

FIG.22. COIL GROOVE DETAIL.

Plastics and ceramics were avoided as materials for the former, as their compressibilities may be 4 to 20 times that of the manganin. On the .58 inch diameter of the former, these compressibilities could lead to a differential contraction on diameter, between wire and former, of .0045 and to .027 inch. In employing a brass former, which has a similar compressibility to that of manganin, the danger of disturbing the position and resistance of the wire, by differential contractions, is eliminated, but the use of a conducting former does present problems of insulation. Throughout construction of the gauge, a close check was kept on insulation resistance, the minimum standard accepted being 100 megohms between any wire and ground.

The manganin coil itself consists of 23 turns of 42 swg (.004 inch diameter) double silk covered wire, which, at 13.4ohms per foot, gives a coil resistance of 44ohms. The gauge resistance was limited by the 48ohm capacity of the resistance bridge available. The coil is silver soldered at each end to two 36 swg double silk covered copper wires, so that the three wires form a Y junction with a single small bead of solder. (Soft soldering of the junctions is thought to lead to instability [136]). The soldering and subsequent cleaning were carried out with the wires held in a jig to maintain correct angles, and the soldered joint was afterwards insulated by wrapping with unspun silk thread, whilst still secured in the jig.

The junctions with the lead wires are laid in enlarged grooves in the former at each end of the 50 t.p.i. thread. The lead wires pass through drillings in the former, and appear at 90 degree intervals around the bottom face of the former. Where the lead wires pass through drillings, they are insulated with PTFE sleeving or tape, and all sharp edges on the brass former are removed. The brass thread is coated with shellac, and the silk insulated manganin wire is wound

loosely in the groove. This looseness was achieved by winding the coil firmly in the thread, backing the wire off by a calculated length, and distributing the slackness, by hand, uniformly along the length of the coil. A brass sleeve, (2), fits closely over the former to prevent the loose coils of manganin from slipping out of their groove. The sleeve is drilled with many small holes to freely ventilate the coil.

Once the sleeve is in place, the coil is protected from any disturbance, and it was in this form that the coil was heat treated. The heat treatment is an attempt to remove the stresses set up in the wire during winding, which, in the case of a large diameter coil, are small. The heat treatment, suggested by Bridman [24], is no more than a recipe, and no information is available as to the best heat treatment for manganin. The coil was cooled to $-70^{\circ}C$ for 2 hours, and heated to $124^{\circ}C$ for 16 hours, after which process the resistance had fallen by $\frac{1}{2}\%$. A precision coil produced by the National Bureau of Standards [106], was found to decrease its resistance on heat treatment by 2%, but the manufacture of that coil produced a good deal of plastic strain in the wire.

The remainder of system shown in Fig.21, forms a capsule around the manganin coil. The bottom header (3), contains four sealed electrodes which connect the lead wires from the manganin coil to the exterior of the capsule. One of the electrodes, (4), was hard soldered in the header, forming a 'ground' connection, and this electrode also locates the former with respect to the header. The remaining three electrodes are similar to (6), consisting of a brass cone sealed and insulated by a Viton sleeve. The electrode is held in place by a nut and a fibre washer.

A brass sleeve (7) was soft soldered to the bottom header, and the coil former assembled in the position shown. In this operation, the copper lead wires projecting from the bottom of the former

were bared and fed through the holes in the electrodes, where they were soft soldered in place to seal the holes. A top header (8), was soldered to the end of the capsule with Wood's metal. On completion of the soldering operations, the gauge was washed with distilled, de-ionised water, to remove flux residues, and oven dried.

The cavity between the coil and the capsule sleeve, (7), is ventilated to the central gallery by radial slots cut in the top header, and by radial slots in the bottom of the former. The capsule is completed by a rubber diaphragm, (9), in the form of a tube of .015 inch wall thickness, passing through the former, and sealed at each end to the top and bottom headers. The capsule is intended to be filled with sodium dried pentane, to provide a low viscosity pressure transmitting fluid, and the function of the diaphragm is to accommodate volume changes in the pentane. Screwed holes in the top header facilitate the filling of the capsule. The capsule is fitted with a base, (10), for attaching the unit to the pressure gauge closure, part (33) in Drawing 1.

A rubber diaphragm was selected to isolate the fluid in the capsule, in preference to a metal bellows, because of the considerable saving in size that this afforded. However, in practice, it has been found that the very small pressure difference across the diaphragm causes diffusion of the pentane. The diaphragm has insufficient capacity to permit loss of pentane by diffusion for more than a few days, and its utilisation for isolating the pentane is, therefore, impractical. By the time this failing of a rubber diaphragm was discovered, the gauge cavity in the pressure equipment had been machined. The gauge could not therefore be adapted for use with a bellows. Instead, the need for dryness in the vicinity of the coil was to some extent satisfied, by drying, over calcium chloride, all the petroleum ether which enters the high pressure system.

A copper-constantan thermocouple adjacent to the gauge cav-

ity measures the gauge temperature. (See Chapter 5.). Its e.m.f. is measured on a Pye Universal Potentiometer, reading to 1 microvolt, in conjunction with a Pye D.C. Microvoltometer, employed as a galvanometer.

The gauge resistance is measured on a Cambridge Smith's Difference Bridge, which is capable of measurement to 10^{-5} ohm up to 48ohms, together with the same microvoltometer as used with the potentiometer. The bridge is oil filled, and it was found that temperature variations throughout the oil were sufficient to cause a large random error in the bridge. To overcome this, the bridge was provided with distributor pipes, and a centrifugal pump circulates the oil through the bridge, and through a water cooler to prevent excessive temperature rise.

Figs. 23 and 24 illustrate the basic circuit employed in the resistance measurement of the gauge. Fig. 23 represents the manganin coil itself, of resistance S, together with four connecting leads of resistance C_1, C_2, C_3, and C_4. Fig. 24 shows the coil connected to the bridge circuit in two ways.

From Fig. 24(a):-

$$R_1/R_2 = \frac{(R + C_3)}{(X_1 + S + C_1)} \qquad 15.$$

From Fig. 24(b):-

$$R_1/R_2 = \frac{(R + C_1)}{(X_2 + S + C_3)} \qquad 16.$$

Then:-

$$S = \frac{(R + C_3)}{(R_1/R_2)} - X_1 - C_1$$

and

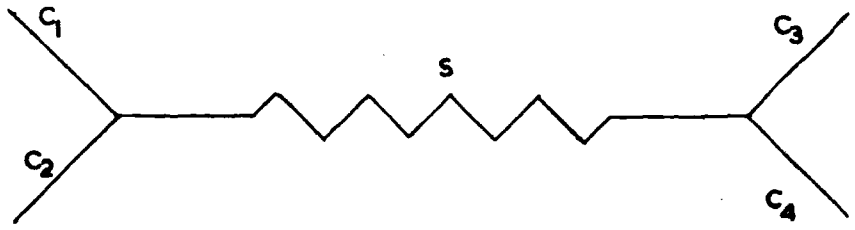

FIG. 23. MANGANIN COIL CONNECTIONS.

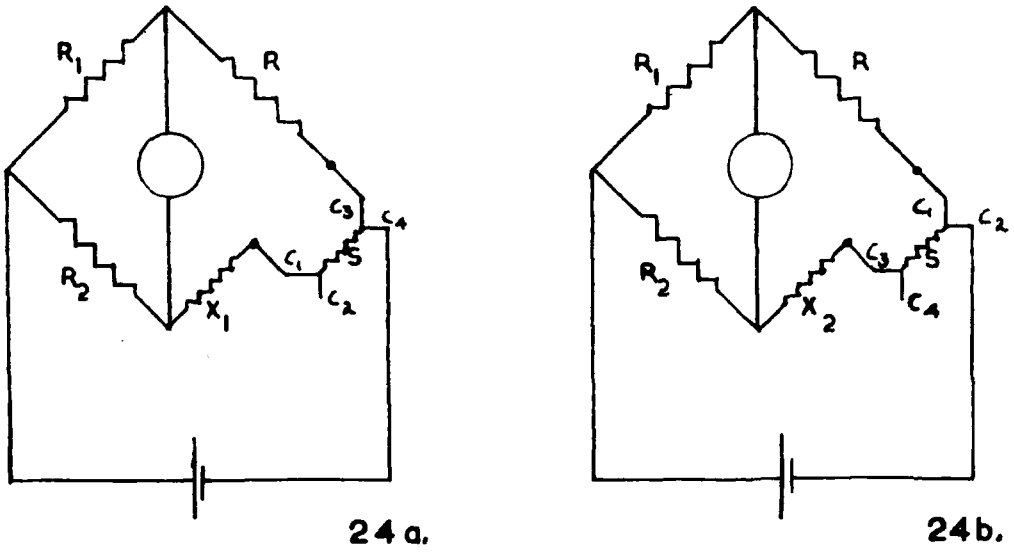

FIG. 24. SMITH'S BRIDGE CIRCUIT.

$$S = \frac{(R + C_1)}{(R_1/R_2)} - X_2 - C_3$$

If $R_1/R_2 = 1$,

$$S = \frac{(R - X_1) + (R - X_2)}{2} \qquad 17.$$

Thus, the lead resistances are eliminated, and the resistance of the manganin between its actual junctions is obtained directly. The Smith's Difference Bridge is provided with a switch, with which the circuit may be arranged as in Fig.24(a) or as in Fig.24(b), enabling X_1 and X_2 to be measured. A second switch allows the external resistance to be short circuited, so that the value of R may be determined against the X arm of the bridge.

(ii) Calibration Requirements.

Calibration of the pressure measuring system involves calibration of the resistance bridge, and a determination of the temperature and pressure effects on the manganin coil.

Before calibration, the manganin coil was subjected to 10,000kg/cm^2 a number of times, to check that its base resistance was pressure stable. Zolotykh [147] reported no effect from pressurising coils to 23,000kg/cm^2, but a slight decrease in resistance was reported for the N.B.S. gauge [106]. The first application of 10,000kg/cm^2 reduced the coil resistance by the equivalent of 10kg/cm^2, after which, no further change was detected.

(iii) Bridge Calibration.

The absolute accuracy of the Smith's Difference Bridge is immaterial, provided the manganin coil is calibrated against the bridge. The requirements of bridge calibration are to check its internal consistency and to measure its temperature dependence.

(a) Internal consistency.

The nominal resistances of the resistors in the X arm of the bridge are:-

1 to 10 x .00001ohm, 1 to 10 x .0001ohm and 1 to 10 x .001 ohm, selected by commutator switches;
.01, 2 x .02, .05, .1, .2, .4, .8, 1.6, 3.2, 6.4, 12.8, and 25.6 ohm coils selected by mercury switches.

Assuming the 10 x .00001ohm coil to be correct, the internal consistency of the bridge was checked at a constant temperature by standard techniques. All resistors were found to equal their nominal value to the nearest .00005ohm, except the 25.6ohm coil, which was .0007ohm high. However, as this particular resistor is used only in the determination of R, the error is self cancelling. As the bridge was 30 years old at the time of calibration, it is assumed that the values are stable. The ratio R_1/R_2 is given in an N.P.L. calibration certificate, dated 1935, as 1. It is assumed also that this ratio is still close enough to 1 for equation 17 to hold, and that the ratio is still stable.

(b) Temperature dependence.

The temperature dependence of the bridge was checked by determining S, from equation 17, at various bridge temperatures, when measuring a constant external resistance. The bridge temperature was controlled by means of the external water cooler, and was measured with the mercury in glass thermometer fitted to the bridge. The manganin coil pressure gauge, maintained at the ice point, was utilised as the constant external resistance. Fig. 25 shows the calculated values of S versus the bridge temperature. Curve fitting, by a 'least squares' method, on a digital computer, to the experimental points in Fig.25, gives:-

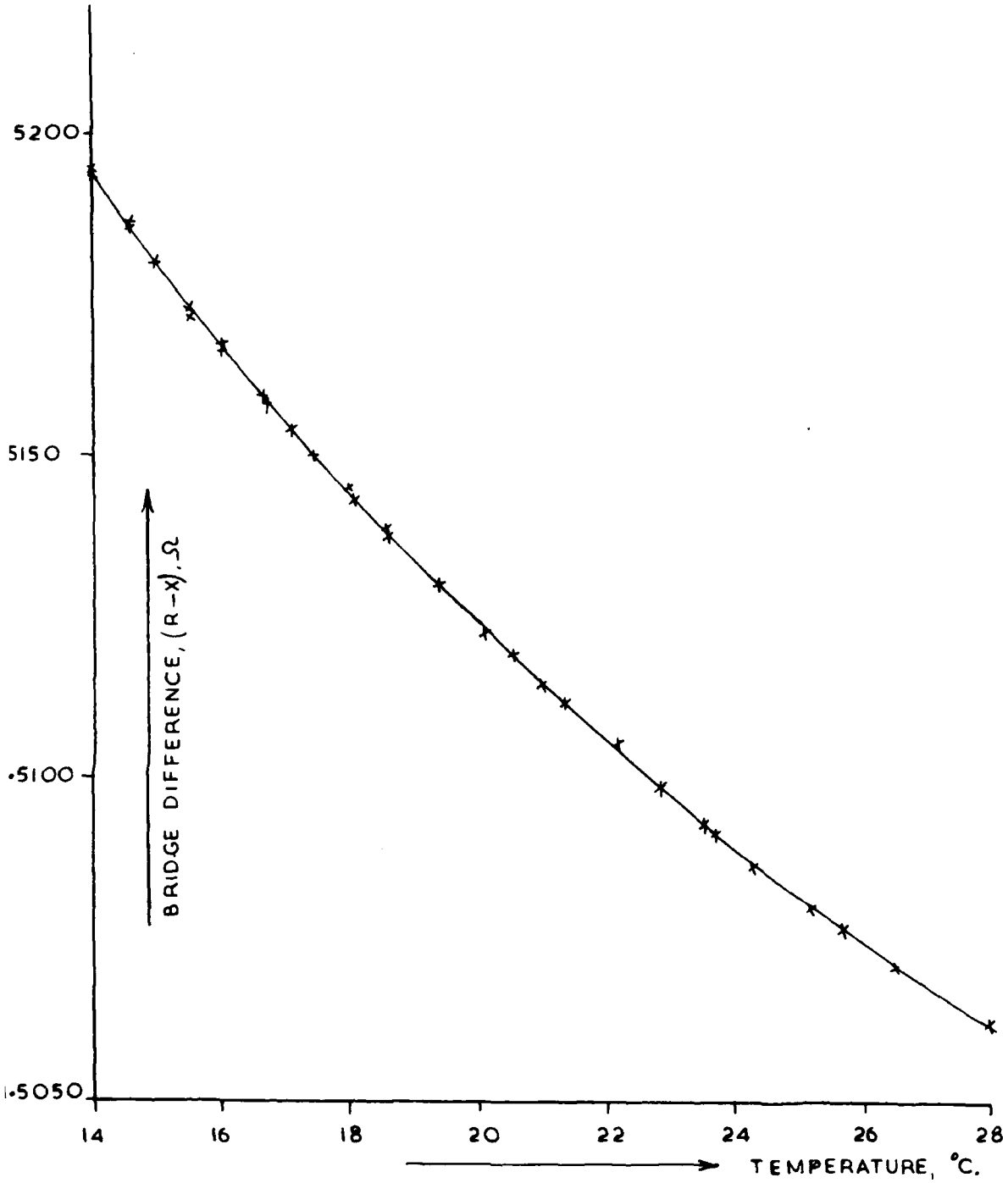

FIG. 25. BRIDGE TEMPERATURE DEPENDENCE.

$$S = 44.587714 - 1.0754940 \times 10^{-2}\, t + 6.4553264 \times 10^{-4} t^2 - 19.180811 \times 10^{-6} t^3 + 21.882985 \times 10^{-8} t^4. \qquad 18.$$

($t = {}^{\circ}C$).

In all subsequent use of the bridge, an arbitary datum was taken at 20°C, and all bridge readings corrected to the datum by means of equation 18. A table of corrections was compiled for this purpose. These corrections are valid only when the external resistance being measured, is equal to that of the manganin coil at 0°C, but in practice, the external resistance is higher, giving a lower value of X than in the calibration. This small difference in the X value must also be corrected for, and the correction is applied by assuming that the resistors, which account for the difference in the X values, have the same temperature characteristics as the overall bridge characteristic shown in Fig.25. The overall bridge characteristic is the temperature variation of (R_1/R_2), which is probably a constamt, combined with the temperature variation of $(R - X)$. If Xa is the value of X during calibration, and Xb is the value of X during a resistance measurement, the bridge temperature correction calculated from 18, must be corrected by the ratio:-

$$\frac{(R - Xb)}{(R - Xa)}$$

As, at all times, the external resistance is the manganin coil, the secondary correction is very small, and rarely exceeds the equivalent of 1.5kg/cm^2. The primary correction can be as high as 50kg/cm^2.

(iv) Gauge Temperature Calibration.

(a) Gauge thermocouple calibration.

The pressure gauge thermocouple was calibrated in-situ in the pressure gauge closure, and as the ceramic cones in this unit require the avoidance of large temperature changes, the thermocouple

was calibrated between 10 and 30°C only. The whole unit was enclosed in a polythene bag, and immersed in water whose temperature was measured with a calibrated mercury in glass thermometer. The connections between the thermocouple and its cold junction were completed by the Plessey plug unit and the Bulgin plug unit employed in the working arrangement. During calibration, these plugs were disconnected and reconnected several times, and it was found that after the re-attainment of thermal equilibrium, the thermocouple e.m.f. remained unaltered. The calibration at the beginning and end of the experimental work is shown in Fig. 26. In both cases, the calibration points lie within .002 mV of standard thermal e.m.f's, and it is assumed, therefore, that the thermocouple calibration did not change by a significant amount during the course of the work.

(b) Manganin coil temperature calibration.

For the purpose of this calibration, the gauge was assembled in its working position in the high pressure equipment, and its temperature measured by the adjacent thermocouple. An air thermostat, constructed around the massive steel assembly, was employed to adjust the gauge temperature. The resistance of the gauge was measured at a number of temperatures between 14 and 32°C, and the results of coil resistance versus thermocouple e.m.f. are plotted in Fig.27, for calibrations at the beginning and end of the experimental work. Although the second calibration gives higher gauge resistances than the first calibration, the resistance difference between the two curves is the same at all temperatures, and the temperature corrections applicable to the coil are assumed, therefore, to be the same throughout the work. As it has been shown that the thermocouple calibration remained unchanged, the difference in the two calibrations in Fig.27 must be due only to drift in the coil resistance.

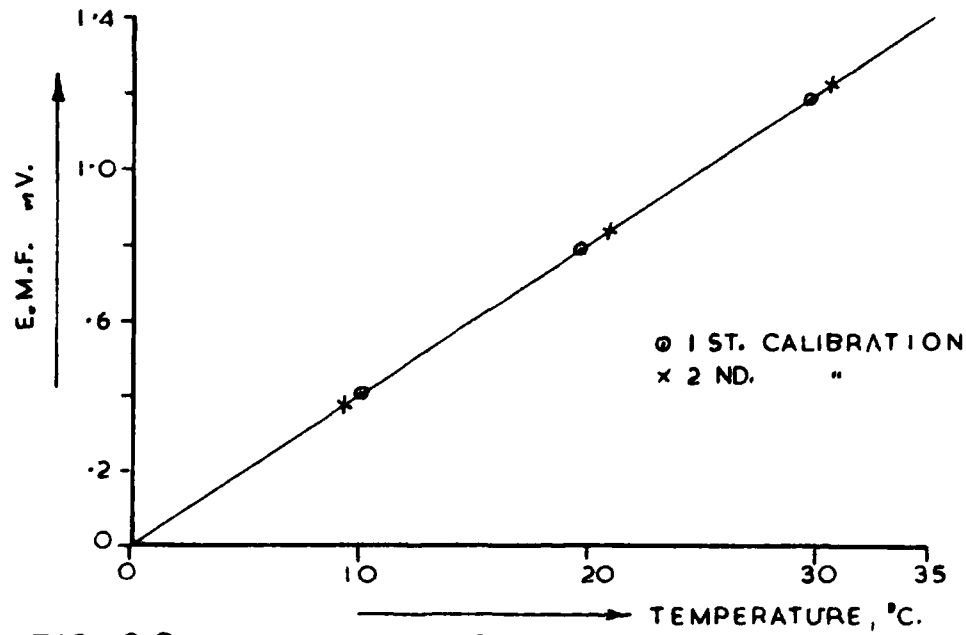

FIG. 26. GAUGE THERMOCOUPLE CALIBRATION.

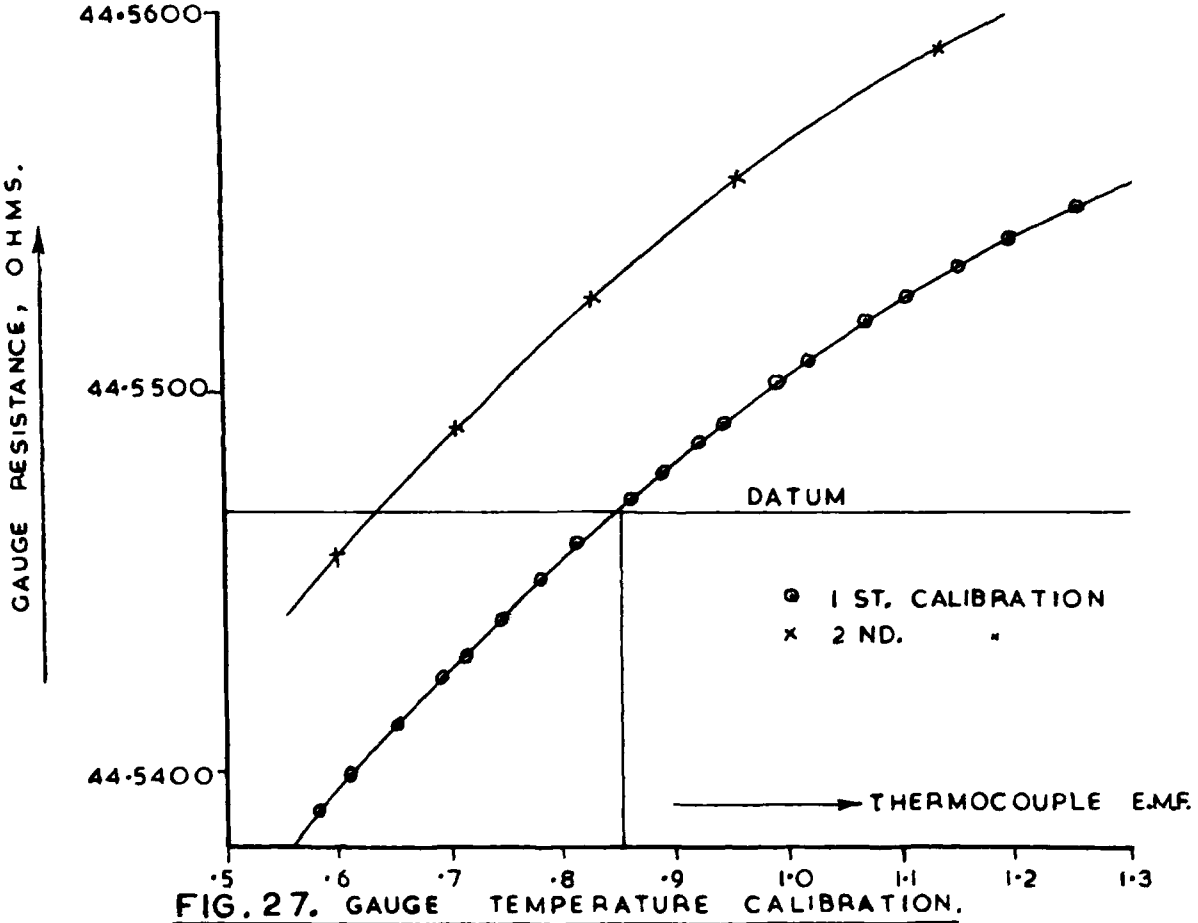

FIG. 27. GAUGE TEMPERATURE CALIBRATION.

An arbitary datum of .85mV. was taken for all gauge measurements, and gauge resistances corrected to this datum. It is assumed that the temperature characteristic of the gauge under pressure is the same as at atmospheric pressure. In calibrating the gauge, an apparent temperature hysterisis, equivalent to 2kg/cm^2, was observed, which occurred if the gauge resistance was measured whilst the whole assembly was drifting upwards in temperature, as is the case during the day, and then re-measured during late evening, when the temperature drifts are reversed. The coil resistance from these two measurements, corrected to the datum, differs by the equivalent of 2kg/cm^2, the first measurement giving the lower value. It is unlikely that there is a real temperature hysterisis, and the probable cause is a temperature lag during drifts, between the gauge and the adjacent thermocouple. A temperature lag of .1°C is sufficient to cause the apparent hysterisis.

(v) Gauge Pressure Calibration.

Ideally, a manganin coil pressure gauge should be calibrated over its whole pressure range against a free piston gauge. However, as such an instrument was not available, the gauge was calibrated up to 3,000kg/cm^2 against a free piston gauge, and at about 7,718kg/cm^2 against the freezing pressure of mercury at 0°C. The remainder of the range is covered by interpolation and extrapolation of the calibrations.

In addition to these calibrations, the 3,000kg/cm^2 gauge itself had to be calibrated.

(a) Calibration of free piston gauge.

The free piston gauge employed for calibrating the manganin coil to 3,000kg/cm^2, was a Budenberg piston and cylinder assembly of .005in^2 nominal cross section, number K347. K347 was calibrated against a similar piston and cylinder assembly, number K346, which had been calibrated at pressures up to 3,000kg/cm^2 by the National Physical

Laboratory, to 1 part in 30,000.

The weights and weight carriers for loading the pistons were all weighed to the nearest .01g on a 15Kg balance, and the balance weights employed for this task were themselves checked against an N.P.L. calibrated weight.

The two pressure balances incorporating the piston and cylinder assemblies were set up as shown in Fig.28. A pressure supply to the system was made by connecting it to the high pressure intensifier, via the let down valve, and a 100,000p.s.i. hand valve was employed as a screw injector for fine adjustment of the pressure. The pressure transmitting fluid used in this experiment was a mixture of 1 part DTD585 hydraulic fluid to 3 parts liquid paraffin, which was found to give a very low leakage rate past the pistons at 3,000 kg/cm^2, yet giving rapid pressure transmission through the 1/16 inch tubing connecting the pistons,

At a number of pressures between 0 and 3,000kg/cm^2, weights were adjusted on to the two pistons, so that, when rotating, each floated on the pressurised fluid without either rising or falling. The balanced loads could be adjusted to a sensitivity of .5g in 100,000g.

Fig.29 shows the piston area of K347 versus pressure, calculated from the balanced loads on the two pistons, and the certified area versus pressure of K346. The calibration is estimated to be correct to 1 part in 15,000.

(b) Calibration of gauge against K347.

The manganin coil was calibrated against free piston gauge K347 at the beginning and end of the experimental work. The equipment was set up as in Fig.28, but with one dead weight tester only, and the same pressure transmitting fluid was used as in experiment (a). A 30 minute period was allowed in each measurement for the attainment

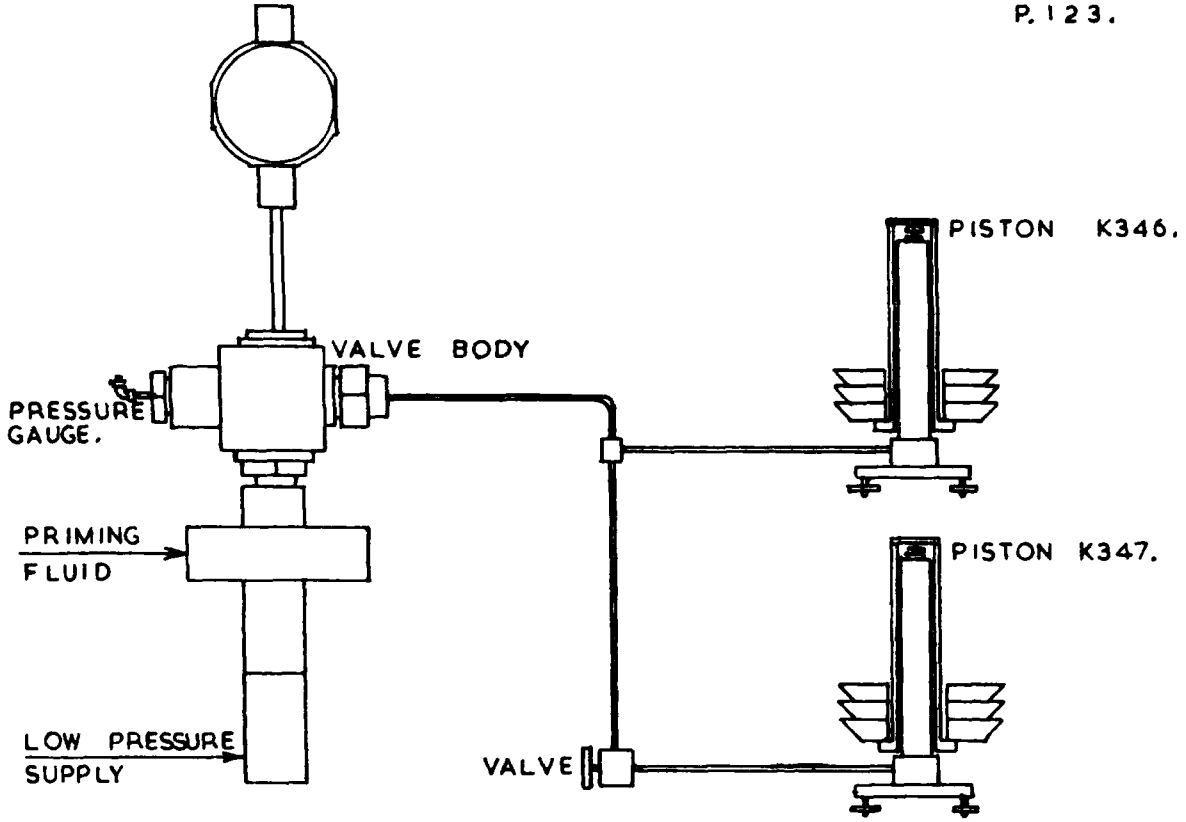

FIG. 28. CALIBRATION OF FREE PISTON GAUGE K347.

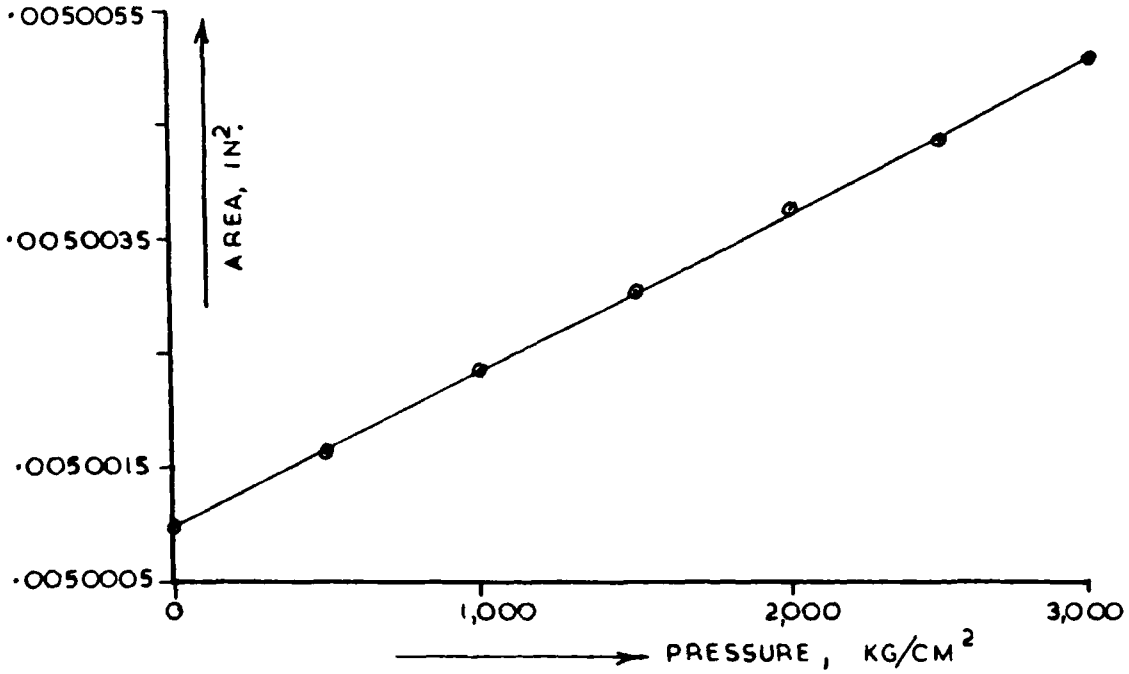

FIG. 29. AREA OF FREE PISTON GAUGE K347.

of pressure and temperature equilibrium.

The results of the calibration, expressed as P versus $\Delta\Omega/\rho$, are shown in Fig.30. The error associated with each experimental point arises from an error in measuring the gauge resistance at atmospheric pressure and at pressure P, and from applying the various temperature corrections. This error is estimated to be the equivalent of $\pm$ 2.0kg/cm^2, and the resulting calibration line through these points is considered accurate to $\pm$ 1.0kg/cm^2.

Referring to Fig.30, calibrations 1 and 2 were carried out at the beginning and end of the experimental work, separated by 9 months, and the resulting pressure coefficients differ by 2 parts per 1,000. During this period, the gauge base resistance at .85mV rose from 44.5479ohms to 44.5508ohms, equivalent to a pressure change of 27kg/cm^2, but gradually fell again towards the end of this period to 44.5496ohms. After calibration 2, the gauge was calibrated against the mercury freezing point, and immediately after this experiment, the insulation of the gauge broke down. A deterioration of the insulation presumably caused the slight decrease in coil resistance, and the fault was traced to the insulation on one of the coil connecting wires being incorrectly applied.

The insulation was repaired without disturbing the coil itself, and on doing so, the coil resistance returned to 44.5507 ohms. The calibration was repeated (calibration 3) as a check on 2, after repair of the insulation, and it can be seen from Fig.30 that the final calibration, 3, is much closer to the first calibration (1), than the calibration with the faulty insulation, 2. A check was made for pressure-resistance hysterisis, but none could be detected.

(c) Calibration of gauge against the freezing pressure of mercury.

The freezing pressure of mercury at 0°C was determined by Bridgman as 7,640 $\pm$ 8kg/cm^2 [17]. More recent determinations by Johnson and Newhall [70], and by Zhokhovskii [145] found the press-

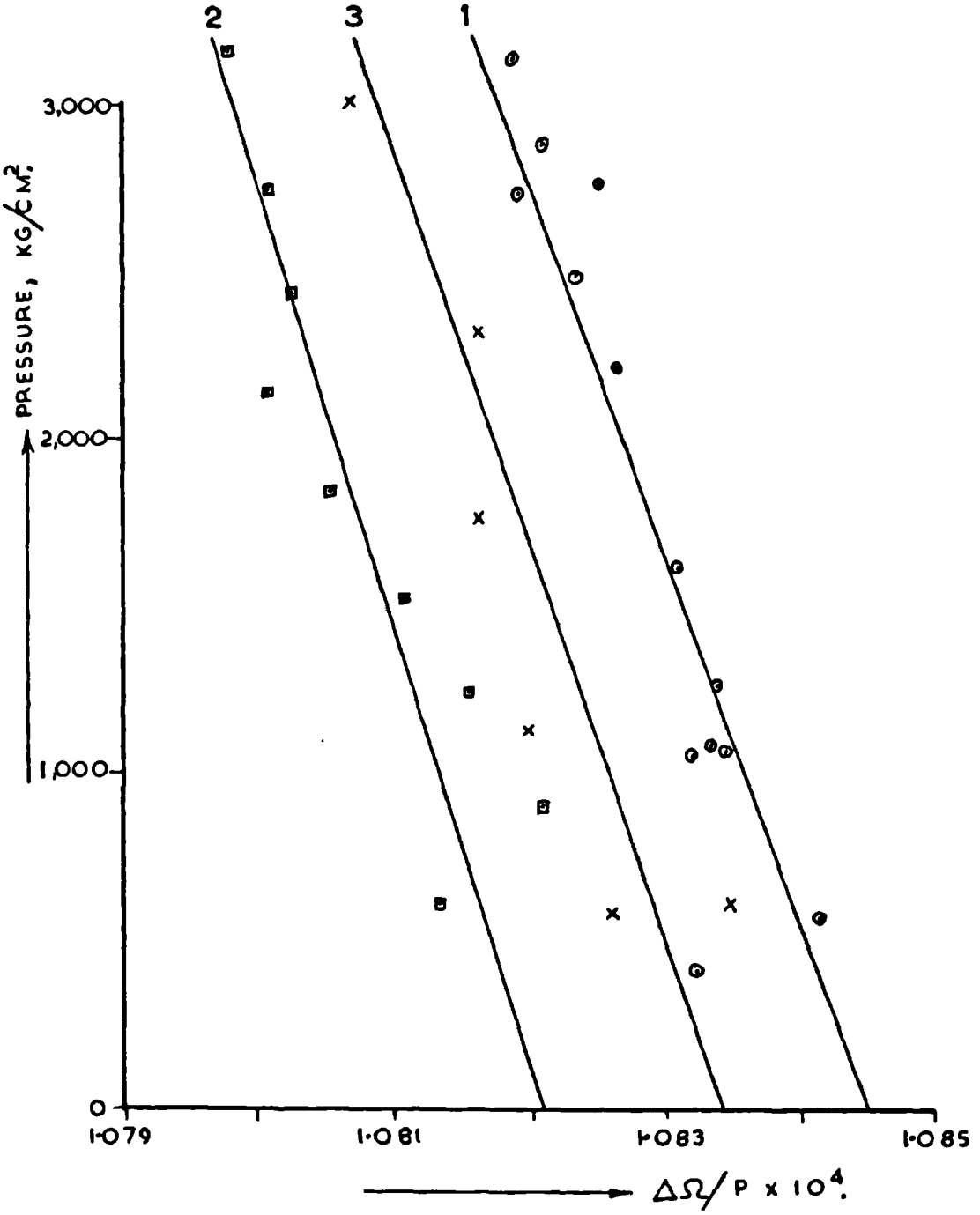

FIG. 30. CALIBRATION OF GAUGE TO 3,000 KG/CM²

ure to be 7,716.0kg/cm^2 and 7,710.0kg/cm^2 respectively. A re-determination by Newhall, Abbot and Dunn [108], the most recently published work, gives the pressure as 7,714.6kg/cm^2, (gauge) $\pm$4kg/cm^2, and a determination by the National Physical Laboratory [32] gives the freezing pressure as 7,718.5 $\pm$ 2kg/cm^2. All of these freezing pressures were determined against a free piston gauge.

The freezing of mercury may be detected either by the decrease in volume or electrical resistance, it being 4% and 75% respectively. As the temperature dependence of the freezing pressure is very sensitive (.0056°C per kg/cm^2), the advantage that the resistance method offers, in keeping heat capacity to a minimum, is important.

The mercury cell constructed for the calibration is illustrated in Fig.31. (The width scale of Fig.31 is expanded for clarity). The mercury is contained in a U tube, (1), made of P.T.F.E. sleeving of .012 inch bore and .018 inch o.d. The U tube is 24 inches high, and only the bottom third is filled, giving a mercury thread 16 inches long. The bend at the bottom of the U is quite sharp, and to prevent it pinching off the mercury thread, a short length of .006 inch diameter nichrome wire is inserted in the capillary at that point. The resistance of the mercury thread is about 8 ohms.

The P.T.F.E. U tube is contained in the 1/16 inch bore of a length of 200,000 p.s.i. Harwood Engineering tubing, (2), which has an outside diameter of $\frac{3}{4}$ inch. The bore of the tube is enlarged to a diameter of $\frac{1}{8}$ inch for a 2 inch length at each end of the tube. Standard 200,000 p.s.i. Harwood Engineering components, (3), (4), and (5) are employed at each end of the pressure tube to couple it to a standard 200,000 p.s.i. elbow (6), at the top, and to an electrode unit (7), at the bottom. The latter consists of a 1.5mm diameter Thermocoax wire, having a single nichrome conductor, hard soldered into an EN26

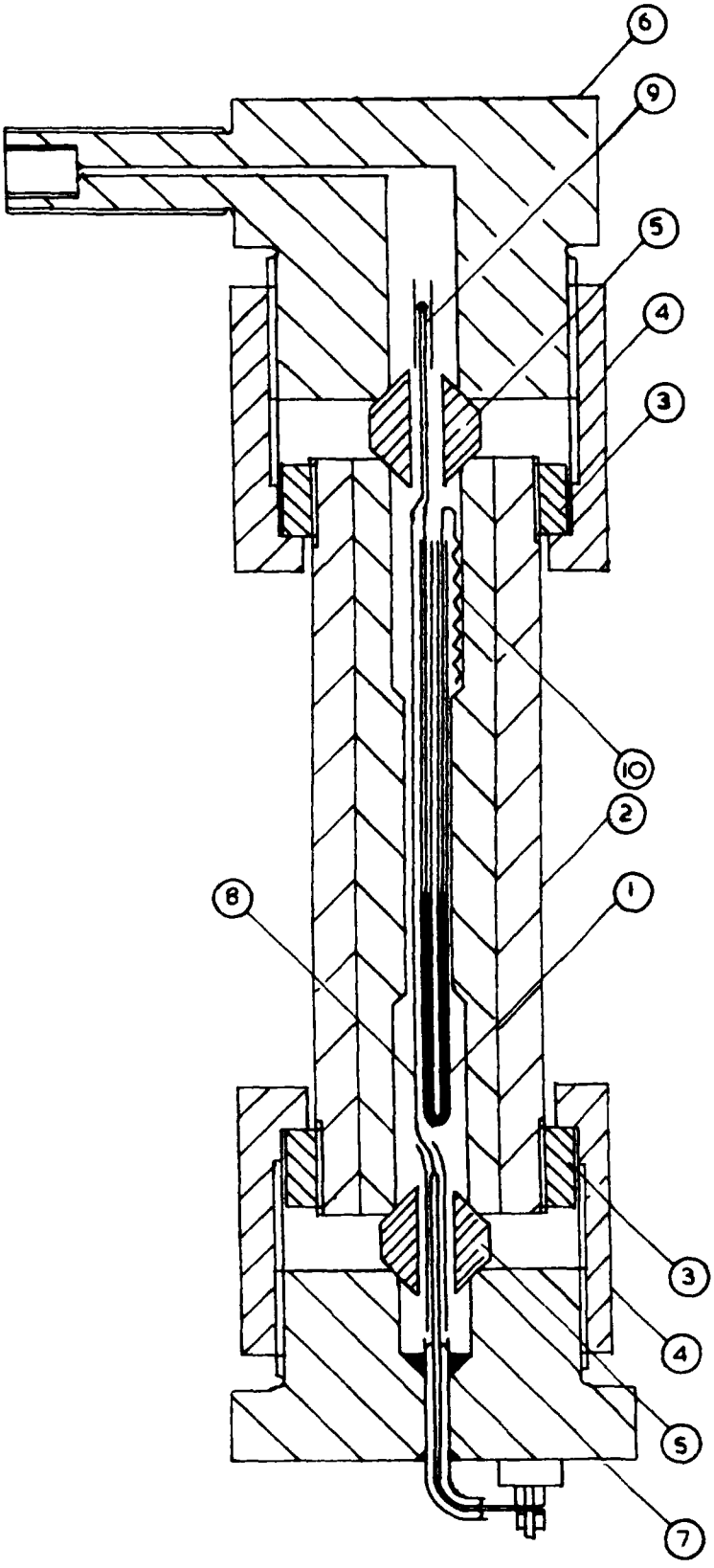

FIG.31. MERCURY FREEZING CELL.

steel plug. A P.T.F.E. insulated wire, (8), is soldered, at its lower end, to the nichrome electrode, and passes up through the 1/16 inch bore. At its top end, at (9), it is soldered to a .006 inch diameter nichrome wire which dips down into one limb of the mercury U. A second nichrome wire, forming an electrode to the second mercury limb, is connected to a beryllium copper corrugated spring, (10), which is forced into the top end of the pressure tube to form a ground connection.

The mercury was limited to the lower third of its U tube, so that heat conduction to the mercury, along the pressure tube, could be eliminated. Also, during development work on the cell, it was found that if the mercury was anywhere near the top of a capillary, it would sometimes overflow in one limb only, on pressurisation, and short circuit the system against the pressure tube.

The capillary was first completely filled with Analar mercury, and to avoid air locks, the filling was achieved by straightening the U to a vertical column, and injecting the mercury at the bottom with a hypodermic syringe. The capillary was then reverted to a U, and both ends immersed in petroleum ether. Raising and lowering the end of one limb then served to drain off the excess mercury, and to fill each limb with petroleum ether. The cell was then completed by assembling as shown in Fig.31, and filling with petroleum ether. In the assembled form, the cell resistance is about 50ohms, most of which is due to the nichrome electrodes.

The manganin coil was calibrated against the mercury cell, as shown in Fig. 32. The cell, coated with silicone grease, was suspended in a $4\frac{1}{2}$ inches diameter glass tube, (1), and was connected by 100,000 p.s.i. tubing to a 100,000 p.s.i. hand valve, which, in turn was connected to the high pressure system in place of the let down valve. The three way hand valve was arranged as a let down valve. The lower half of the glass tube, (1) was surrounded by a 12 inches

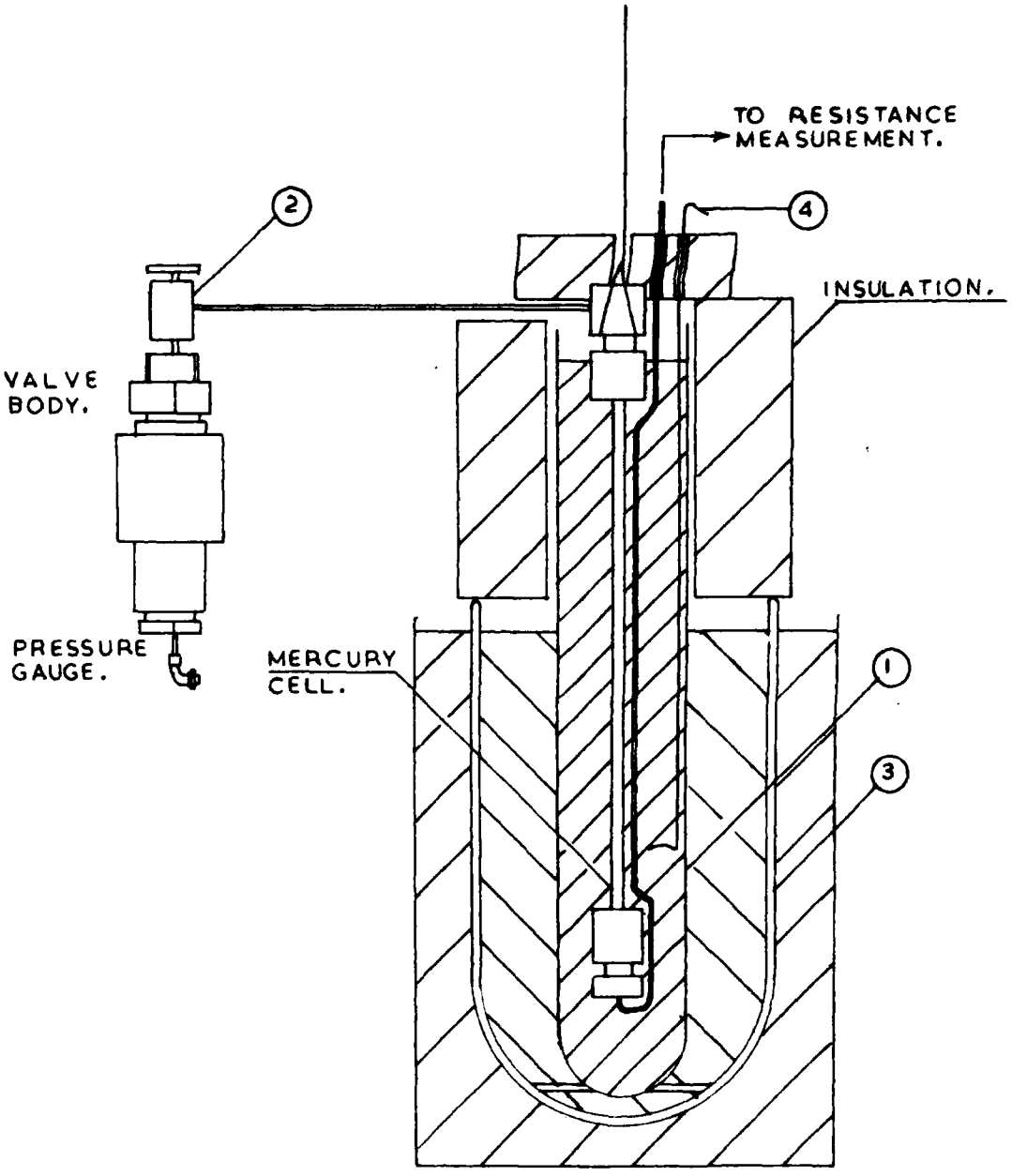

FIG. 32 . CALIBRATION OF GAUGE AGAINST MERCURY CELL.

diameter dewar (3), contained in an insulated box, and a Wheatstone bridge was used to measure the cell resistance.

During preliminary experiments with the cell, it was found that the mercury could be taken considerably above its freezing pressure without freezing. It was also found that the kinetics of the melting of the mercury were extremely fast, whereas the kinetics of freezing, when both phases were present, were so slow that at pressures several kg/cm^2 above the freezing pressure, no change in the quantity of solid phase could be detected during a 1-hour period.

As the freezing pressure of mercury is close to 110,000 p.s.i. the tubing and valve employed in the equipment are overloaded by 10%, leaving no significant margin in hand for superpressing the mercury. In practice, the mercury was frozen initially by cooling the cell to $-10^{\circ}C$, with alcohol and solid carbon dioxide in dewar (3), and raising the pressure in the system to $7,780 kg/cm^2$. Once the mercury was frozen, glass tube (1) was filled with small cubes of ice, prepared from distilled deionised water, dewar (3) was filled with crude ice, and insulation applied as shown.

The pressure in the system was adjusted by controlling the temperature of the main pressure vessel with its thermostat, and the pressure was reduced quite rapidly on the first attempt, to approximately locate the freezing pressure against the manganin coil resistance. The mercury was then refrozen, and the pressure reduced very slowly to approach the melting point of the mercury. The complete melting of the mercury gave a rise in resistance of 6 ohms in the cell. The middle third of this resistance change was utilised as the calibration point, as this is likely to represent the purest portion of the mercury, and it was found that the chosen 2 ohm melting range could be spread over a 30-minute period, with no detectable pressure change in the system. During the melting period, the pure ice and water surrounding the cell was agitated frequently with a stainless steel rod, (4).

As the viscosity of the pressure transmitting fluid employed in this experiment (petroleum ether) is very low, and the physical size and capacity of the mercury cell is small, any temperature or pressure error arising in the detection of the melting point of the mercury is small, but a $\pm$ 1kg/cm^2 error is placed on the result to allow for possible error in temperature control. In addition, it is estimated that the error in detecting the resistance of the manganin gauge, at the freezing pressure of mercury, is the equivalent of $\pm$ 2.0kg/cm^2. Superimposed on this error is the uncertainty of the value of the freezing pressure of mercury. Considering the mean values of Newhall et al [108] and the N.P.L. [32], and the mean of their errors, the freezing pressure of mercury is taken, for the purpose of this work, as 7,716.6 $\pm$ 3kg/cm^2. The total error in calibrating the manganin gauge against the freezing pressure of mercury, is, therefore, $\pm$ 6.0kg/cm^2.

The results of the calibrations of the manganin gauge against the freezing pressure of mercury are shown in Fig.33, together with the calibrations up to 3,000kg/cm^2. The first, second and third calibrations with mercury were carried out immediately after the corresponding calibrations at 3,000kg/cm^2. It was after the second calibration with mercury that the gauge insulation failed, and the third calibration was completed shortly after the repair. Only calibrations 1 and 3 are considered for the purpose of calculating pressure, and it is assumed that the small difference which exists between the initial and final calibrations has occurred uniformly and gradually over the time period between the calibrations.

It is estimated that the extrapolation of the calibration to 10,000kg/cm^2 leads to an error of $\pm$ 10kg/cm^2 on measurements at that pressure. Between 6,000 and 8,000kg/cm^2, the error in measuring pressure is estimated at $\pm$ 8kg/cm^2; between 4,000 and 6,000 kg/cm^2 it is $\pm$ 5kg/cm^2, and below 4,000kg/cm^2, $\pm$ 3kg/cm^2.

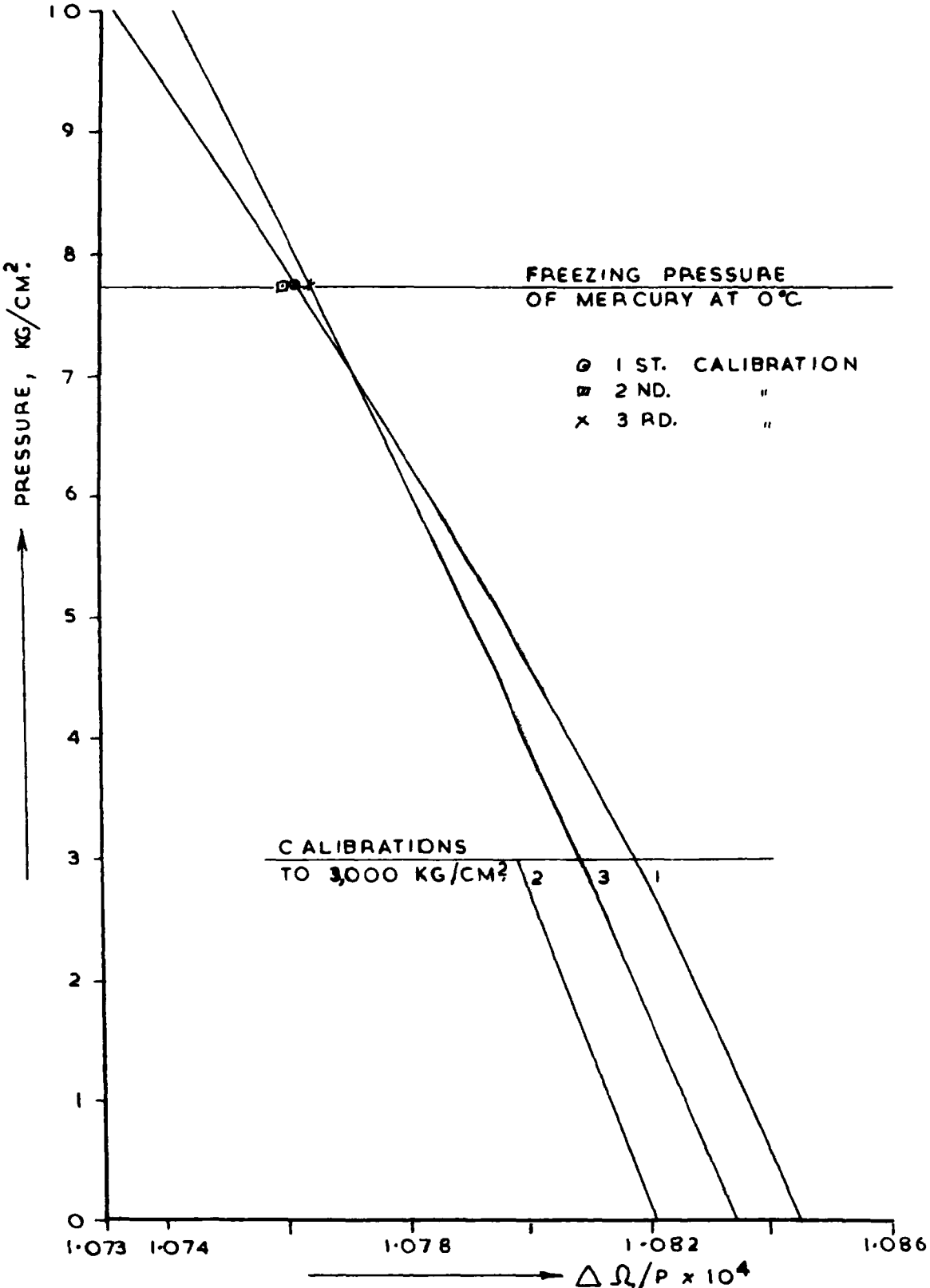

FIG. 33. CALIBRATION OF MANGANIN COIL PRESSURE GAUGE.

The resistance of the manganin gauge is certainly not linear with pressure, but is concave to the pressure axis. The increase in the base resistance of the gauge during the course of the work appears to have decreased the pressure coefficient at low pressure, and increased it at high pressure, with the result that the gauge approaches a little closer to linearity.

CHAPTER 8.

ANCILLARY EQUIPMENT.

(i). Main Structure.

The main framework, carrying all the equipment except the instruments, is shown in Plates 5 and 6. The emphasis in its construction is on rigidity, and it is assembled mainly from $2\frac{1}{2} \times 2\frac{1}{2} \times \frac{1}{4}$ inch mild steel angle, bolted together, and, in some places, welded. The framework is mounted at six points on "Tico" vibration pads, $\frac{1}{2}$ inch thick, and loaded to 50p.s.i. These pads are sufficiently stiff and stable to maintain the framework level.

A thermostat tank, fabricated from $\frac{1}{8}$ inch plate, welded and galvanised, is bolted at its base to the framework, with a layer of heat insulating material interposed between the two. The top of the tank is bolted to the framework so that lateral loads are transmitted, but relative vertical movement between the two may take place. In this way, the tank adds to the rigidity of the structure, and allows the hot tank to expand with respect to the cool framework. The tank is insulated on its sides by a 1 inch layer of cork, and a layer of hardboard.

A welded steel subframe, for carrying the pressure vessel, is suspended in the tank, as shown in Fig. 34. This rigid assembly is bolted at the top to the mainframe, and at its lower end, it is located by set screws bearing against the sides of the tank, permitting thermal expansion movement.

The high pressure system, other than the vessel, is surrounded by $\frac{1}{4}$ inch mild steel plate, except at the top. Two sides of the plate enclosure are in the form of three hinged doors, which have been removed in Plate 5.

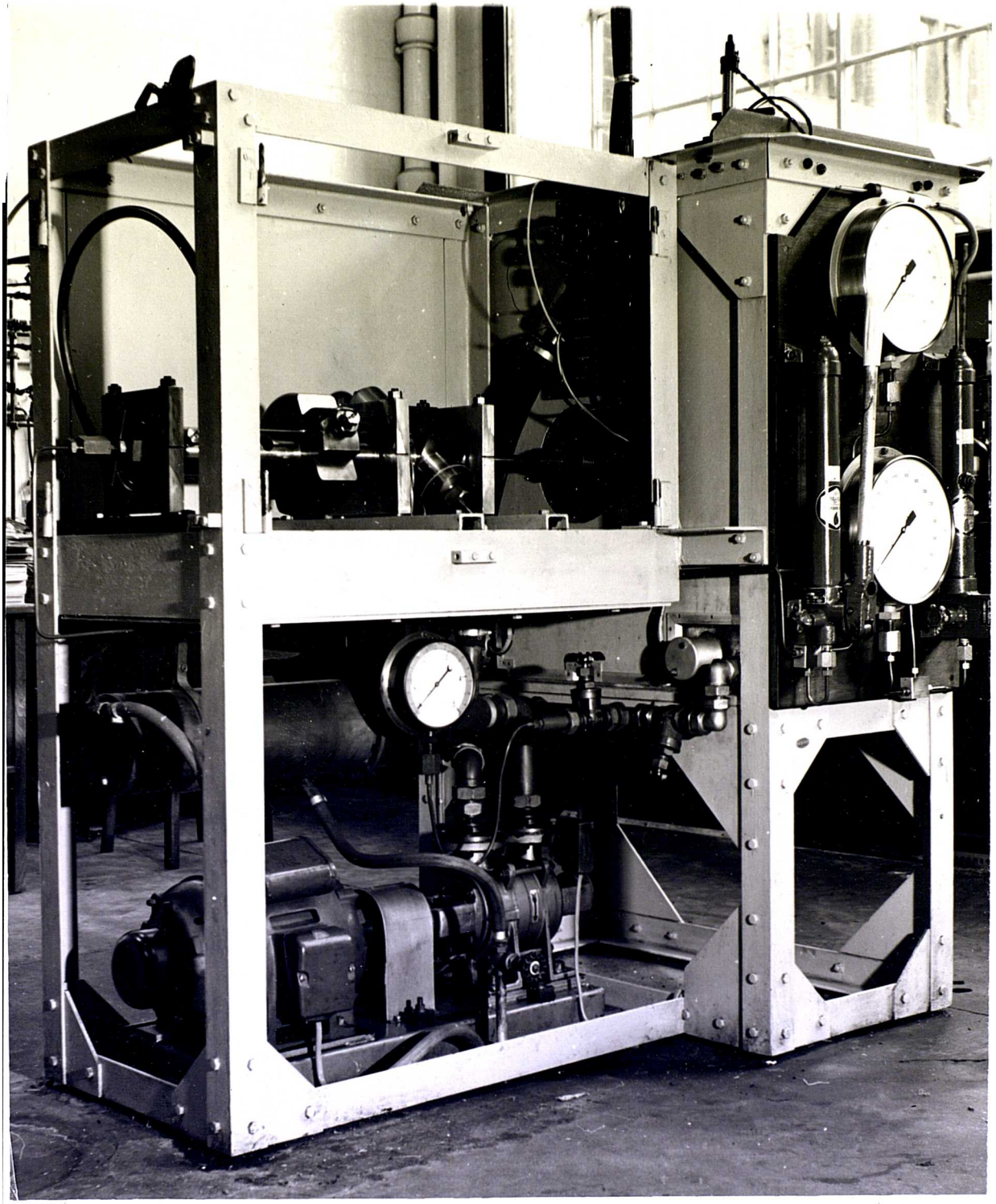

PLATE 5.

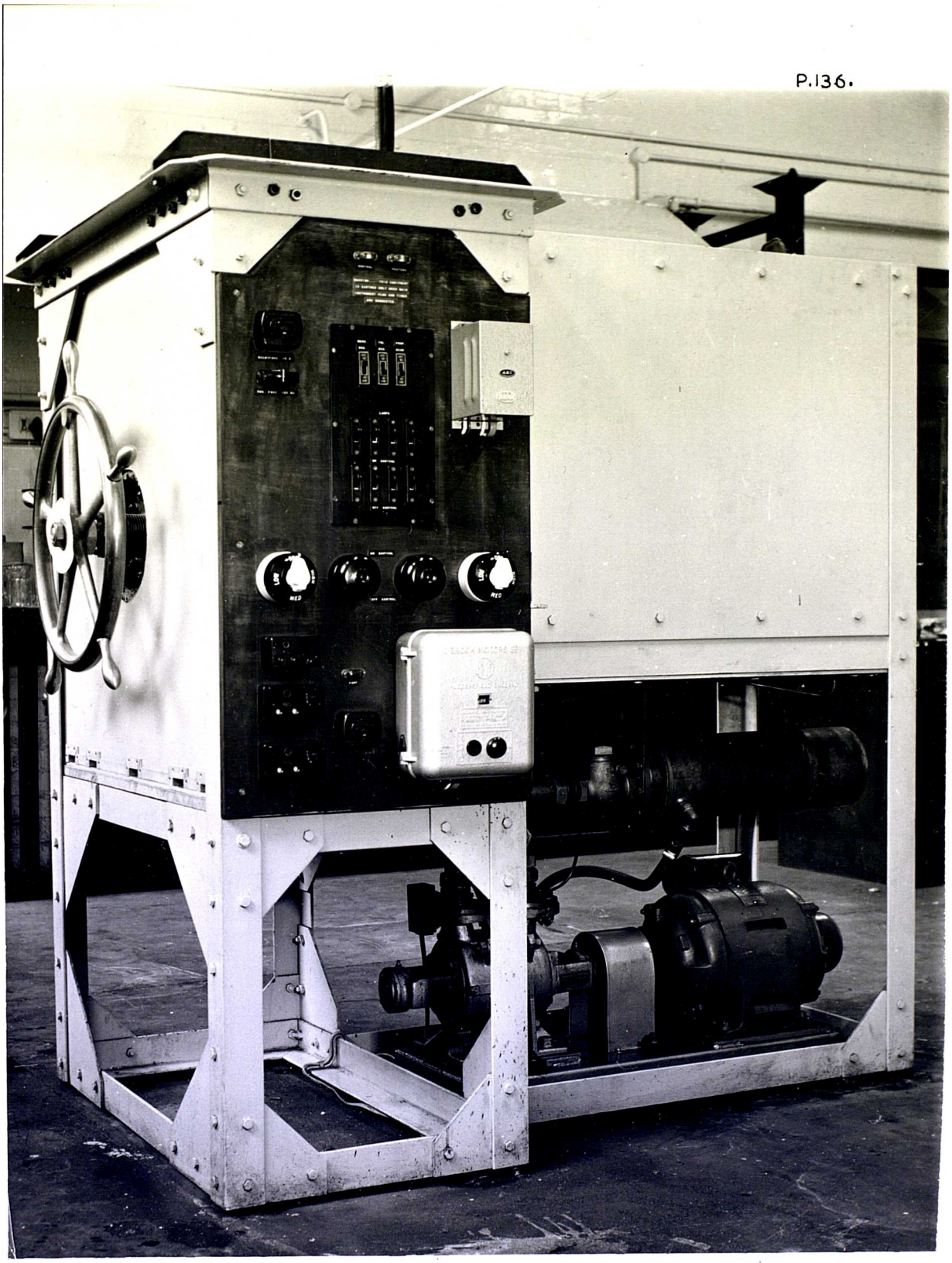

PLATE 6.

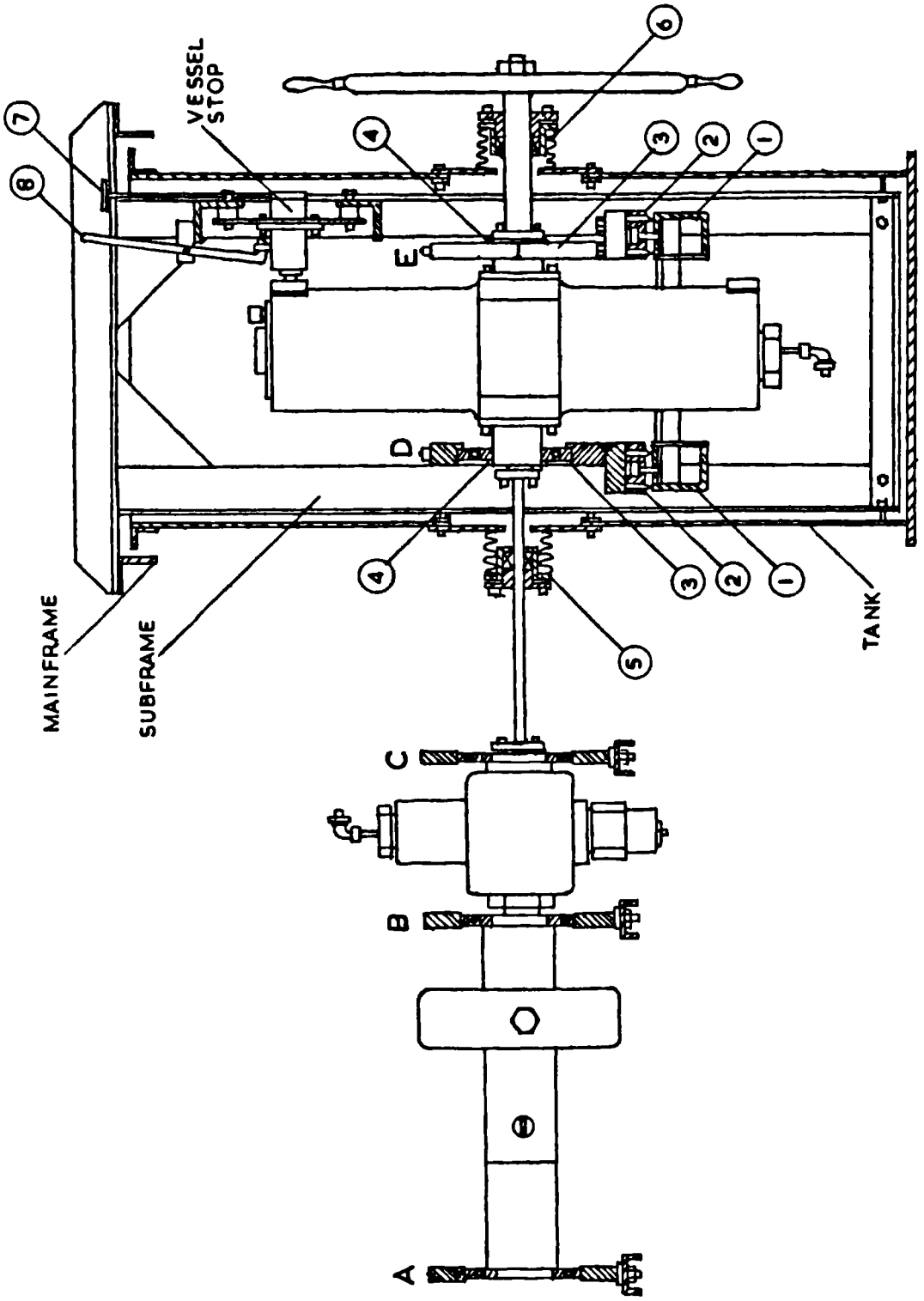

FIG. 34. MOUNTING OF THE HIGH PRESSURE SYSTEM

(ii). Mounting of the High Pressure System.

The important aspect of mounting the pressure system, is the alignment of the vessel, illustrated in Fig. 34.

The vessel is supported on two horizontal 3 x 2 inch channel sections, (1), which are an integral part of the welded subframe. The channels have plates welded on their open sides to improve torsional rigidity. Attached to the top of each channel is a length of 2 x 1 inch steel ground flat stock, (2), fixed by an arrangement of countersunk cap screws, and cone pointed socket set screws, so that the level of the ground flat surface may be adjusted. The surfaces were adjusted horizontal and level with each other to an accuracy of .0005 inch in 10 inches with a precision spirit level. During this operation, the framework was loaded with weights to simulate the effect on the vibration pads, of the weight of the pressure vessel and a tank load of thermostating fluid.

The strips of ground flat stock form an accurately aligned bed for the pressure vessel bearings. The mild steel bearing housings, (3), are of welded construction and are split. In manufacturing these, the boring operations were completed first, and the pair of housings were assembled on a cylindrical mandrel of the same diameter as the bearing outer race. When so assembled, their bases were surface ground in one operation, producing a pair of housings whose height from base to axis is identical. The bearing housings are bolted to their adjustable beds, and the vessel is assembled in its bearings as shown in Fig. 34. The vessel is located longitudinally by the screwed rings, (4). By this method of construction, the vessel ends are maintained horizontal, in the plane of the bearing axis, to .001 inch in 10 inches.

Bearings A, B and C are mounted in simple aluminium alloy housings, bolted to horizontal channel sections on the main framework.

As the bearings are self aligning, only the position, and not the plane of the housings, needed adjustment, and this was achieved by shimming. The aluminium housings were set up with respect to bearings D and E with a long, straight, ground bar passing through the whole assembly. The axis of ABC was set .005 inch below the axis of DE. As the thermostat temperature rises, axis DE drops, and at 100°C, it is .010 inch below the axis ABC.

The provisions for rotation are completed by glands, (5), on the pressure pipe, and (6) on the handwheel shaft. These are conventional stuffing box arrangements, except that a bellows accommodates the 1/32 inch relative movement between the shafts and the tank.

(iii). Vessel Stop.

A cross section of the vessel indexing system, is shown in Fig. 35. It consists of a rigidly mounted cylinder, and a closely fitting piston, loaded, with a pair of concentric coil springs, to about 40lbs. thrust. A pin, (1), screwed into the side of the piston, and projecting through a longitudinal slot in the cylinder, allows the piston to be pushed back against its springs by a lever, not shown in Fig.35. A hardened wheel, (2), on the end of the piston, engages a V-shaped slot in a hardened steel ramp, (3). A ramp is bolted to each end of the pressure vessel, allowing it to be locked either end up.

Projecting out of the top end plate (4), (but not shown in Fig. 35), is an adjustable orifice, which controls the degree of hydraulic damping of the piston movement. The vessel stop is normally immersed in thermostating fluid, which provides the piston damping.

The indexing mechanism is shown in its working position in Fig. 34, bolted to the subframe. The lever for withdrawing the piston is shown at (8) and the damping valve is shown at (7). When the vessel rotates towards the vertical position, the piston rides up the ramp,

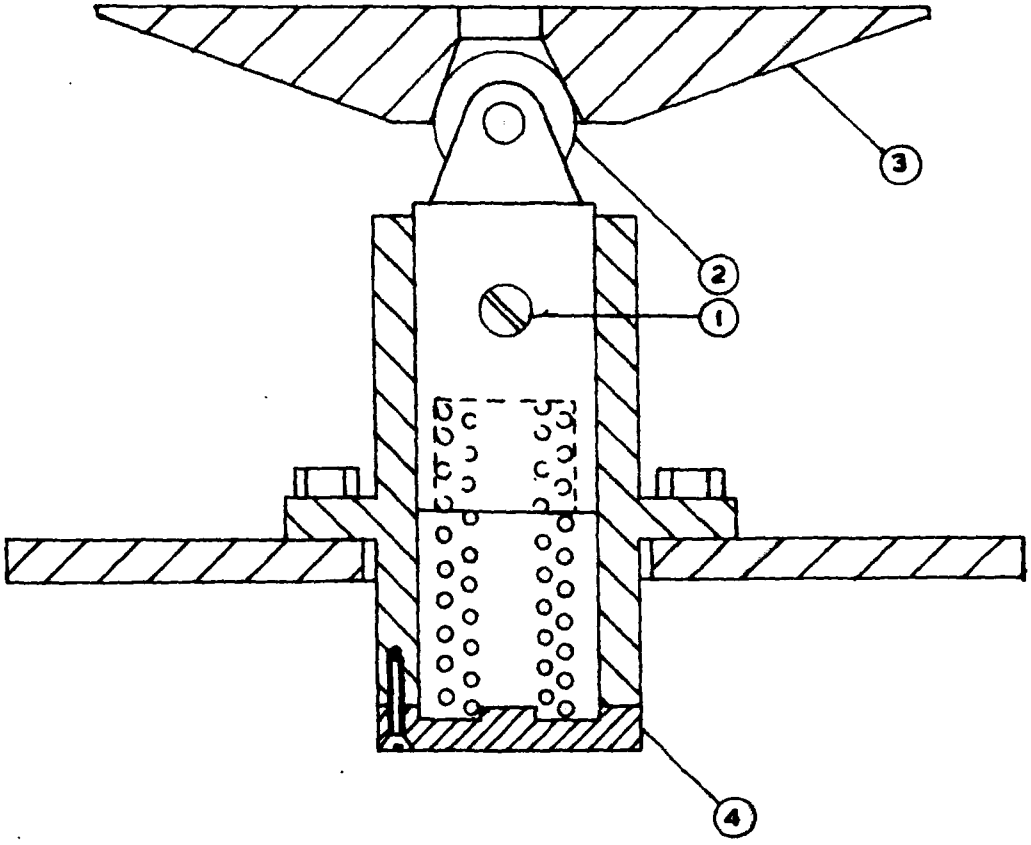

FIG. 35. VESSEL STOP.

and retards the vessel by virtue of the spring loading, and the hydraulic pressure behind the piston. If the vessel has slowed sufficiently by the time it is vertical, the piston engages the slot, and locks the vessel. If the vessel is moving fast, the piston will partially engage the slot, but the momentum of the vessel will drive the piston back up the V-ramp, and allow the vessel motion to continue. This mechanism prevents accidental overloading of the system, and limits the torque transmission along the pressure pipe. In service, the damping valve, (7), is adjusted to give the system the desired characteristics.

The indexing mechanism was adjusted by altering the position of the ramps on the vessel, this adjustment being carried out with the precision spirit level. The vessel is maintained vertical in the plane of rotation, by its stop, either end up, to an accuracy of .0015 inch per 10 inches.

(iv). Temperature Control.

For controlling the temperature of the pressure vessel, the tank is filled with 60 gallons of thermostating fluid. At temperatures above 20°C, Shell Tellus 23 oil was employed, which was replaced at lower temperatures by demostic kerosene. The fluid is circulated by an external turbine pump, which can be seen in Plates 5 and 6. The delivery of the pump at low heads is 1,200g.p.h., and is driven by a 2 h.p. single phase motor. The pump base is not attached to the main-frame, but is mounted on the floor on vibration pads. Sections of rubber hose in the pipe lines help to isolate pump vibration from the main-frame. The thermostat fluid is drawn from the tank at a point 4 inches below fluid level. The pump delivery passes through a specially designed 5 sq. ft. water cooler, and then divides into two streams. The fluid enters the tank at the bottom corners (see Plate 5), and distributor pipes inside the tank eject the two streams of fluid

across the bottom of the tank, so that they meet head on, and create a considerable degree of turbulence. A non return valve in the pump delivery line prevents the escape of the tank contents in the event of a hose failure, and a pressure sensitive switch, also in the pump delivery, stops the pump in the event of such a failure. The pipework is arranged so that the pump may be utilised for emptying and filling the thermostat tank.

The thermostat is heated by two $1\frac{1}{2}$ Kilowatt, three heat immersion heaters. The end of one of these can be seen in Plate 5, and they are placed directly in the fluid stream from the distributor pipes. Low powered heating is supplied also by four 100 watt lamps completely immersed in the fluid.

Heating is controlled by a mercury-toluene regulator, fitted with a standard proportioning head, or alternatively, a mercury contact thermometer. The latter can be pre-set, and is employed as a control during warm up. Both controllers perform their switching through an electronic relay. The heating system is wired so that each heater may be controlled or uncontrolled, and the system is operated with an uncontrolled heat load and a superimposed controlled load.

The thermostat will work satisfactorily at 25°C when use is made of the water cooler, and lower temperatures may be achieved by circulating a chilled coolant through the heat exchanger.

At any temperature, the thermostat control system caused a cyclic temperature variation of .01°C, with zero short term drift, and the temperature drift over a 24 hour period was .05°C. This drift which was caused by a change in ambient conditions affecting the operation of the proportioning head, was slow, and therefore easily corrected. Temperature variations throughout the tank were found to be .03°C, but no cyclic or random variation could be detected inside the pressure vessel.

The thermostat temperature was measured by mercury-in-glass

thermometers, and the point selected for temperature measurement was found to correspond to the temperature inside the pressure vessel. The thermometers were calibrated against a platinum resistance thermometer, to the nearest .01°C., which, in turn, was calibrated against the ice, steam and sulphur points.

It is estimated that the temperature of the viscometer inside the pressure vessel, was measured correct to $\pm$.02°C.

CHAPTER 9.

CALIBRATION AND PERFORMANCE OF VISCOMETER.

(i) Timer.

The accuracy of the timing system is dependent on the stability of the time period counter, and the reproducibility of the position of the sinker at which triggering occurs. The performance of the system at atmospheric pressure and temperature has been dealt with in Chapter 3, and under these conditions, it was found that the triggering position was dependent on how well the bridge was balanced, and that the balance point was sufficiently reproducible to give .02% reproducibility on the triggering position.

When the pressure and temperature are changed, it is found that the timing bridge circuits go out of balance, the balance point being highly temperature dependent, and only slightly pressure dependent. The main cause of these temperature and pressure effects is that each coil of a pair on the viscometer tube is not of identical resistance. A change in temperature, or pressure, changes the coil resistance; as the coils are not identical, the change in each coil differs slightly, and there is, therefore, a change in the ratio of the impedance of the pair of coils, putting the bridge out of balance. The high temperature-resistance coefficient of copper, compared with its pressure coefficient, explains the difference in the order of the two effects.

It was found that to re-balance the bridge required mostly readjustment of the resistive part of the balancing system, but a small degree of phase shift was also required, which was achieved by means of the variable capacitance in the circuit. It is thought that most of the phase shift is caused by the inductive winding of the potentiometer which forms the resistance adjustment.

The need for rebalancing the timing circuits, on changing temperature and pressure conditions, introduces an uncertainty as to whether or not the rebalancing changes the position of the magnetic centres of the pairs of coils, apart from changes caused by normal expansion and contraction of the length of the viscometer tube.

The method of checking the temperature and pressure dependence of the timing system is illustrated in Fig.36. In place of the normal sinkers in the viscometer tube is a solid stainless steel sinker body whose length is a little shorter than the distance between the coil triggering positions, L. A stainless steel screwed rod protrudes from each end of the sinker body, and on each of these, there is screwed a soft iron disc of the same dimensions as the pellet carried in the normal sinkers, and a stainless steel locknut. The distance between the centres of the soft iron discs is adjusted to be slightly less than L, i.e. L - h. When this long sinker is allowed to fall through the coils, soft iron disc (a), will first trigger coils (1) and start the timer. On travelling a short distance, h, soft iron disc (b) will trigger coils (2) and stop the timer.

By suspending the sinker on a cathetometer base and measuring the vertical motion of the sinker between starting and stopping the timer, h was found to be .127cm.
Since L = 17.8cm., $\frac{h}{L}$ = 0.71%.

The principle of the experiment is to measure any small change in L by detecting a large change in h. By this means, low accuracy determinations of h, at various temperatures and pressures, allow an accurate assessment of any change in L.

If the viscometer is filled with a fluid whose temperature and pressure viscosity dependence is known approximately, variations in h may be determined by comparing the known relative viscosity

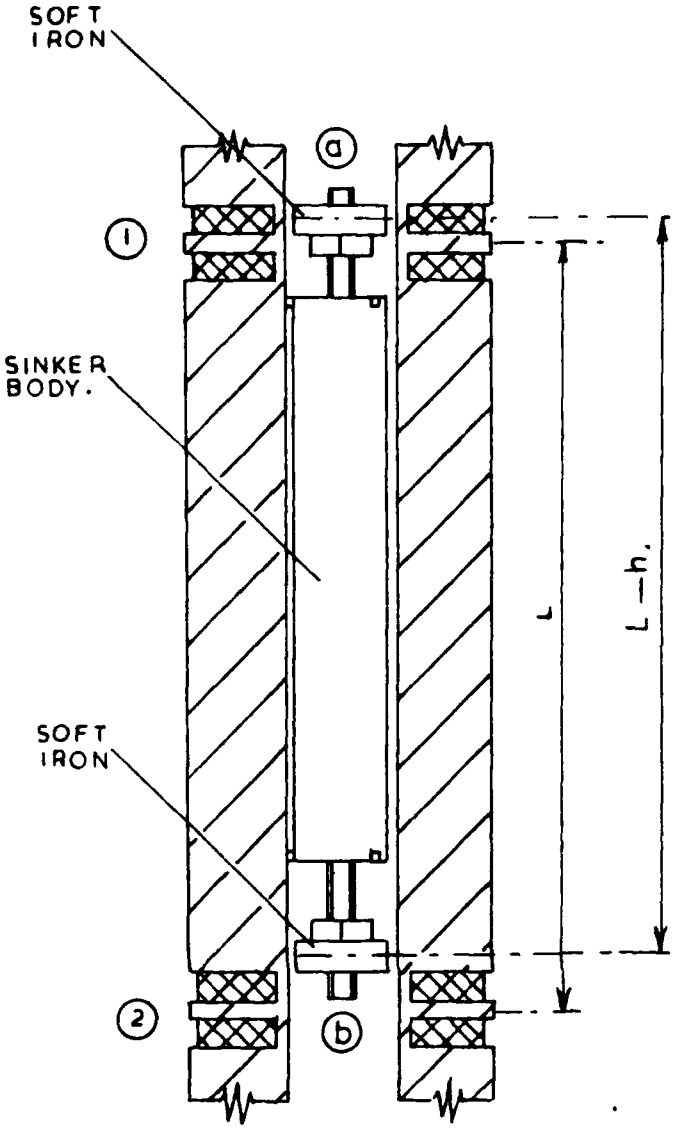

FIG. 36. THE LONG CALIBRATION SINKER.

with the relative viscosity calculated from measurements with the long sinker. For example, if the relative viscosity, calculated from the fall time of the long sinker, is found to be double the known relative viscosity, then h has doubled, and the distance between the magnetic coil centres has increased from 17.8cm. to (17.8 + .127)cm.

Any change in length of the viscometer tube, due to normal temperature and pressure effects, is compensated for by an identical change in the long sinker, except for the thermal and compressibility changes in the length h.

The accuracy of the experiment was limited by the accuracy of the viscosity data employed, and by the consistency with which the sinker fall times could be determined. The latter gave 12% variations, on means, caused by the tube and sinker not being perfectly straight, and the data were corrected to 3%.

The temperature dependence between 25 and 100°C, and the pressure dependence between 0 and 10,000kg/cm^2, were studied by using water in the viscometer, and the data employed ~~was~~ were that of Bingham and Jackson [13], for the temperature dependence, and some preliminary results from the present work for the pressure dependence of viscosity, calculated on the assumption that L does not change with pressure. The calculated viscosity changes were found to be the same as the known changes, within the experimental error, for both temperature and pressure variations, and it is concluded that h is constant, to within 15%, and L is constant, to within .1%.

(ii) Viscometer.

(a) General behaviour.

Most of the operating experience was gained with a stainless steel sinker of .004 inch radial clearance, constructed to the design shown in Fig.5e. However, other sinkers employed to a lesser

extent, showed the same behaviour as the .004 inch clearance sinker.

The fall time of a sinker was extremely sensitive to any contamination in the form of a second phase, either liquid or solid, and introduction of the slightest amount of contaminant into the viscometer was found to produce erratic fall times, causing variations of perhaps 5% or more in bad cases. In an extreme case the sinker would stick in the tube if solid particles comparable in size with the gap were present. When sufficiently free of contamination, the scatter of the fall times was normally within .2% for 8 or 10 falls, and often within .1%, giving a standard deviation of .05%.

All of the sinkers were found to possess a direction effect in their times of fall. The sinkers were reversed in the viscometer tube, and the directional effects were found to persist, showing that the effects were a property of the sinker rather than the tube. Because of the existence of this effect, the sinkers were always assembled in the tube the same way round. Similar effects were prevalent in the viscometers employed by Bridgman [19] and by the A.S.M.E. [5].

The .004 inch clearance stainless steel sinker was found to have the greatest directional effect, the difference in fall times in the two directions being 1%. If the bursting disc end of the viscometer is designated end 1, and the bellows end is designated as end 2, then, when assembling the viscometer the end of the sinker nearest the joint in the sinker body, (see Fig.5) was always placed nearest to end 2. It was found that the sinker falling from 1 to 2 gave a longer fall time than falling from 2 to 1.

A stainless steel sinker of .006 inch radial clearance, of similar construction to the .004 inch clearance sinker, and assembled in the same manner, was found to have a .2% directional effect. The fastest direction of fall was the same as for the .004 inch clearance sinker. An aluminium alloy sinker constructed with a symmetrically

placed joint in its body, as in Fig.5f, had a .1% directional effect.

The directional effect was probably caused by asymmetrical shape effects. In particular, the shapes of the ends of the sinkers were found to be difficult to produce symmetrically, with the machinery available. It may also be significant that the sinkers with an asymmetrically placed joint exhibited the greatest directional effect. The joints introduced a small circumferential valley on the sinker body, and the two halves were not properly matched. The smaller the radial clearance, the larger the effect of these imperfections would be, and this is reflected in the .004 inch clearance sinker having the largest directional effect. Apart from the joint in the aluminium alloy sinker being symmetrically placed, the two halves were the most accurately matched and this probably accounts for its superior performance.

Asymmetric mass distribution in the sinker would affect its tendency to tilt and fall eccentrically, and this factor, too, could introduce directional effects. Additional factors which could lead to this defect in a sinker are eccentricity and out of roundness in the machining operations, and the pieces of wire, forming the guiding pins, being of unequal length.

No special effort was made in the manufacture of this first generation of sinkers, as the extent of the problem was not appreciated at that time. In this study, no attempt has been made to improve on the performance of the sinkers, and their inherent defects have been allowed for in their calibration.

The directional effects were found to be constant over a certain range of fall times. No lower limit of time was found, but for each sinker, there was an upper limit of time above which the behaviour pattern of the sinker deviated from that already described. Beyond this limit, it was found that the fall time in one direction, i.e. the direction of shortest fall time, went through a period of

instability as the fall time increased. At even longer fall times, stability would again be achieved, but the directional effect would increase to perhaps 4%, rising, with increasing fall times, to perhaps 10%, together with a return to instability. This period of increasing directional effect was followed by a period of decreasing direction effect. The reasons for this behaviour are discussed in connection with the sinker calibration.

(b) Effect of a non-vertical viscometer.

The viscometer was assembled containing water and the .006 inch clearance stainless steel sinker. The vessel stop was adjusted so that the vessel was locked as near to vertical as could be measured with the existing arrangements, and the fall time of the sinker determined for these conditions. The indexing mechanism was then readjusted to lock the vessel at a variety of inclinations to the vertical, and the fall times again determined.

The results of these experiments are summarised in Fig.37. The first few minutes of inclination make very little difference to the fall time, but greater angles produce a reduction in the fall time. Inclination of the viscometer tube makes the sinker tilt relative to the tube, so as to provide hydrodynamic "lift", and the sinker will also take up a degree of eccentricity. The effect of eccentricity was shown in Chapter 4 to produce an increase in terminal velocity. However, the tilting of the sinker to produce lift tends to increase the drag on the sinker, and the overall effect of inclination depends on the relative magnitude of the effects of eccentricity and tilting. Scott [125] found that inclination of the viscometer could initially either increase or decrease the terminal velocity, depending on the length of the sinker, and Awbery & Griffiths [6] found a decrease in velocity. At substantial inclinations, the guiding pins come into contact with the

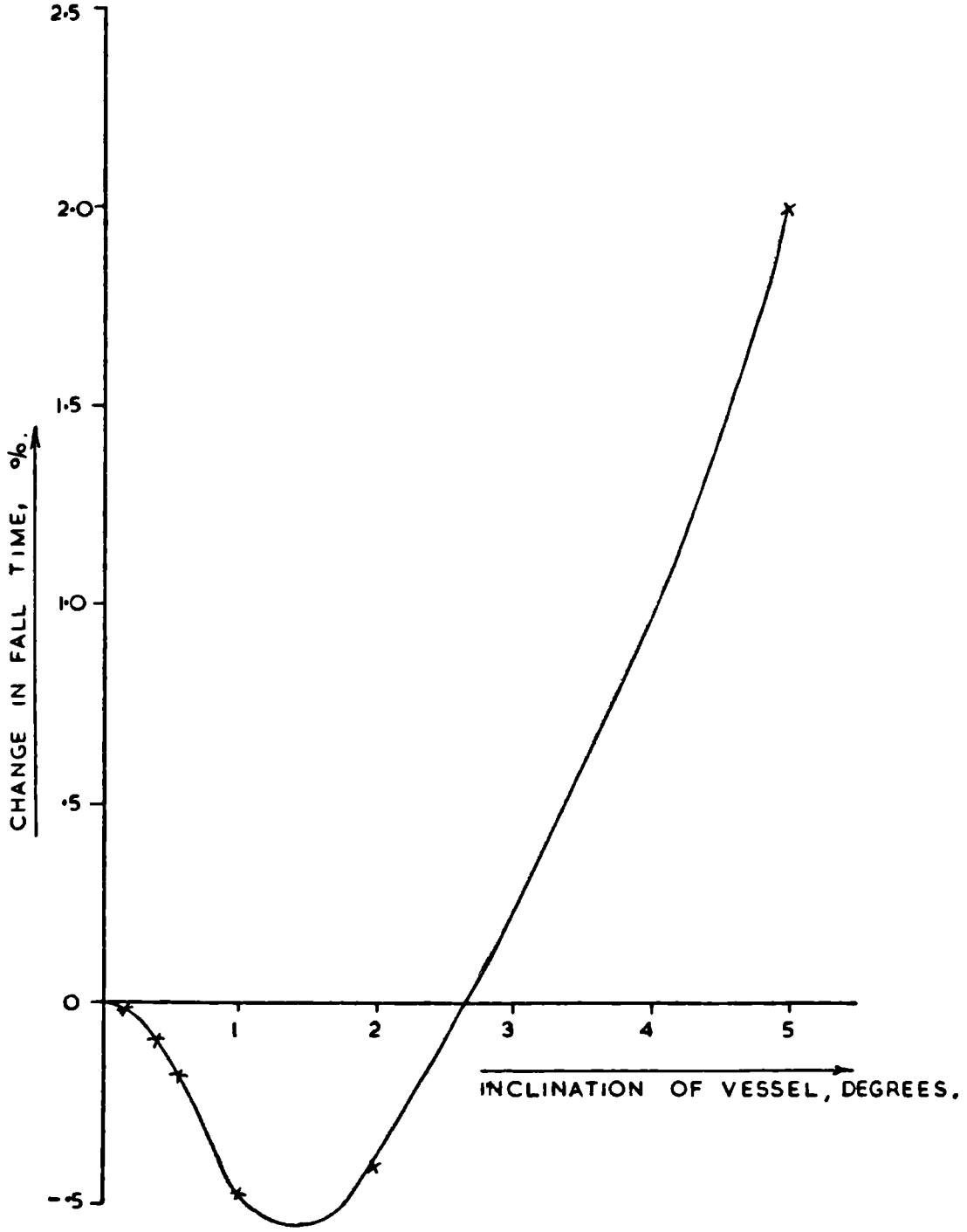

FIG. 37. EFFECT OF VISCOMETER INCLINATION.

tube, and friction then has a large effect, producing a sharp increase in fall time. A 17° inclination, which is too large to be shown on the scale of Fig. 37, increases fall time by 35%, and at these large inclinations, the results tend to be erratic.

At all times, the inclination of the viscometer tube is well within .004 inch per 10 inches to the vertical. This corresponds to an angle of 1.5 minutes, which would produce an error, from Fig. 37, of only .005% on the fall time.

(c) Calibration of stainless steel sinker of .004 inch clearance.

The sinker was calibrated by determining its fall time in a number of fluids of known relative viscosity. The fluids selected were not of high purity, but their relative viscosities were all determined in the same standard U tube viscometer. The U tube viscometer was employed in a thermostat at $25^{\circ}C$, and the minimum transpiration time experienced was 113 seconds.

The viscometer was supplied with a calibration certificate by the manufacturer in the form Kinematic viscosity = $AT^{*} - B/T^{*}$ where T^{*} is the transpiration time. The absolute accuracy of the constants A and B is unimportant for the purpose of the sinker calibration, only the relative magnitudes of A and B being required.

The fluids employed for the calibration, together with their viscosities, as determined from the U tube viscometer, were :-

Pentane,	.21242cp.	Allyl alcohol	1.21688cp.
Hexane,	.31029cp.	Butanol,	2.56337cp.
Heptane,	.44272cp.	Octanol,	7.55032cp.
n Octane,	.50116cp.	A mineral oil,	20.7255 cp.
n Decane,	.84204cp.		

The fall time of the sinker was determined in each of these fluids, and all the times corrected to the same fluid density. The uncorrected mean fall times of the sinker in each fluid, are given in Table 3.

TABLE 3.

Fluid	Start end 1		Start end 2		Difference, %
	Mean time.s.	Scatter %	Mean time.s.	Scatter %	
Pentane.	9.905	.2	9.793	.2	1.1
Hexane.	14.152	.1	13.998	.2	1.1
Heptane.	19.981	.2	19.719	.3	1.3
n Octane.	22.496	.1	22.191	.2	1.3
n Decane.	37.750	.1	37.281	.15	1.2
Allyl alcohol	55.072	.15	54.401	.2	1.2
Butanol.	115.086	.1	107.1	1.0	6.9
Octanol.	339.843	.2	307.3	1.0	9.6
Mineral oil.	915.046	.1	849.8	.8	7.1

Where the difference between the fall times in the two directions is in the region of 1%, the mean of the two times is considered for calibration. In the last three cases, only the times starting from end 1 are considered, and these are decreased by .6% to make them comparable with the mean times.

The ratio, $\frac{\text{Corrected fall time}}{\text{Fluid viscosity}}$, or T^*/η, is plotted against log. t^* in Fig.38, where t^* is the uncorrected fall time. Included in Fig. 38 are additional calibration points, considered later.

All the points in Fig. 38 lie near a smooth curve, except the point of longest fall time. Over most of the fall time range studied, T^*/η is not a constant, and it is not until a fall time of about 70 seconds is reached that the viscometer constant, k, in equation 5, becomes a constant. The range above t^* = 70 seconds is assumed to correspond to completely laminar flow conditions,

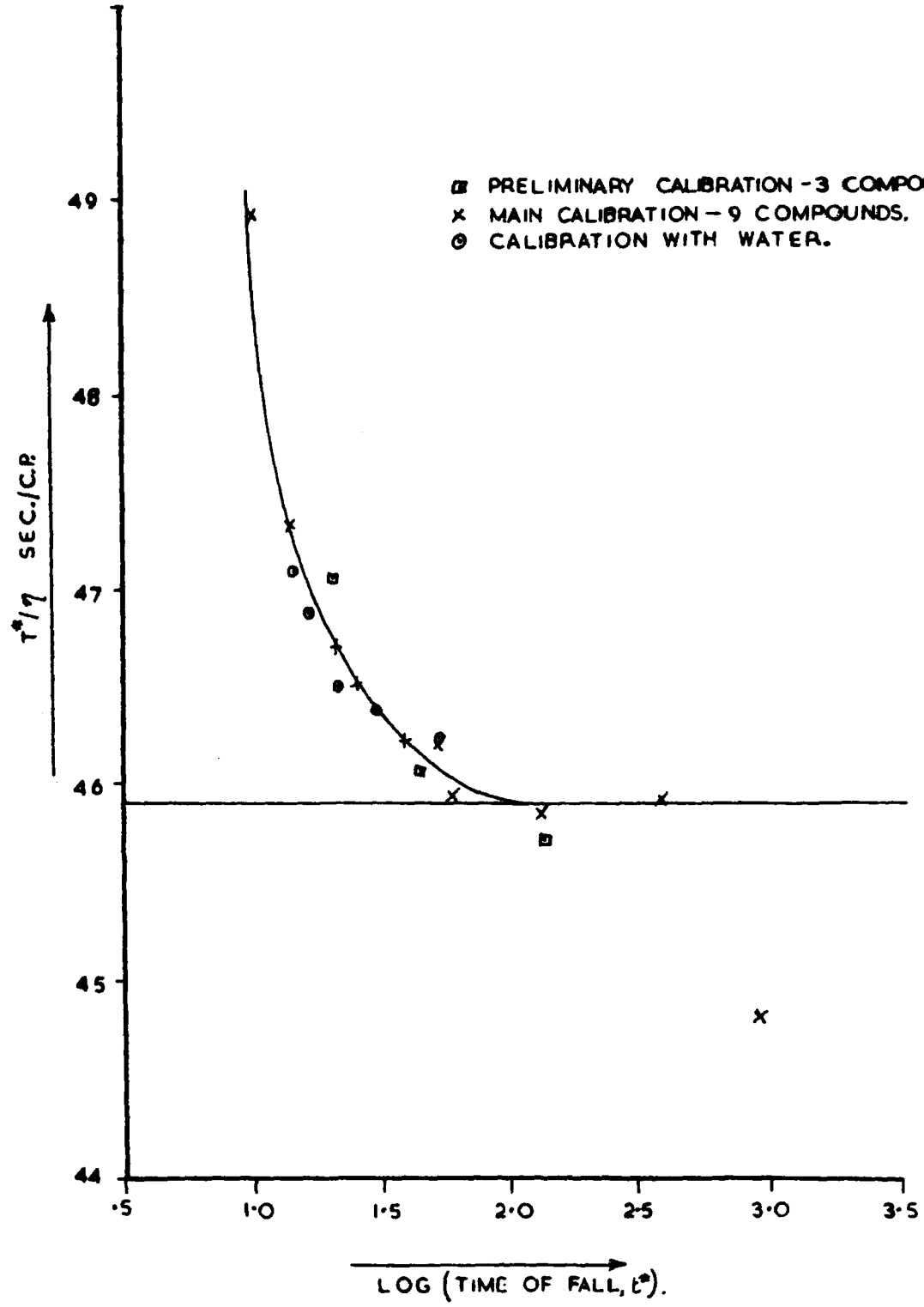

FIG. 38. CALIBRATION OF ·004 IN. CLEARANCE SINKER.

and below this value, an increasing degree of turbulence sets in with decreasing fall time. Lorhenz, Swift and Kurata [84] found that laminar flow conditions persisted up to N_{Re} = .1 to .2, but according to the work of Scott [125], the flow conditions never become completely laminar. However, this cannot be experimentally verified, as the kinetic energy corrections become so small at low velocities that they are easily lost in experimental error. From Fig.38, the value of N_{Re} at which the flow conditions begin to exhibit turbulence is .04. However, at N_{Re} = .1, the fall time is only .3% slower than it should be for completely laminar conditions. At fall times in the region of 10 seconds, the effects of turbulence are quite large.

An examination of Table 3 shows that up to a fall time of 55 seconds, the sinker behaves in a similar manner in both directions. However, for fall times of about 115 seconds, falls from end 2 are 6.9% faster than those from end 1, and at 340 seconds, this difference has increased to 9.6%. The conformity of the fall times from end 1 with Fig. 38 indicates that the fault lies with the fall times from end 2, and the larger scatter of the results for end 2 supports this.

It was shown in Chapter 4 that eccentricity produces an increase in terminal velocity. It is estimated, from the guiding pin dimensions, that the maximum displacement of the axis of the sinker is .0005 inch, i.e. 2d = .00254cm. Then, from Fig. 13, the possible increase in terminal velocity is 12%. It was also shown that a low terminal velocity tends to produce eccentricity. It is probable, therefore, that the anomolous behaviour of the sinker in falling from end 2, in the fall time region of 55 to 340 seconds, is due to the sinker falling eccentrically. The observed increase in terminal velocity corresponds approximately with that to be expected from the maximum possible eccentricity of the sinker.

At the longest time of fall investigated in Table 3, it is seen that the difference between the two directions decreases, and the fall time from end 1 falls below the calibration curve in Fig. 38. Presumably, the sinker, in falling from end 1, has taken up a degree of eccentricity at this very low velocity, causing it to depart from the calibration curve, and to become closer to the already eccentric fall time from end 2. A condition of fall where the sinker wanders about its concentric axis was observed by Scott [125] at low velocities, and in her experiments, employing square ended cylinders, eccentric fall generally occurred at a velocity equivalent to between 60 and 180 seconds fall time.

The upper limit of fall time at which this particular sinker may be employed is, therefore, somewhere between 340 and 915 seconds. Below 10 seconds, the corrections for turbulence become large.

In addition to the calibration with 9 fluids, a preliminary calibration was carried out at 30°C employing :-

Heptane,	.36189cp.
Water,	.79212cp.
Pentadecane,	2.25972cp.

The results of this calibration are included in Fig. 38. With the pentadecane, a fall time of 99 seconds produced a difference in the two directions of 4%.

Also included in Fig. 38 are the results of determining the fall time of the sinker in water over the temperature range 30 to 95°C. For this, the viscosity data of Bingham and Jackson [13] were employed.

For a fall time greater than 20 seconds, there is no doubt that the viscometer was vertical and stationary well before the sinker started the timer. At a 10 seconds fall time, this is by no means certain, and it is possible, therefore, that the sinker does not achieve

terminal velocity at the shortest fall times. Any such effects are included in the calibration curve.

The correlation between T^*/η and t^* should allow for the fact that the calibrations were carried out on fluids covering a range of densities. The correlation should, therefore, relate to t^*/ρ_f rather than to t^* as implied by Lohrenz, Swift and Kurata's correlation between viscometer constant and Reynolds number, and by Scott's equation 13. In the case of Scott's work, the experimental results agreed well with equation 13, but only in the region of perfectly steady fall. The correlation of the present calibration results with t^*/ρ_f is not very good, especially at the high velocity end of the calibration, and correlation with t^* is very much better. The term t^*/ρ_f does not take into account the effects of oscillation at high velocities, caused either by the natural tendency of a sinker to behave in this manner, (as shown by Scott), or by instability induced in the fall of the sinker by the vessel coming quickly to rest in the vertical position. A correlation with t^* takes these effects into account more precisely than t^*/ρ_f, and at fall times where it would be more significant to correlate the turbulence correction with t^*/ρ_f rather than with t^*, the corrections are sufficiently small to make the neglecting of ρ_f relatively unimportant. As the turbulence correction has not been investigated sufficiently to be more explicit about its correlation, a 15% error is placed on the correction.

From Fig. 38 is constructed Fig. 39, which gives the percentage of corrected fall time T^* which must be subtracted from T^* to correct for turbulence and instability.

(d) Calibration of stainless steel sinker of .006 inch clearance.

As this sinker was not employed for any serious experimental work, it was not given a thorough calibration. However, determinations of its fall time in water at various temperatures showed it to have a similar turbulence effect to the .004 inch clearance sinker.

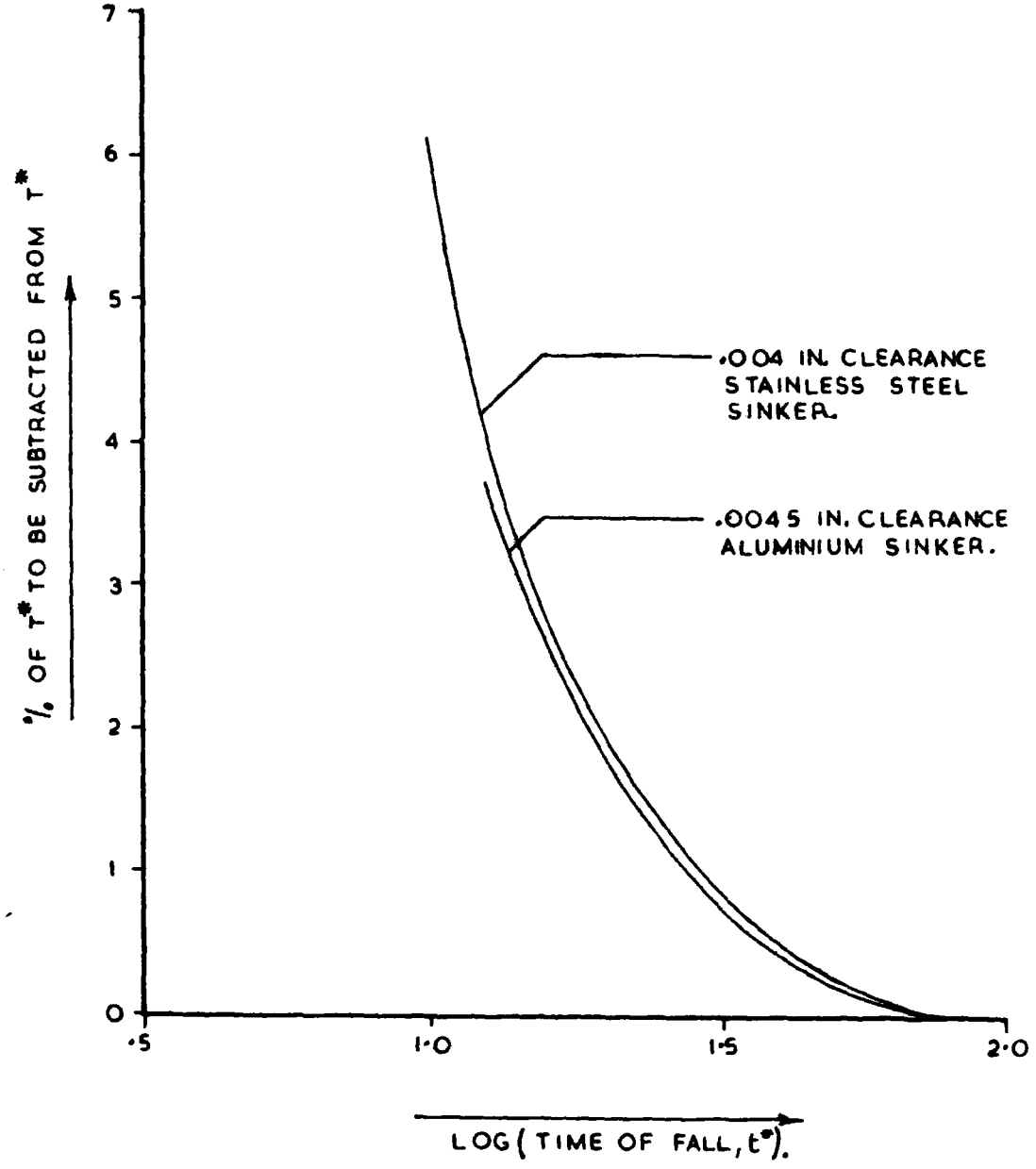

FIG. 39. SINKER TURBULENCE CORRECTIONS.

During some preliminary trials on the viscometer at high pressure, this sinker achieved fall times of 2,000 seconds, and coaxial fall conditions in both directions were maintained up to more than 1,000 seconds. This, together with its smaller directional effect, indicates that the .006 inch clearance sinker to have a more satisfactory performance than the .004 inch clearance sinker. However, the larger clearance sinker was unsuitable for the viscosity range covered in this study.

(e) Calibration of Aluminium Alloy sinker of .0045 inch clearance.

The aluminium sinker was calibrated in a similar manner to the .004 inch clearance stainless steel sinker, employing pentane, heptane, decane, butanol and octanol.

The result of the calibration, in the form,

$$\frac{\text{corrected time } T^*}{\text{fluid viscosity}} \text{ vs. } \log t^*,$$

is shown in Fig. 40, and the form of the calibration curve is similar to that of the stainless steel sinker in Fig. 38. Fig. 39 includes the time corrections, derived from Fig. 40, which must be applied to the aluminium alloy sinker. For a given fall time, the aluminium alloy sinker is seen, in Fig. 39, to require a slightly smaller turbulence correction than the stainless steel sinker, even though N_{Re} for the former sinker is the larger of the two, indicating that the stainless steel sinker tends to produce a greater degree of turbulence than the aluminium alloy sinker.

The aluminium alloy sinker maintains a constant directional effect up to a fall time of 150 seconds, and at greater times it falls eccentrically in one direction. The other direction of fall is satisfactory at 450 seconds, above which time the sinker has not been used. At this fall time, the directional effect is 5%.

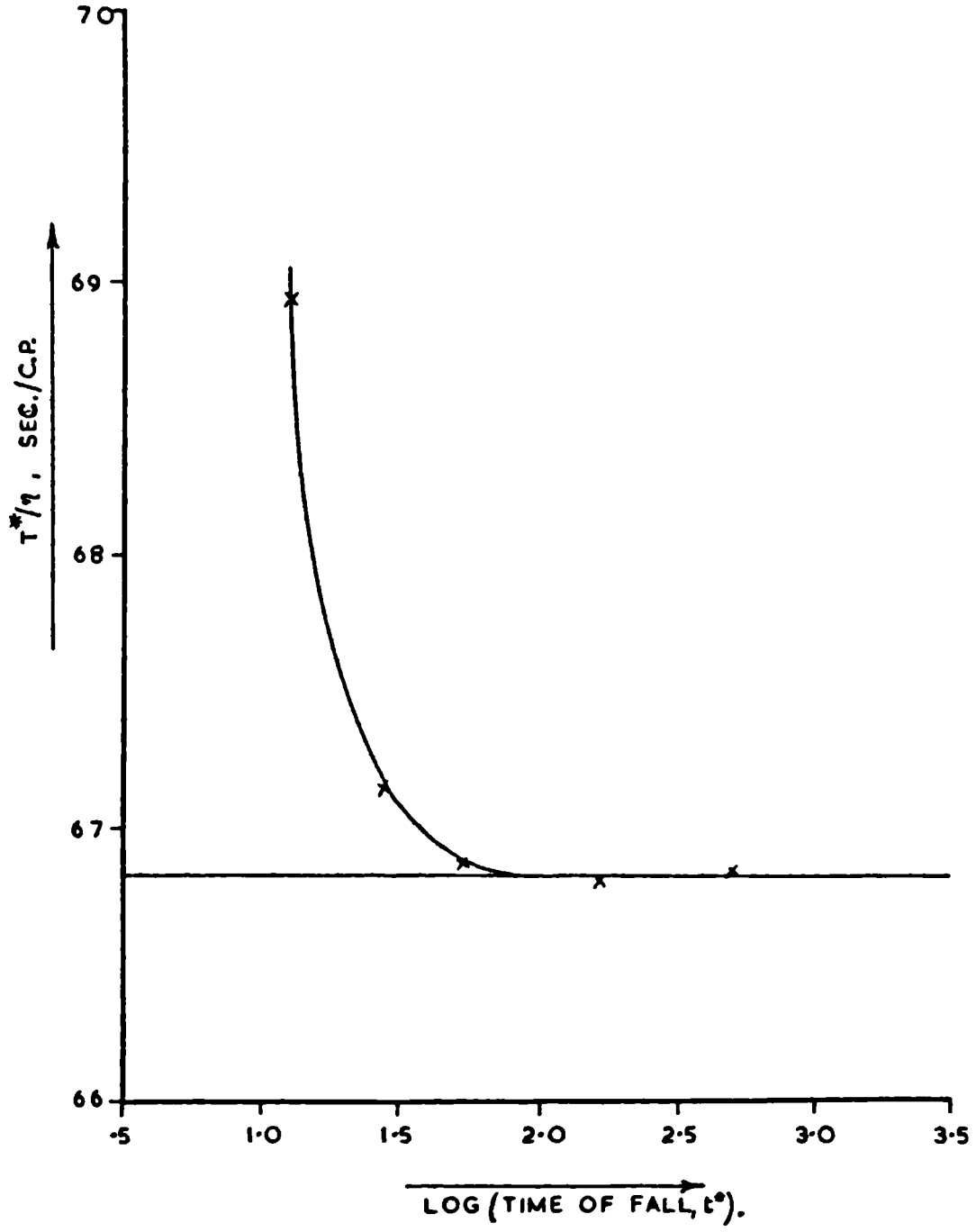

FIG. 40. CALIBRATION OF ·0045 IN. CLEARANCE SINKER.

(iii) Performance at High Pressure.

As Bridgman's viscometer is the only other instrument of similar pressure range which has ever been used, the availability of high pressure data for comparison is extremely limited. Unfortunately, of all the pure compounds that have been studied above 3,000kg/cm^2 in Bridgman's instrument, none have been studied by other workers to more than a few tens or hundreds of kg/cm^2.

There being no fluid whose viscosity is particularly well defined up to 10,000kg/cm^2, n-pentane was selected for a trial of the viscometer from among the fluids studied by Bridgman to this pressure, mainly because this would allow the use of the same sinker that was employed for the results given in Chapter 12. The viscosity of n-pentane was determined up to 10,000kg/cm^2 at 30°C, with the .004 inch clearance stainless steel sinker. The .0045 inch clearance aluminium alloy sinker was also employed in this experiment to determine how well the two sinker method could predict the density of n-pentane under pressure. The results of the density determinations are dealt with in Chapter 10.

The composition of the pentane employed for this experiment was determined by vapour phase chromatography as :-

n-pentane	=	98.0%.
iso-pentane	=	1.88%.
propane	=	0.12%.

The orientation of the two sinkers in the viscometer tube was the same as for calibrations (c) and (e), and the aluminium alloy sinker was nearest end 2 of the viscometer.

In calculating the viscosity of pentane under pressure, from the fall times of the stainless steel sinker, the fall times in both directions were considered where possible. At the longer fall times, the time for direction 1 only was considered, and relative viscosities for these conditions were calculated by compar-

ing the uni-directional time at atmospheric pressure with the uni-directional time under pressure. The fall times were corrected for the changing density of the pentane, the data employed being that of Bridgman [24]. (See Chapter 10). Corrections were also applied for the dimension changes of the viscometer and tube under presure as indicated in Chapter 4. Finally, the fall time of the sinker was corrected by means of Fig. 39 for the effects of turbulence. All of these corrections were applied in the manner shown in the specimen calculation in Appendix 4.

The results for pentane are shown in Fig. 41 in the form of log η_p/η_o vs. pressure. Included in Fig. 41 for comparison are Bridgman's results [19].

The maximum difference in η_p/η_o occurs at about 1,000 kg/cm^2, and is 4%. At higher pressures, the two results converge to reach a common value at 9,000kg/cm^2. However, as Bridgman based his pressure measurement on a mercury freezing point of 7,640kg/cm^2, his pressure scale must be expanded for a proper comparison of the results. The effect of this at low pressures is small, but at 10,000kg/cm^2, Bridgman's results should be 100kg/cm^2 higher than shown in Fig. 41. Under these conditions, the present work gives the relative viscosity 1.5% higher than Bridgman at the highest pressure. From the work of Hubbard and Brown[66], who measured the viscosity of n-pentane up to 1,000 p.s.i. with a rolling ball instrument, the relative viscosity at 30°C and 100kg/cm^2, obtained by interpolation and extrapolation of their results, should be 1.130. However, the accuracy of their work is claimed to be only 5%. Their result compares with the value of η_p/η_o in Fig. 41 at 100kg/cm^2, η_p/η_o = 1.122. The initial pressure coefficient is therefore in agreement within the error of Hubbard and Brown's experiments.

An interesting feature of the experiment on pentane is that in falling from end 1, the stainless steel sinker was able to achieve

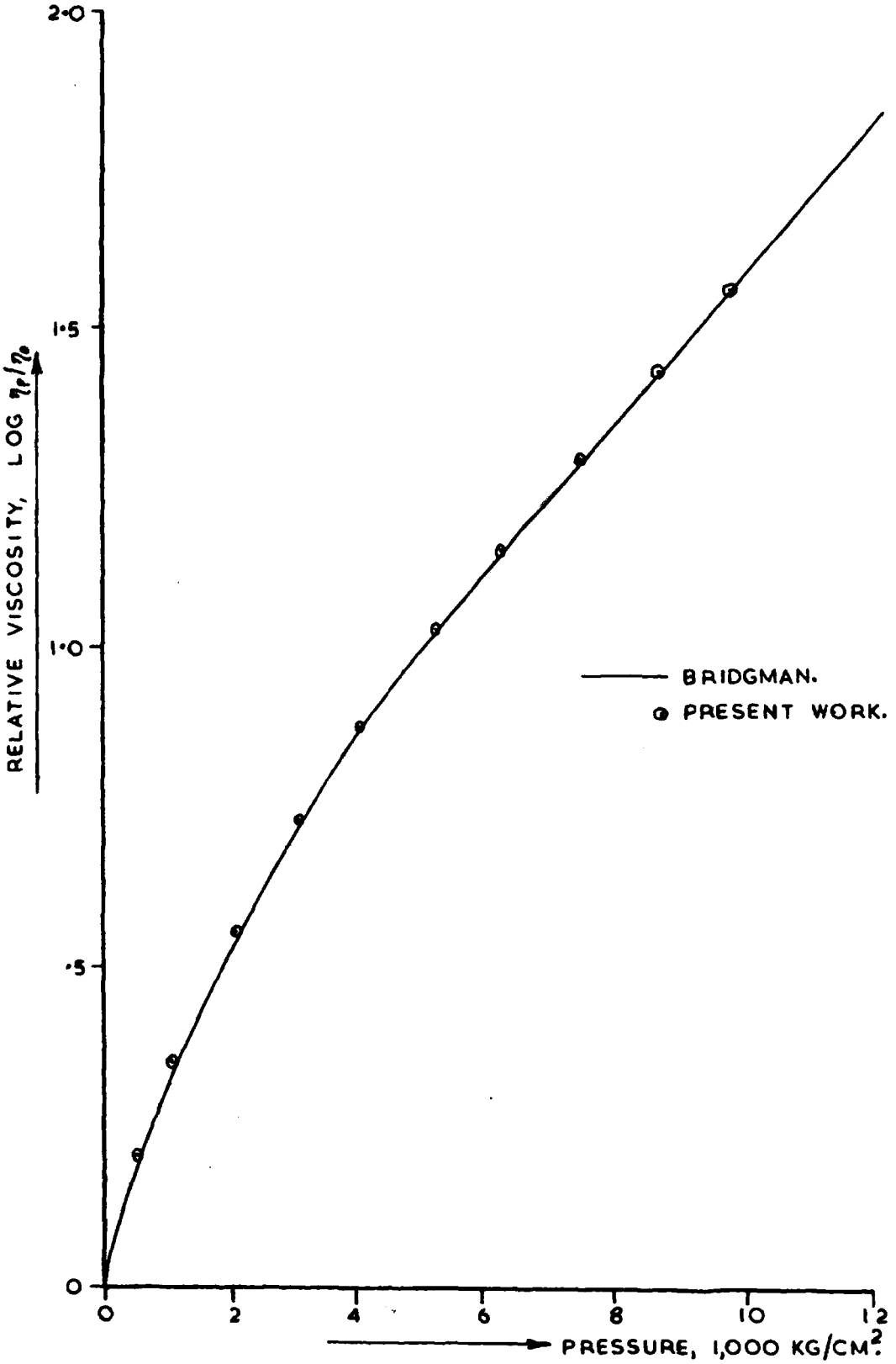

FIG. 41. VISCOSITY OF N-PENTANE AT 30°C.

its terminal velocity in a similar manner as in its calibration. However, in falling from end 2, the presence of the aluminium alloy sinker meant that the stainless steel sinker had a shorter distance in which to fall before starting the timer. Under these conditions, the directional effect was 1.11% at a 9.3 second fall time. At a similar fall time, during calibration, the directional effect was 1.15%. If, during the experiment on pentane, the fall from end 2 was appreciably altered by terminal velocity effects, the fall time from end 2 would be increased, and would decrease the directional effect. The fact that the directional effect during the calibration and during the pentane experiment is substantially the same, indicates that any terminal velocity effects at a 9 or 10 second fall time are very small.

The calculation of the distance required to achieve terminal velocity under these conditions is made rather difficult by the fact that the sinker starts falling well before the vessel is vertical, by the effects of instability of fall, and by the slight bell-mouthing of the viscometer tube introduced in its manufacture.

CHAPTER 10.

DENSITY MEASUREMENT.

The use of two sinkers in the viscometer, and its application to density measurement, was described in Chapter 3. The object of the method is to measure fluid density, under pressure with sufficient accuracy for buoyancy corrections to be made on the fall time of the sinker. When employing a stainless steel sinker, the fluid density must be known to 4% in order to determine viscosity to an accuracy of .2%.

If the viscosity of a liquid, at atmospheric pressure, employing a high density sinker, (e.g. stainless steel), is given by:-

$$\eta_o = \frac{k_s t^*_{so}}{L}, \qquad 19.$$

then the viscosity of the fluid under pressure is,

$$\eta_p = \frac{k_s t^*_{sp}}{L} \frac{(\rho_{sp} - \rho_{fp})}{(\rho_{so} - \rho_{fo})} \cdot \frac{\rho_{so}}{\rho_{sp}} \qquad 20.$$

The viscosity of the same fluid, employing a low density sinker, (e.g. aluminium alloy), is given by,

$$\eta_o = k_a \frac{t^*_{ao}}{L} \qquad 21.$$

$$\text{and,} \quad \eta_p = k_a \frac{t^*_{ap}}{L} \frac{(\rho_{ap} - \rho_{fp})}{(\rho_{ao} - \rho_{fo})} \cdot \frac{\rho_{ao}}{\rho_{ap}} \qquad 22.$$

$$\text{then,} \quad \frac{\eta_p}{\eta_o} = \left(\frac{t^*_p}{t^*_o}\right)_s \cdot \frac{(\rho_{sp} - \rho_{fp})c_s}{\rho_{sp}} = \left(\frac{t^*_p}{t^*_o}\right)_a \cdot \frac{(\rho_{ap} - \rho_{fp})}{\rho_{ap}} . c_a \qquad 23.$$

where $c_s = \dfrac{\rho_{so}}{(\rho_{so} - \rho_{fo})}$, and $c_a = \dfrac{\rho_{ao}}{(\rho_{ao} - \rho_{fo})}$.

From 23, $$\rho_{fp} = \frac{(t^*_p/t^*_o)_a \cdot c_a - (t^*_p/t^*_o)_s \cdot c_s}{\left(\frac{t^*_p}{t^*_o}\right) \cdot \frac{c_a}{\rho_{ap}} - \left(\frac{t^*_p}{t^*_o}\right) \cdot \frac{c_s}{\rho_{sp}}} \qquad 24.$$

Thus, by determining the fall times of two sinkers of different density, the density of a fluid under pressure may be calculated from 24. The time ratios, t^*_p/t^*_o must be corrected to the same temperature, and they must also be corrected for dimensional changes under pressure, in the tube and sinker, and for turbulence effects.

All the fluids studied in the viscometer, so far, have been of known compressibility, and the facility which the viscometer provides for the measurement of density has not been required. However, in the viscosity determination of n-pentane, described in Chapter 9, two sinkers were employed so as to assess the practicability of employing this method for density measurements.

The determination of $(t^*_p/t^*_o)_s$ is the same as that for calculating the relative viscosity of the pentane in Chapter 9, and the specimen calculation in Appendix 4, except that the correction for buoyancy changes is not applied.

Calculation of $(t^*_p/t^*_o)_a$, for the aluminium alloy sinker, is the same as that for $(t^*_p/t^*_o)_s$, except for the correction for dimensional changes.

The first order theory of the viscometer, in Chapter 4 gives,

$$v = \frac{wg}{2\pi l \eta} \cdot \frac{c^3}{(3r_1^2 c + 3r_2^2 c + 3r_1^2 r_2 + 4r_2 c^2)} \qquad 10.$$

As the stainless steel sinker is of the same material as

the tube, the fall time of the sinker has only to be corrected for changes in the length of the tube, L, and in the length of the sinker, l. In Chapter 4, this correction was shown to be twice the linear compressibility of the material, and at 10,000kg/cm^2, it amounts to only .4%. In the case of the aluminium alloy sinker, the term,

$$\frac{c^3}{(3r_1^2c + 3r_2^2c + 3r_1^2r_2 + 4r_2c^2)},$$

is no longer a constant, and the change in its value must be determined from the compressibilities of the tube and of the sinker.

The elastic constants of samples of the EN58JM stainless steel, and of the RR77 aluminium alloy, were determined by ultrasonic techniques by the National Physical Laboratory.

For EN58JM, $E = 28.0 \times 10^6$ p.s.i., and $c = 0.295$. (Poisson's ratio).

For RR77, $E = 7.22 \times 10^{11}$ dynes/cm^2., and $c = .340$.

The volume compressibility at atmospheric pressure is related to E and c by the expression:-

$$\beta = \frac{3(1 - 2c)}{E} \qquad (c = \text{Poisson's ratio}). \qquad 25.$$

Then, $\beta_s = 6.248 \times 10^{-7}$ per kg/cm^2,

and, $\beta_a = 13.04 \times 10^{-7}$ per kg/cm^2.

The linear compressibilities are 1/3 of these.

From the compressibilities, and the values of r_2, r_1 and c at atmospheric pressure, the values of r_2, r_1 and c under pressure may be calculated. From these values, the term,

$$\frac{\left(\dfrac{c^3}{3r_1^2c + 3r_2^2c + 3r_1^2r_2 + 4r_2c^2}\right)_p}{\left(\dfrac{c^3}{3r_1^2c + 3r_2^2c + 3r_1^2r_2 + 4r_2c^2}\right)_o}$$

may be determined, and is the factor by which the fall time under

pressure must be multiplied to correct it to the radius ratio of the viscometer at atmospheric pressure. In addition, the usual small factor for changes in the lengths L and l must be included. It was found that the two factors combined, may be represented by the multiplying factor, $1 + 2.2822 \times 10^{-5}P + 1.7334 \times 10^{-10}P^2$. At 10,000kg/cm^2, this factor is equal to 1.24556. Thus, the correction factor under these conditions is very much larger than the factor for dimensional changes for tube and sinker of common material.

The corrected time ratios, $(t^*_p/t^*_o)_a$ for the aluminium alloy sinker, and $(t^*_p/t^*_o)_s$ for the stainless steel sinker, were calculated from the experiment on n-pentane. In Fig. 42, $(t^*_p/t^*_o)_a - (t^*_p/t^*_o)_s$, expressed as a percentage of $(t^*_p/t^*_o)_a$, is plotted against pressure.

The curve in Fig. 42 should pass through the origin, whereas it intercepts the P = 0 axis at -1.4%. The values of t^*_p/t^*_o must, therefore, be in error. The likely source of this error is the value of t^*_{os}, the fall time of the stainless steel sinker in n-pentane at atmospheric pressure and 30°C, which was 9.3 seconds. From Fig. 39, the turbulence correction at this fall time is very large, it being 7.2%. Referring to Fig. 38, it can be seen that one experimental calibration point only is available for determining the line of the calibration curve in the region of high turbulence correction, and the error in applying the turbulence correction to t^*_{os} is therefore considerable. If the zero error in Fig. 42 arises entirely from an error in t^*_{os}, then t^*_{os} is 1.4% too small. This error would make all the results for the relative viscosity of n-pentane, quoted in Chapter 9, 1.4% too high.

To allow for errors in t^*_{os}, and possibly t^*_{oa} (where the turbulence correction is 3.6%), the y axis zero is moved to the intercept at -1.4%. From Fig. 42, smoothed values of:-

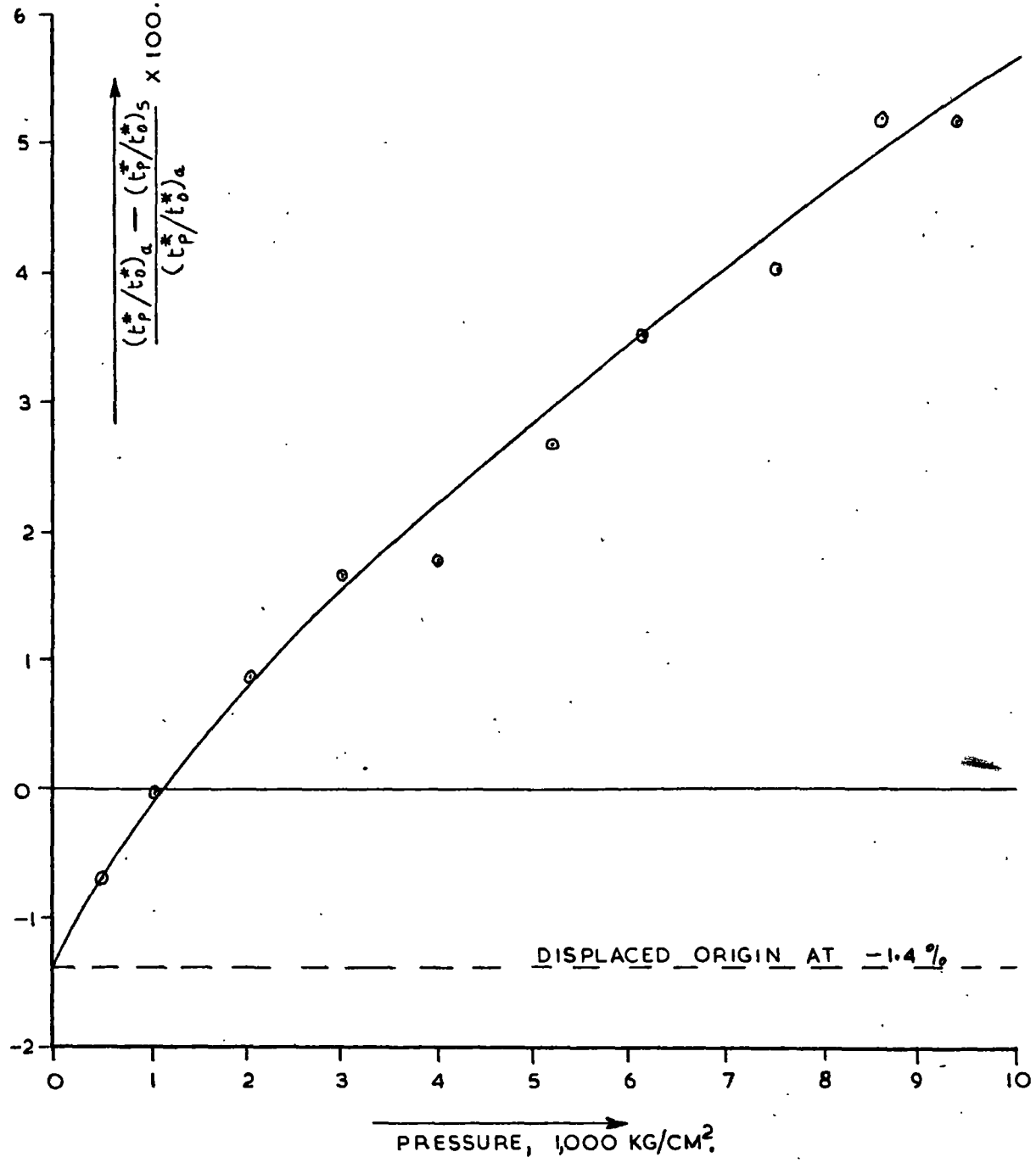

FIG. 42. COMBINED FALL TIMES OF TWO SINKER METHOD.

$$\frac{\left(\frac{t^*_p}{t^*_o}\right)_a - \left(\frac{t^*_p}{t^*_o}\right)_s}{\left(\frac{t^*_p}{t^*_o}\right)_a} \times 100$$

are taken, and these, together with the original values of $(t^*_p/t^*_o)_a$, are used to calculate smoothed values of $(t^*_p/t^*_o)_s$.

These values of $(t^*_p/t^*_o)_a$ and $(t^*_p/t^*_o)_s$ are inserted in 24 to determine ρ_{fp}, and for this purpose, the atmospheric pressure densities of the materials, and their compressibilities, are used to calculate values of ρ_{ap} and ρ_{sp}.

The calculated values of ρ_{fp} for n-pentane are shown in Fig. 43, and included in Fig. 43 are Bridgman's results [24] for the density of n-pentane under pressure. Between 0 and 4,000kg/cm^2, the calculated densities are within 3% of Bridgman's values, and mostly within 1.5%. However, above 4,000kg/cm^2, the values diverge rapidly, and at 10,000kg/cm^2, the calculated density is 13½% above Bridgman's value. The buoyancy correction for pentane at 10,000kg/cm^2 is 3.7%, and even if the calculated density were used to compute the buoyancy correction, the error in viscosity, arising from a 13½% error in density, would be only .5%.

The large dimensional corrections for $(t^*_p/t^*_o)_a$ are the prime cause of the 13½% error in the calculated density at the higher pressures. This error could be caused by $(t^*_p/t^*_o)_a$ being 1.8% too high, and as the dimension correction at 10,000kg/cm^2 is 24½%, calculated from a first order theory only, the error in applying the correction is not surprising. The error in the correction, which could account for a 1.8% error in $(t^*_p/t^*_o)_a$, is 7.3% of 24.5%. It was shown in Chapter 4 that the approximation of the annular gap, around the sinker, to the gap between parallel surfaces, leading to equation 10,

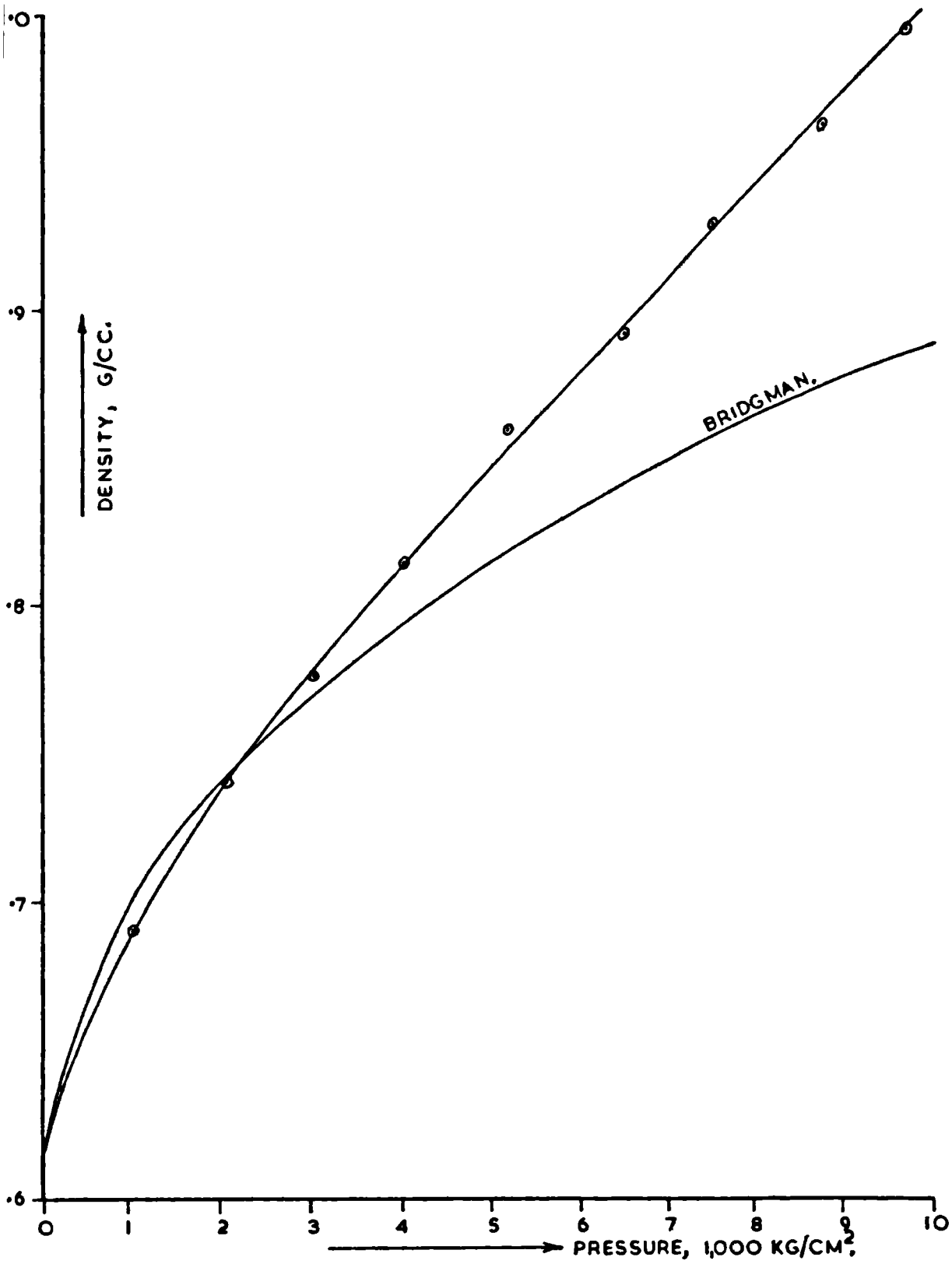

FIG. 43, DENSITY OF N-PENTANE AT 30°C.

results in only a very small error in calculating the effects of dimensional changes. However, Lohrenz, Swift & Kurata [84], (see Chapter 4), showed that large dimensional corrections could be predicted from the properties of the tube and sinker materials, to an accuracy of only 5%. The theory leading to equation 10 takes no account of the effect of dimensional changes on the drag on the guiding pins or on the ends of the sinker, and the error in the dimensional correction is, therefore, reasonable. Errors in the dimensional correction factor may also be due to the use of inaccurate compressibility data. Firstly, the compressibilities of the tube and sinker materials were calculated from the elastic constants, rather than measured. Secondly, the calculated compressibility is assumed to be constant over the whole pressure range. In practice, this is rarely true, and it is usual for the compressibility to decrease with increasing pressure. For example, the volume compressibility of pure aluminium and iron is given by Bridgman as [18]:-

Aluminium. $$-\frac{\Delta V}{V_o} = 13.43 \times 10^{-7}P - 5.0 \times 10^{-12}P^2$$

Iron. $$-\frac{\Delta V}{V_o} = 5.87 \times 10^{-7}P - 2.1 \times 10^{-12}P^2$$

At 10,000kg/cm^2, the second order correction to $\Delta V/V_o$ amounts to 3.7%. If the stainless steel and aluminium alloy exhibit similar second order compressibility effects to the materials measured by Bridgman, the dimensional correction factor would be reduced by 3.9% of 24.5% at 10,000kg/cm^2. This factor alone reduces by a half the error in the calculated density at the highest pressure.

Having compared the calculated density of a fluid with the known density, the error in applying the dimensional correction to the aluminium sinker may be assessed from the difference. On subsequent

use of the two sinker method, the dimensional correction itself may be corrected, permitting the determination of fluid density certainty to within 2 or 3%. The avoidance of employing sinkers in the region of very high turbulence corrections would be particularly helpful in increasing accuracy.

The use of materials of lower density than aluminium alloy would help to provide density determinations of a fluid of higher accuracy. The materials which could be considered for sinker construction having suitable density, are magnesium, of density 1.74g/cc., and beryllium, of density 1.82g/cc. It is estimated that a sinker could be constructed from these materials having an effective density of 2.72g/cc., as compared with the density 3.80g/cc. for the aluminium alloy sinker. Comparing these sinkers in a fluid of density .7g/cc., the buoyancy corrected density of the aluminium alloy sinker would be 3.1g/cc., and that of a magnesium or beryllium sinker would be 2.02g/cc. Thus, a change in fluid density would produce an effect on the fall time of a magnesium or beryllium sinker $1\frac{1}{2}$ times that of the aluminium alloy sinker. The accuracy of the experiment should, therefore, be increased by a similar factor, i.e. to better than 2%.

The volume compressibility of magnesium [18] is 29.5×10^{-7} per kg/cm^2, and that of beryllium [18] is 8.55×10^{-7} per kg/cm^2. These compare with 6.248×10^{-7} per kg/cm^2 for the stainless steel and 13.04×10^{-7} per kg/cm^2 for the aluminium alloy. The dimensional corrections for a magnesium sinker would be about 4 times larger than for an aluminium alloy sinker, which would completely outweigh the advantage of magnesium's lower density. However, the dimensional corrections for beryllium would be only $\frac{1}{4}$ of those of aluminium alloy, which is very favourable. It is likely, therefore, that the use of a beryllium sinker would allow the determination of fluid densities to within 1%, provided turbulence corrections are not large, and the difficulties of machining beryllium can be overcome.

CHAPTER 11.

EXPERIMENTAL PROCEDURE.

(i). Filling the Viscometer.

Assembly of the viscometer completely free of contamination is an essential pre-requisite to filling. (The assembly procedure has been described in Chapter 3).

The apparatus used for filling the viscometer, is illustrated in Fig. 44. A brass tube, (1), is sealed into the top of the viscometer with an O ring, and the upper end of the brass tube is sealed to a glass B7 cone with Araldite. A sintered glass filter unit, (2), terminating in a B7 socket at its lower end, and cone at its upper end, fits onto the filling tube, (1). The liquid with which the viscometer is to be filled is contained in a glass bulb, (3), of 100ml. capacity. The lower end of the bulb is joined to a two-way vacuum cock, (4), and the neck of the bulb is formed by a B19 cone and vacuum cock, (5). The system is completed by a rotary vacuum pump, a vacuum gauge, and a vapour trap. A screwed rod, (6), is attached to the viscometer bellows unit, and arranged so that the free end of the bellows can be supported or extended by a nut, (7).

The filling procedure depends on the nature of the fluid being handled. When filling the viscometer with the impure calibration fluids discussed in Chapter 9, no de- aeration was required, and the fluid was not exposed to a vacuum for a prolonged period, otherwise a small change in composition would have occurred. Under these circumstances, a 10mm. Hg. vacuum was applied at B, to evacuate the viscometer, and fluid was then drained through the cock, (4), into the viscometer, and residual bubbles removed by working the bellows up and down.

The pure compounds which have been handled in the viscometer, n-pentane, water, and heavy water, were first de-aerated by applying

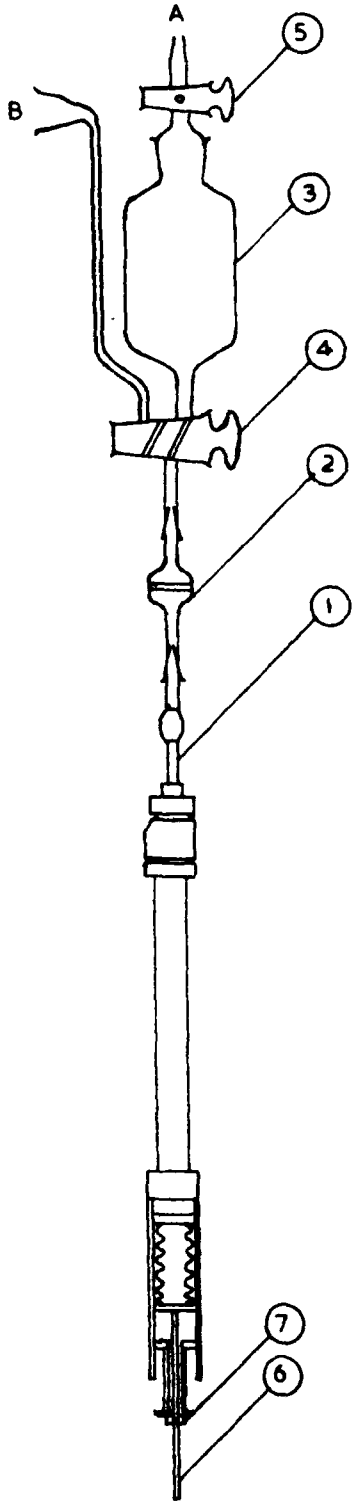

FIG. 44. VISCOMETER FILLING APPARATUS.

a vacuum at A. In the case of H_2O and D_2O, the de-aeration is most important because the presence of O_2 and CO_2 in the water produces corrosion of the stainless steel viscometer. There is no visible effect of this corrosion in the viscometer, but it causes an increase of $\frac{1}{2}\%$ in viscosity, and water from the viscometer which has not been properly de-aerated, produces a slight brown precipitate on prolonged exposure to air. De-aeration of water is continued until the pressure is reduced to 1mm. Hg., during which time about 15% of the water is evaporated. Pressure over the liquid is then produced by warming to near the boiling point. Again, the viscometer is evacuated at B, to 1mm. Hg., and liquid admitted through the two-way cock. Flexing of the bellows provides a check for the existence of any bubbles.

The bellows are almost fully extended and supported before disconnecting the filling tube. After this operation, the O ring in the filling hole is removed, and replaced with a copper disc and a screw with which to seal it. Before tightening the seal, the bellows are relaxed a little to flush away any air near the seal. The rod, (6), is then removed, and the viscometer is ready for loading in the pressure vessel.

(ii). Viscosity Determinations.

After loading the vessel with the viscometer, it is inverted a few times to check that the sinker is not sticking, and that the timing circuits are functioning satisfactorily. The alignment of the vessel is checked, and the thermostat tank is then filled with fluid, and its temperature adjusted to the desired value.

A two hour period was found to be necessary before the thermostat and the viscometer reached the same temperature. Normally, the rig is left running overnight for temperature equilibrium to be achieved, but, if not, a minimum of two hours is allowed. Before the

commencement of measurements, the timing circuits are balanced, the bridge and potentiometer are connected to their cells, and the oil circulating through the bridge allowed to attain temperature equilibrium. The thermocouple cold junction is filled with pure ice and distilled water, and all of the electronic equipment allowed a warming up period.

The sequence of events in determining the viscosity at one pressure point on an isotherm is as follows:-

1. Adjust potentiometer.
2. Measure gauge thermocouple e.m.f.
3. Measure bridge temperature.
4. Measure internal bridge resistance, R. (Two measurements).
5. Measure gauge resistance. (Two measurements).
6. Measure thermostat temperature.
7. Balance timing circuits, and adjust level of reference voltage on trigger circuits.
8. Set timing system for direction 1.
9. Reset time period counter and trigger circuit 1.
10. Invert vessel. Circuit 1 triggers and starts timer.
11. Reset trigger circuit 2. Circuit 2 triggers and stops timer.
12. Note time of fall.
13. Set timing system for direction 2.
14. Reset time period counter, and trigger circuit 2.
15. Invert vessel. Circuit 2 triggers and starts timer.
16. Reset trigger circuit 1. Circuit 1 triggers and stops timer.
17. Note time of fall.
18. Repeat 8 to 17 until sufficient observations have been made.
19. Repeat 6, 5, 4, 3, 2.

The pressure is then raised or lowered to the next point, and the whole procedure repeated. A pressure change produces a temperature change in the vessel, and time must be allowed to regain equilibrium. It was found that 30 minutes were sufficient for a 500

kg/cm^2 change, and 45 minutes for a 1,000kg/cm^2 change.

Viscosity determinations were carried out at 1,000kg/cm^2 intervals, except near the origin, where the first point after atmospheric pressure was determined near 500kg/cm^2. However, on some of the isotherms for H_2O and D_2O, it was necessary to work at 200 or 300kg/cm^2 intervals in the region of minimum viscosity.

The determination of the viscosity of n -pentane, discussed in Chapter 9, involved the use of two sinkers in the viscometer tube. For the purpose of this experiment, procedure steps 8 to 17 were modified, so that the sinkers were timed as follows:-

1. Time aluminium alloy sinker from end 1.
2. Time stainless steel sinker from end 1.
3. Time stainless steel sinker from end 2.
4. Time aluminium alloy sinker from end 2.

CHAPTER 12.

RESULTS.

The experimental viscosity results obtained with the high pressure viscometer are:-

Isotherms on H_2O at 2.2, 10, 20, 25, 30, 35, 50, 75 and 100°C.

An isotherm of D_2O at 25°C.

An isotherm on n-pentane at 30°C.

An isotherm on the pressure transmitting fluid at 25°C.

The experimental results, together with a specimen calculation, are set out in Appendix 4.

(i). Water.

The results for water have been smoothed by plotting the isothermal relative viscosity, η_p/η_o, vs. pressure, and cross plotting with interpolated isobaric viscosity, log η_p vs. temperature. The smoothed interpolated data are tabulated in Appendix 4. Included in the tables are smoothed extrapolated figures for the viscosity of water at 0°C. In calculating the absolute viscosity, η_p, from the relative viscosity, η_p/η_o, the viscosity-temperature data of Bingham & Jackson [13] was employed.

Figs. 45 to 53 show the experimental results for each temperature plotted as η_p/η_o vs. pressure. The curves drawn through the points are the smoothed curves, and included on the graphs for 10, 30, and 75°C are Bridgman's results for water at these temperatures. Fig. 54 gives the extrapolated smoothed results for 0°C for comparison with Bridgman's results for that temperature, while Figs. 55 and 56 give all the smoothed isothermal and isobaric viscosity results together.

The only experimental points which lie appreciably off

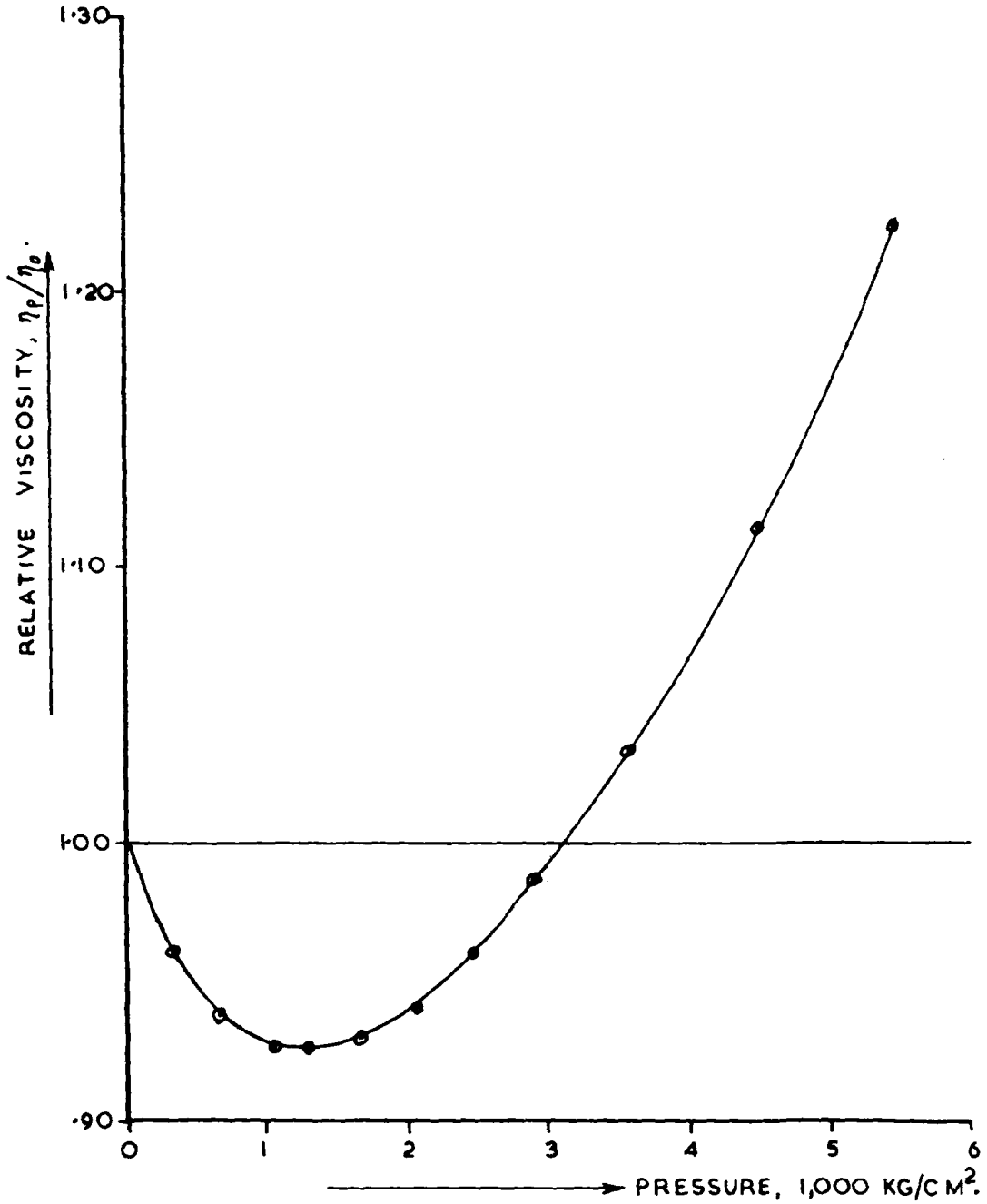

FIG. 45. VISCOSITY OF WATER AT 2·2 °C.

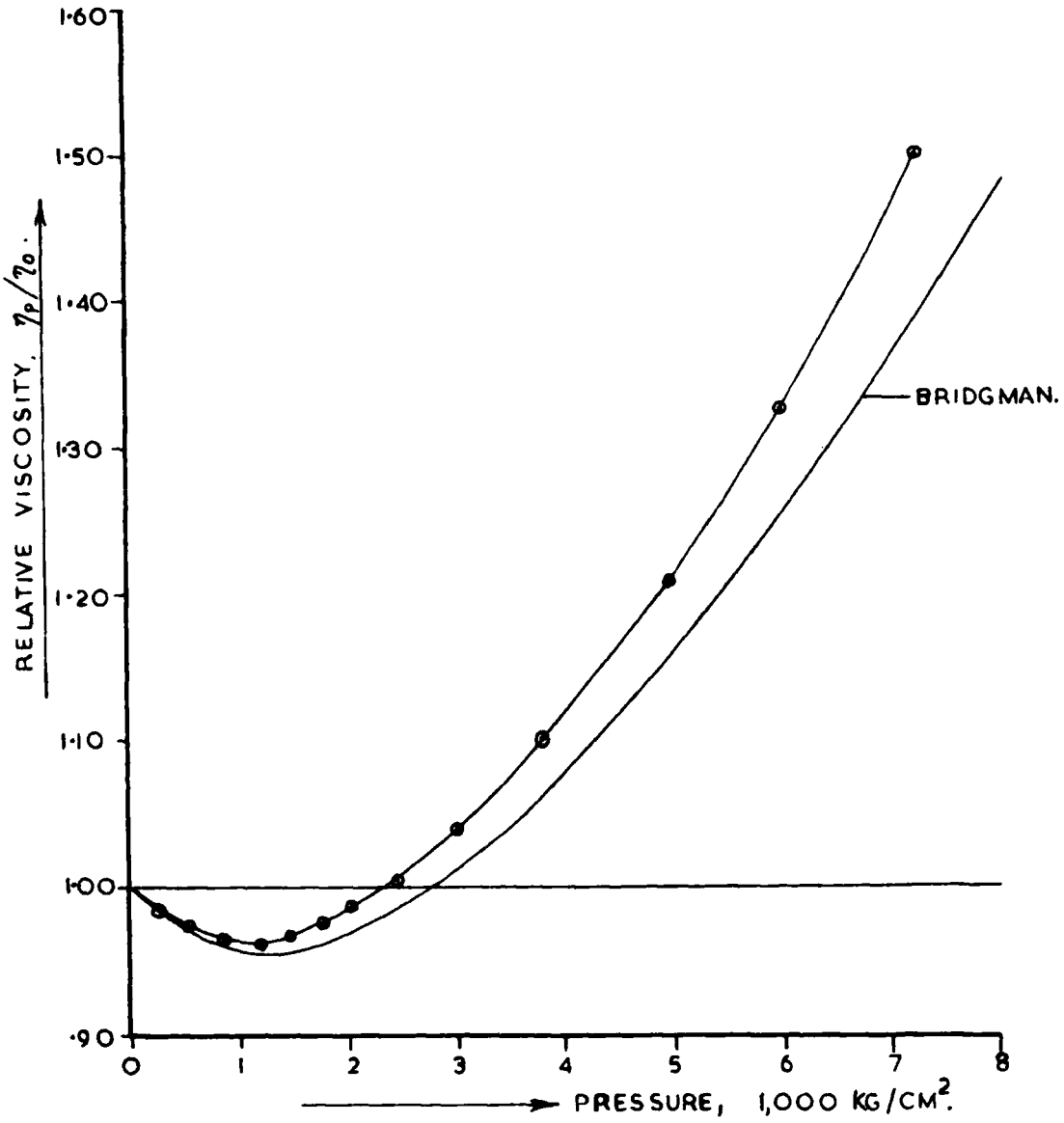

FIG. 46. VISCOSITY OF WATER AT 10 °C.

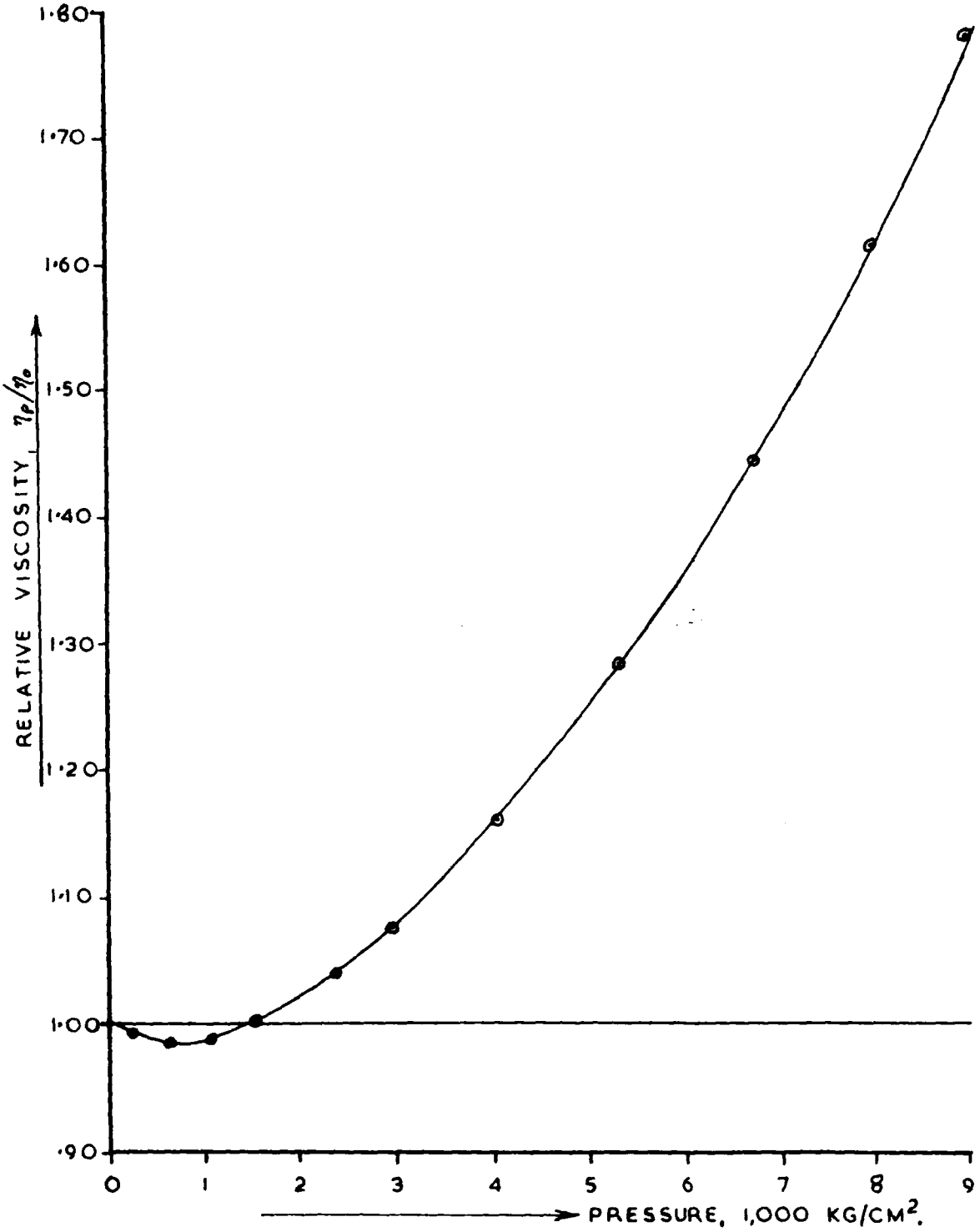

FIG. 47. VISCOSITY OF WATER AT 20°C.

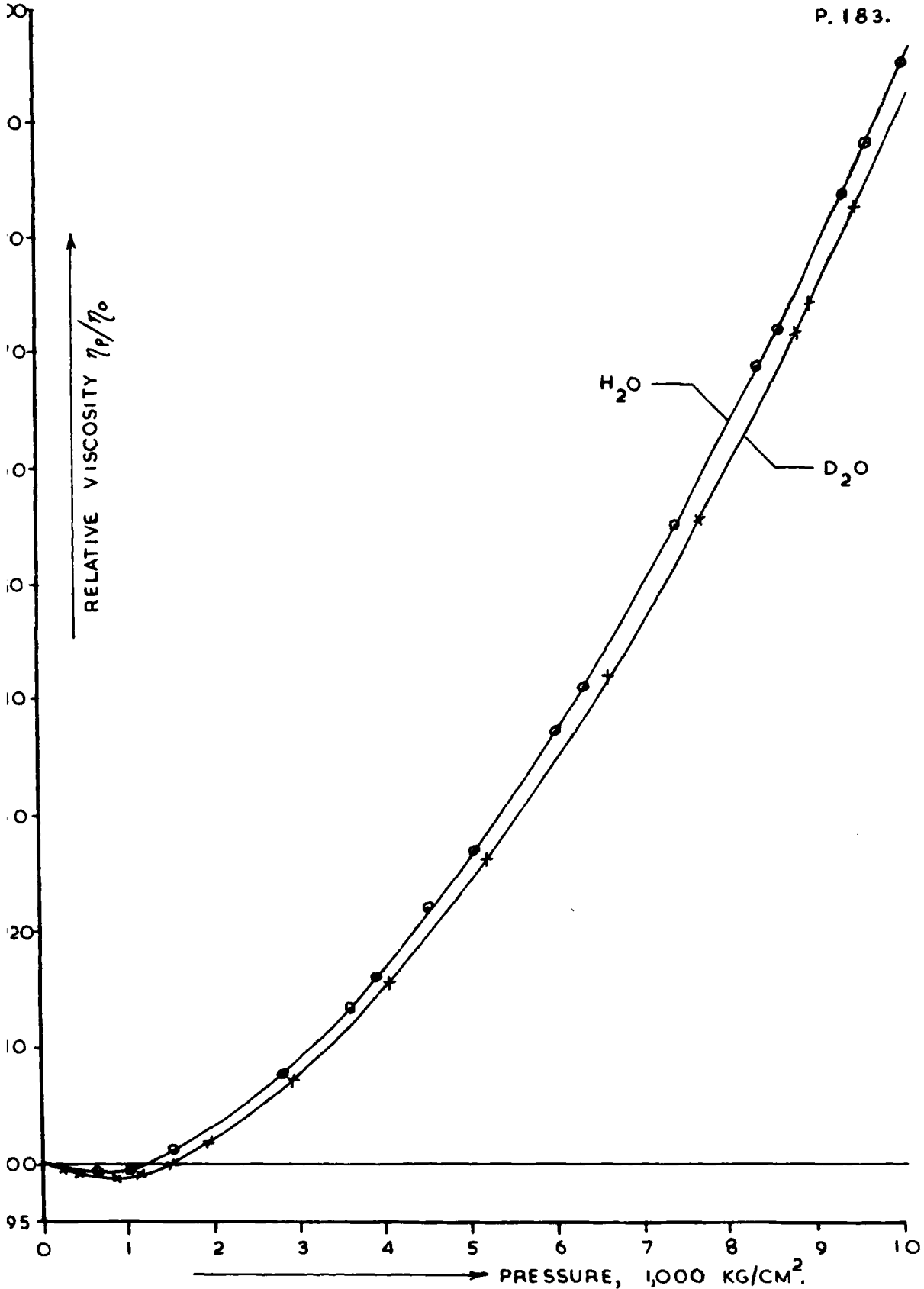

FIG. 48. VISCOSITY OF WATER AND HEAVY WATER AT 25 °C.

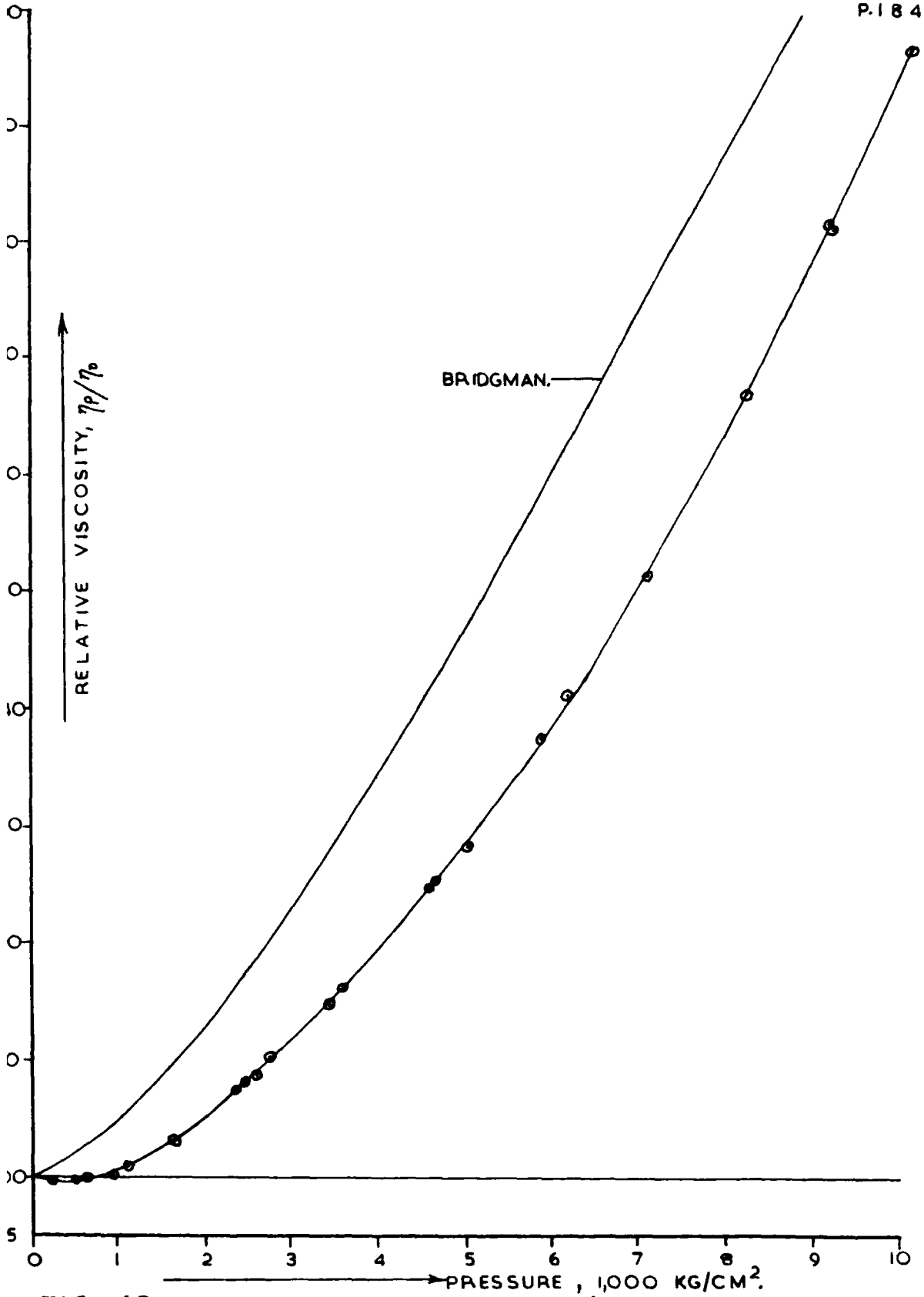

FIG. 49. VISCOSITY OF WATER AT 30°C.

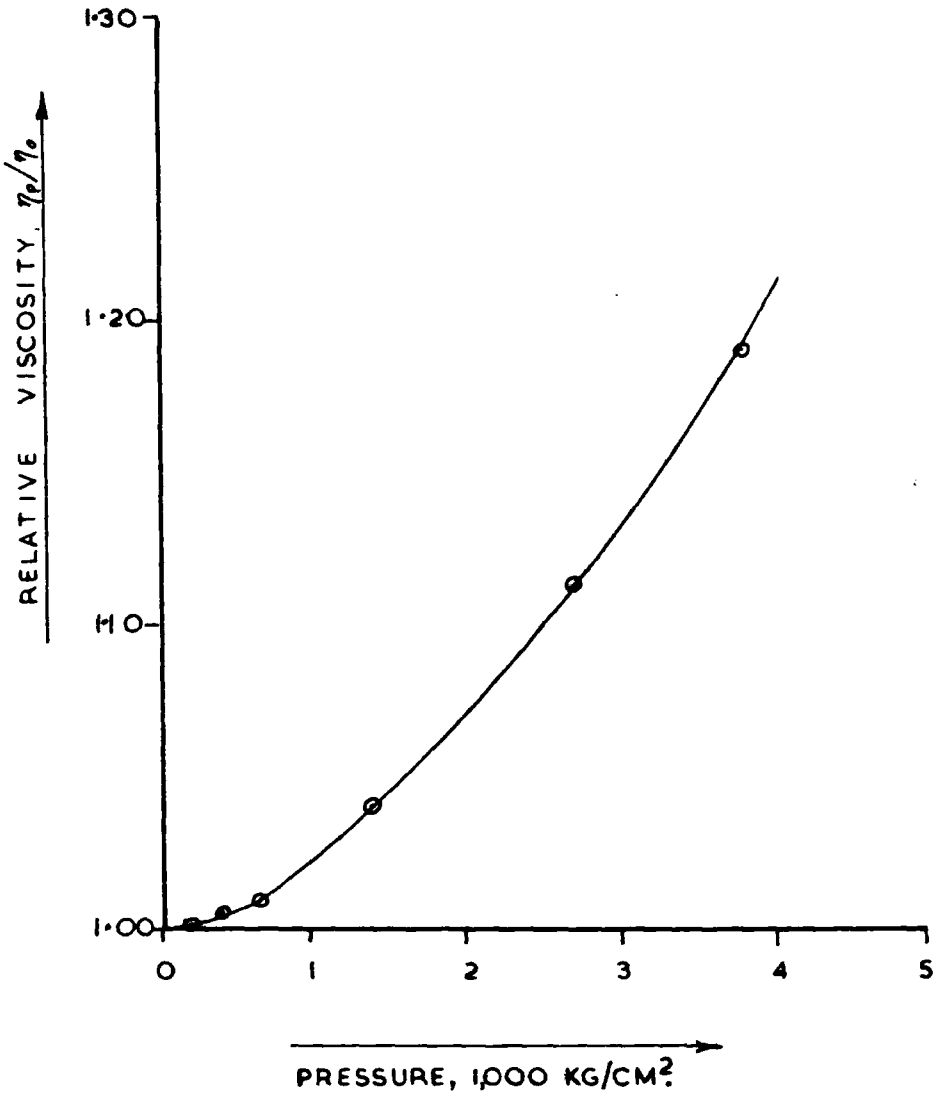

FIG.50. VISCOSITY OF WATER AT 35 °C.

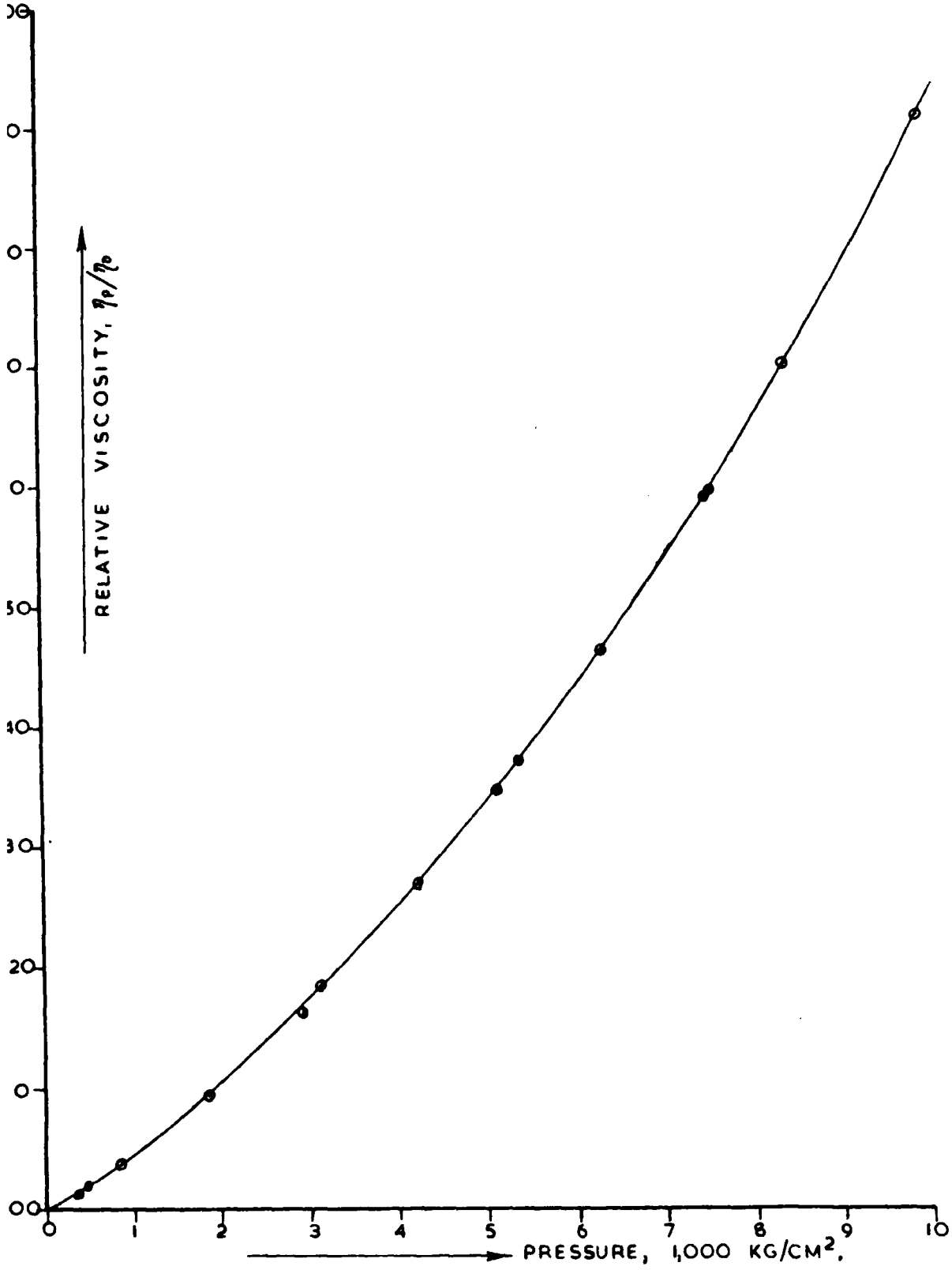

FIG. 51. VISCOSITY OF WATER AT 50°C.

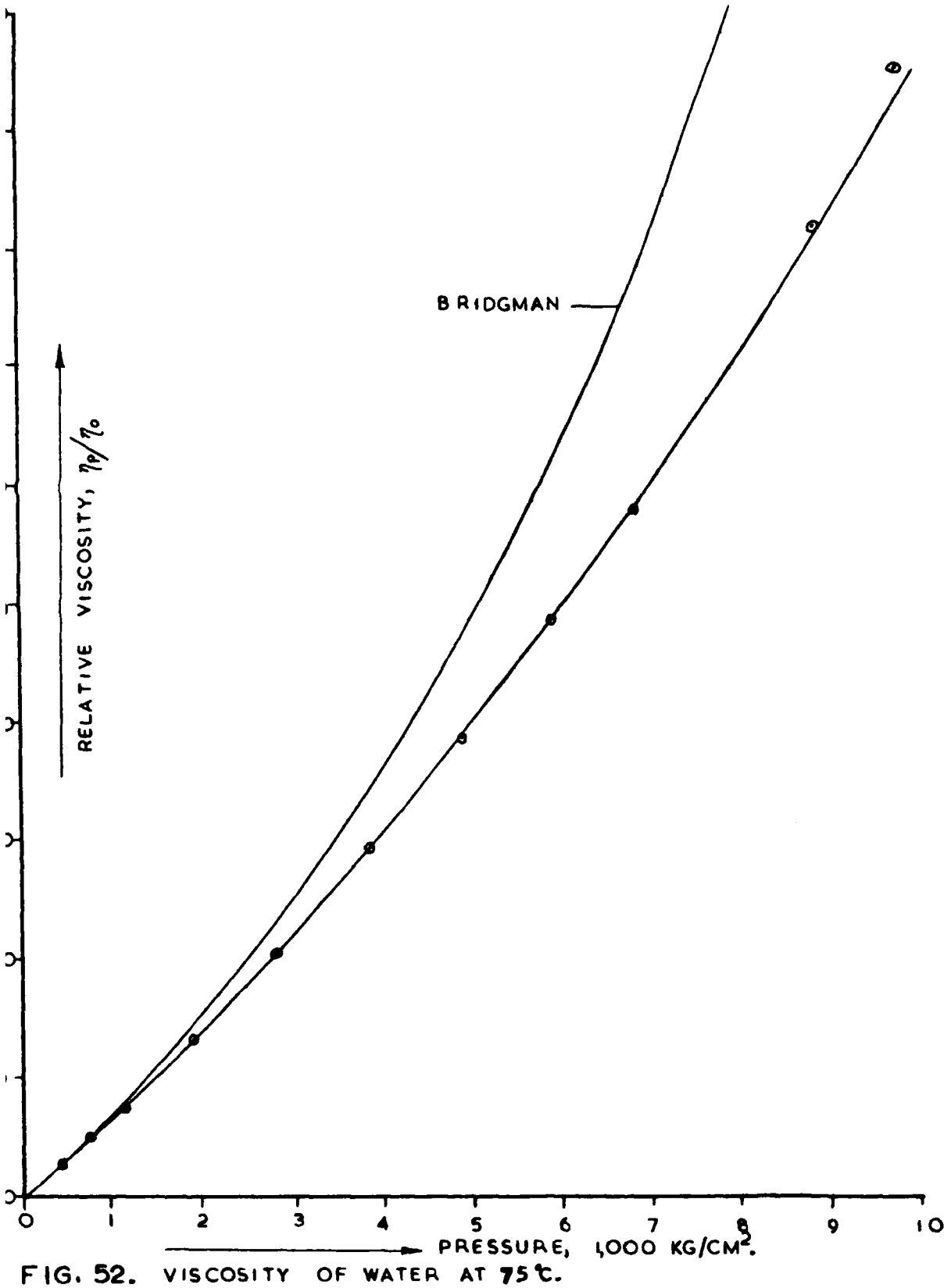

FIG. 52. VISCOSITY OF WATER AT 75°C.

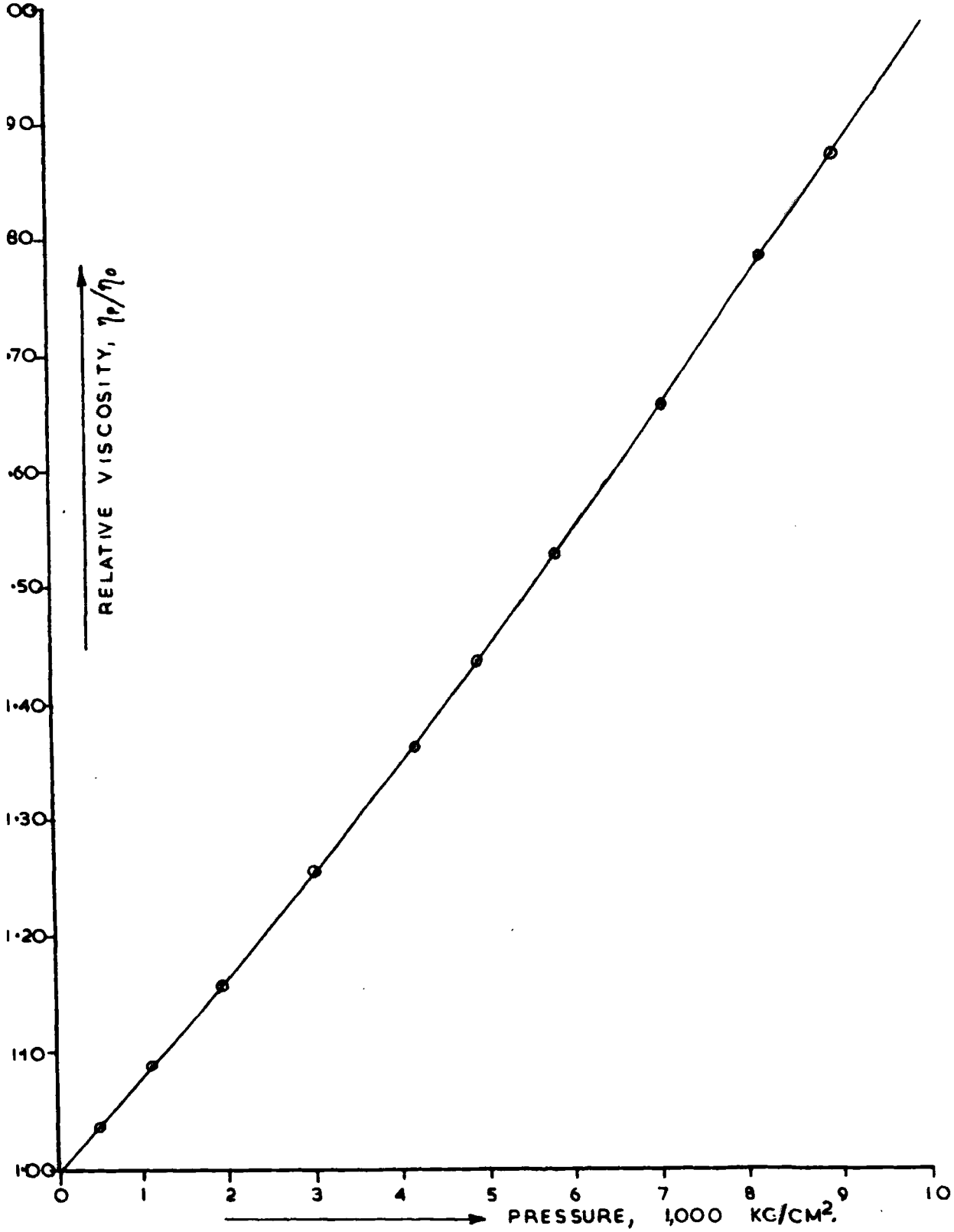

FIG. 53. VISCOSITY OF WATER AT 100°C.

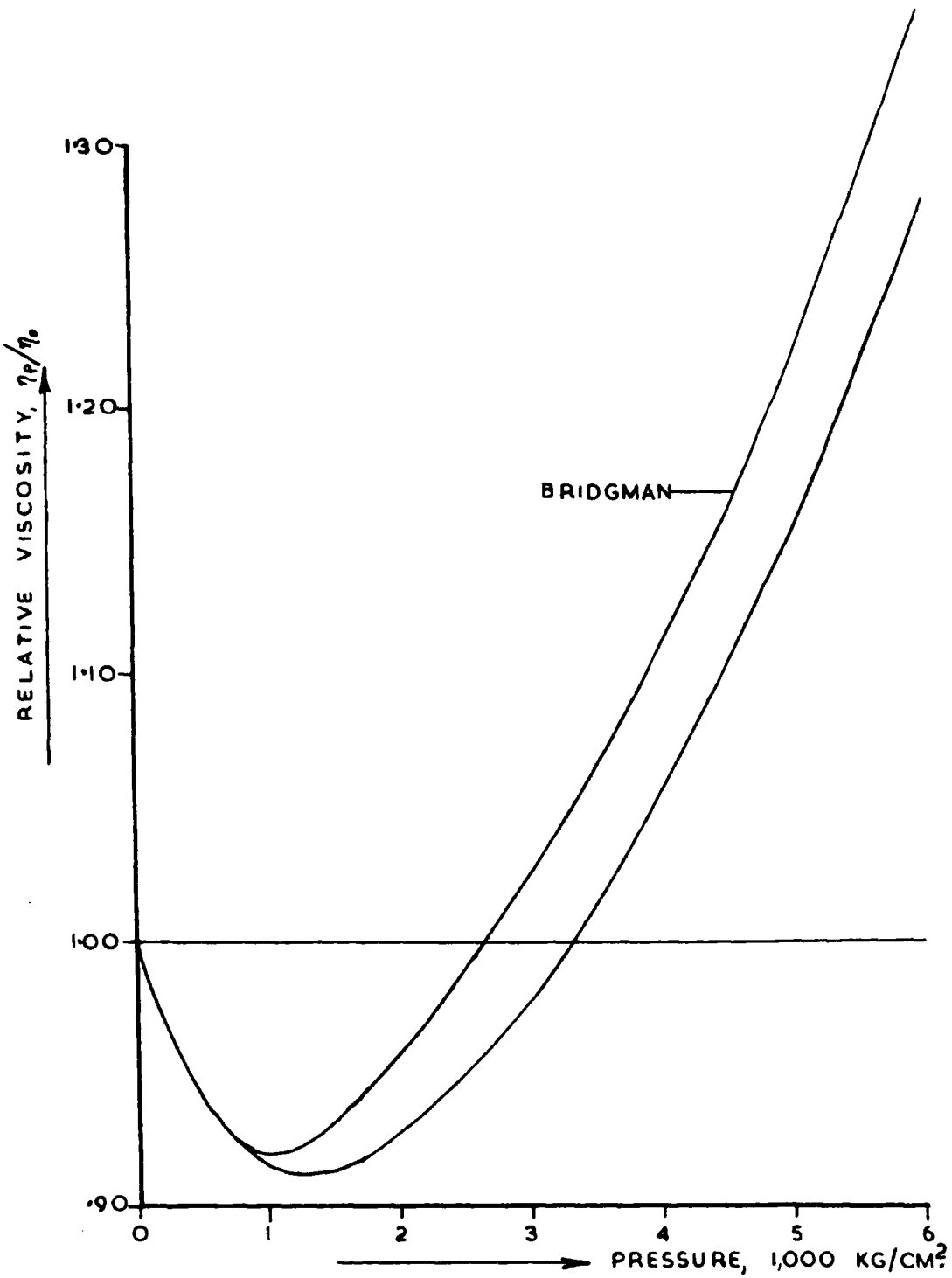

FIG. 54. VISCOSITY OF WATER AT 0°C (EXTRAPOLATED)

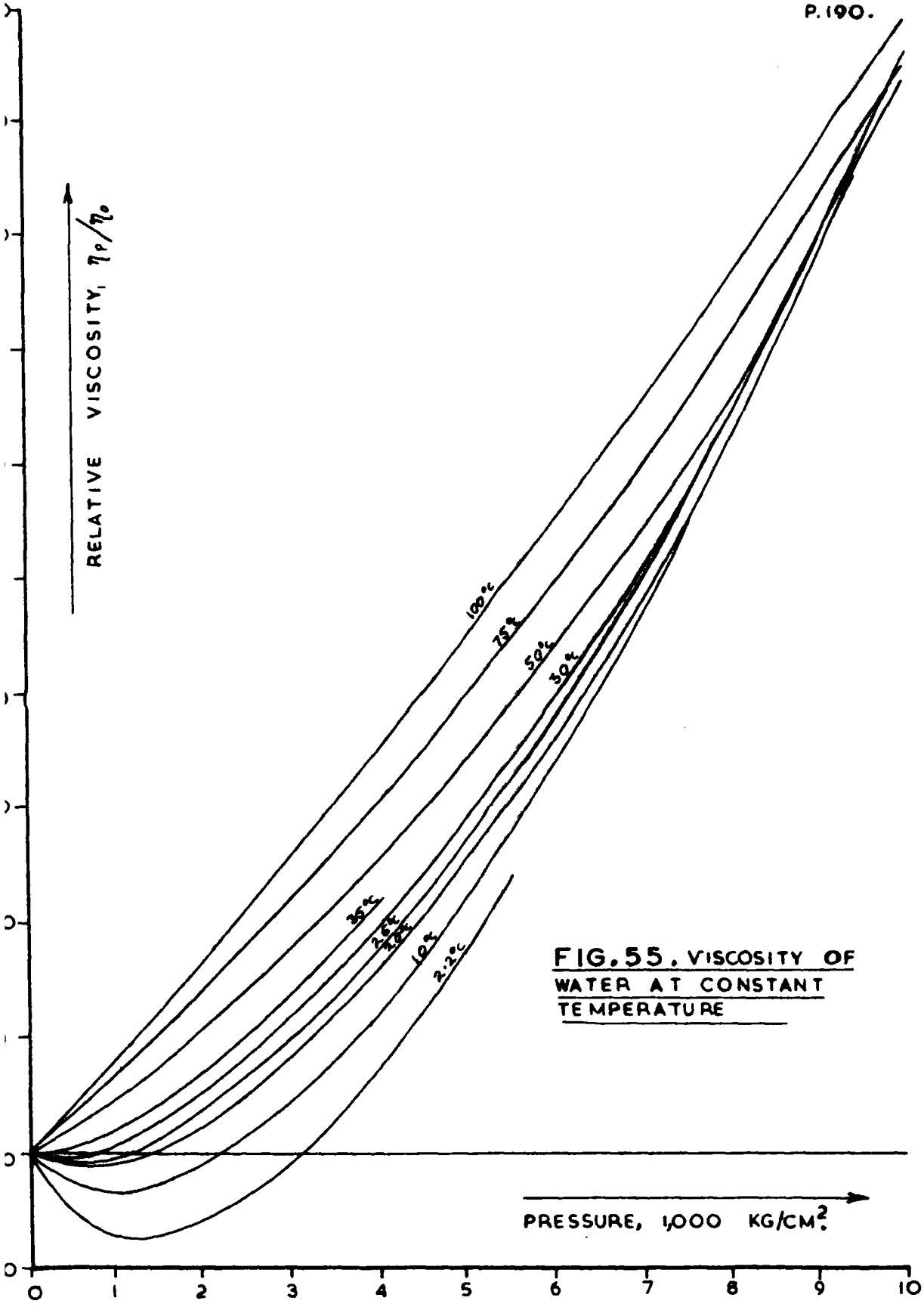

FIG. 55. VISCOSITY OF WATER AT CONSTANT TEMPERATURE

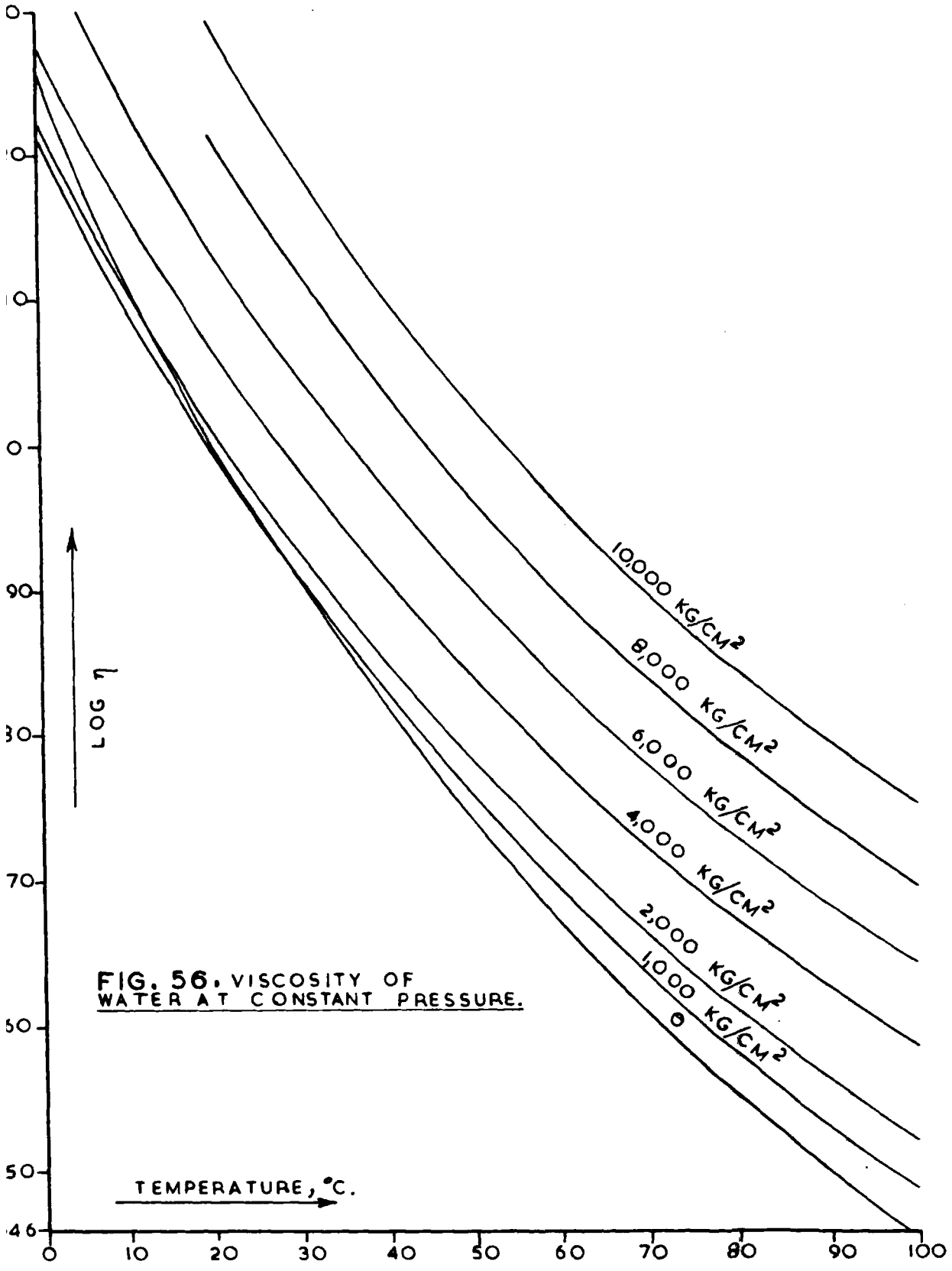

FIG. 56. VISCOSITY OF WATER AT CONSTANT PRESSURE.

the smoothed curves are the results for 75°C at the high pressure end of the isotherm. These results give a relative viscosity 1% higher than the smoothed results. In measuring these particular points, one of the soldered connections, in the timing circuit within the pressure vessel, became faulty at high pressure, and these conditions caused the malfunctioning of the timer. All other experimental points are within .5% of the smoothed results. The standard deviations are within .2%, and on half of the isotherms they are within .1%.

The isotherms for water are seen to exhibit an initial reduction in relative viscosity at the lower temperatures. In Fig. 57 is plotted the minimum relative viscosity achieved, vs. temperature, and the pressure at which the minimum occurs is plotted vs. temperature in Fig. 58. In Fig. 57, the axis $\eta_p / \eta_o = 1$, is intercepted at 33.5°C, and in Fig. 58, the axis P = 0 is also intercepted at this temperature. These intercepts correspond to the temperature at which the initial pressure coefficient of viscosity is zero.

(ii). Deuterium Oxide.

The experimental results for deuterium oxide are given in the specimen calculation in Appendix 4. As measurements were made at 25°C only, the results were smoothed only by fitting a curve to the points. However, the standard deviation from a smooth curve is less than .1%. The interpolated smoothed results are given in Appendix 4, and included in the table are values for the ratio ofthe viscosities of D_2O and H_2O. The results for the relative viscosity of D_2O at 25°C are plotted in Fig. 48 for comparison with the viscosity of H_2O at the same temperature. Fig. 59 gives the ratio of viscosities vs. pressure. The absolute viscosity of D_2O was taken from the data of Hardy & Cottingham [56].

(iii). Normal Pentane.

The experimental results for n-pentane are tabulated in

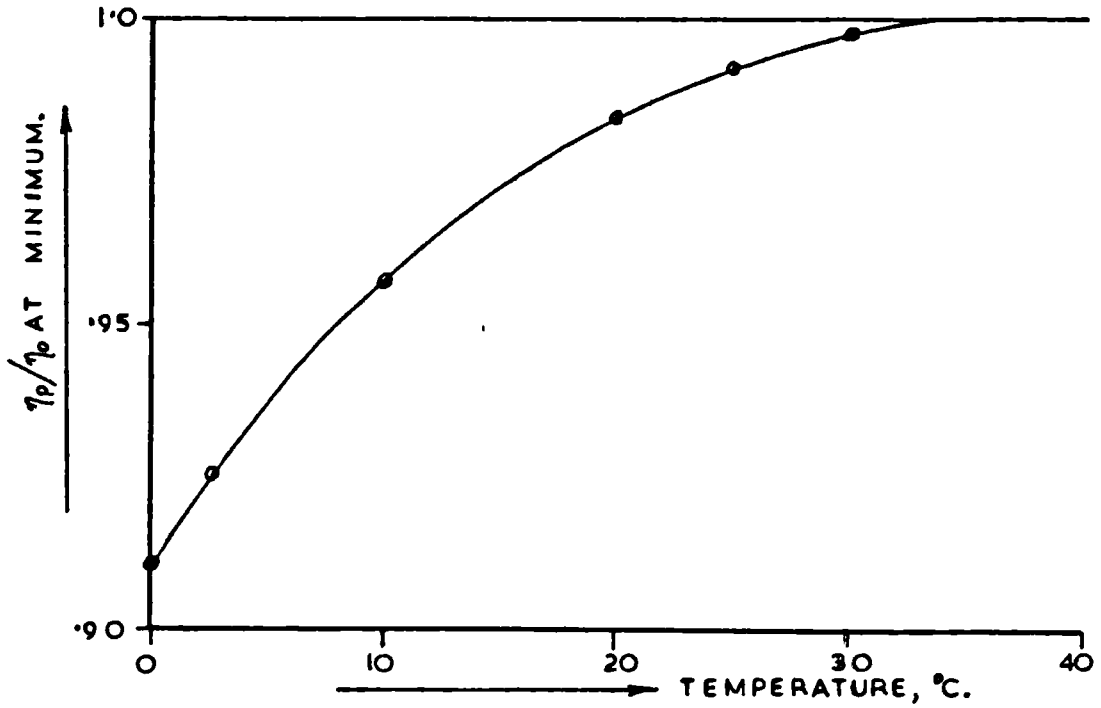

FIG. 57. TEMPERATURE OF VISCOSITY MINIMA FOR WATER.

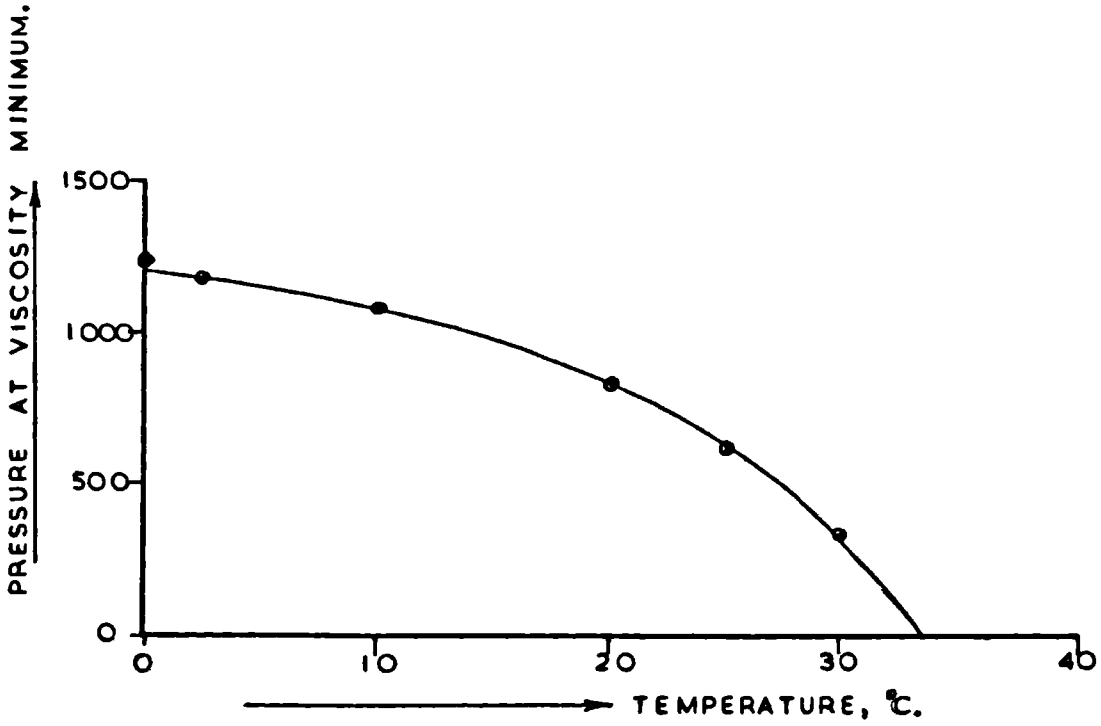

FIG. 58. PRESSURE OF VISCOSITY MINIMA FOR WATER.

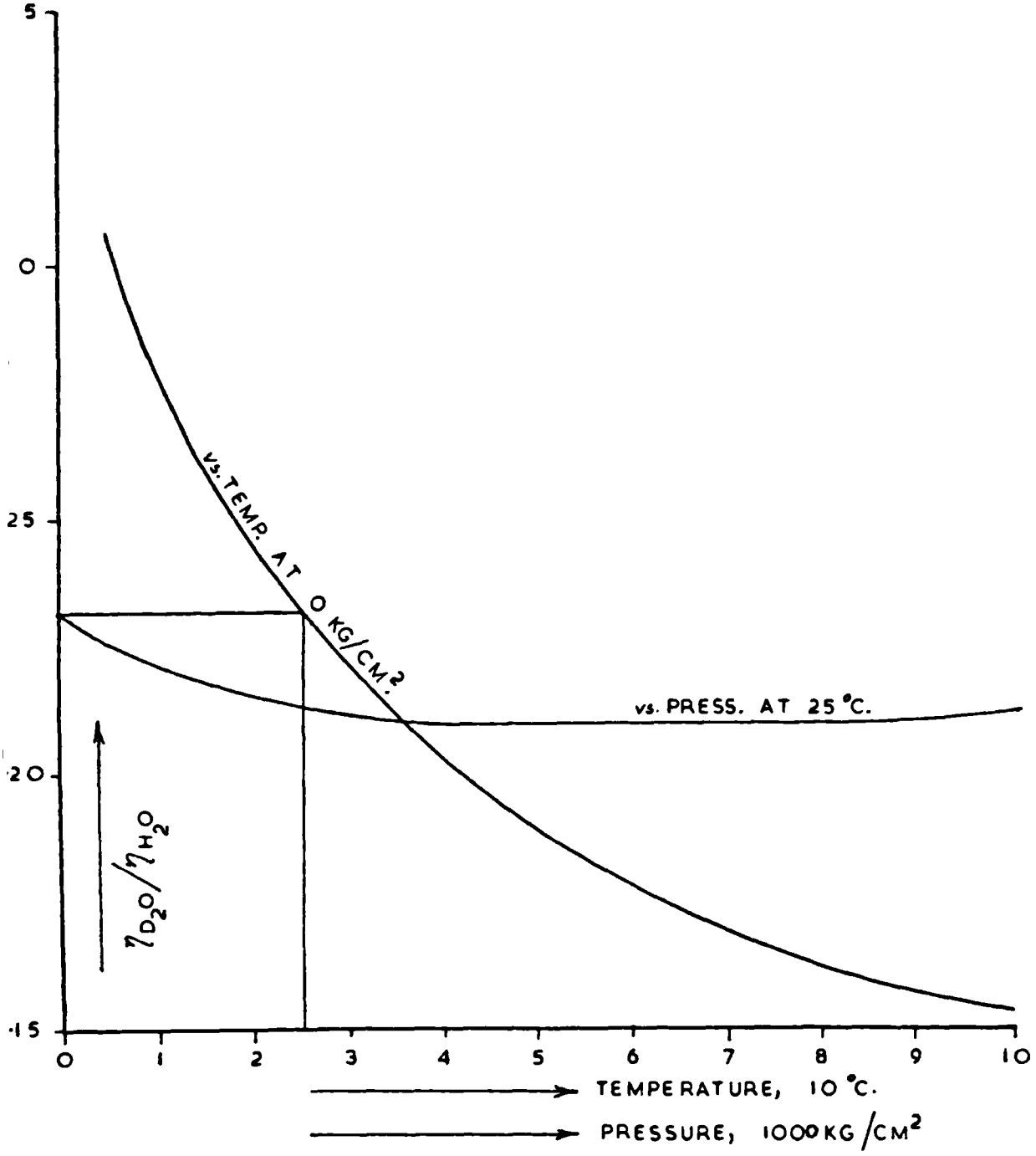

FIG. 59. VISCOSITY RATIO FOR H_2O AND D_2O.

Appendix 4. and the results are plotted in Fig. 41, for comparison with Bridgman's data. It was deduced in Chapter 10 that the experimental results were all 1.4% too high, and before smoothing, the results were adjusted by this amount. The smoothed results, obtained by plotting log (η_p / η_o) vs. pressure and interpolating, are tabulated in Appendix 4.

(iv). Pressure Transmitting Fluid.

See Appendix 4.

(v). Accuracy of Results.

The sources of errors, and their estimated magnitude, are as follows:-

1. Stability of time period counter = .02%.
   ∴ Possible error = $\pm$.02%.
2. The resolution of the triggering circuits is one cycle of the operating frequency, i.e. .002 seconds for each circuit. The maximum error for starting and stopping for one determination is therefore .004 seconds. At a fall time of 10 seconds, this would lead to an error of .04%. However, on averaging several determinations of the fall time, the error would become negligible.
3. In Chapter 9, it was shown that the maximum uncertainty in the distance between triggering positions is .1%. The possible error from this source is therefore, $\pm$.1%.
4. It was shown in Chapter 9 that the maximum error arising from the possible inclination of the viscometer tube is $\pm$.005%.
5. The fall time exhibits a random variation, most probably due to the fact that imperfections exist in the roundness and parallelism of the tube and of the sinker. These variations in fall time usually amount to .2%, and the mean of 8 or 10 falls

is normally reproducible to .05%. Also, an uncertainty exists in the fall time due to the possibility of contamination in the viscometer. When the level of contamination is sufficient to appreciably affect the results, its presence is obvious. The error in fall time that could be caused by an undetectable level of contamination is estimated as +.3%. The maximum error in determination of fall time is therefore +.35%, -.05%.

6. The maximum correction to the fall time for buoyancy changes under pressure is 4%. It is estimated that the density data employed lead to an error in this correction of 1%. The error in applying the correction is therefore $\pm$ .04%.
7. The maximum correction arising from dimensional changes under pressure amounts to .4%. As the correction is known to better than 5% (See Chapters 4 and 10), the error in applying the correction is $\pm$ .02%.
8. For water, the correction for turbulence in the worst case (100°C) amounts to $3\frac{1}{2}$%. It is estimated that the turbulence corrections are known to 15%. The error in the turbulence corrected time at 100°C, zero pressure, is then $\pm$ .52%. At 75°C, the correction is 2%, giving an error of $\pm$ .3%, and at 50°C, it is 1.2%, leading to an error of $\pm$ .18%, while at lower temperatures, the error rapidly approaches zero. For water at 100°C, 10,000kg/cm^2, the correction falls to 1%, giving a $\pm$ .15% error. In the case of n-pentane, the correction at atmospheric pressure was very large, and it was shown in Chapter 10, that the corrected fall time under this condition was in error by 1.4%. Consequently, the smoothed results for n-pentane have been adjusted accordingly.
9. The error in measuring temperature (See Chapter 8) leads to a $\pm$ .02% error in the results.
10. An error of $\pm$ 10kg/cm^2 at 10,000kg/cm^2 leads to an error of

$\pm$ .05% for water, and $\pm$ .2% for n-pentane.

The errors apply to the determination of the true fall time (referred to density and dimension conditions at atmospheric pressure) for the stated temperature and pressure. Relative viscosity is calculated from the ratio of corrected fall times under pressure and at atmospheric pressure. The individual time errors lead to errors in the ratio as follows:-

From 1, error = $\pm$ .04%.

From 2, error = 0.

From 3, the error at atmospheric pressure is zero, and increases with pressure to a maximum of $\pm$ .1%. The maximum error in the ratio is therefore $\pm$ .1%.

From 4, error = 0.

From 5, the error from reproducibility in the ratio would be $\pm$ .1%, and the error from contamination uncertainty is $\pm$ .3%. Then total error = $\pm$ .4%.

From 6, the error at atmospheric pressure is zero, and increases to a maximum of $\pm$ .04% at 10,000kg/cm^2. Then maximum error in ratio is $\pm$ .04%.

From 7, similarly, the maximum error is $\pm$ .02%.

From 8, the error in the turbulence correction tends to zero when the ratio of times is very close to 1, and the maximum error in the ratio occurs when one time of fall has a zero turbulence correction, the error being the same as the error on the shortest time. The errors from this source, therefore, vary from zero to $\pm$ .52%.

From 9, the ratio error is $\pm$ .04%.

From 10, the error varies from zero at atmospheric pressure, to $\pm$.05% for water, and $\pm$ .2% for pentane, at 10,000kg/cm^2.

The total error for a single relative viscosity at the stated temperature and pressure is between $\pm$ .48% and $\pm$ 1.21% for water, and up to $\pm$ 1.36% for pentane. The smoothing of the results

to some extent reduces the error on the interpolated results.

(vi). Accuracy of Smoothed Results.

Water. The effect of fitting a curve to the plots of relative viscosity vs. pressure is to reduce the random errors due to the variations in timer stability, reproducibility of fall time, and measurement of temperature. The cross plotting of interpolated isobars reduces the random errors arising from uncertainty of contamination and the systematic turbulence correction errors. It is estimated that all these errors have been reduced by smoothing to a half, giving an overall error, from these sources, of $\pm$ .5%. Smoothing does not reduce the systematic errors arising from constancy of fall distance, buoyancy correction, dimensional correction, and pressure measurement. These amount to $\pm$ .21%.

The overall accuracy of the results for water is therefore estimated to be $\pm$ .7%.

Heavy Water. As only one isotherm is available, the results could not be cross plotted. The errors from timer stability, reproducibility, and temperature measurement are reduced, by plotting the isotherm, to $\pm$ .09%. The contamination uncertainty is $\pm$ .3%, but as the maximum turbulence correction was only .2%, the error from this source is only $\pm$ .03%. The additional errors are the same as for water at $\pm$ .21%. The overall error for heavy water is therefore $\pm$ .6%.

Normal Pentane. Again, only one isotherm is available, giving a smoothed error on timer stability, reproducibility, and temperature, of $\pm$ .09%, and an uncertainty due to contamination of $\pm$ .3%. The 7.2% turbulence correction at atmospheric pressure could give an error of 1.1%, and it was shown in Chapter 10 that the probable error was in fact 1.4%. The results have been adjusted by this amount, but the 1.4% error was determined by a second sinker which itself had a $3\frac{1}{2}$%

turbulence correction. The turbulence error is therefore taken as 15% of $3\frac{1}{2}$%, i.e. .52%. Additional errors are the same as for water, except for the pressure error, in all amounting to .36%.

The overall error for n-pentane is, therefore, estimated as being $\pm$ 1.27% at the highest pressure, and $\pm$ .8% below 5,000kg/cm^2.

CHAPTER 13.

DISCUSSION A.

(i) Comparison of Results.

The estimated accuracy of the results in Chapter 12 is concerned mostly with factors which have been experimentally determined or verified. It is, however, difficult to verify what happens to the viscometer when pressure is applied.

Although the small corrections which have been applied for the effects of pressure have been derived entirely from theoretical considerations, the calculation of the density of n-pentane, in Chapter 10, has shown the essential correctness of this theory as it affects pressurisation.

In comparing the viscosity results for n-pentane with those of Bridgman, it was shown in Chapter 9 that, after allowing for Bridgman's error in pressure measurement, the two results differ by a maximum of 4% at 1,000kg/cm^2, falling to 1.5% at 10,000kg/cm^2. Itwas shown in Chapter 10 that the present results were 1.4% too high, which makes the two sets of results coincide at 10,000kg/cm^2, and gives a maximum difference of 2.6% at 1,000kg/cm^2. It is remarkable that the maximum difference should occur at the low pressure end of the experiments, and the explanation of this is to be found in Bridgman's assumption that viscosity was directly proportional to fall time of the sinker at all velocities. Bridgman calibrated the sinker with which the majority of his work was executed in a number of pure compounds which gave fall times covering the range 2.17 to 28.9 seconds. As these were for a 3cm. fall, the times compare with 12.9 to 173 seconds in the present instrument. After making corrections for the fact that, in Bridgman's instrument, the timing commenced as soon as the sinker moved with the tube in the inclined position, the ratio $\frac{\text{corrected time}}{\text{fluid viscosity}}$, as determined from

Bridgman's calibrations and published viscosity data, covered a range of values varying by 15%. Undoubtedly, a good deal of the variation was due to the unreliability of absolute viscosity data, but it is very likely that a non-linear effect was hidden in the large scatter of the calibration results.

The corrections which Bridgman had to apply to his viscometer, to take into account the inclination of the viscometer at the commencement of timing, and the acceleration to terminal velocity, were estimated as .0515 second at a fall time of 2 seconds. This 2.6% correction might in itself be in considerable error.

Further doubt is cast on Bridgman's results by comparing his ratio, $\frac{\text{viscosity at } 75^{\circ}C}{\text{viscosity at } 30^{\circ}C}$, with published values. Table 4 gives these ratios for some of the fluids listed in his investigation of 43 liquids under pressure.[19]

TABLE 4.

Compound	η_{30}/η_{75} Bridgman.	η_{30}/η_{75} from I.C.T.	% difference.
Methyl alcohol	1.702	1.722	-1.16
Ethyl "	2.203	2.134*	3.23
n-Propyl "	2.523	2.574	-1.98
n-Butyl "	2.845	2.696	5.53
i-Propyl "	3.141	3.031	3.63
i-Butyl "	3.597	3.299	9.03
i-Amyl "	3,805	3.132	21.49
n-Hexane.	1.574	1.475	6.71
n-Octane.	1.549	1.575	-1.65
Ethylene dibromide.	1.754	1.730	1.39
Ethyl bromide.	1.567	1.502	4.33
Ethyl iodide.	1.455	1.451	0.28
Ethyl acetate.	1.459	1.551	-5.93
Oleic acid.	3.811	4.109*	-7.25
Carbon tetrachloride.	1.738	1.703	2.06
Chloroform.	1.387	1.453	-4.54
Ether.	1.324	1.466	-9.96
Benzene.	1.718	1.680	2.26
Chlorobenzene.	1.535	1.571	-2.29
Bromobenzene.	1.581	1.650	-4.18
Aniline.	2.812	2.709	3.80
Diethyl aniline.	2.042	2.095	-2.53
Toluene.	1.600	1.566	2.17
o-Xylene.	1.710	1.631	4.84
m-Xylene.	1.589	1.551	2.45
p-Xylene.	1.596	1.581	0.95

* From Timmermans.

If it is assumed that a turbulence correction was applicable to Bridgman's work, similar to that found for the .004 inch clearance stainless steel sinker in the present work, a correction may be made to Bridgman's results for n-pentane. The fall time at atmospheric pressure, and 30°C, was 2.32 seconds, which corresponds to 13.7 seconds in the present instrument. Referring to Fig.39, this fall time should be corrected by reducing it by 3.2%. At 1,000kg/cm^2, the viscosity of n-pentane is 2.1 times its viscosity at atmospheric pressure, and Bridgman's fall time at 1,000kg/cm^2 would therefore have corresponded to 28.8 seconds, after buoyancy and dimensional corrections. Before corrections, the fall time would correspond to 29.1 seconds. Again, referring to Fig.39, the turbulence correction at this fall time is 0.9%. The net effect of these corrections would be to increase Bridgman's result by 2.3% at 1,000kg/cm^2, and by 3.2% at 10,000kg/cm^2. Comparing these corrected results with the present work, Bridgman's result is only .3% low at 1,000kg/cm^2, and 3.2% high at 10,000kg/cm^2. The agreement at the low pressure end of the experiment is therefore excellent, and the divergence of the results increases with pressure by a small amount only. The most likely explanation of the difference in the results is the purity of n-pentane employed, the purity of Bridgman's sample being unknown. The common impurity in n-pentane is iso-pentane, and according to Bridgman [19], the relative viscosity of iso-pentane at 10,000kg/cm^2 is 18% higher than that of n-pentane. If Bridgman's n-pentane was, in fact, sufficiently contaminated with iso-pentane to cause a 3.2% error, the difference in relative viscosities of the two isomers is 21%. Assuming a simple mixing law, a 15% concentration of iso-pentane in Bridgman's n-pentane would, therefore, account for the difference in the results at the highest pressure.

The results for water are compared with those of Bridgman in

Figs. 46, 49, 52 and 54. A comparison of the results reveals no general pattern of behaviour, for, at 75, 30 and 0°C, Bridgman gives a higher relative viscosity, whereas at 10°C, his relative viscosity is lower. At 0 and 10°C, Bridgman's results yield similar values for the minima in the curves, but at 30°C, the trends at low pressure are quite different. Except at 30°C, the results are in reasonably good agreement up to 1,000 or 1,500kg/cm^2. The best overall agreement is at 0°C, where Bridgman had the least difficulty with his apparatus; and at 5,000kg/cm^2, the two results differ by 6%. At 10°C and 7,000kg/cm^2, the difference in the results is 7%. At 30°C Bridgman's results exhibit no minimum in the relative viscosity curve, and the initial pressure coefficients are very different and of opposite sign. The largest difference in the viscosity values at 30°C occurs at 6,000kg/cm^2, where it is almost 16%. At 75°C the agreement at low pressure is good, but at high pressure, the two results diverge sharply. At 10,000kg/cm^2, Bridgman's relative viscosity is over 25% higher than the results of this work.

Bridgman's results for water are subject to the same criticisms and corrections as for those of pentane. However, as he gives no indication of the fall times employed for water, the necessary turbulence corrections cannot be assessed, and the correction for rotation of the viscometer, as a proportion of the atmospheric pressure fall time, is not known.

Bridgman experienced a great deal of trouble in applying his viscometer principle to water, and to polar liquids generally, the difficulty being caused by the unreliability of his break and make contact system of timing. For water, he employed three viscometers, one of carbon steel, and two of different grades of rustless iron. It was found that the carbon steel viscometer ionised the water so quickly as to form a permanent short circuit in the timing system, and the published results were obtained with a rustless iron tube.

At all temperatures, difficulty was experienced with conductivity in the water, and this became rapidly worse at rising temperatures. Further difficulty was caused by arcing between the sinker and tube causing an insulating film on the surface of the rustless iron, leading to unreliable operation of the timer; this effect also worsening rapidly with rising temperature. The malfunctioning of the timing system under these conditions is reflected in the large scatter of Bridgman's experimental points for water; at 75°C, the deviation of the points from a smooth curve is as much as 10%. Additional doubt is cast on Bridgman's results for water by the fact that for 0 and 10°C, half of the sinker was of a different grade of rustless iron to that of the tube, and at 30 and 75°C, a nickel sinker was employed. There is no indication in his publication that the results were corrected for the differential compressibilities which arise from the introduction of materials other than that of the viscometer tube. Finally, it can be seen from Table 5 that the temperature variation of viscosity derived from Bridgman's work compares unfavourably with the data of Bingham and Jackson [13].

TABLE 5.

TEMP. °C.	η_t/η_o Bridgman.	η_t/η_o Bingham and Jackson.	% difference.
0	1.0	1.0	-
10	0.779	0.729	6.5%
30	0.488	0.447	8.4%
75	0.222	0.212	4.5%

It is not surprising, therefore, that large discrepancies exist between the present results for water and those of Bridgman.

Above 900kg/cm^2, Bridgman's results for water are the only ones available for comparison. Below this pressure, however, water has received a little more attention. Roentgen [120], and Warburg & Sachs [138], carried out the first viscosity pressure measurements on water up to 20kg/cm^2 and 100kg/cm^2 respectively, at 6 and 30°C. Cohen [27] extended the pressure range on water to 900kg/cm^2, working at 1, 15 and 23°C, and Hauser [57] covered the temperature range 18 to 100°C up to 400kg/cm^2. These early workers, employing capillary instruments, all found a negative pressure-viscosity coefficient for water at the lower temperatures. Only Hauser, who worked at higher temperatures, observed a positive pressure-viscosity coefficient, and he found that the change in sign of the coefficient occurred at 32°C, which is close to the value of 33.5°C determined in this work. Hauser measured the transpiration time through a capillary at atmospheric pressure and at 400kg/cm^2, and his results are expressed in Fig.60 as % viscosity change at 400kg/cm^2, vs. temperature. Included for comparison in Fig.60 are corresponding results from the present work. It can be seen that the agreement with a smooth curve through Hauser's results is within .2%, except for 75°C, where it is .4%.

Cohen's results up to 900kg/cm^2, are represented in Fig.61, alongside suitable results from the present work. Although none of the isotherm temperatures coincide, it can be seen that the agreement between the two sets of data is within .2%. It is a tribute to these early high pressure experimenters that their work is in such good agreement with modern results, especially considering the handicap under which they laboured, of having to open their pressure vessels for every viscosity determination.

More recently, Moszinski [102] has studied the absolute viscosity of water over the temperature range 20 to 186°C, and up to 340kg/cm^2, employing an oscillating sphere viscometer. Moszinski's results were obtained for temperatures scattered fairly widely about

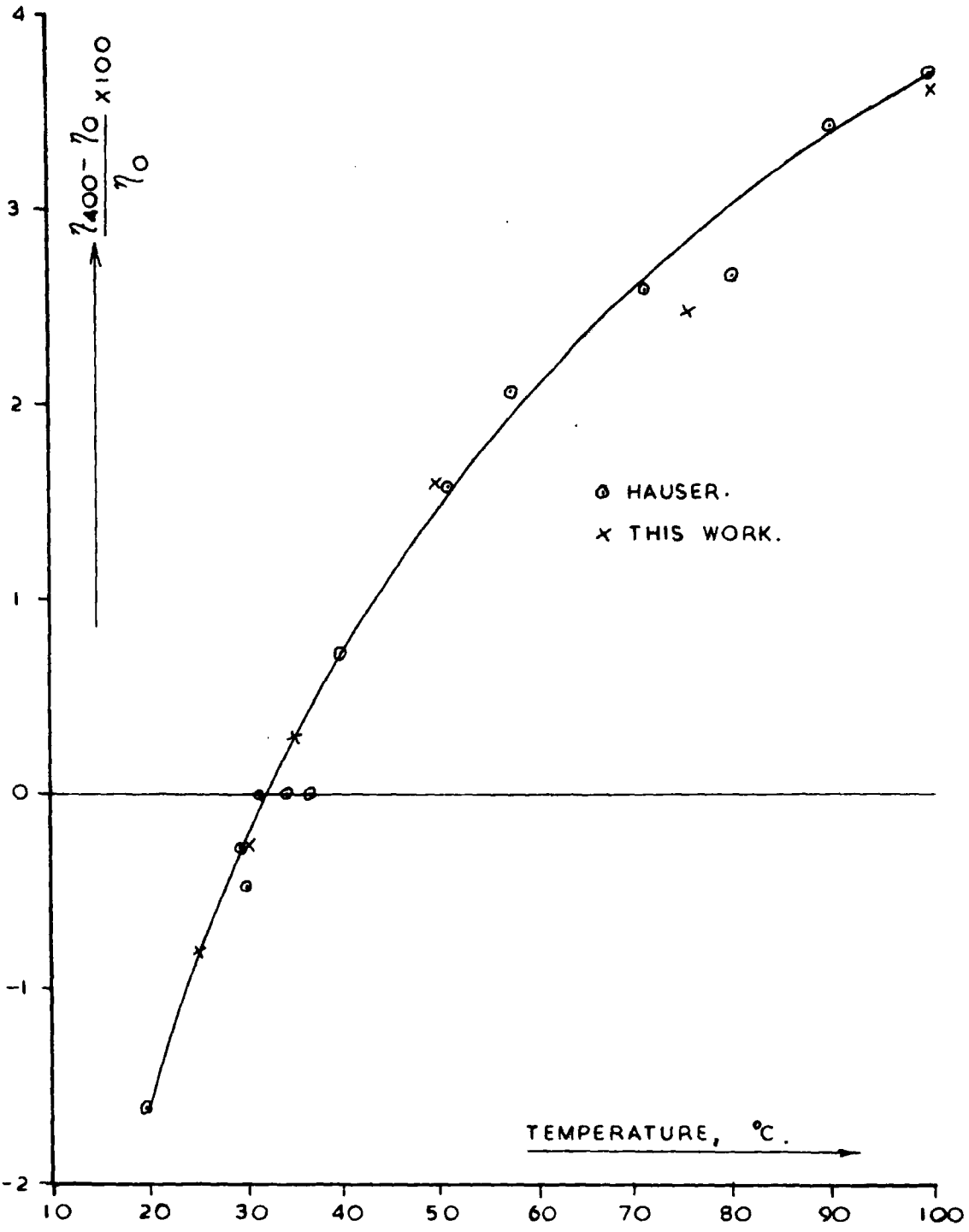

FIG. 60. VISCOSITY OF WATER AT 400 KG/CM^2, HAUSER.

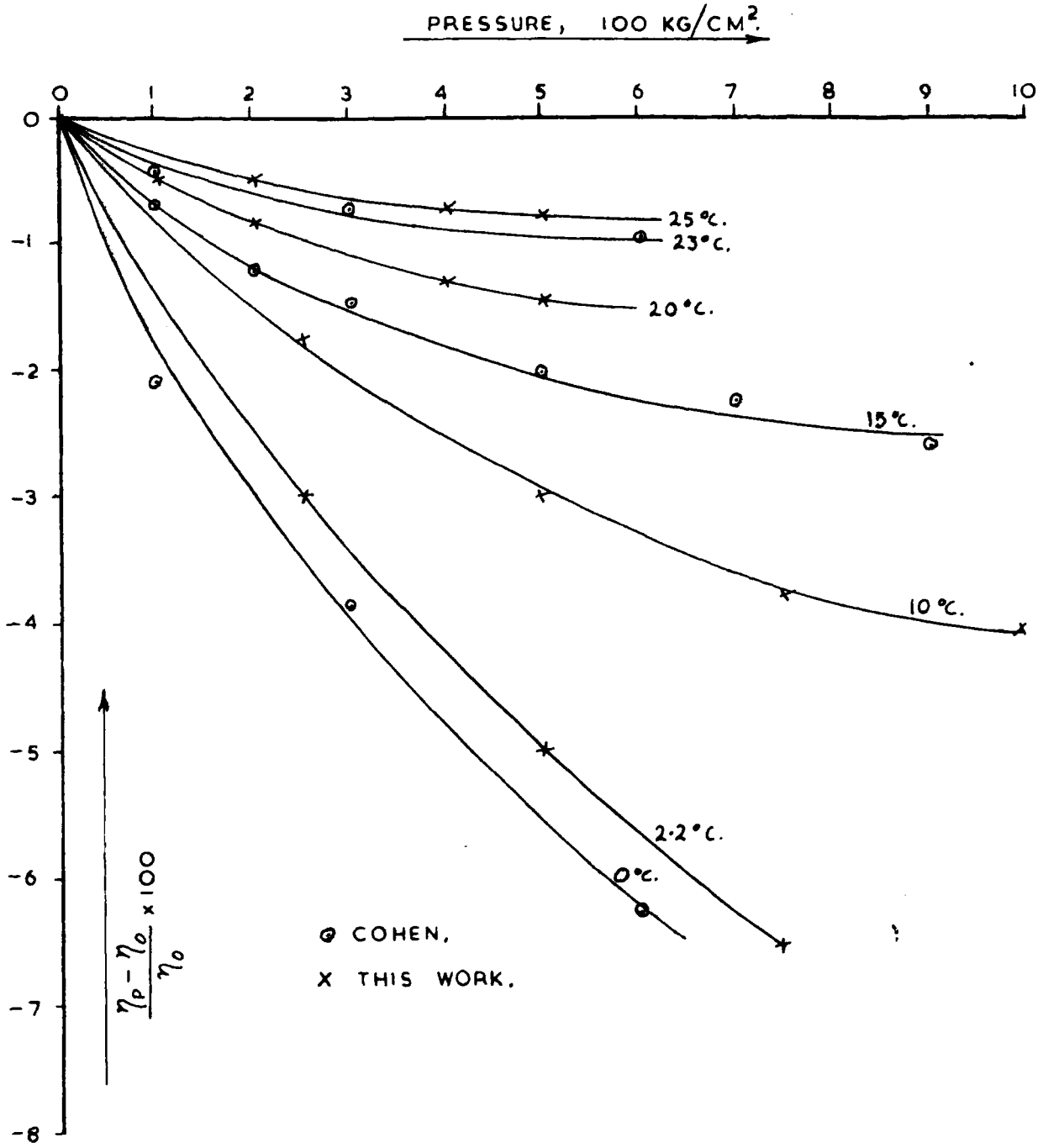

FIG. 61. VISCOSITY OF WATER, COHEN.

a nominal isotherm, and his results, expressed in Fig.62, have all been corrected to the nominal temperature. The agreement at 100 and 75°C is good, but Mosżinski's results at 28, 24, and 20°C are confused, and it is unlikely that the crossing of these isotherms, as indicated by Mosżinski's work, is real. The results for these temperatures do, however, fall into a similar range of values as the present work. Mosżinski found that at 20°C, his apparatus gave substantially different results for the viscosity of water before and after pressurisation, the effect being random. No explanation of this phenomenon has been offered, and the anomalous results of Mosżinski at the lower temperatures might be associated with this observation.

Weber [141] has recently published viscosity data for water up to 500kg/cm^2, over the temperature range 20 to 160°C. Weber's results are summarised and compared with this work in Fig. 63. The agreement at 20 and 25°C is very good, and Weber's isotherm for 32°C compares favourably with the 30°C isotherm. Also, the 32°C isotherm shows a slight negative pressure-viscosity coefficient, indicating the temperature of zero coefficient to be slightly higher than 32°C. The agreement between the 50 and 100°C isotherms is not quite so good, and at 500kg/cm^2, Weber's results lie ½% above those of the present work.

Weber's instrument consisted of a metal sphere rolling down an inclined glass tube. The most unsatisfactory feature of his apparatus is the large correction arising from the high compressibility of the glass, and the small compressibility of the metal sphere, and the increase in fall time of the sphere at 500kg/cm^2, caused by differential compressibilities alone, varied from 12 to 22%, depending on the diameter of the sphere. This large correction applies to an experiment where the observed viscosity change is almost zero at 32°C, and a maximum of 4% at 100°C. Weber sought to overcome this great disadvantage by repeating

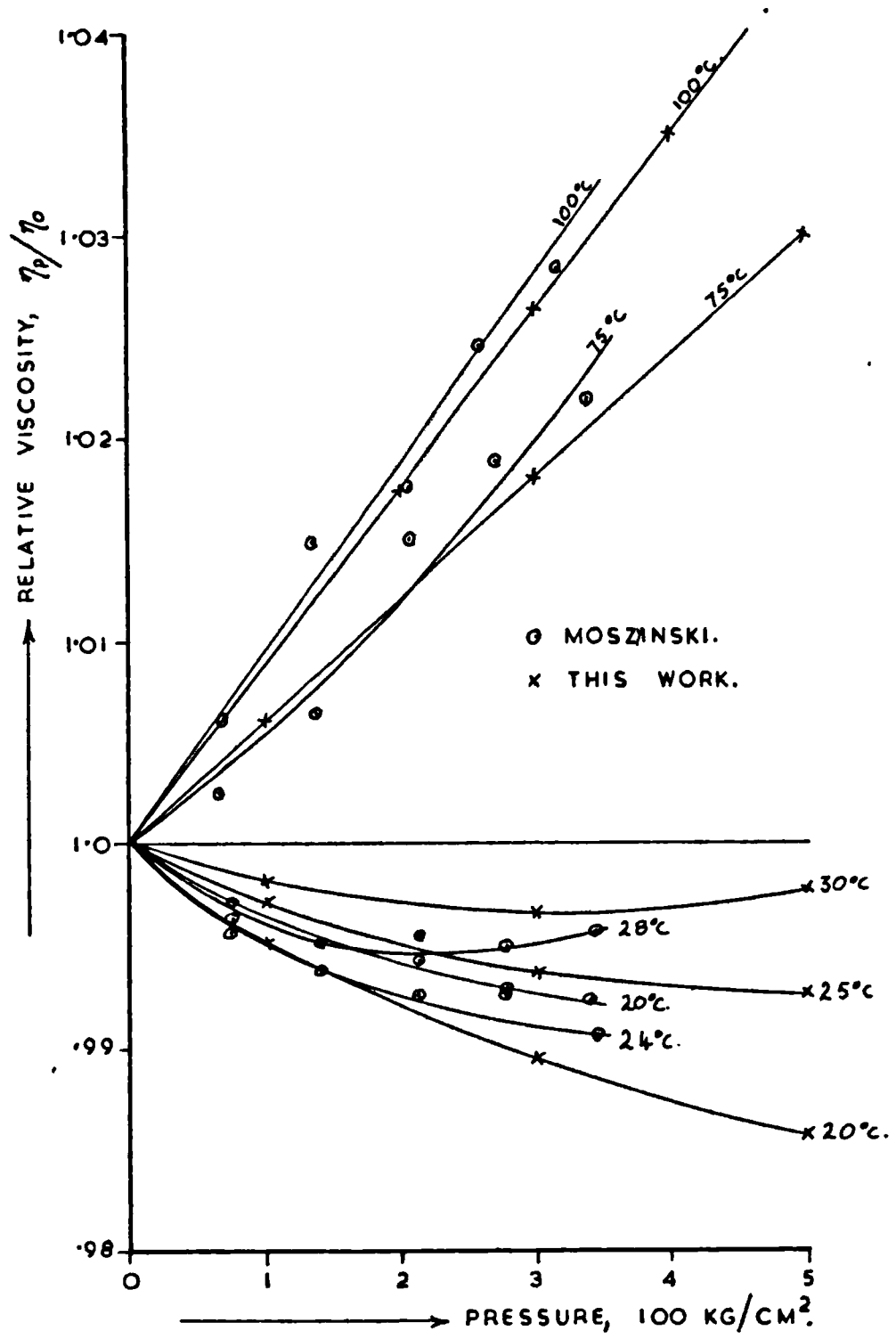

FIG. 62. VISCOSITY OF WATER, MOSZYNSKI.

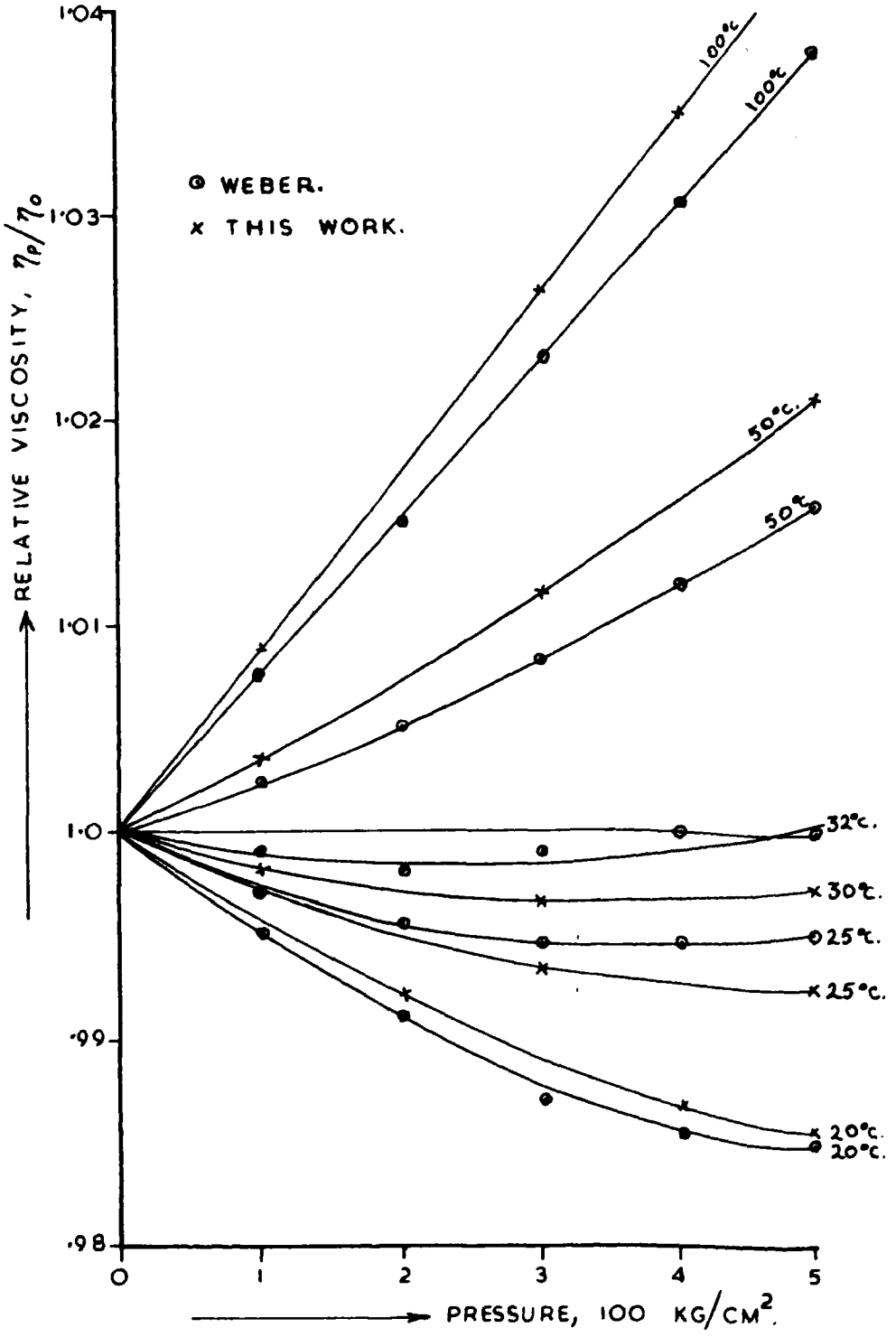

FIG. 63. VISCOSITY OF WATER, WEBER.

the experiment many times with spheres of different diameters, and at various inclination. In fact, 10,000 experiments are claimed to have been made to determine the reported results for water. An assumption made in order to eliminate the errors of the large compressibility correction is that the viscometer constant is directly proportional to the sine of the angle of inclination. As the inclinations to the horizontal varied from 80° to 88°, the assumption of proportionality is not valid, as the film thickness under the rolling ball, and the degree of slipping of the ball, would be dependent on the angle of inclination in this region. Furthermore, buoyancy corrections of the sphere are neglected, and no correction is made for the change in length of the viscometer tube caused by the increase in pressure. As the compressibility of the tube is so high, the latter effect would be significant, even at $500 kg/cm^2$.

Thus, the agreement with existing low pressure data is generally good, and well within the experimental error, in spite of the fact that most of the data have been obtained at a pressure below that of the first observation in the present work.

(ii) Improvement of the Apparatus.

As the object of constructing this high pressure viscometer was to provide viscosity data for a wide range of fluids, suggestions for the improvement of the apparatus, after this relatively brief experience of operation, is of some importance. Improvements should be directed towards increasing the accuracy of the instrument, although this is already good, and to extending the velocity range over which an individual sinker may be employed. To some extent, these two basic requirements are inter-related.

(a) High pressure system.

The operation of the high pressure system, in so far as it affects the accuracy of the viscometer, and the convenience of its operation, is satisfactory except for the behaviour of the let down valve. This tends to lower the pressure in the system in a rather erratic manner, making smooth reduction of pressure difficult. Gradual pressure change is important in order to achieve fine adjustment of pressure and obviate the detrimental effects that sudden pressure reductions have on the sealing of the viscometer. The erratic nature of the valve is caused by slight sticking of the valve spindle in its seat, rather than by sensitivity of adjustment, and it is suggested that the angle on the valve spindle should be changed from 60° to 90°, or to an even larger angle if found to be necessary.

The error in viscosity introduced by errors in pressure measurement are small in the case of water (.04%), and pentane (.2%). However, when dealing with fluids possessing considerably higher pressure coefficients than these, the pressure error can become significant. The largest error in pressure measurements, is caused by the accuracy with which the freezing pressure of mercury is known, and the fact that only a single calibration point exists in the high pressure region. This

error may be reduced to some extent by calibrating the manganin gauge directly against a dead weight pressure gauge over the whole pressure range to 100,000 p.s.i. Errors in measuring the gauge resistance may also be reduced. A considerable correction is introduced by the temperature variations of the manganin coil, and a further error is caused by the hysterisis inherent in its temperature measurement. The manganin coil pressure gauge, should, therefore, be thermostated for improvement in accuracy, as should the Smith's bridge.

(b) Viscometer.

The greatest weakness in the existing viscometer is the sealing arrangement. As stated previously, the viscometer was designed to operate with O ring seals, and subsequently had to be adapted for use with metal compression seals. These are satisfactory for rising and steady pressures, but tend to leak on reducing the pressure. The first requirement of an improved viscometer must be a better sealing arrangement. If metal seals are to be retained, an improvement should be made by providing the viscometer with heavier threads, allowing a greater pre-loading of the seal, and by designing the seal so that the seal and the thread diameters are as similar as possible. By this means, the effect of temperature gradient through the seal would be reduced.

An alternative approach to the sealing problem might be to use PTFE as the sealing material, in spite of its phase change at 6,000kg/cm^2, and its combination of low elasticity and high compressibility. Two suggested methods for applying PTFE viscometer seals are illustrated in Figs. 64a and b. The principle of both of these is that the contraction on the diameter of the PTFE ring, caused by compressibility, forces the ring against a ramp, and so maintains the vertical component of compression required to form a seal. If a seal of this kind is found to be satisfactory under the conditions of high hydrostatic pressure, the simplicity of an O ring can be retained without the disadvantage of "swell pumping" observed with elastomers

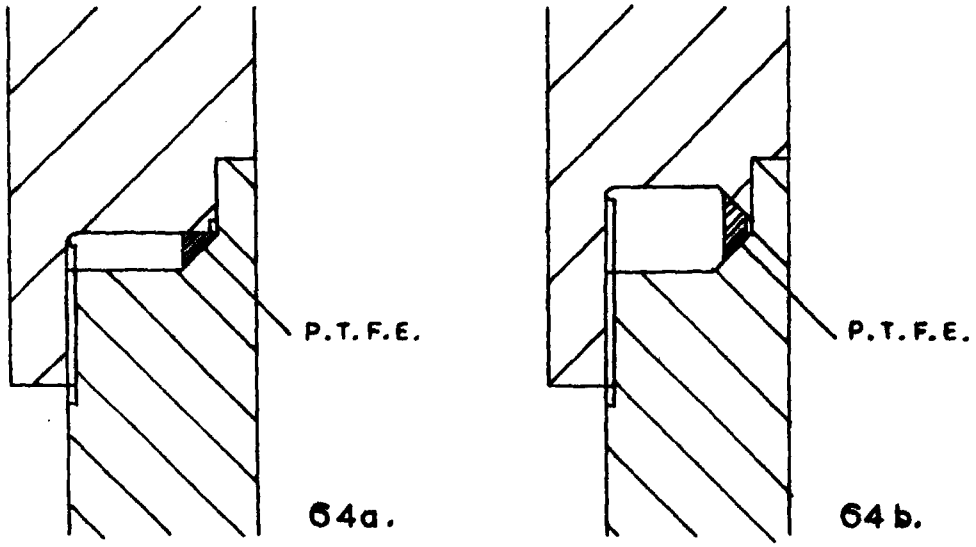

FIG. 64. VISCOMETER SEALS.

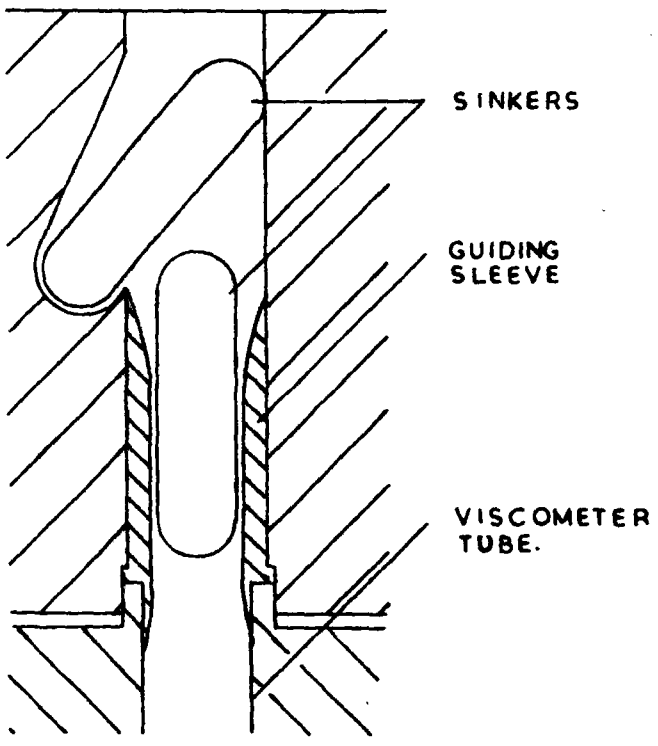

FIG. 65. SINKER GUIDE.

under these conditions.

Small variations in the roundness and diameter of the viscosmeter tube cause large variations in the radial clearance around the sinker, and this is detrimental in two respects. Firstly, such variations help to introduce random variations in the fall time of the sinker, and therefore introduce an error. An improved tube would permit slightly greater accuracy and reduce the number of observations of fall required, which is particularly important at long times of fall. Secondly, and this is perhaps of greater significance, variations in the clearance around the sinker introduce forces on the sinker which cause it to deviate from the axis of the tube. At low terminal velocities, where the sinker has the greatest tendency to fall eccentrically, or to wander about its coaxial position, a better tube than the existing one might extend the fall time at which a given sinker will fall satisfactorily. The present tube has variations of .0003 inch on its diameter, and any improvement on this would contribute towards better performance.

No attempt has been made to produce better sinkers than the ones employed in this study, but the operating experience, together with the work of Scott [125], and of Lohrenz, Swift & Kurata [84], has pointed the way to a better design.

Perhaps the most important question to be answered, in connection with sinker design, is whether or not guiding pins are necessary. Their drawbacks are considerable, and in certain respects, their elimination would be very advantageous. The disadvantages of guiding pins are as follows:-

1. They are very difficult and tedious to make, and complicate the design of the sinker in that their inner ends must be ventilated.
2. The depth of the pins embedded in the body of the sinker is not uniform, and symmetrical spacing of the pins is difficult

to achieve. Both of these lead to asymmetric mass distribution in the sinker, which helps to cause the onset of eccentric fall at low velocities.

3. Asymmetric spacing of the guiding pins causes asymmetric shear stress distribution over the surface of the sinker. This also provokes instability in the sinker at low velocities.

4. As the clearance between the ends of the guiding pins and the tube wall is very small, a high shear stress exists on the ends of the guides. It is impossible to produce all the pins of identical length, and the shear stress on the end of each pin will not be identical. The guiding pins, therefore, lead to yet another source of asymmetrical shear stress distribution.

5. The pins are in a region of high velocity flow, and the degree of turbulence around the pins is much greater than in the remainder of the annulus. At the higher terminal velocities, turbulent wakes will exist behind the pins, which are undesirable, as they add to the kinetic energy losses which limit the maximum velocity at which a sinker may be employed. Also, the turbulent wakes cause buffeting against the side of the sinker, which helps to provoke the instabilities at high velocities observed by Scott [125], and so limits the maximum velocity at which the sinker may be used.

On inverting the viscometer, the guiding pins fulfill a useful function when the pressure vessel is suddenly retarded near its vertical position. As the sinker falls, it is thrown by the retardation to one side, and the guiding pins limit the eccentricity and steady the motion of the sinker. If the pins were eliminated, the system employed by Jobling and Lawrence [69] could be used, in which the sinker commences its fall in a tube only slightly larger

than the sinker, and concentric with the viscometer tube. Fig. 65 illustrates the principle as it should be applied to a 'two-sinker' viscometer. The guiding sleeve at each end of the viscometer would have to be, say, .001 inch larger than the largest sinker, (the high density sinker), and the low density sinker could be an extra .001 inch smaller. (The clearance may be increased for increased sinker-tube clearances). The fall times of the high and low density sinkers could be made similar, even with their similar diameters, as indicated later.

The guiding sleeve method would be superior to the guiding pin method of steadying the initial fall of the sinker in several respects. The extent to which a sinker could oscillate about its coaxial axis in a guiding sleeve would be similar, or only slightly greater, than is the case with guiding pins. However, because of the small clearance between the body of the sinker and the guiding sleeve, the damping forces and the centralising forces are very much greater than for the guiding pin method. The guiding sleeve will, therefore, be very much more efficient at stabilising the motion of the sinker. An additional advantage of the guiding sleeve is that the terminal velocity of the sinker in the sleeve is much lower than in the tube. Thus, even at the shortest fall times, it would be a simple matter to stop the rotation of the vessel well before the sinker starts to fall in the viscometer tube. At long fall times, this low terminal velocity is a disadvantage, as a considerable delay will be incurred as the sinker passes through the sleeve. Also, a disadvantage is that a set of sleeves must be provided for each set of sinkers.

At fall times where the motion of the sinker is steady, and the centralising forces on the sinker are sufficient to maintain concentric fall, the guiding pins have no effect. It was shown in Chapter 9 that the onset of eccentricity or instability at low vel-

ocities was sudden. The behaviour of the sinker was either stable or unstable, and no intermediate degrees of stability were observed. Under these conditions, by the time the sinker is sufficiently eccentric or unstable for the pins to be of any use, the results are of no value for the calculation of viscosity. Thus, at low velocities, guiding pins do not perform a useful function.

At high terminal velocities, the oscillatory and lateral instability which Scott observed (see Chapter 4), can become so violent that a sinker without guiding pins can collide with the viscometer tube. In Scott's work, employing unguided sinkers, the fall time at which instability began was equivalent to about 4 or 5 seconds, and collisions occurred at fall times equivalent to 2 or 3 seconds. Thus, under high velocity conditions, guiding pins serve no useful purpose, for as already mentioned, their presence probably provokes oscillation at a lower velocity, and almost as soon as oscillation sets in, the pins collide with the tube and introduce friction effects.

It is considered that the advantages of guiding pins are few, and the disadvantages numerous. What useful purpose the pins fulfill may be provided by other means, and it is recommended, therefore, that an improved viscometer be based on unguided sinkers with the provision of guiding sleeves at each end of the viscometer.

Scott's investigation into the performance of the falling body viscometer was carried out mainly with square ended sinkers, and a few observations on hemispherical and 90° cone ended sinkers showed no difference in their general behaviour in comparison with square ends. This is not surprising, as the cross section at a very small distance away from the annulus entrance or exit, is very much greater than in the annulus, and the shapes so far employed would therefore have little effect. Also, at the higher terminal velocities, the high velocity stream emerging from the annulus is presented with much

the same widely divergent conditions whether the end be square, hemispherical, or 90° conical. The section at the annulus exit diverges so rapidly that the fluid stream breaks away from the sinker surface, and the kinetic energy is dispersed in a turbulent region a short distance behind the sinker. This turbulent region was actually observed by Scott with a square ended sinker falling in a glass tube, filled with a colloidal suspension of acetone in water.

The sinker shape recommended for further work is illustrated in Fig.66. It is a square ended cylinder, with a slight conical section at each end. The external shape has been kept as simple as possible, so that mass and shear stress distribution may be as perfect as possible. Also, to ensure a uniform mass distribution, the sinker is solid (and non-magnetic), and contains no soft iron pellet. The good mass and shear stress distribution of such a sinker should go a long way towards improving performance at low velocity.

The purpose of the conical sections is twofold. At velocities where the kinetic energy of the annular fluid stream is significant, it is desirable to recover as much of the kinetic energy as possible, in order that turbulence may be reduced. A reduction of turbulence reduces the correction that must be made to the fall time at high velocities, and also reduces the disturbances which cause instability in the sinker at high velocities. Any improvement along these lines will allow the sinker to be used at shorter fall times, which is very important. In the suggested design, a good deal of the kinetic energy would be recovered in the diverging section at the annulus exit. In venturi meter practice, diverging angles up to 7° are found satisfactory for recovering 80 to 90% of fluid stream kinetic energy. At angles greater than this, breakaway begins to set in, resulting in turbulence. A diverging angle of 2 to 5° is recommended, therefore, as being capable of good kinetic energy

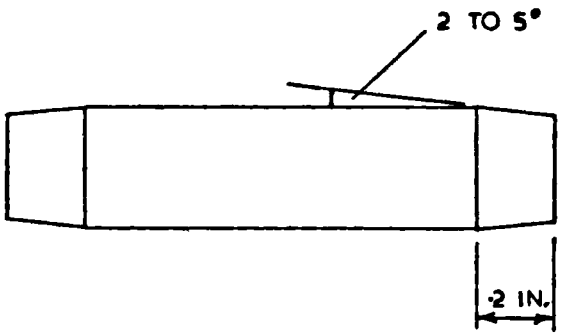

FIG. 66. SUGGESTED SINKER DESIGN.

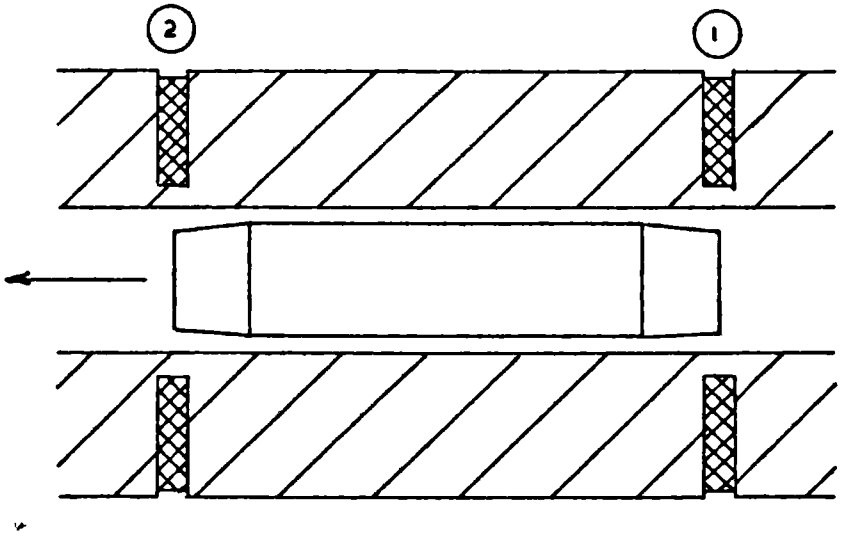

FIG. 67. SUGGESTED TIMING SYSTEM

recovery. An angle of 2° increases the radial clearance by .035 inch per inch length of sinker, and by .087 inch per inch in the case of 5°. If the conical section were .2 inch long, a .004 inch clearance sinker with a 2° cone increases the cross section available for flow by a factor of almost 3 at the very end of the sinker. A .009 inch clearance sinker, with a 5° cone, increases the flow section by a factor of just over 3. In both these cases, the velocity of the fluid stream is reduced by a factor of about 3 before breaking away from the sinker, which reduces the kinetic energy by a factor of 9. Assuming the divergent sections to be 80% efficient in recovering kinetic energy, the kinetic energy loss is reduced by a factor of 7. Thus, the possible reductions in the turbulence corrections at high velocities are considerable.

The gradual fluid acceleration into, and retardation out of the annulus, brought about by the conical sections at each end of the sinker, produces centralising pressure forces in the convergent and divergent sections. This is advantageous at low velocities, and the conical sections should contribute to the extension of satisfactory performance of the sinker into the low velocity region.

The use of a solid non-magnetic sinker will require some modification of the timing technique. It may be recalled from Chapter 3 that in the development of the timing system, trouble was experienced with eddy currents induced in the sinker when operating at 6kc/s. The eddy current effect on the timing coils was sufficient to trigger the timer, and the operating frequency had to be reduced to 500 cps to eliminate the interference. The proposed timing system is based on the reduced inductance of a coil by eddy currents, instead of the increased inductance by ferro-magnetism, and the system suggested is illustrated in Fig. 67. The distance between the coil centres is equal to the length of the sinker, and the coils are

wound exactly as before as part of an a.c.bridge. As the sinker enters coil 1, the coil inductance is reduced by eddy currents induced in the sinker, and puts the bridge out of balance. As the sinker approaches the position shown in Fig.67, the inductance of coil 2 decreases, and that of coil 1 increases. Thus a bridge balance point and phase change occurs just as in the present system. Apart from the repositioning of the coils and the reversal of the reference signal, the whole timing system may be used as it stands. The eddy current signal was considerable at 6kc/s, but if the circuit is operated at 24kc/s, the signal will be 16 times as great. This operating frequency should be satisfactory, as the amplifiers and Schmitt triggers are suitable for use at 30kc/s, and the signal generator is capable of 50kc/s. The proposed system should have a sensitivity equal to the present system, yet allow considerable simplifications to be made in the sinker design.

The only problem remaining is to endow a high and low density sinker with similar fall times. To facilitate symmetrical mass distribution, both sinkers must be solid. Also, they must be of similar diameter in order that the guiding sleeve may work properly. However, by making the low density sinker, say, .001 inch smaller than the high density sinker at small sinker clearances, a considerable increase in terminal velocity of the low density sinker may be achieved. At larger clearances, the diameter difference between the two sinkers may be increased. The two sinkers must be of the same length, but by making the length of the conical portions on the low density sinker greater than those on the high density sinker, a further increase in the terminal velocity of the low density sinker can be produced.

CHAPTER 14

DISCUSSION, B.

(i) Anomalous Behaviour of Water.

In common with almost every other property of water, the viscosity-pressure relationship, shown in Fig.55, is clearly anomalous. Normal behaviour is typified by the results for n-pentane, plotted as $\log(\eta_p/\eta_o)$ vs pressure in Fig.41, from which it may be seen that the first 2,000kg/cm^2 or so produces a greater than exponential rise in viscosity, followed by an almost exactly exponential viscosity-pressure relationship. Apart from the first 2,000kg/cm^2, the viscosity of n-pentane may be expressed at constant temperature as

$$\eta_p = A\exp(PB) \qquad 26.$$

where A and B are constants.

The first and most obvious anomaly in the viscosity behaviour of water is the existence of negative viscosity-pressure coefficients, and minima in the viscosity isotherms at the lower temperatures. No other compound has been found to exhibit this property. Secondly, the effect of pressure on the viscosity of water is very much smaller than for other materials, (except the liquid metals). Under a pressure of 10,000kg/cm^2, the viscosity of water increases by a factor of 2, whereas the next smallest pressure effect is that for methanol, whose viscosity increases by a factor of 9. Lastly, in the case of water, the viscosity-temperature ratio, $\eta t_1/\eta t_2$, at 10,000kg/cm^2 is about the same as at atmospheric pressure, whereas it is normal for this ratio to increase with pressure. For example, Bridgman's results for n-pentane give η_{30}/η_{75} as 1.5 at atmospheric pressure, and 2.0 at 10,000kg/cm^2.

The abnormal behaviour of water may be better illustrated by plotting $\log(\eta_p/\eta_o)$ vs pressure, as is usual for normal liquids. Fig.68 shows such a plot for the data at 100, 50, and 30°C. Although the magnitude of the pressure effect is small, it can be seen that water at 100°C exhibits normal behaviour in that above 2,500kg/cm^2, its viscosity increases exponentially with pressure. The behaviour at 50°C is 'normal' above 5,000kg/cm^2, but below this pressure, the curve is concave to the pressure axis instead of the more usual convex form. At 30°C this behaviour is even more exaggerated, and normal behaviour is not achieved until 6,000kg/cm^2. Thus, the greatest abnormality occurs at low temperature, and normal behaviour is approached at high temperatures. Except over a limited range of pressure-temperature conditions, the viscosity of water cannot be described by the general group of empirical and semi-empirical equations of the form

$$\eta_p = f_1(V,T)\exp(f_2(P,V,T))$$

In Appendix 5, the expression,

$$1/\eta \left(\frac{\partial \eta}{\partial P}\right)_T \simeq C/\beta_T \qquad 27.$$

is derived on the basis of the dependence of molecular collision frequency on volume, suggesting that the viscosity-pressure coefficient is a function of compressibility only. As a test of this expression, and its application to water, $1/\eta\,(\partial\eta/\partial P)_T$ is plotted against the isothermal compressibility coefficient $-1/V\,(\partial V/\partial P)_T$, for water, and for various other compounds at 30°C, in Fig.69. The density and viscosity data used for this purpose are those of Bridgman,[19,24] except the viscosity results for water, taken from the present work. Unfortunately, most of the data are not sufficiently detailed or precise to evaluate $(\partial\eta/\partial P)_T$ and $(\partial V/\partial P)_T$ accurately, especially the

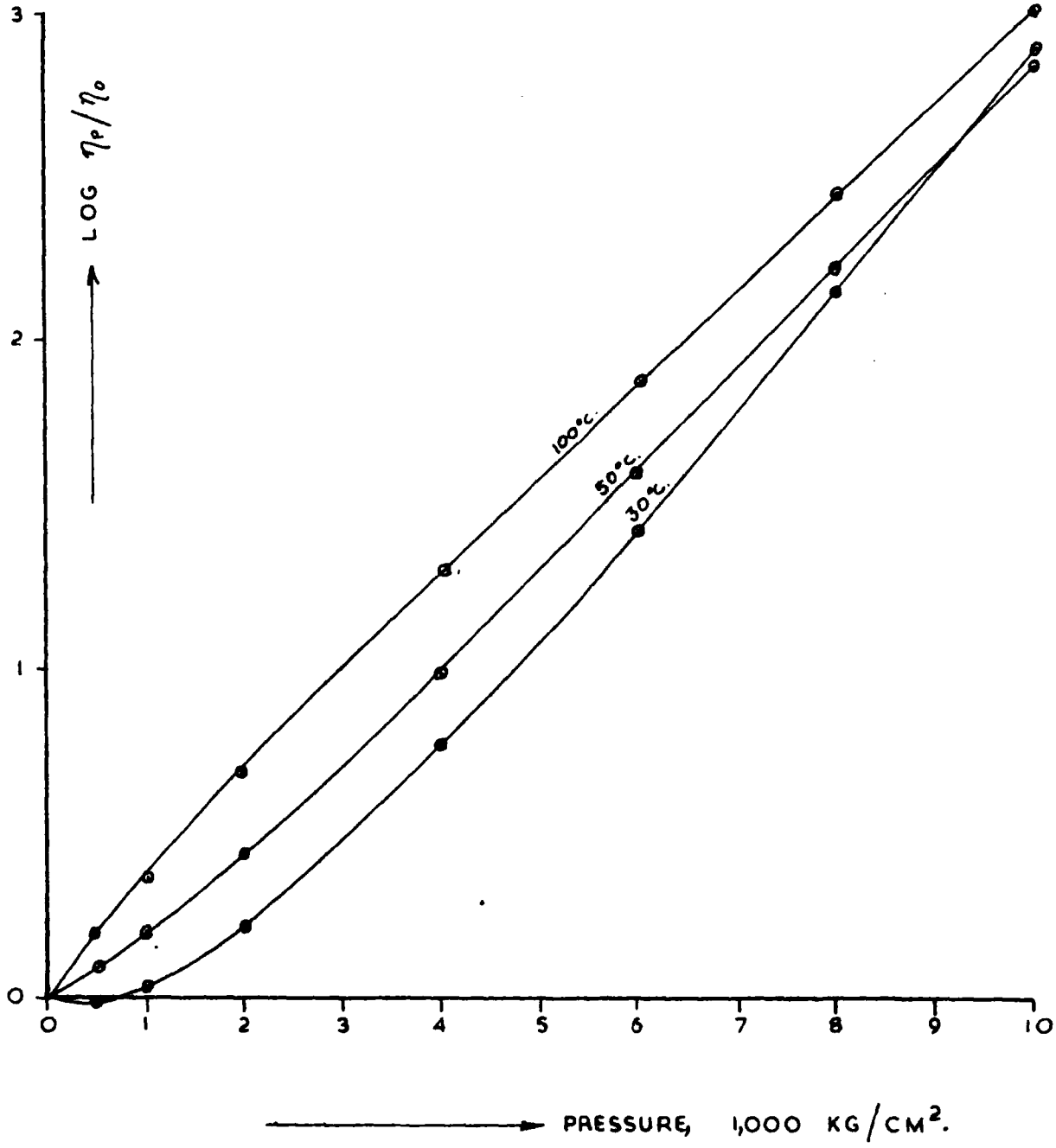

FIG. 68. LOGARITHMIC PLOT OF WATER VISCOSITY.

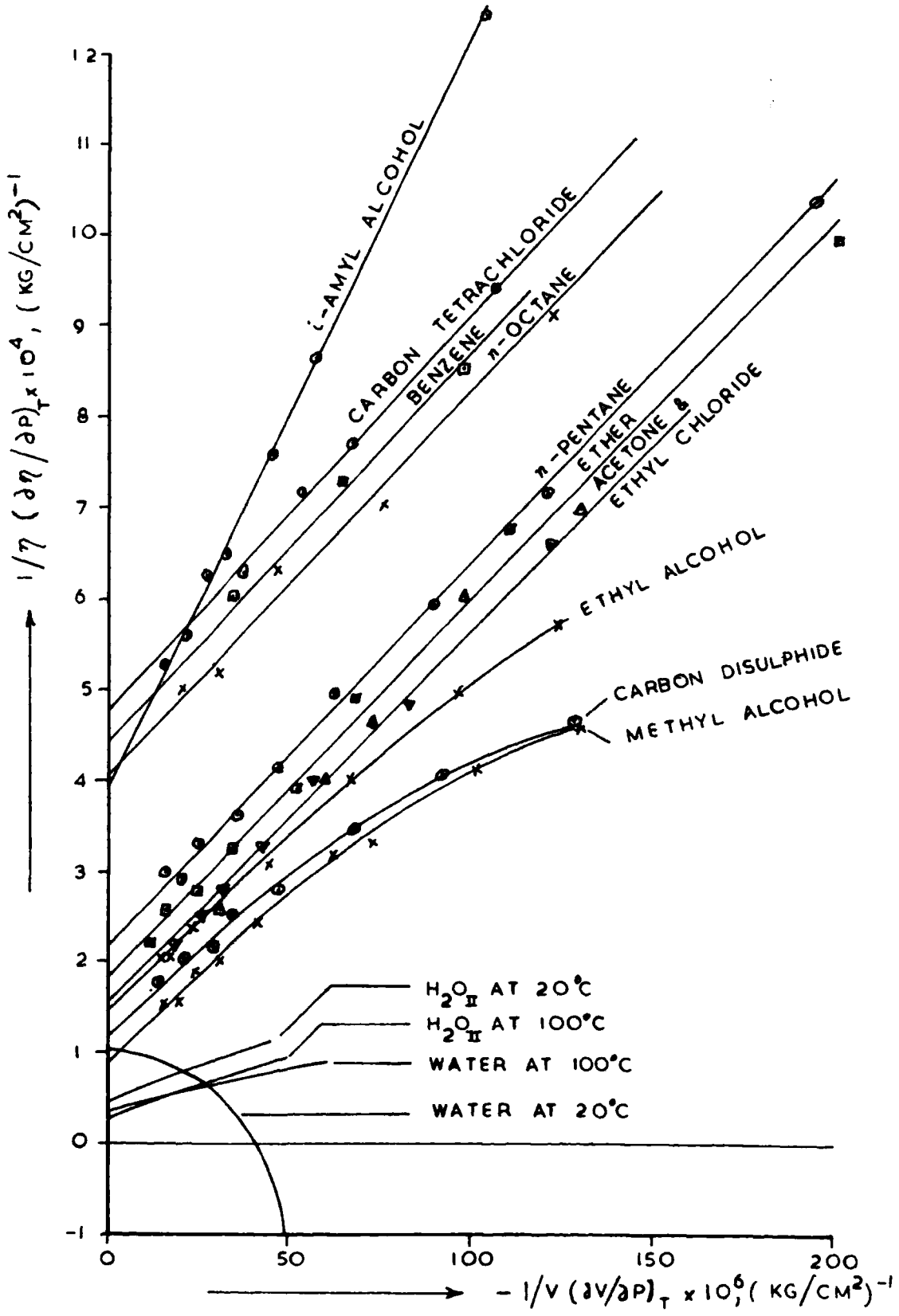

FIG. 69. VISCOSITY AS A FUNCTION OF COMPRESSIBILITY.

density data which have to be interpolated and extrapolated over quite large temperature ranges. However, within the limitations of the data available, it can be seen from Fig.69 that n-pentane, n-octane, acetone, ether, ethyl chloride, carbon tetrachloride, benzene and i-amyl alcohol all give a linear relationship between viscosity-pressure coefficient, and compressibility. However, the relationship is not as predicted by equation 27, but is of the form

$$1/\eta \left(\partial\eta/\partial P\right)_T = C\beta_T + D. \qquad 28.$$

It is interesting that all the compounds so far mentioned, except iso-amyl alcohol, have a common value of C, equal to 4.2, which compares favourably with the approximate value, 3.3, predicted in Appendix 5. The value of C for iso-amyl alcohol is 8.4. Ethyl and methyl alcohol do not conform to the general pattern at low pressures, where compressibility is large, but at high pressure, the curve becomes a straight line with the common slope, 4.2. Presumably, the hydrogen bonding in these two compounds causes the anomaly at low pressure, and it is significant that methyl alcohol, which has the greater degree of bonding, exhibits the greater deviation from normal behaviour. Carbon disulphide, which one would have expected to show normal behaviour, exhibits the same tendencies as the low alcohols. There is no explanation apparent for this anomaly, except, perhaps, the use of inaccurate data.

Thus, Fig.69 shows that most liquids, of widely differing molecular structure and size, and of greatly differing pressure-viscosity effects, may be represented by equation 28. Included in Fig.69 are the results for water at 20°C and 100°C. Again, at 100°C, water can be seen to be approaching 'normal' behaviour, but at 20°C, it can be seen that $1/\eta \left(\partial\eta/\partial P\right)_T$ is negative at high compressibilities, and that the slope is of opposite sign to all other liquids.

The effect of pressure on the viscosity of water, therefore, is without any doubt, fundamentally different from normal behaviour.

(ii). Isotopic Substitution.

If the dimension t is eliminated from the dimensions of viscosity, $\eta = ml^{-1}t^{-1}$, by writing $t = m^{\frac{1}{2}}l^{-\frac{1}{2}}k^{-\frac{1}{2}}T^{-\frac{1}{2}}$, the dimensions of viscosity become [86], $\eta = m^{\frac{1}{2}}l^{-2}k^{\frac{1}{2}}T^{\frac{1}{2}}$. 29. where k is Boltzmann's constant.

If the molecules of the liquid interact with a central potential, characterised by the parameters ε and σ (as in the Lennard-Jones potential), then equation 29 can be re-written by dimensional considerations, in the dimensionless 'reduced' form, [96]

$$\eta^* = \eta\sigma^2\varepsilon^{-\frac{1}{2}}m^{-\frac{1}{2}}. \qquad 30.$$

When a molecule is isotopically substituted, the mass is changed, but the intermolecular potential parameters ε and σ remain virtually unchanged. If subscript i refers to an isotopic species, then, from 30,

$$\eta_i/\eta = (m_i/m)^{\frac{1}{2}}. \qquad 31.$$

This relationship applies only to systems where momentum transfer involves only convection or vibration of the molecules. In the case where momentum transfer involves only rotation of the molecules, the molecular mass must be replaced in equation 31 by the moment of inertia, I, whence,

$$\eta_i/\eta = (I_i/I)^{\frac{1}{2}}. \qquad 32.$$

Isotopic substitution can, therefore, provide information on the mechanism of transport processes.

In the case of the H_2O - D_2O system, the masses are such that,

$(m_i/m)^{\frac{1}{2}} = 1.054$

The three principle moments of inertia are, (63)

$(I_{Ai}/I_A)^{\frac{1}{2}} = 1.340$; $(I_{Bi}/I_B)^{\frac{1}{2}} = 1.414$; $(I_{Ci}/I_C)^{\frac{1}{2}} = 1.390$,

The mean of these gives, $(I_i/I)^{\frac{1}{2}} = 1.381$

The results of Hardy and Cottingham[56] for $\eta D_2O / \eta H_2O$, between the melting point of D_2O at 5°C, and 100°C, are plotted in Fig.59, together with the same ratio at 25°C, up to 10,000 kg/cm^2, calculated from the present results. It can be seen that the ratio falls from 1.301 at 5°C to 1.151 at 100°C, and at all times, η_i/η lies between $(m_i/m)^{\frac{1}{2}}$ and $(I_i/I)^{\frac{1}{2}}$, indicating that, in the case of water, rotation, as well as convection and/or vibration is involved in momentum transfer at atmospheric pressure, The viscosity ratio at 25°C falls from 1.231 at atmospheric pressure to 1.208 at 4000kg/cm^2, and is then constant at this value with increasing pressure. Between 8000 and 10,000kg/cm^2, the ratio rises by .2%, but this could well be due to experimental error. It appears, therefore, that, whereas the mechanism of momentum transfer changes considerably with rising temperature, the transport mechanism is substantially constant with rising pressure, and includes a significant rotational contribution.

(It is noteworthy that in the case of energy transport, i.e. thermal conductivity, a similar relationship to equation 31 can be derived, and $\lambda H_2O / \lambda D_2O = (m_i/m)^{\frac{1}{2}}$. (96)).

(iii). The Structure of Water.

It is a generally accepted fact that the structure of water is strongly influenced by the existence of extensive hydrogen bonding, and that the explanation of most of the anomalous properties of water is to be found in its structure.

Theories of the structure of water have been reviewed by Némethy & Scheraga.[107] Modern theories are represented by those of Pople[113] and Frank & Wen [49, 50], and these two theories are an interesting contrast in that Pople's is based on a completely hydrogen bonded homogenous single species structure, whereas Frank & Wen proposed a partially hydrogen bonded dual species structure.

In the model of Pople, water retains the tetrahedral hydrogen bonded structure which is found in ice, but the O-H---O bonds are bent. Also, bonds are continually broken and remade, which provides a degree of mobility to the structure and introduces long range disorder. The co-ordination number remains at 4, as in ice, but because of the bending of the bonds, some of the molecules in the second and third shell are able to collapse into the first shell around a particular molecule, thus explaining the apparent increase in co-ordination number found by Morgan & Warren, [101] in their X-ray scattering studies. On the basis of this model, Pople was able to calculate a radial distribution function which was in good agreement with that measured by X-ray techniques. Also, calculated dielectric constants were found to be of the same order as observed values. The reduction in volume of ice on melting was explained by the partial collapse of the second and third shells into the first shell, but no other properties of water have been explained in terms of this theory.

Frank & Wen postulate that water consists of two species, one of which, designated H_2O_I is ice-like, and the other, designated H_2O_{II} water like. H_2O_I consists of clusters of molecules which are hydrogen bonded into a tetrahedral, ice like structure, (but not necessarily with the hexagonal packing found in ice) with little or no bending of the bonds.

H_2O_{II} consists of unbonded molecules which have a closer packing than H_2O_I, and although this species is unbonded, the large dipole-dipole interactions exert a considerable influence on the motion and orientation of the molecules. H_2O_I is in equilibrium with H_2O_{II} on a macroscopic scale, but on a molecular scale, H_2O_I is continuously breaking up and reforming in other regions as a consequence of local energy fluctuations. Frank & Wen have termed the ice structure in water as "flickering clusters", as a description of their mode of existence. The presence of these distinct hydrogen bonded clusters is based on Frank's hypothesis[50] that hydrogen bonding is a co-operative phenomenon. The essence of this theory is that when two water molecules form a hydrogen bond, the resulting charge distribution is such that additional hydrogen bonding with adjacent molecules is favoured. Consequently, bonds tend to form and break down in groups rather than individually. Both temperature and pressure displace the equilibrium between H_2O_I and H_2O_{II} in the same direction, because $H_2O_I \rightarrow H_2O_{II}$ involves both a reduction in volume, and an increase in energy (required to break the hydrogen bonds).

Némethy & Scheraga[107] have calculated the energy of the hydrogen bond in Frank & Wem's model, and have also calculated the size of the clusters, the degree of hydrogen bonding, the internal energy(U), Helmholtz function(A), entropy(S), specific heat at constant volume(Cv)and molecular volume (V) of water. They have elaborated the 'flickering cluster' model by assuming that the clusters contain molecules with 4, 3, 2 and 1 hydrogen bonds, those molecules inside the cluster being tetrahedrally bonded, and those near the surface having one or more bonds broken.

Their calculations show that the energy required to

break a bond, but leave the molecule on its tetrahedral lattice site, is 3.57 Kcal/mole. The energy to remove the molecule from the lattice site to the vapour phase is 2 x 2.25Kcal /mole. However, when the molecule moves from its lattice site in H_2O_I to its closer packed condition in H_2O_{II}, its potential energy decreases, and the net energy required to break a hydrogen bond for the transformation $H_2O_I \rightarrow H_2O_{II}$, is only 1.32Kcal/mole. Thus, the energy of dipole-dipole interaction, and other forces between the unbonded molecules is very large.

The estimate of the number of molecules per cluster varies from 90.6 at 0°C to 21.0 at 100°C, and the fraction of unbroken hydrogen bonds falls from .528 at 0°C to .325 at 100°C. The calculated values of A, U and S agree to within 3% of observed values, but agreement with Cv and V is not so good. However, the discrepancies here could be explained by the number of unbroken bonds at the higher temperatures being too high. Also, the agreement with the observed radial distribution function is good.

The Frank & Wen model is also able to explain the thermodynamic properties of solutions, [50,107]. in that non-polar solutes help to stabilise the clusters, whereas polar solutes tend to break up the clusters. Various other properties, too, may be described qualitatively in terms of this theory. The maximum density of water at 4°C is easily explained by the rapid breaking of the hydrogen bonds by a rise in temperature in this region. The breaking of bonds causes a reduction in volume below 4°C which is greater than the normal increase in volume due to an increase in intermolecular distances. The specific heat at constant pressure, Cp, normally rises with temperature for a liquid, but a component of the specific heat of water is derived from the energy required to break hydrogen bonds. The rate

of breaking is highest at low temperature, and the bond energy component of C_p will, therefore, be highest at low temperature. Thus, a minimum occurs in the specific heat of water at 35°C. The compressibility of water is abnormally low because the intermolecular attractions in both H_2O_I and H_2O_{II} are exceptionally high. Application of pressure moves the equilibrium in favour of H_2O_{II}, providing an additional component to compressibility. As this effect is greatest at low temperatures, the minimum in the compressibility of water at 50°C is qualitatively explained, The thermal expansion of water may be explained in the same terms as the density of water. Finally, in the Frank & Wen model, the large heat of vaporisation of water does not rely on the existence of large numbers of hydrogen bonds, as is the case with the Pople model.

Some thermodynamic calculations on a variant of the two species model of water structure have recently been made by Marchi and Eyring[91]. Although a bonded ice like structure was considered to co-exist with an unbonded species, their model is fundamentally different from that of Frank & Wen in that Marchi & Eyring propose large units of bonded lattice containing voids filled with freely rotating monomer.

(iv). Momentum Transport in Water.

In considering the viscosity behaviour of water, Pople's theory of the structure of water must be discredited on two counts. Firstly, the theory implies a constant mechanism of transport at all temperatures, whereas the isotopic substitution of water at atmospheric pressure shows a behaviour to the contrary. Secondly, it cannot explain the reduction in viscosity which water exhibits on application of pressure at low temperature and it would seem that the theory is far removed from a model of the true

structure of water.

On the basis of the Marchi and Eyring theory, it seems that the whole bonded structure would have to be broken down before any flow could occur, and once the structure is broken, the mechanism of transport is much the same regardless of how much hydrogen bonding existed before shear. In these terms, the viscosity behaviour of water under pressure cannot be explained.

Before applying the Frank & Wen theory to the viscosity of water at high pressure, it is necessary to consider the mechanism of momentum transport in terms of this theory. Early estimates of the energy of the hydrogen bond have been in the region of 4.5Kcal/mole. (e.g.[111]). Wang, Robinson & Edelman[137] determined the activation energy of viscous flow in water at atmospheric pressure as 4.6Kcal/mole, and they also found the same value for dielectric relaxation and for self-diffusion. Frank & Wen concluded, therefore, that all of these processes took place in the H_2O_I phase of water. It is unlikely that the major part of momentum transport takes place in the H_2O_I phase, for the following reasons:-

1. The energy required to separate molecules in the H_2O_I phase is greater than in the H_2O_{II} phase.
2. If appreciable momentum transport occurred in the H_2O_I phase, the equilibrium $H_2O_I \rightleftharpoons H_2O_{II}$ would be dependent on rate of shear of the liquid. If this were so, water would behave in a non-Newtonian manner, which has not been observed.
3. The bond forces in ice are not very much greater than those in H_2O_I on the Frank & Wen model. The viscosity of ice has been estimated as 10^{13} poise,[37] and is shear rate dependent.

It is postulated, therefore, that momentum transport in water occurs in the unbonded H_2O_{II} structure. It is interesting to note that Miller[99] treated the viscosity of water at atmospheric pressure on a free volume basis, using a modified Arrhenius equation, and has empirically identified his calculated volume available for viscous flow with the fraction of unbonded molecules, calculated by Nèmethy and Scheraga[107] on the Frank & Wen model. Also, of interest, is the similarity between the generally accepted estimate of the hydrogen bond energy, 4.5Kcal/mole, with the energy required to separate unbonded molecules on the Frank & Wen model, 2 x 4.5Kcal/mole.

In Section (ii), it was shown that momentum transport involves a rotational contribution which decreases with rising temperature. However, at low temperatures, the rotational contribution need not be as large as it appears from the closeness of η_i/η to $(I_i/I)^{\frac{1}{2}}$, for at 5°C, one is comparing D_2O at its melting point with H_2O 5°C above its melting point. It is likely, therefore, that part of the high ratio of η_i/η, at low temperature, is due to a greater degree of cluster formation in D_2O than in H_2O. This argument is fortified by reference to Fig. 48 showing that at 25°C, the minimum in the viscosity of D_2O occurs at a higher pressure than for H_2O, and the reduction in viscosity caused by that pressure is considerably greater than for H_2O.

At low temperatures, therefore, it is suggested that viscous flow occurs in water by setting up a velocity gradient in the unbonded water molecules, and that the equilibrium $H_2O_I \rightleftharpoons H_2O_{II}$, and its resonant nature, is largely unaffected by the shear stresses. Flow between adjacent layers of molecules occurs mainly by overcoming the dipole-dipole interactions, and rolling the molecules in the direction of flow, making the mom-

ent of inertia of the molecule important in momentum transfer. As the bonded clusters constitute a large part of the liquid volume, the number of layers of unbonded molecules between the clusters will be of the order 2 to 6, and momentum transport between unbonded H_2O_{II} and the molecules on the surface of the H_2O_I clusters will also contribute to the viscosity mechanism. As the temperature rises, the mole fraction of unbonded water molecules increases, causing a reduction in viscosity. Also, the rising internal energy of the molecules reduces the energy required to overcome the intermolecular forces, causing a further reduction in viscosity, and the translational energy of the molecules increases, causing an increase in the convective component of momentum transport. The latter effect reduces the contribution of rotation, and hence a change in the mechanism of momentum transport. The high viscosity of water is due to the combination of flow occuring in only part of the volume of the liquid, and to the large dipole-dipole interactions. The abnormally high temperature-viscosity coefficient of water is due to the fact that in addition to the normal increase in internal energy and intermolecular distances with temperature, the number of molecules available for momentum transport also increases with temperature. The failure of water to fit the usual Arrhenius relationship,

$$\eta = A\exp(B/T),$$

is due to the last mentioned phenomenon.

Application of pressure to water decreases the intermolecular distances, and at the same time displaces the $H_2O_I \rightleftharpoons H_2O_{II}$ equilibrium in favour of the unbonded species. The latter effect is greatest at low temperatures, and this is reflected in the reduction in the viscosity of water caused by pressure at temperatures below $33.5^{\circ}C$.

The lower the temperature, the greater is the potential shift in the equilibrium by pressure, and the larger is the reduction in viscosity. As the pressure rises, the equilibrium shift becomes less significant and the viscosity therefore increases in the normal manner. At temperatures above 33.5°C, the effect of pressure on the $H_2O_I \rightleftharpoons H_2O_{II}$ equilibrium is sufficiently small to be less significant than the normal pressure effects. At 100°C, it can be seen from Fig.68 that at a relatively low pressure, all of the H_2O_I species has been eliminated by pressure, and the liquid exhibits the usual exponential pattern.

The trends of the $\eta D_2O/\eta H_2O$ ratio, shown in Fig.59, throw some light on the viscosity mechanism under pressure. After a slight fall in the ratio, a constant value is achieved over a wide range of pressure, showing that a constant momentum transport mechanism must be operating. Under these high pressure conditions, the convective contribution to transport would be negligible, and the $\eta D_2O/\eta H_2O$ ratio shows that a large rotational contribution is evident throughout the high pressure range. The mechanism is thought, therefore, to be similar to the rolling action at low temperature and atmospheric pressure. The initial fall in the ratio in the first few thousand kg/cm^2 is interpreted as being due to a slight difference in the degree of association in D_2O and H_2O at 25°C. At high pressures, the restriction on molecular translation would be much the same at all temperatures between 0 and 100°C, and it is likely that the same transport mechanism will exist under pressure regardless of temperature. It is predicted, therefore, that at all temperatures, the $\eta D_2O/\eta H_2O$ ratio will rise or fall under pressure to about the same value as found at 25°C, i.e. 1.208.

(v). Viscosity of H_2O_{II}.

The viscosity of water, is, in effect, the viscosity of a suspension, whose particle size and concentration is variable with temperature and pressure. Némethy and Scheraga [107] predict that even at 100°C, a considerable 'particle' concentration exists, and varying temperature alone does not allow measurement on 'pure' H_2O_{II}. Measurements at high pressure take us nearer to this goal, and it seems likely from Fig. 68 and the $\eta D_2O/\eta H_2O$ ratio in Fig.59 that under high pressure H_2O_{II} alone exists.

The isobars for water in Fig.56 are plotted in terms of the Arrhenius relationship, i.e. log η vs I/T, at 0, 2,000, 4,000, 6,000, 8,000, and 10,000kg/cm^2 in Fig.70. At atmospheric pressure, at no point does the curve approximate to a straight line. However, at higher pressures, it can be seen from Fig.70 that a straight line can be drawn through the high temperature end of the isobar, and at increasing pressure, a greater range of the isobar lies on the straight line. The straight line portions have been extrapolated into the low temperature region in Fig.70. They are not quite parallel, but of slightly increasing slope at increasing pressures. Lines have been drawn through the isobars at 10,000, 8,000, 6,000 and 4,000kg/cm^2 only, as Fig.68 indicates that at 100°C and 2,000kg/cm^2, H_2O_I structure might still exist. The 2,000kg/cm^2 line has been determined by extrapolating back to 2,000kg/cm^2 the viscosities given by the straight lines at higher pressures, at 6 temperatures. The 2,000kg/cm^2 line is the best line through these 6 points.

The interpretation of Fig.70 is consistent with the idea that H_2O_I tends to disappear at high pressures. It is suggested that the straight line portions of the isobars are due to the water being completely free of the H_2O_I species, and the port-

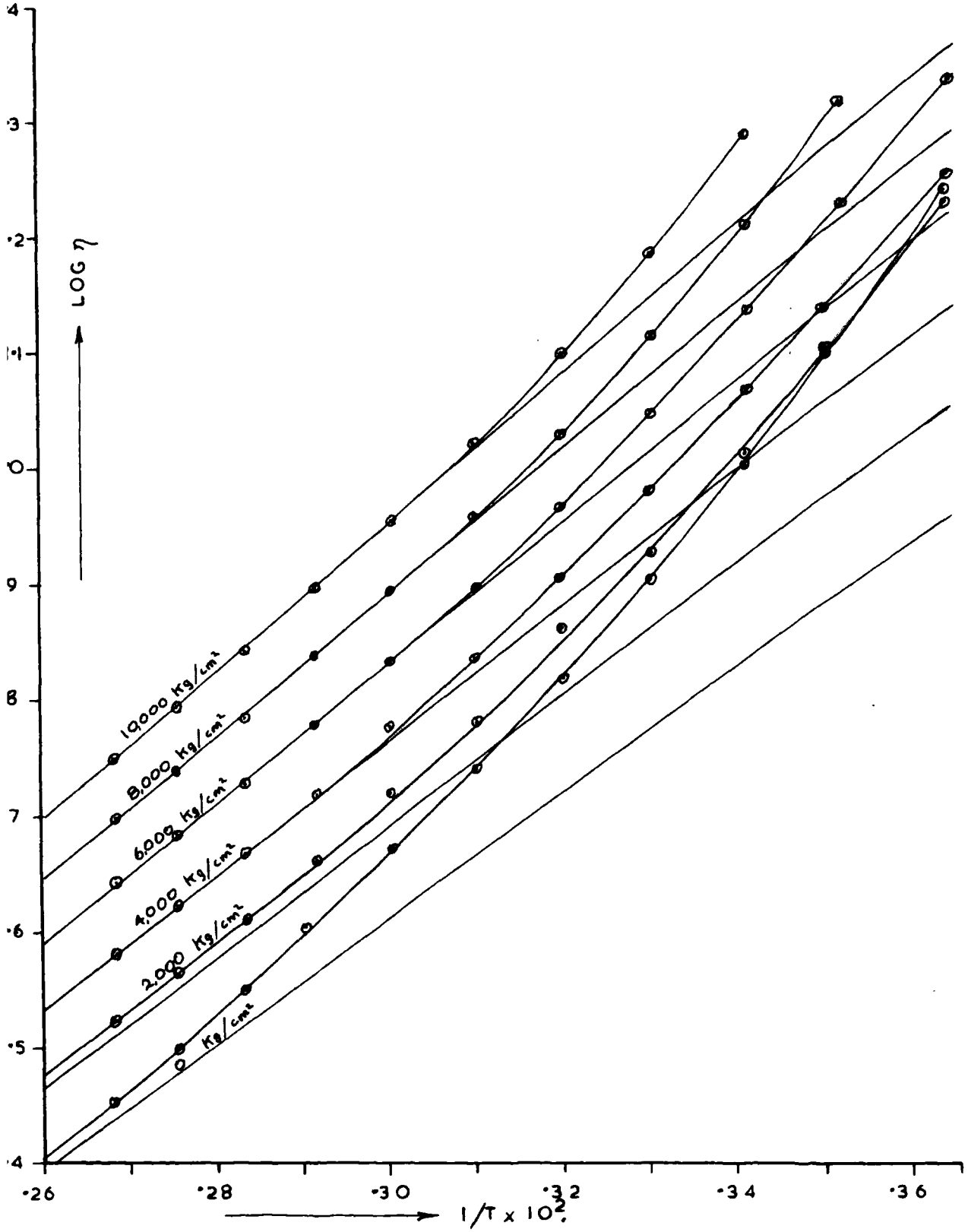

FIG. 70. ARRHENIUS PLOT OF WATER VISCOSITY.

ion of the plot which deviates from the straight line is interpreted as a transport mechanism the same as for the H_2O_I free condition of water, but with the apparent viscosity increased by some of the molecules remaining in H_2O_I clusters unable to take part in momentum transport. The point at which the curved part of the isobar joins the straight line portion gives the temperature at which all H_2O_I has disappeared. From Fig.70, the approximate temperatures are:-

P kg/cm^2.	2,000.	4,000.	6,000.	8,000.	10,000.
t °C.	-	75.	60.	55.	50.

The grid formed by the straight lines in Fig.70 represents the viscosity of 'pure' H_2O_{II} at all temperatures between 0 and 100°C, and above 2000kg/cm^2. Isotherms of H_2O_{II} may be produced from the grid in Fig.70, and extrapolated back to atmospheric pressure. The results of this extrapolation give the lowest straight line in Fig.70, and represents the viscosity of H_2O_{II} between 0 and 100°C, at atmospheric pressure.

The logarithms of relative viscosity, calculated from the grid in Fig.70, are plotted in Fig.71 against pressure, and it can be seen that at both 0°C and 100°C, the predicted viscosity of 'pure' H_2O_{II} exhibits the normal exponential behaviour. Also, no minima exist in the H_2O_{II} isotherms.

The ratio of the predicted viscosity of 'pure' H_2O_{II} at atmospheric pressure, and the measured viscosity of water, should not be very much greater than the mole fraction of unbonded water at the same temperature. In this respect, the findings of this work are in poor agreement with Némethy & Scheraga's interpretation of Frank & Wen's theory. The ratio is .52 at 0°C and .97 at 100°C, whereas the mole fraction of unbonded water is given by Némethy & Scheraga as .224 and .437. As momentum transport will take place between unbonded molecules,

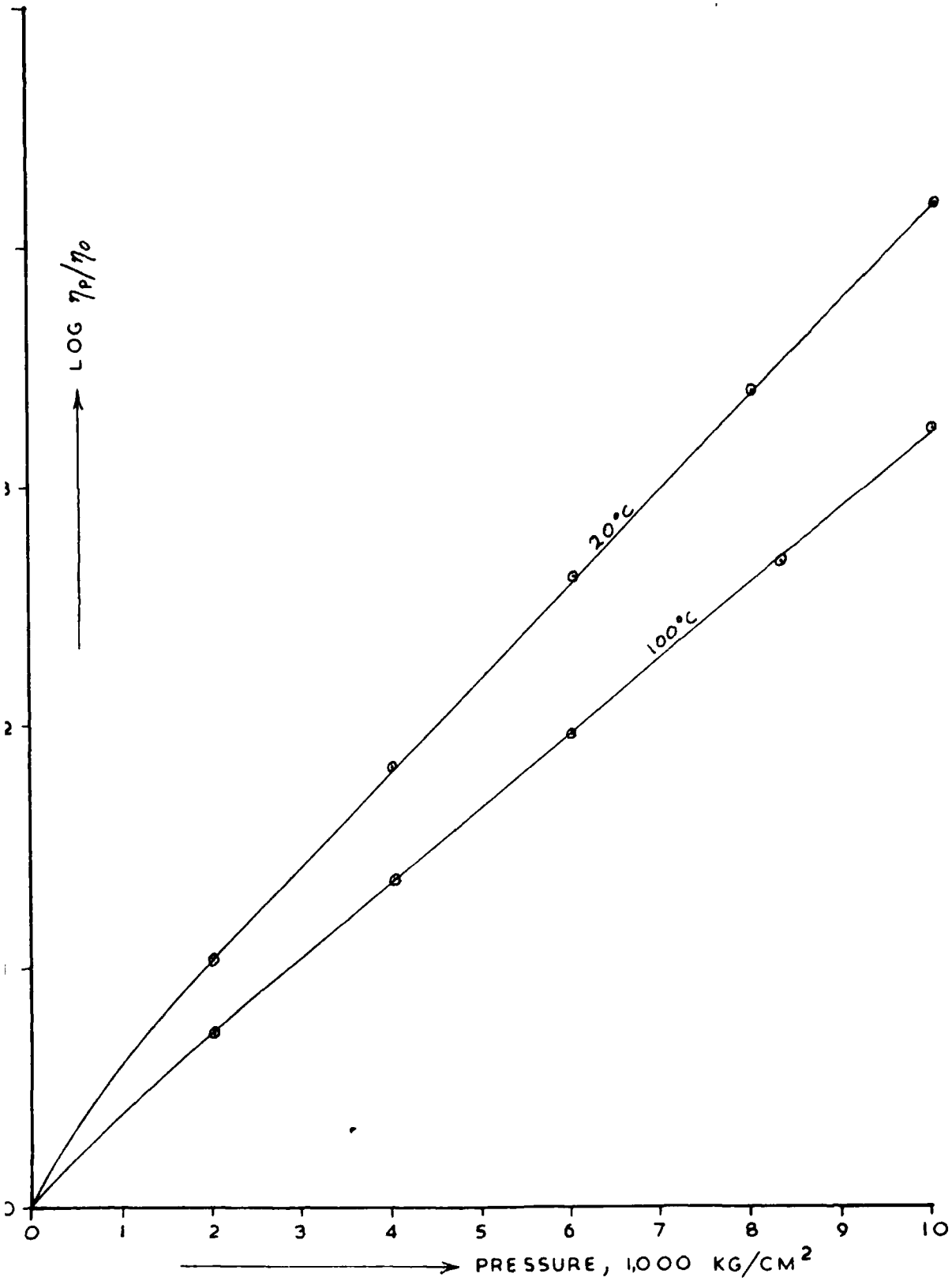

FIG. 71. LOGARITHMIC PLOT OF H_2O_{II} VISCOSITY.

and bonded molecules on the surface of the clusters, it can be assumed that the surface molecules contribute to the velocity gradient to the extent of half the contribution of the unbonded molecules. An estimate of the number of surface cluster molecules in the Némethy & Scheraga model brings the mole fraction of molecules free to engage in momentum transport to .48 at 0°C and .62 at 100°C. In their five state model, Némethy & Scheraga estimate the mole fraction of molecules with 1, 2, 3 and 4 hydrogen bonds as :-

Number of bonds.	1.	2.	3.	4.
Mole fraction 0°C.	.214	.029	.214	.300
Mole fraction 100°C.	.249	.032	.140	.142

The number of molecules tied up with one bond might not be as high as this, and the actual number of unbonded molecules could be considerably greater than their predictions without drastically altering their model. (e.g. a greater number of molecules with 2 bonds).

TABLE 6.

Viscosity of H_2O_{II}.

P kg/cm^2.	viscosity c.p. 0°C.	20°C.	40°C.	60°C.	80°C.	100°C.
0	.927	.681	.520	.410	.334	.275
2,000	1.164	.841	.634	.494	.399	.325
4,000	1.419	1.016	.762	.585	.470	.380
6,000	1.722	1.213	.895	.684	.543	.436
8,000	2.028	1.419	1.045	.787	.621	.496
10,000	2.415	1.667	1.213	.906	.708	.561

The estimated viscosity of 'pure' H_2O_{II} is given in Table 6 at various temperatures and pressures. From these values, $1/\eta\ (\partial\eta/\partial P)_T$ has been calculated for 20°C and 100°C, for comparison with the results given by water at these temperatures in Fig.69. For this purpose, it is assumed that the presence of any H_2O_I has little effect on the compressibility of water in the region of 100°C, and the compressibility of H_2O_{II} at all pressures at 100°C has, therefore, been taken as the compressibility of water at this temperature. This argument is not valid at low temperatures, and the compressibility of H_2O_{II} at 20°C and atmospheric pressure has been estimated by extrapolating the compressibility-temperature curve in the 100°C region back to 20°C. By a similar argument for water at 100°C, the compressibility of H_2O_{II} at 20°C and 10,000kg/cm^2 is taken as the value for water under the same conditions. Compressibilities for intermediate pressures have been obtained by interpolating between these two points on a 'typical' compressibility curve. The values derived are approximate only, but are adequate for demonstrating the viscosity relationship of H_2O_{II}.

The viscosity-compressibility results for 'pure' H_2O_{II} at 20 and 100°C are plotted in Fig.69, and it can be seen that, although similar behaviour to water is exhibited at 100°C, the line for H_2O_{II} at 20°C is totally different from that of water, and conforms to normal behaviour. This is additional evidence that, although the viscosity behaviour of water is abnormal, this behaviour can be adequately explained if only the actual molecules contributing to flow are considered.

(vi). The Pressure Dependence of Viscosity.

Liquids whose viscosity-pressure relationships are characterised by equation 28 may have their viscosity expressed at constant temperature by the following expression, derived by integrating equation 28.

$$\ln(\eta_p/\eta_o) = -C\ln(V_p/V_o) + PD + E \qquad 33.$$

where C and D are given by the slope and intercept in Fig.69, and E is the integration constant. Putting P = 0, then E = 0.

$$\therefore \quad \eta_p = \eta_o(V_p/V_o)^{-C}\exp(PD). \qquad 34.$$

Equation 34 is similar in its pre-exponential term to Andrade's expression for viscosity under pressure:-

$$\eta_p/\eta_o = (V_o/V_p)^{1/6}.\ (\kappa_o/\kappa_p)^{\frac{1}{2}}\exp(c/T(1/V_p - 1/V_o))$$

where V_o and V_p are molar volumes, κ_o, κ_p, are adiabatic compressibilities, and c is an empirical constant.

The term $(V_p/V_o)^{-C}$, which is the predominant factor at low pressures, has been derived theoretically, but the theory relating viscosity to volume change, does not account for the constant factor D arising from Fig.69. The term PD, which is usually contained in empirical relationships, has commonly been interpreted as referring to a volume which must be created in the liquid in order that a molecule may move to another position, relative to its neighbours, under the influence of a shear stress.

Unfortunately, Bridgman's viscosity and density data are inadequate to distinguish conclusively between his viscosity data at 30°C and that at 75°C on the viscosity-compressibility plot in Fig.69. All that can be said is that the data available indicate that the value of C, i.e. the volume effect, is independent of temperature, and the value of D adjusts it-

self so that, if D = F/T, then F is a constant. If this is so, then equation 34 may be rewritten so as to describe viscosity at any temperature and pressure by putting,

$\eta_o = A\exp(E_p/RT)$.

i.e. $$\eta = A/V_p/V_o)^{-C}\exp(PF/T + E_p/RT) \qquad 35.$$

where $E_p = \frac{(\partial \ln \eta)}{(\partial 1/T)_p}$ at atmospheric pressure.

As pointed out by Jobling & Lawrence,[69] E_p is not of any real theoretical significance, because this so called activation energy takes into account viscosity changes due to changes in internal energy, changes in volume, and changes in transport mechanism due to varying degrees of molecular convection. Thus, it would seem to be fortuitous that $\eta_o = A\exp(E_p/RT)$ fits the viscosity data of a large number of liquids well. V_o in equation 35 is the molar volume of the system at atmospheric pressure at the same temperature at V_p.

Jobling & Lawrence also pointed out that the activation energy at constant volume, $E_v = \frac{(\partial \ln \eta)}{(\partial 1/T)V}$, was a better description of the energy a molecule must possess in order to engage in momentum transport. They measured the viscosity of benzene at constant volume up to $400 kg/cm^2$, and found that its viscosity could be described by:-

$$\eta = A\exp(E_v/RT) \qquad 36.$$

Jobling & Lawrence also interpolated some of Bridgman's results at constant volume, and found that equation 36 was applicable.

E_v has been calculated for n-pentane at four densities from Bridgman's data, and has been plotted vs the pressure at 30^oC at each density. It can be seen from Fig.72 that E_v may be described by:-

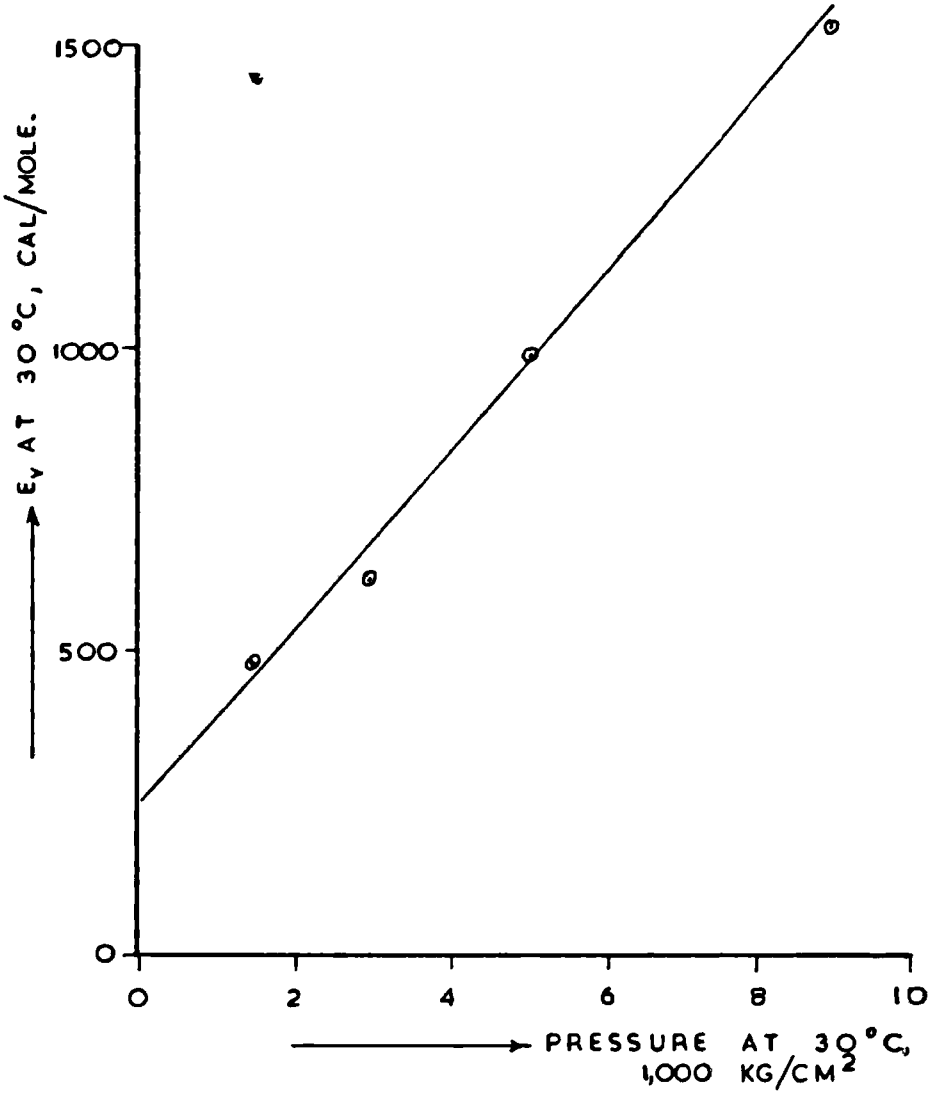

FIG. 72. ACTIVATION ENERGY AT CONSTANT VOLUME, FOR n-PENTANE AT 30 °C.

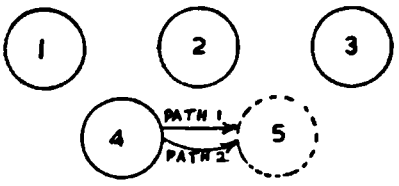

FIG. 73.

$$E_v = E_{vo} + HP \qquad 37.$$

where H is the slope, and E_{vo} the value of E_v at atmospheric pressure.

Then $1/R(dE_v/dP)_T = H/R.$

From Fig.69, $D = F/T = 2.2 \times 10^{-4}(kg/cm^2)^{-1}.$

From Fig.72, $H/RT = 2.3 \times 10^{-4}(kg/cm^2)^{-1}.$

Thus, for pentane, F/T in equation 35 may be identified with H/RT, or $1/RT(dE_v/dP)_T$.

As $(dE_v/dP)_T$ is independent of P, then,

$$P/RT(dE_v/dP)_T = \Delta E_v/RT, \text{ where } \Delta E_v = E_v - E_{vo}.$$

Equation 35 may be written,

$$\eta = A\,(V_p/V_o)^{-C} \exp\,(\Delta E_v/RT + E_p/RT) \qquad 38.$$

The term E_{vo} is included in E_p together with other factors which determine the variation of viscosity with temperature at atmospheric pressure.

The energy E_v, which a molecule must possess in order to change its position in the liquid lattice structure, consists of two parts. Referring to Fig.73, in order that molecule 4 may move to position 5, it must overcome attractive forces between 1 and 4, and move against repulsive forces between 2 and 4. The energy required to do this is termed E_A. The difference in the energy requirements at atmospheric pressure and pressure P is ΔE_A. ΔE_A, at any given pressure, is at maximum when the molecule 4 moves straight to position 5,(path 1). However, if molecule 4 moves along path 2, it must expand the surrounding liquid structure by an amount ΔV, and must therefore do work $P\,\Delta V$ against the external pressure. The activation energy is the sum of these two energies, and the distribution of molecules possessing sufficient energy for 'flow' is given by:-

$$\exp(\Delta E_v/RT) = \exp(\Delta E_A/RT + P\,\Delta V/RT).$$

Equation 38 then becomes,

$$\eta = A(V_p/V_o)^{-C} \cdot \exp(\Delta E_A/RT + P\Delta V/RT + E_p/RT). \qquad 39.$$

The distribution of ΔE_v between ΔE_A and $P\Delta V$ is not known. When path 1 is followed, ΔV is zero, and $\Delta E_A = \Delta E_v$. ΔE_A might lie anywhere between ΔE_v, which is positive, and some negative unknown value. The order of magnitude of ΔV may be obtained by making ΔE_A zero, in which case $D = \Delta V/RT$.

Table 7 gives values for ΔV, based on this assumption, for all the liquids considered in Fig.69, together with their molar volumes.

TABLE 7.

Compound.	D x 10^4.	ΔVcc/mole.	V molar volume	ΔV/V.
Carbon tetrachloride.	4.7	12.1	94	.129
Benzene.	4.3	11.1	89	.125
n-Octane.	4.1	10.5	160	.066
n-Pentane.	2.2	5.7	116	.049
Ether.	1.8	4.6	103	.044
Acetone.	1.6	4.1	71	.058
Ethyl Chloride.	1.6	4.1	68	.060
Carbon disulphide.	1.2	3.1	60	.050
i-amyl alcohol.	3.9	10.0	109	.092
Ethyl alcohol.	1.5	3.9	59	.066
Methyl alcohol.	.9	2.3	40	.058
H_2O_{II} at 20°C.	.45	1.2	18	.067

In empirical relationships of the form, $\eta = A\exp(P\Delta V/T)$, it has been estimated that ΔV is about 1/3 or ¼ of the molar volume.(100) None of the values of $\Delta V/V$ in Table 7 is as high as

this, and only the spherical molecules benzene and carbon tetrachloride are larger than 1/10. The rest of the compounds lie between 1/10 and 1/20. It should be noted that, in this respect, H_2O_{II} appears to be quite normal.

The form of equation 39 is similar to the Eyring theory of viscous flow in which the formation of 'holes' in the liquid lattice is the fundamental rate process. Eyring gives the viscosity as :-

$$\eta = \frac{1.09 \times 10^{-3} M^{\frac{1}{2}} T^{3/2}}{V^{2/3} \Delta U_v} \exp(E/RT).$$

where E is the energy of activation associated with the formation of a hole into which a molecule can move. E is related to ΔU_v and PV. The fundamental difference between Eyring's theory and that arising from the present work is that Eyring does not recognise the importance of volume change. Also, the exponential term in Eyring's model refers to the formation of a hole, whereas the present work associates the similar term with the displacement of a molecule from its lattice site. Eyring assumes that once a hole is formed, molecular diffusion will cause the hole to be filled by an adjacent molecule.

(vii). Viscosity of Water at Constant Volume.

By interpolation of Bridgman's density data, and the viscosity data of the present work, the viscosity of water at 4 volumes has been plotted in Fig.74 in the form log η vs 1/T. The pattern of behaviour shown in Fig.74 is similar to that in the plot at constant pressure shown in Fig.70. At low volumes, a linear relationship is applicable at the higher temperatures, while at lower temperatures and greater volumes, the deviations from linearity become increasingly great. The interpretation of Fig.74 is the same as for Fig.70, and the slopes of the straight

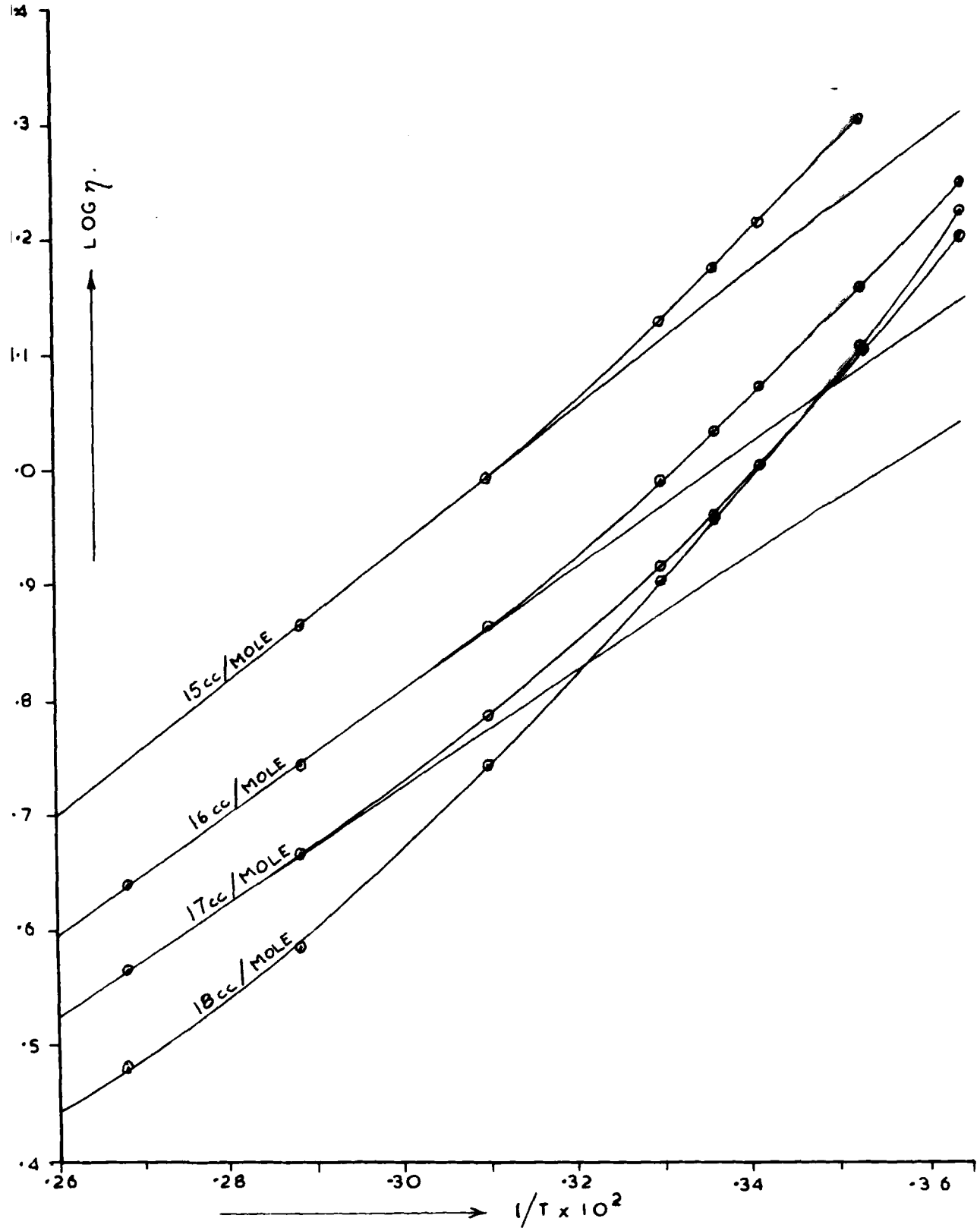

FIG. 74. VISCOSITY OF WATER AT CONSTANT VOLUME.

lines in Figs. 70 and 74 are virtually identical, showing that E_p and E_v for H_2O_{II} are of almost the same value. This is a reflection of the very small value of the constant C in equation 28, estimated for H_2O_{II} from Fig.69; that is, a change in volume has little effect on the viscosity of H_2O_{II}. The indication that rotation of the molecules provides a considerable contribution to the viscosity of water partly explains why the increase in collisional frequency caused by a volume decrease has an exceptionally small effect in H_2O_{II}.

The value of E_v for H_2O_{II} has been calculated from Fig.74 as 1185cal/mole at 15cc/mole, and 1020cal/mole at 17cc/mole. By a similar method as used in the previous section for pentane, it is found that,

$H/RT = .42 \times 10^{-4}$ $(kg/cm^2)^{-1}$ at 20^oC,

which compares well with $D = .45 \times 10^{-4}$ $(kg/cm^2)^{-1}$ from Fig. 69.

Comparing the values of E_v for H_2O_{II} with those of pentane in Fig.72, the activation energy of water is higher than normal at low pressures, as was suggested in Section (iv), but changes very little on raising the pressure.

The small change might be due to the small ΔV that water has by virtue of its low molecular volume, or to the attractive intermolecular forces in water being so large that the application of pressure produced little change in E_A i.e. ΔE_A is small.

CHAPTER 15.

CONCLUSIONS.

(a) A viscometer has been designed and constructed, which is capable of measurements on liquids in the temperature range 0 to 100°C, at pressures up to 10,000kg/cm^2, with an estimated accuracy which varies between .6 and 1.2%.

(b) The density of a fluid at high pressure may be determined with sufficient accuracy for computation of viscosity, by employing a viscometer based on a high density and a low density sinker. A low density sinker of beryllium is suggested as being capable of giving density results of the order of $\pm$ 1%.

(c) Bridgman's viscosity results for n-pentane should be corrected for kinetic energy losses at low fall times, and it is likely that similar corrections should be applied to all his viscosity data.

(d) Bridgman's viscosity results for water are not in agreement with the present work or with the data of other workers up to 900kg/cm^2, and it is likely that his data contain large errors arising from the unsuitability of his instrument for strongly polar liquids.

(e) The anomalous pressure dependence of the viscosity of water can be explained in terms of liquid water existing as an equilibrium between a hydrogen bonded ice like structure, surrounded by an unbonded close packed monomer with strong dipole-dipole interactions. Raising temperature or pressure displaces the equilibrium in favour of the unbonded species, and under suitable conditions of temperature and pressure, only the unbonded species exists. Momentum transport occurs in the unbonded species of water, and between the unbonded species and

the boundaries of the bonded structures.

(f) Momentum transport in water includes a large rotational contribution which is independent of pressure above 4,000kg/cm^2 at 25°C, and is probably independent of temperature, too, above this pressure.

(g) The effect of pressure on the viscosity of many liquids may be represented over all or part of the pressure range by:-

$$1/\eta \ (\partial \eta / \partial P)_T = C\beta_T + D,$$

or, $$\eta_p / \eta_o = (V_p/V_o)_T^{-C} \exp(PD).$$

where the volume term represents the dependence of collisional frequency on volume, and the term exp(PD) is equal to exp(ΔE_v/ RT).

(h) If momentum transport in water is considered to occur only in the unbonded species, the expressions in (g) are applicable to the predicted viscosity of water free of all bonded structures.

In addition, it has been found that there is a limit to the pressure an O ring will seal, which is a function of the O ring material, and the temperature. Failure of the seal at its upper pressure limit is of a "pressure relief valve" nature, similar to failures encountered at low temperatures, and the lower the temperature at which a material maintains its flexibility, the higher the pressure it will seal. Also, the upper pressure limit of the seal may be raised by increasing the temperature. O rings are unsuitable for complete separation of two fluids, under conditions of variable pressure, if one or both of the fluids is able to swell the O ring elastomer.

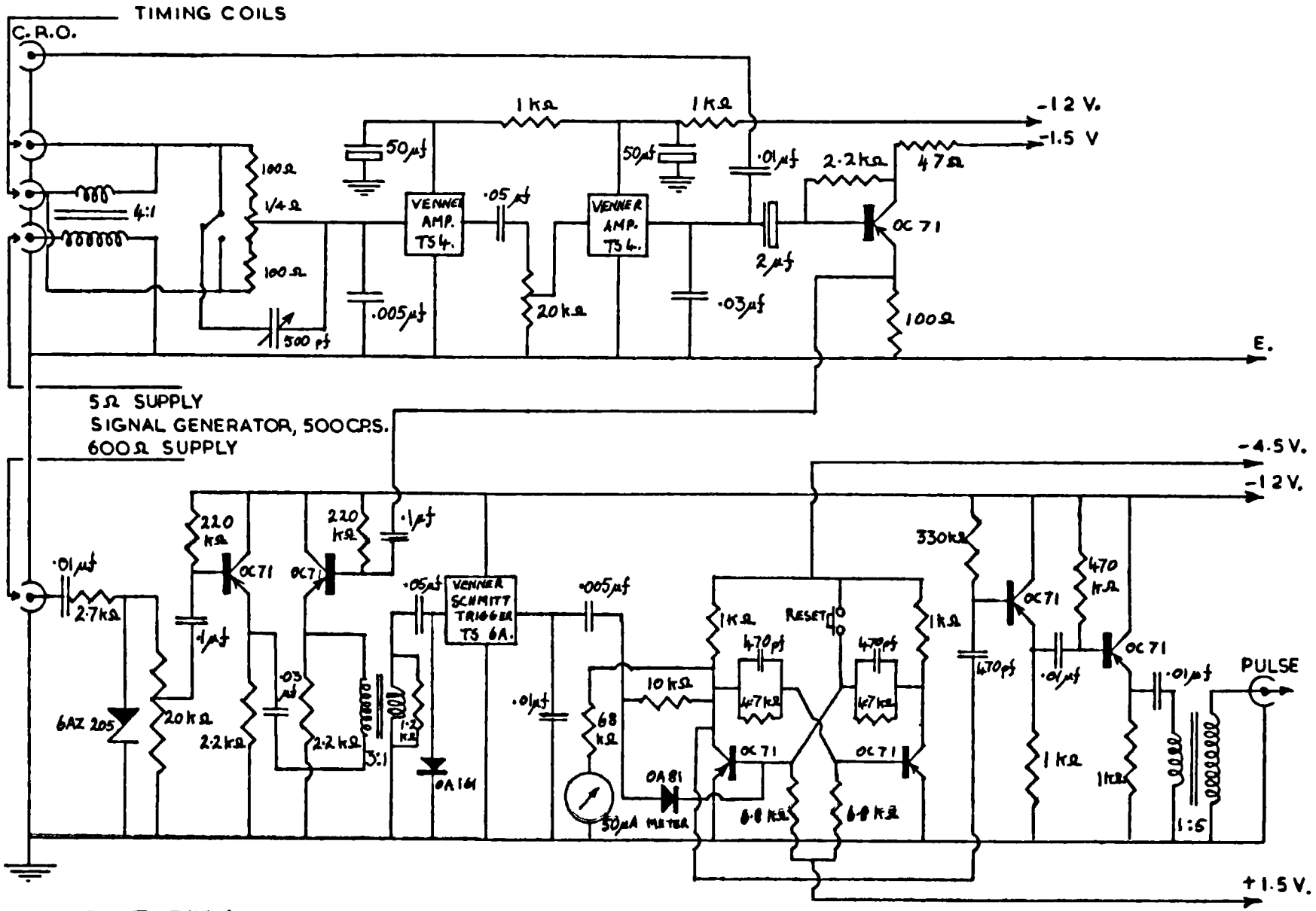

APPENDIX 1. TRIGGER CIRCUIT — ONE CHANNEL ONLY

APPENDIX 2.

DERIVATION OF VISCOMETER RELATIONSHIPS.

(i). Concentric Conditions.

The following derivation assumes that:-

1. The sinker falls concentrically with the viscometer tube.
2. Laminar flow conditions are maintained at all times in all regions of flow around the sinker.
3. A negligible contribution to the total viscous drag on the sinker is made by the guiding pins and by the ends of the sinker.
4. Development of fluid flow into and out of the annulus produces a negligible pressure change on the ends of the sinker.
5. The sinker achieves terminal velocity before timing commences.

Fig. 1.A2 represents the sinker falling in the viscometer tube at velocity v, and P_1 and P_2 are the pressures prevailing at each end of the sinker, exclusive of any pressure due to the head of fluid. λ is the shear force acting on the cylindrical surface of the sinker, and wg represents the effective weight of the sinker after buoyancy correction.

The shear stress at any point in the annulus is given by:-

$$\tau = \frac{\eta \, du_s}{ds} \qquad 1.A2.$$

The weight of the sinker is balanced by the viscous shear force on the sinker surface, and by the pressure difference across its ends, and may be expressed by:-

$$-wg + \lambda + \Delta P \pi r_1^2 = 0 \qquad 2.A2.$$

where $\Delta P = P_2 - P_1$.

Considering the vertical forces acting on an annulus of fluid between the surface of the sinker and a boundary at radius s, it may be shown that:-

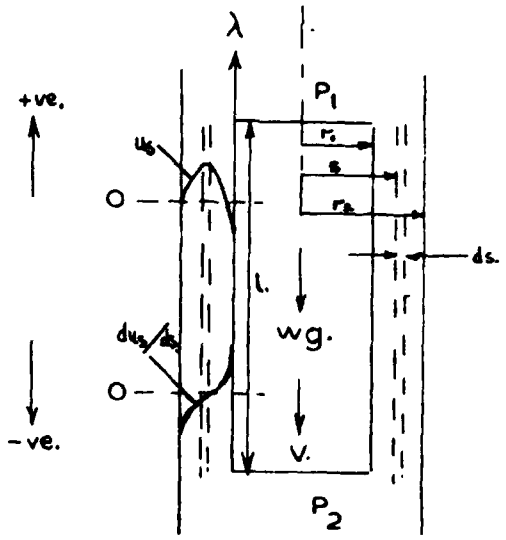

FIG. 1.A2.

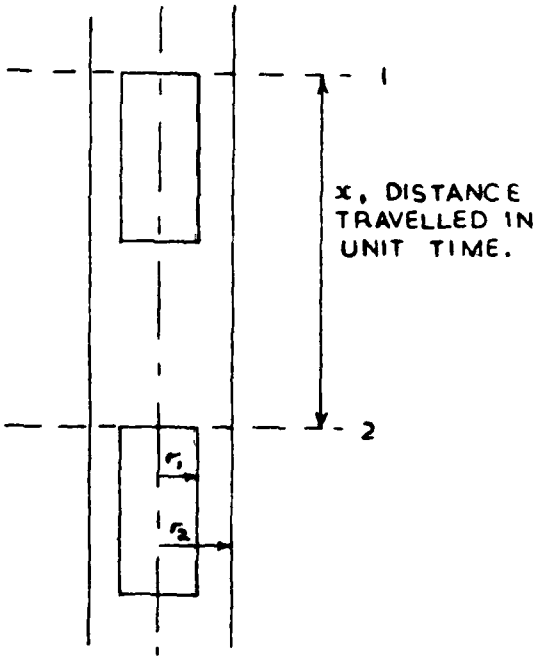

FIG. 2.A2.

$$\Delta P(s^2 - r_1^2) - \lambda + 2\pi s l \eta . \frac{du_s}{ds} = 0 \qquad 3.A2.$$

Adding 2 and 3, rearranging and integrating, gives:-

$$u_s = \frac{wg\ln.s}{2\pi l \eta} - \frac{\Delta P s^2}{4 l \eta} + K \qquad 4.A2.$$

Inserting boundary conditions, $u_s = -v$, $s = r_1$,

$u_s = 0$, $s = r_2$,

in 4, gives:-

$$K = -\frac{wg\ln.r_1}{2\pi l \eta} + \frac{\Delta P r_1^2}{4 l \eta} - v$$

and $$\Delta P = \frac{2wg\ln.(r_2/r_1)}{\pi(r_2^2 - r_1^2)} - \frac{4lv\eta}{(r_2^2 - r_1^2)}$$

Substituting for ΔP and K in 4,

$$u_s = \frac{wg\ln.(s/r_1)}{2\pi l \eta} - \frac{wg(s^2 - r_1^2)\ln.(r_2/r_1)}{2\pi l \eta (r_2^2 - r_1^2)} + v.\frac{(s^2 - r_2^2)}{(r_2^2 - r_1^2)}$$

5.A2.

Flow through an incremental annulus of thickness ds, is given by:-

$$dQ = 2\pi s u_s . ds \qquad 6.A2.$$

Inserting 5 in 6,

$$dQ = \frac{wgs\ln.(s/r_1)}{l\eta}.ds - \frac{wgs(s^2 - r_1^2)\ln.(r_2/r_1)}{l\eta(r_2^2 - r_1^2)}.ds + 2\pi s v.\frac{(s^2 - r_2^2)}{(r_2^2 - r_1^2)}.ds$$

7.A2.

Integration of 7, between the limits r_1 and r_2, gives:-

$$Q = \frac{wg}{4l\eta}.\left\{(r_2^2 + r_1^2)\ln.(r_2/r_1) - (r_2^2 - r_1^2)\right\} - \frac{\pi v}{2}.(r_2^2 - r_1^2) \qquad 8.A2.$$

Q, the volume flow rate of fluid through the annulus, may be

evaluated by referring to Fig. 2.A2. When the sinker moves a distance x, the volume of fluid between boundaries 1 and 2 is:-

$$Q = \pi r_2^2 x. \qquad 9.A2.$$

All of this fluid must have passed the sinker. Then, from 8 and 9,

$$\eta = \frac{wgT^*}{2\pi lL} \cdot \frac{\left\{(r_2^2 + r_1^2)\ln.(r_2/r_1) - (r_2^2 - r_1^2)\right\}}{(3r_2^2 - r_1^2)} \qquad 10.A2.$$

(ii). Eccentric Conditions.

(Eccentricity here refers to the sinker and tube axes being displaced but parallel).

Except for concentricity, the same assumptions as for the concentric condition, are made for the treatment of the eccentric condition. However, the following derivation is an approximation only.

A cross section of the sinker, falling eccentrically in the viscometer tube, is illustrated in Fig. 3a.A2. The cross section is split into a number of equiangular sectors, centred at a point midway between the tube and sinker centres, and each part of the annular clearance, contained in these sectors, is approximated to a series of parallel surfaces, as shown in Fig. 3b.A2. The gap between each pair of parallel surfaces is taken as c, the clearance along a line bisecting a sector, and the total width of the series is approximated to the circumference of the viscometer tube, $2\pi r_2$.

This procedure is valid for conditions of r_2/r_1 close to 1, and its accuracy will depend on the number of sectors chosen. Each sector may be treated as a fraction of a sinker falling concentrically, with a clearance equal to that of the sector. Thus, the eccentric condition may be regarded as a series of concentric sinkers having a range of clearances equivalent to those in the eccentric case. If the cross section of an eccentrically falling sinker is divided into n sectors,

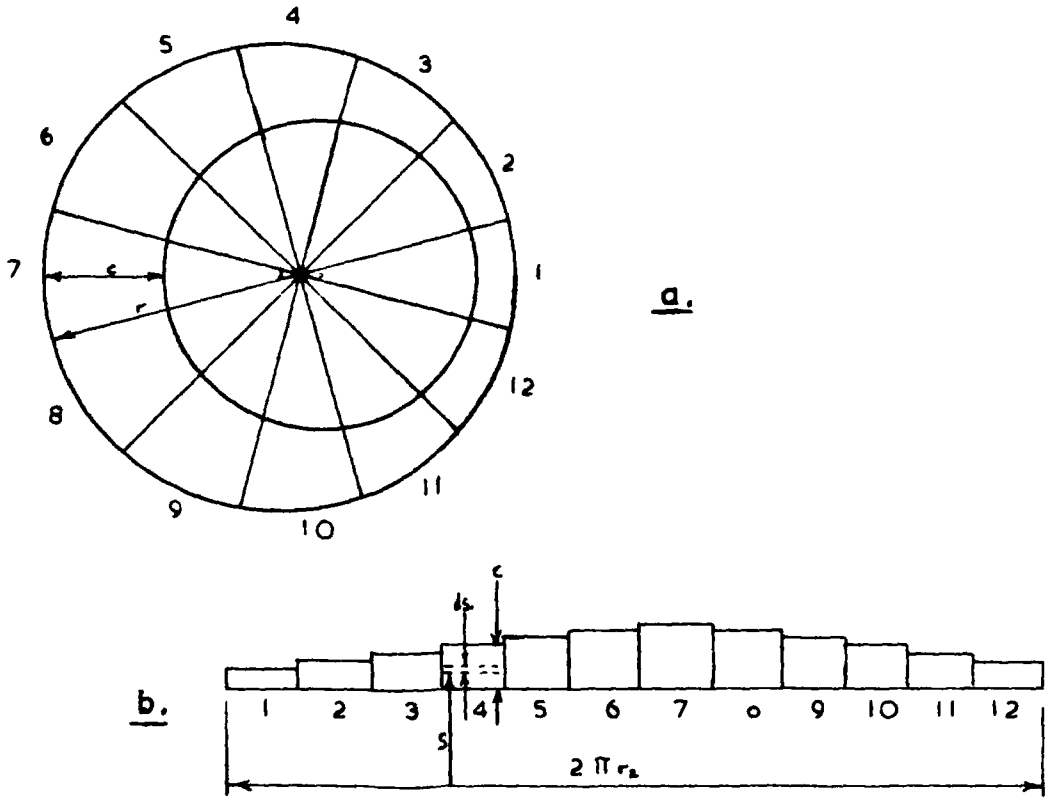

FIG. 3.A2.

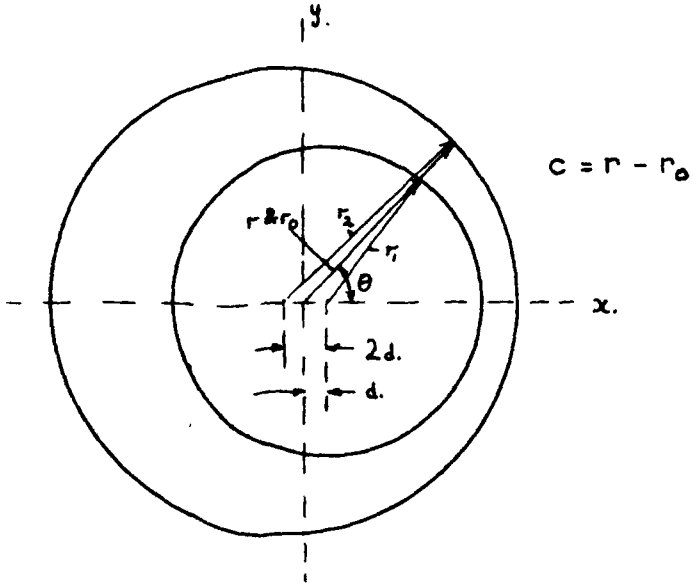

FIG. 4. A2.

then n tubes and concentric sinkers must be considered. Each sinker is subjected to the same buoyancy corrected gravitational force, wg, and the ends of all the tubes are connected, so that each sinker has the same pressure difference, ΔP, across its ends. Each sinker is constrained by an external force, f, so that they all fall at the same terminal velocity, v. For the sinkers of largest clearance, f will be positive, and for those of smallest clearance, f will be negative. Also, $\sum_n f_1 = 0$. Finally, the mean flow past the series of n sinkers is equal to the flow past the eccentric sinker.

$$\text{i.e.} \quad 1/n.\sum_n Q_1 = Q$$

Considering one sinker of a series of n sinkers,
a force balance on the sinker gives:-

$$-wg + f_1 + \lambda_1 + \Delta P \pi r_1^2 = 0 \qquad 11.A2.$$

A force balance on an annulus of fluid between the sinker surface and a boundary at radius s gives:-

$$2\pi r_2 s \Delta P - \lambda_1 + 2\pi r_2 l \eta . \frac{du_s}{ds} = 0 \qquad 12.A2.$$

Adding 11 and 12, rearranging and integrating gives:-

$$u_{s1} = \frac{s}{2\pi r_2 l \eta}.(wg - f_1) - \frac{\Delta P}{2 r_2 l \eta}.(r_1^2 s + r_2 s^2) + K \qquad 13.A2.$$

Inserting boundary conditions, $u_{s1} = -v$, $s = 0$,
$u_{s1} = 0$, $s = c_1$

in 13 gives:- $K = -v$

and $$\Delta P = \frac{(wg - f_1)}{\pi(r_1^2 + r_2 c_1)} - \frac{2v r_2 l \eta}{(r_1^2 c_1 + r_2 c_1^2)} \qquad 14.A2.$$

Substituting for ΔP and K in 13 gives:-

$$u_{s1} = \frac{(wg - f_1)}{2\pi l\eta} \cdot \frac{(sc_1 - s^2)}{(r_1^2 + r_2c_1)} - v\left\{1 - \frac{(r_1^2 s + r_2 s^2)}{(r_1^2 c_1 + r_2 c_1^2)}\right\} \qquad 15.A2.$$

Flow through an incremental annulus of thickness ds is given by:-

$$dQ_1 = 2\pi r_2 u_{s1} \cdot ds \qquad 16.A2.$$

Substituting for u_{s1} in 16, and integrating between the limits 0 and c_1, gives the flow past sinker 1 as:-

$$Q_1 = \frac{r_2(wg - f_1)}{6l\eta} \cdot \frac{c_1^3}{(r_1^2 + r_2c_1)} - \frac{\pi r_2 v}{3} \cdot \frac{(3r_1^2c_1 + 4r_2c_1^2)}{(r_1^2 + r_2c_1)} \qquad 17.A2.$$

Now $Q = 1/n \cdot \sum_n Q_1 = v\pi r_2^2$ 18.A2.

From 17 and 18,

$$v\pi r_2^2 = \frac{wgr_2 \cdot 1/n}{6l\eta} \cdot \sum_n\left\{\frac{c_1^3}{(r_1^2 + r_2c_1)}\right\} - \frac{r_2 \cdot 1/n}{6l\eta} \cdot \sum_n\left\{\frac{f_1c_1^3}{r_1^2 + r_2c_1}\right\} -$$

$$\frac{\pi r_2 v \cdot 1/n}{3} \cdot \sum_n\left\{\frac{3r_1^2c_1 + 4r_2c_1^2}{r_1^2 + r_2c_1}\right\} \qquad 19.A2.$$

From 14,

$$f_1 = wg - \frac{2\pi r_2 l\eta v}{c_1} - \pi\Delta P(r_1^2 + r_2c_1) \qquad 20.A2.$$

Now, $\sum_n f_1 = 0.$

$$\therefore\ 0 = nwg - 2\pi r_2 l\eta v \cdot \sum_n(1/c_1) - \pi\Delta P \cdot \sum_n(r_1^2 + r_2c_1)$$

$$\therefore\ \pi\Delta P = \frac{nwg}{\sum_n(r_1^2 + r_2c_1)} - \frac{2\pi r_2 l\eta v \cdot \sum_n(1/c_1)}{\sum_n(r_1^2 + r_2c_1)} \qquad 21.A2.$$

From 20,

$$\frac{f_1 c_1^3}{(r_1^2 + r_2 c_1)} = \frac{wgc_1^3}{(r_1^2 + r_2 c_1)} - \frac{2\pi r_2 l \eta v c_1^2}{(r_1^2 + r_2 c_1)} - \pi \Delta P c_1^3 \qquad 22.A2.$$

Substituting for $\pi\Delta P$ in 22, and summing for n sinkers,

$$\sum_n \left\{ \frac{f_1 c_1^3}{(r_1^2 + r_2 c_1)} \right\} = wg(1 - n) \cdot \sum_n \left\{ \frac{c_1^3}{(r_1^2 + r_2 c_1)} \right\} - 2\pi r_2 l \eta v \cdot \sum_n \left\{ \frac{c_1^2}{(r_1^2 + r_2 c_1)} \right\}$$

$$+ 2\pi r_2 l \eta v \cdot \sum_n \left\{ \frac{c_1^3 \cdot \sum_n (1/c_1)}{\sum_n (r_1^2 + r_2 c_1)} \right\} \qquad 23.A2.$$

Substituting for $\sum_n \left\{ \frac{f_1 c_1^3}{(r_1^2 + r_2 c_1)} \right\}$ in 19,

$$v = \frac{wg}{6\pi l \eta} \cdot \frac{\sum_n \left\{ \frac{c_1^3}{\sum_n (r_1^2 + r_2 c_1)} \right\}}{\left\{ r_2 + \frac{1}{3n} \cdot \sum_n \left\{ \frac{3r_1^2 c_1 + 4r_2 c_1^2}{r_1^2 + r_2 c_1} \right\} + \frac{r_2}{3n} \cdot \sum_n \left\{ \frac{c_1^3 \cdot \sum_n (1/c_1)}{\sum_n (r_1^2 + r_2 c_1)} \right\} - \right.}$$

$$\left. \frac{r_2}{3n} \cdot \sum_n \left\{ \frac{c_1^2}{(r_1^2 + r_2 c_1)} \right\} \right\} \qquad 24.A2.$$

If the sinker falls concentrically, equation 24 may be simplified, by inserting n = 1, to:-

$$v = \frac{wg}{2\pi l \eta} \cdot \frac{c^3}{(3r_1^2 r_2 + 3cr_2^2 + 3cr_1^2 + 4c^2 r_2)} \qquad 25.A2.$$

Determination of c_1, c_2 etc.

Fig. 4.A2 shows the axis of the sinker displaced a distance 2d from the axis of the tube. The clearance c along a line defined by θ, is $c = r - r_o$ 26.A2.

Now, $r_1^2 = y^2 + (x - d)^2$

and, $r_o^2 = y^2 + x^2$

then $r_o^2 = r_1^2 - (x - d)^2 + x^2$

also, $x/r_o = \cos\theta$

$\therefore\ r_o^2 - 2r_o d\cos\theta + (d^2 - r_1^2) = 0$

$$r_o = \frac{2d\cos\theta \pm \sqrt{(2d\cos\theta)^2 - 4(d^2 - r_1^2)}}{2} \qquad 27.A2.$$

Similarly, $$r = \frac{-2d\cos\theta \pm \sqrt{(2d\cos\theta)^2 - 4(d^2 - r_2^2)}}{2} \qquad 28.A2.$$

Equations 26, 27, and 28 allow c_1, c_2 etc. to be calculated as a function of θ and d.

APPENDIX 3.

STRESS CALCULATIONS.

(i). Radius Ratio of High Pressure Cylinder.

The procedure for designing an autofrettaged cylinder is based on the Manning method [90] for constructing a design chart from the shear properties of the cylinder material. The chart gives radial stress and tangential strain at any radius in the section of an infinitely thick cylinder. It covers the radius ratio 1 to 10 on a logarithmic scale, and the strain at radius ratio $\gamma = 1$ is selected so that the shear strain in the cylinder falls to the value of the shear strain at yield approximately in the middle of the chart; i.e. the elastic-plastic boundary falls at the geometric mean radius of the cylinder.

The design chart for EN26 steel, hardened to 80 tons/in^2, is taken from Manning's work [90], and the following design is based on the chart reproduced in Fig. 1.A3.

Final diameter of cylinder bore = .375 inch.

Design pressure = 12,000kg/cm^2.

If the yield pressure of final cylinder is taken as 1.5 times the design pressure, i.e. 18,000kg/cm^2, or, 118.5 tons/in^2, then the radial stress difference between bore and outside of cylinder = 118.5 tons/in^2. This stress difference is fitted to Fig. 1.A3., so that the intercepts on the stress curve are equidistant from the elastic-plastic boundary line. In effect, in a cylinder of infinite radius ratio, with an internal pressure of 137.5 tons/in^2, two imaginary boundaries in the cylinder section are considered, one at radius ratio 1.1, where the radial stress has fallen to 125.5 tons/in^2, and the other at radius ratio 7.7, where the radial stress is 7 tons/in^2. This is equivalent to a cylinder of radius ratio 7, with an internal pressure of 118.5 tons/in^2, and a superimposed hydrostatic pressure of 7 tons/

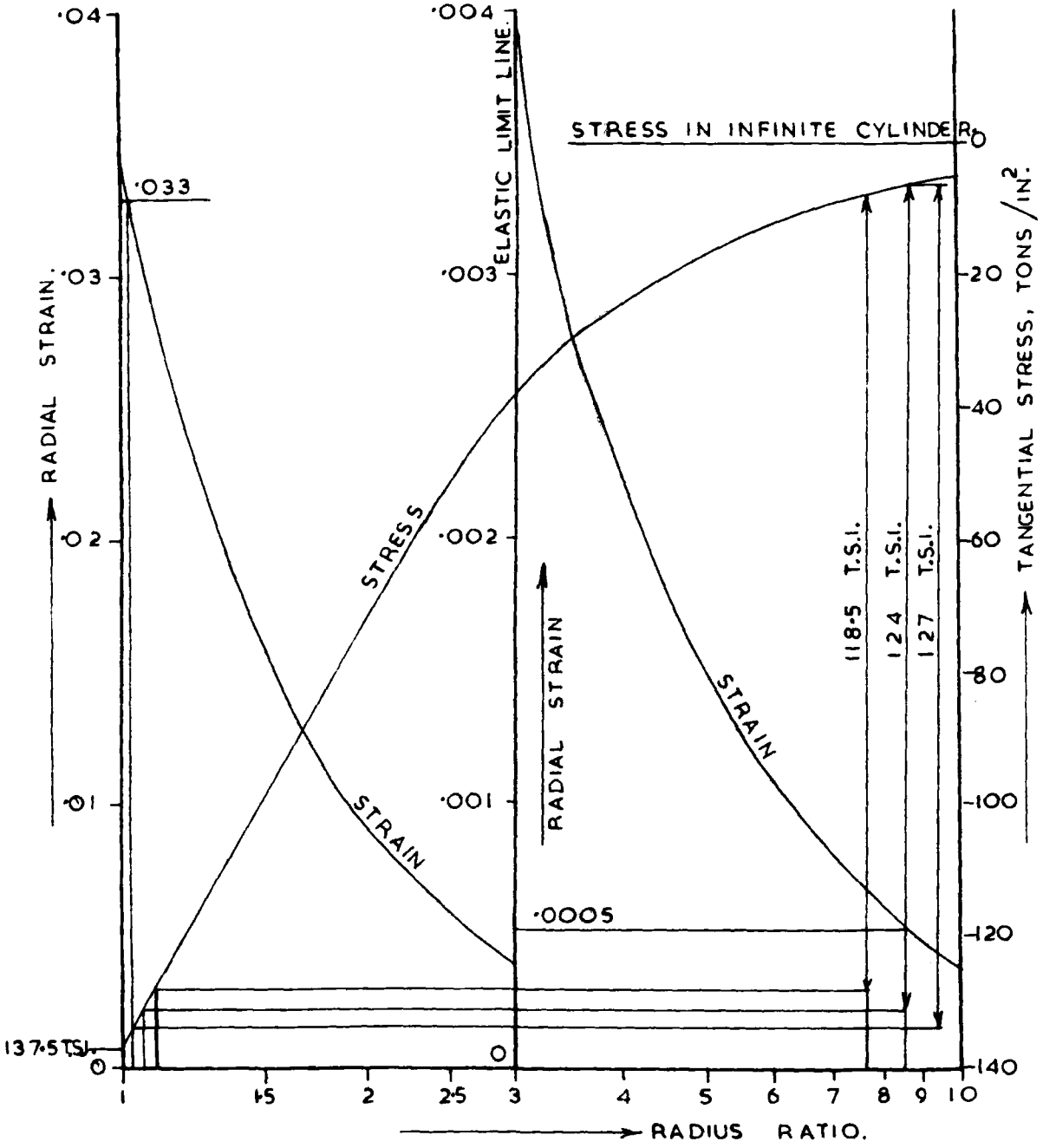

FIG. 1.A3. AUTOFRETTAGE DESIGN CHART FOR EN 26 STEEL AT 80 T.S.I. U.T.S.

in^2. The outside diameter of such a cylinder would be 2.65 inches. The high pressure cylinder of the intensifier should have an allowance for the possibility of a rebore, and the outside diameter selected is 2.86 inches, giving $\gamma = 7.62$. From Fig. 1.A3, the internal pressure required to move the elastic-plastic boundary to the geometric mean radius of the cylinder, when $\gamma = 7.62$, is 124 tons/in^2.

Under these conditions, the diameter of the elastic-plastic boundary is $.375\sqrt{7.62}$ inch, i.e. 1.03 inches.

An allowance must be made for reboring the cylinder after autofrettage to produce uniform dimensions. The initial diameter of the cylinder bore should therefore be .360 inch. The radius ratio then becomes 7.94. Keeping the elastic-plastic boundary at 1.03 inches diameter, its radius ratio becomes 1.03/.360 i.e. 2.86.

As the elastic-plastic boundary is at $\gamma = 3$ on the chart, the reduced bore corresponds to $\gamma = 3/2.86$, i.e. 1.05. Moving the bore to 1.05 on the chart corresponds to a rise in radial stress, or pressure of 3 tons/in^2. The cylinder must therefore be subject to a pressure of 127 tons/in^2, or 19,500kg/cm^2. After enlarging the bore to .375 inch, its elastic limit will be 18,000kg/cm^2.

(ii). Strains in High Pressure Cylinder.

From Fig. 1.A3, the tangential strains during autofrettage are .033 at the bore, and .0005 at the outside diameter. To these strains must be added the effect of removing the superimposed hydraulic pressure of 7 tons/in^2, to give the true autofrettage strains.

Linear compressibility of steel $= \frac{(1 - 2c)}{E}$

The tangential strains produced by removing hydrostatic pressure $= \frac{7(1 - 2c)}{E}$

$= .00023.$

Then autofrettage strains are .03323, or .012 inch at bore, and .00073, or .00209 inch at outer diameter.

The strains on returning to atmospheric pressure may be determined by assuming that the cylinder recovers elastically. The elastic strains are given by [11]:-

$$\frac{P}{E(\gamma^2 - 1)} \cdot \left\{(1 - 2c) + \gamma^2(1 + c)\right\} \qquad 1.A3.$$

at the bore, and

$$\frac{P}{E(\gamma^2 - 1)} \cdot (2 - c) \qquad 2.A3.$$

at the outside diameter.

Then elastic strain on removing 127 tons/in^2 from bore is:-

.0125, or .0045 inch at bore,
and .000264, or .00075 inch at outside diameter.

The permanent deformation due to autofrettage is the difference between the autofrettage strain and the elastic recovery. Thus, the permanent deformations are:-

.0075 inch at bore,
and .0013 inch at outside diameter.

The elastic strains on applying 10,000kg/cm^2 to the cylinder, may be determined from equations 1.A3. and 2.A3. They are:-

.0024 inch at bore,
and .00039 inch at outside diameter.

(iii). Bursting Pressure.

Provided there are no metallurgical faults in the steel, the cylinder would extend the region of plastic strain to the outside diameter before bursting. Work hardening of the steel would permit an even higher bursting pressure. The pressure at which the cylinder

becomes fully plastic may be determined very approximately by extrapolating the near straight line portion of the stress curve in Fig. 1.A3., into the region of higher strain. Taking radius ratio 3 on the chart as the outside diameter of the cylinder, a radius ratio of 7.62 gives a radial stress difference of about 180 tons/in^2. The bursting pressure, therefore, is in excess of 27,000kg/cm^2.

(iv). Radius Ratio of Low Pressure Cylinder.

The radius ratio required to maintain the yield pressure of the cylinder above 15,000 p.s.i. is 1.108. This may be predicted by applying the relationship,[11] :-

$$p_y = \frac{\sigma_y}{2} \frac{(\gamma^2 - 1)}{\gamma^2} , \qquad 3.A3.$$

giving yield pressure as a function of tensile yield stress, assuming the maximum shear stress criterion of failure.

However, when $\gamma = 1.108$, the cylinder bore strain is .006 inch at 10,000 p.s.i. This is given by the expression for tangential strain at the bore of a cylinder[11] :-

$$\varepsilon_t = \frac{P}{E(\gamma^2 - 1)} \left\{(1 - 2c) + \gamma^2(1 + c)\right\} \qquad 4.A3.$$

The problems of sealing the cylinder are lessened by a smaller bore strain, and the 1.68 radius ratio of the low pressure cylinder gives a diameter change of .0015 inch at 10,000 p.s.i.

(v). Design of Vessel Top Closure.

The screwed ring and cap screw assembly, parts (61) and (62) in Drawing 1, presents a complex design problem which cannot be carried out rigorously. The design is based on simplified calculations only, to determine approximately the principle stresses in the screwed ring and cap screws. The tensile yield stresses of these components

are 50 and 70 tons/in^2 respectively.

With the dimensions of the closure finally arrived at, the stresses in the closure which are considered to be of greatest importance are as follows:-

Pressure in vessel	= $1\frac{1}{2}$ x working pressure.
End load	= 100 tons.
Superficial shear area of cap screw threads	= 52in^2.
Superficial shear stress on cap screw threads	= 1.92 tons/in^2.
Area of end face of cap screws	= 3.38in^2.
Maximum compressive stress in cap screws	= 32.1 tons/in^2.
Superficial shear stress on screwed ring thread	= 3.03 tons/in^2.
Maximum bursting load in screwed ring	= 14.1 tons/in^2.

APPENDIX 4.

RESULTS.

(i). Specimen Calculation.

The example selected to illustrate the calculation procedure is the determination of the viscosity of D_2O at 25°C.

(a). Calculation of pressure.

The complete set of observations and calculations for pressure measurement are shown in Table 1.A4. Each pressure measurement involves observations before and after a viscosity determination. The columns in the table are arranged as follows:-

1. Bridge temperature, °C.
2. Coil temperature, mV, measured with the thermocouple adjacent to the manganin coil.
3. Bridge balance, (or measurement of the resistance of the R arm of the bridge). Value of X arm with commutator in position A.
4. Bridge balance; value of X arm with commutator in position B.
5. Mean of columns 3 and 4.
6. Coil balance, (or measurement of the external gauge resistance). Value of X arm with commutator in position A.
7. Coil balance; value of X arm with commutator in position B.
8. Mean of columns 6 and 7.
9. Uncorrected resistance of manganin coil; columns 5 minus 8. (See Chapter 7).
10. Coil resistance corrected to arbitary datum of 0.85mV coil temperature, by means of Fig. 27.
11. Coil resistance corrected to arbitary datum of 20°C Bridge temperature, by means of table derived from Fig. 25. Primary correction. (See Chapter 7).
12. Coil resistance corrected to arbitary datum of 20°C Bridge tem-

perature. Secondary correction. (See Chapter 7). Mean of initial and final observation.

13. Corrected coil resistance under pressure, minus corrected coil resistance at atmospheric pressure.

14. Coil factor, from Fig. 33. Column 13 is first converted to approximate pressure so that Fig. 33 can be used.

15. Pressure, columns 13 divided by 14.

(b). Determination of relative viscosity.

Calculation of the relative viscosity requires the following data:-

(1). Density of sinker.

The density of the sinker is determined by the density of its component parts;

Weight of stainless steel in sinker = 3.6164g.

Weight of soft iron in sinker = 0.5230g.

Density of stainless steel at $0^{\circ}C$. (Measured). = 7.9748g/cc.

Density of soft iron at $0^{\circ}C$ [97] = 7.8800g/cc.

Then, density of sinker at $0^{\circ}C$ and $0kg/cm^2$

$$= \frac{(3.6164 \times 7.9748) + (0.5230 \times 7.8800)}{4.1394} \qquad 1.A4.$$

The densities of the soft iron and stainless steel at other temperatures and pressures are calculated from the following data:-

Volume compressibility of stainless steel, (see Chapter 10) $= 6.248 \times 10^{-7}/kg/cm^2$.

Volume compressibility of soft iron [18] $= 5.80 \times 10^{-7}/kg/cm^2$.

Coefficient of linear expansion, stainless steel [97] $= .000016/^{\circ}C$.

Coefficient of linear expansion, soft iron [97] $= .0000126/^{\circ}C$.

From the densities of the materials at various temperatures and pressures, the density of the sinker is calculated as in

equation 1.A4. The sinker densities are summarised in Fig. 1.A4.

(2). Density of D_2O.

The density of deuterium oxide has been determined under pressure by Bridgman.[21] His results for 25°C, obtained by interpolation, are summarised in Fig. 2.A4.

Table 2.A4. shows a complete set of observations and calculations for determining relative viscosity. The columns in the table are arranged as follows:-

1. Pressure, from table 1.A4.
2. Bath temperature, after correction of the thermometer reading in accordance with its calibration against a platinum resistance thermometer.
3. Mean time of fall from end 1. Seconds.
4. Scatter of fall times from end 1.
5. Mean time of fall from end 2. Seconds.
6. Scatter of fall times from end 2.
7. Percentage difference between 3 and 5.
8. Mean of columns 3 and 5. Where column 7 indicates eccentric fall from end 2, only column 3 is considered. At atmospheric pressure, the second figure is from column 3. Seconds.
9. Column 8 corrected to 25.00°C. This small correction is applied by calculating the temperature-viscosity coefficient from atmospheric pressure data. Seconds.
10. Column 9 corrected to buoyancy of sinker at atmospheric pressure. Multiplying factor is

$$\frac{(\rho_{sp} - \rho_{fp})}{(\rho_{so} - \rho_{fo})} \cdot \frac{\rho_{so}}{\rho_{sp}}$$

The data for this correction is from Figs. 1.A4. and 2.A4. Seconds.

11. Column 10 corrected to the tube and sinker dimensions at atmospheric pressure. Seconds. Multiplying factor is
(1 + 2P x (linear compressibility stainless steel)).

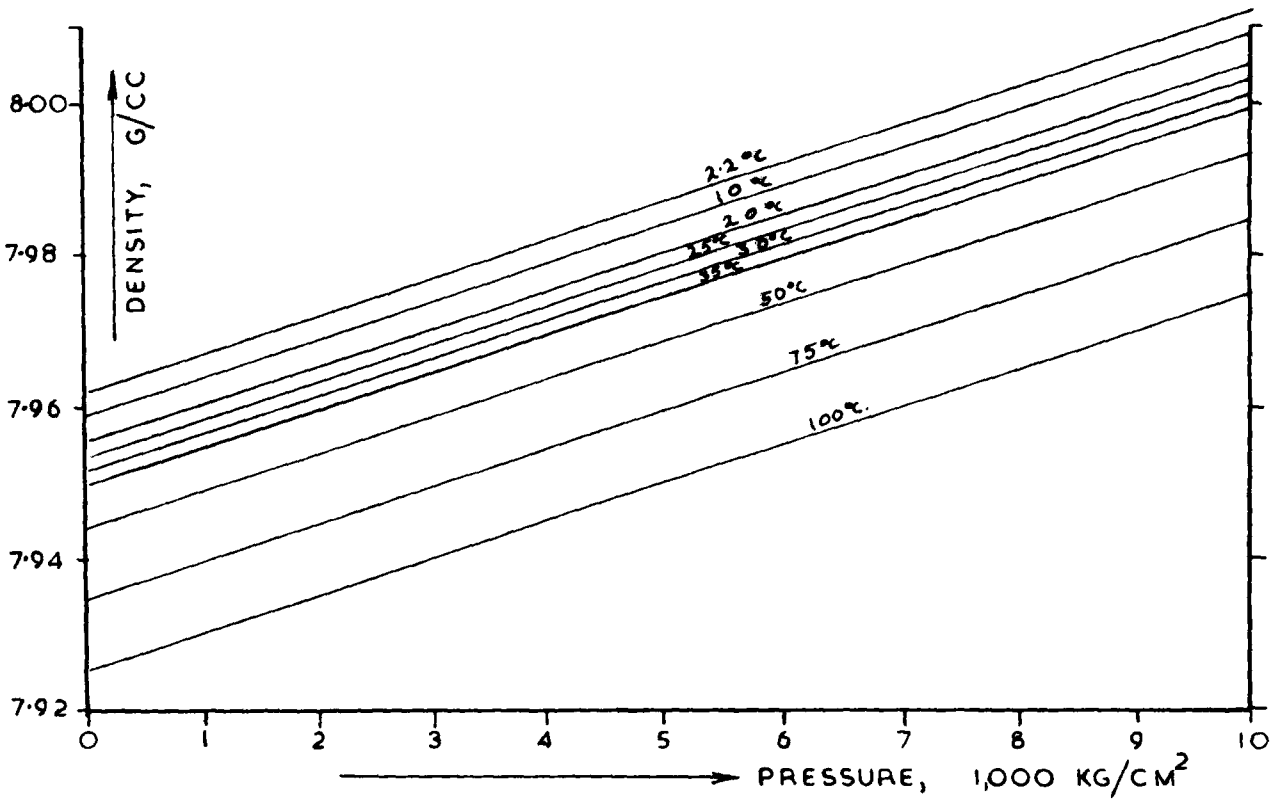

FIG. 1.A4. DENSITY OF ·004 IN. CLEARANCE SINKER.

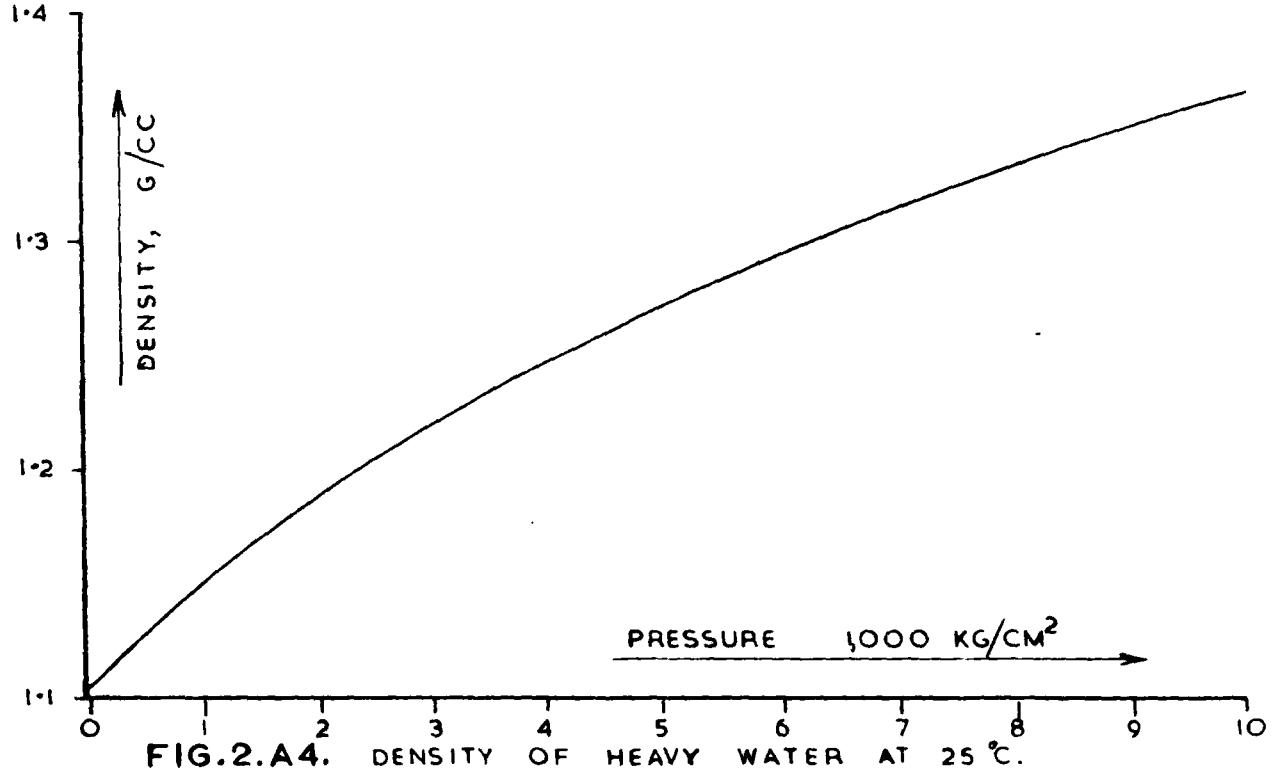

FIG.2.A4. DENSITY OF HEAVY WATER AT 25 °C.

12. Logarithm of 8.

13. Column 11 corrected for turbulence. The correction is determined from Fig. 39 and Column 12.

14. Relative viscosity. Corrected fall time under pressure, divided by corrected fall time at atmospheric pressure (mean of initial and final value). Where only column 3 was considered in column 8, the corrected time is divided by the second figure at atmospheric pressure in column 13.

In addition to the data already mentioned, the density of water is required under pressure. Bridgman's data for water densities,[21] interpolated for the temperatures employed in this study, are summarised in Fig. 3.A4.

(ii). Summary of Experimental Results.

In the following tables of results, the columns are arranged as follows:-

1. Pressure, kg/cm^2.
2. Temperature, ^{o}C.
3. Mean time of fall of sinker from end 1, for atmospheric pressure, and for pressures where the fall conditions are concentric in one direction only. Seconds.
4. Mean time of fall of sinker from both ends, for pressures where fall conditions are concentric in both directions. Seconds.
5, and 6. Fall times from columns 3 and 4 corrected to the nominal temperature of the experiment, corrected for density changes in the fluid and sinker under pressure, corrected for dimensional changes under pressure in the tube and sinker, and corrected for the effects of turbulence. Seconds.
7. Relative viscosity, given by the corrected fall time under pressure, divided by the corrected fall time at atmospheric pressure.

(a). Water.

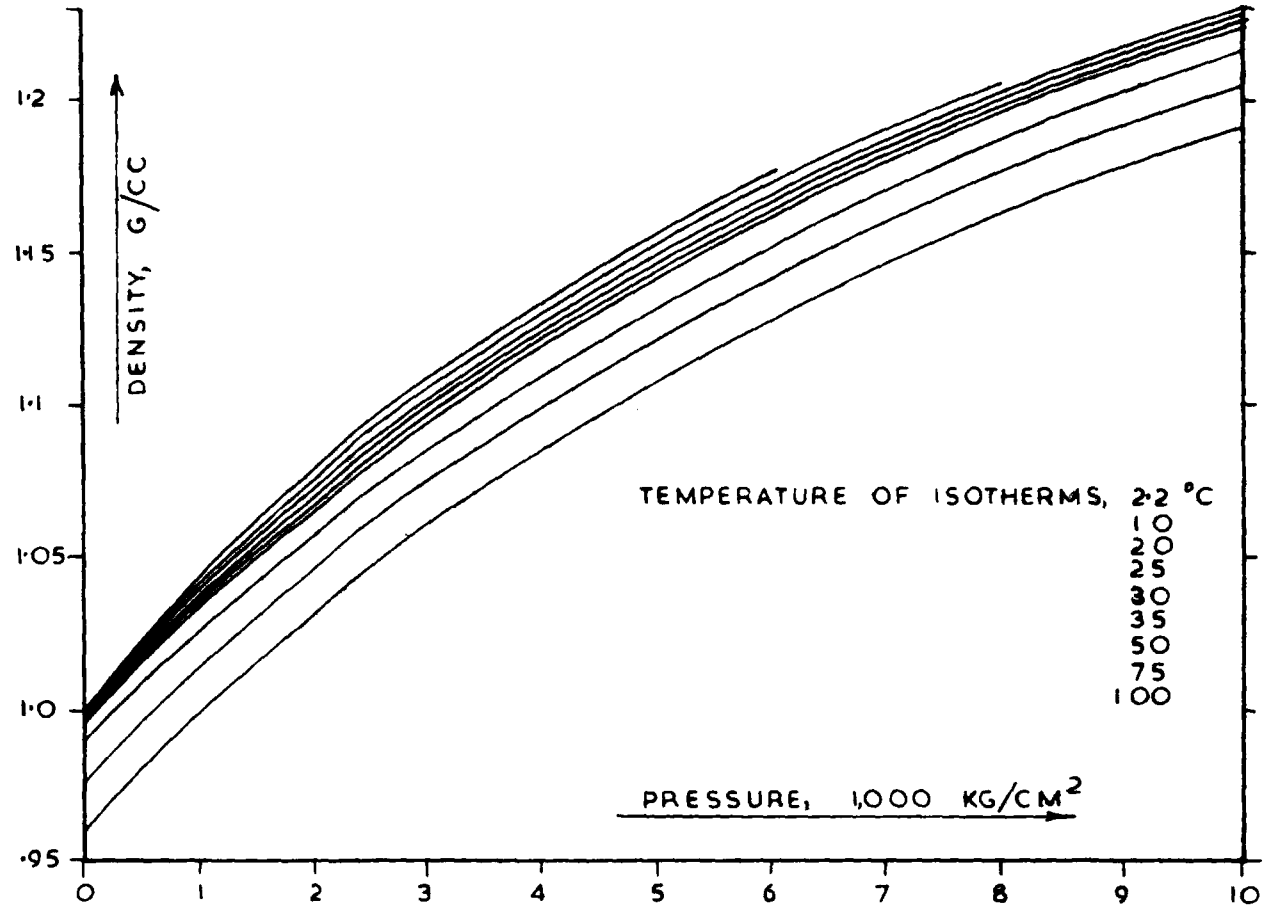

FIG. 3.A4. DENSITY OF WATER

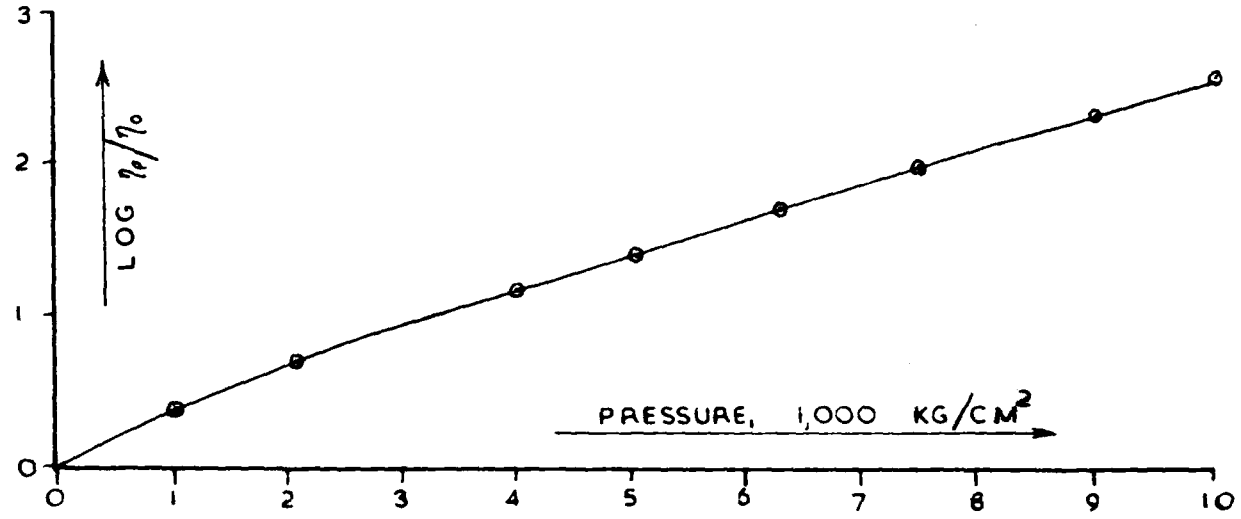

FIG. 4.A4. VISCOSITY OF PRESSURE TRANSMITTING FLUID AT 25 °C.

TABLE 1.A4.

1.	2.	3.	4.	5.	6.	7.	8.
Bridge Temp.	Coil Temp.	Bridge Balance. A	B	Mean.	Coil Balance. A	B	Mean.
24.70	.774	48.00220	48.00330	48.00275	3.48510	3.43270	3.45890
24.65	.775	48.00240	48.00320	48.00280	3.48520	3.43250	3.45885
25.15	.777	48.00210	48.00350	48.00280	3.44160	3.38900	3.41530
25.20	.779	48.00230	48.00340	48.00285	3.44170	3.38950	3.41560
25.45	.781	48.00220	48.00350	48.00285	3.40260	3.35000	3.37640
25.45	.782	48.00250	48.00340	48.00295	3.40260	3.35030	3.37645
25.05	.786	48.00300	48.00270	48.00285	3.36760	3.31480	3.34120
25.00	.786	48.00330	48.00270	48.00300	3.36750	3.31490	3.34120
24.85	.790	48.00250	48.00330	48.00290	3.32810	3.27560	3.30185
24.85	.791	48.00280	48.00320	48.00300	3.32820	3.27560	3.30190
24.70	.796	48.00240	48.00360	48.00300	3.27720	3.22440	3.25080
24.80	.798	48.00350	48.00260	48.00305	3.27700	3.22450	3.25075
24.70	.800	48.00290	48.00300	48.00295	3.16720	3.11420	3.14070
24.70	.801	48.00270	48.00350	48.00310	3.16710	3.11460	3.14085
24.85	.806	48.00260	48.00340	48.00300	3.04460	2.99370	3.01915
24.95	.807	48.00280	48.00320	48.00300	3.04470	2.99390	3.01930
25.20	.796	48.00260	48.00320	48.00290	2.92350	2.87290	2.89820
25.15	.796	48.00330	48.00260	48.00295	2.92370	2.87320	2.89845
25.10	.796	48.00300	48.00280	48.00290	2.77040	2.71960	2.74500
25.10	.796	48.00320	48.00280	48.00300	2.77050	2.71990	2.74520
25.20	.799	48.00260	48.00310	48.00285	2.52150	2.47090	2.49620
25.20	.799	48.00300	48.00250	48.00275	2.52970	2.47870	2.50420
24.70	.894	48.00270	48.00310	48.00290	2.65600	2.60430	2.63015
24.75	.908	48.00290	48.00300	48.00295	2.65570	2.60440	2.63005
24.85	1.263	48.00300	48.00300	48.00300	2.46440	2.41210	2.43825
24.70	1.245	48.00290	48.00330	48.00310	2.46820	2.41580	2.44200
25.10	1.237	48.00280	48.00310	48.00295	2.53430	2.48210	2.50820
25.20	1.239	48.00300	48 00290	48.00295	2.53450	2.48240	2.50845
24.10	.767	48.00280	48.00290	48.00285	3.46260	3.41240	3.43750
24.10	.780	48.00260	48.00330	48.00295	3.46240	3.41220	3.43730

TABLE 1.A4. CONT.

9. Diff.	10. Correct for C. temp.	11. Correct for B. temp.	12. Corrected mean C. resist.	13. Resist. change.	14. Coil factor, $\times 10^4$	15. Pressure. kg/cm^2.
44.54385	44.54593	44.55001	44.55001			
44.54395	44.54601	44.55005				
44.58750	44.58950	44.59395	44.59379	.04378	1.0846	403.7
44.58725	44.58919	44.59368				
44.62645	44.62833	44.63299	44.63297	.08296	1.0843	765.1
44.62650	44.62836	44.63302				
44.66165	44.66337	44.66773	44.66775	.11774	1.0840	1086.2
44.66180	44.66352	44.66784				
44.70105	44.70267	44.70686	44.70684	.15683	1.0835	1447.4
44.70110	44.70270	44.70689				
44.75220	44.75368	44.75776	44.75776	.20775	1.0831	1918.1
44.75230	44.75370	44.75785				
44.86225	44.86359	44.86767	44.86760	.31759	1.0821	2934.9
44.86225	44.86357	44.86765				
44.98385	44.98505	44.98924	44.98911	.43910	1.0809	4062.4
44.98370	44.98486	44.98914				
45.10470	45.10620	45.11068	45.11046	.56045	1.0793	5192.7
45.10450	45.10600	45.11044				
45.25790	45.25840	45.26380	45.26363	.71362	1.0774	6623.5
45.25780	45.25830	45.26370				
45.50665	45.50805	45.51253	45.50833	.95832	1.0750	8914.6
45.49855	45.49995	45.50443				
45.37275	45.37167	45.37575	45.37554	.82553	1.0763	7670.1
45.37290	45.37146	45.37558				
45.56475	45.55659	45.56079	45.55888	1.00887	1.0740	9393.5
45.56110	45.55320	45.55728				
45.49475	45.48699	45.49139	45.49115	.94114	1.0753	8754.8
45.49450	45.48672	45.49120				
44.56535	44.56761	44.57125	44.57119	.02118	1.0849	195.2
44.56565	44.56755	44.57119				

TABLE 2.A4.

1. Pressure kg/cm^2.	2. Temp. °C.	3. Fall time.s. 1.	4. Scatter 1. %	5. Fall time.s. 2.	6. Scatter 2. %	7. Diff. %
0	25.04	50.528	.02	50.071	.1	.9
403.7	25.03	50.116	.2	49.621	.05	1.0
765.1	25.02	50.083	.1	49.600	.15	.97
1086.2	25.02	50.366	.1	49.869	.15	1.0
1447.4	25.03	50.922	.1	50.416	.12	1.0
1918.1	25.02	51.924	.1	51.413	.01	1.0
2934.9	25.03	55.012	.1	54.482	.1	1.0
4062.4	25.02	59.585	.16	59.015	.08	1.0
5192.7	24.99	65.121	.06	64.547	.08	.9
6623.5	25.00	73.579	.06	72.830	.05	1.05
8914.6	25.01	90.819	.3	89.739	.2	1.2
7670.1	24.99	80.751	.08	79.893	.1	1.1
9393.5	24.99	94.813	.25	92.1	2.1	2.86
8754.8	25.00	89.212	.03	88.2	.4	1.3
195.2	24.99	50.251	.2	49.800	.2	.9

TABLE 2.A4. CONT.

8. Mean time s.	9. Correct to 25°C. s.	10. Correct for density. s.	11. Correct for dimensions. s.	12. Log. time.	13. Correct for turbulence. s.	14. η_p / η_o
50.300	50.345	50.345	50.345	1.702	50.244	1.0000
50.528	50.574	50.574	50.574		50.473	
49.868	49.901	49.774	49.782	1.698	49.677	.9887
-	-	-	-		-	
49.842	49.865	49.624	49.639	1.697	49.535	.9859
-	-	-	-		-	
50.118	50.141	49.804	49.825	1.699	49.720	.9896
-	-	-	-		-	
50.669	50.703	50.254	50.284	1.704	50.183	.9988
-	-	-	-		-	
51.669	51.692	51.108	51.149	1.713	51.057	1.0162
-	-	-	-		-	
54.747	54.784	53.909	53.974	1.738	53.898	1.0727
-	-	-	-		-	
59.300	59.327	58.112	58.210	1.773	58.163	1.1576
-	-	-	-		-	
64.834	64.819	63.243	63.380	1.812	63.355	1.2609
-	-	-	-		-	
73.205	73.205	71.105	71.301	1.865	71.301	1.4191
-	-	-	-		-	
90.279	90.299	87.183	87.507	1.956	87.507	1.7416
-	-	-	-		-	
80.322	80.304	77.846	78.024	1.905	78.024	1.5529
-	-	-	-		-	
-	-	-	-	1.977	-	1.8183
94.813	94.792	91.416	91.775		91.775	
-	-	-	-	1.951	-	1.7132
89.212	89.212	86.155	86.470		86.470	
50.026	50.015	49.957	49.957	1.700	49.352	.9922
-	-	-	-		-	

Experimental results - Water.

	1.	2.	3.	4.	5.	6.	7.
	Press. kg/cm^2.	Temp. °C.	Mean fall time. sec. End 1.	Mean fall time. sec. Both ends.	Corrected fall time. sec. End 1.	Corrected fall time. sec. Both ends.	η_p/η_o
2.2°C.	0	2.20	76.404		76.404		1.0000
	342	2.20	73.383		73.225		.9584
	658	2.22	71.789		71.548		.9364
	1041	2.22	71.077		70.693		.9253
	1303	2.20	71.183		70.664		.9249
	1656	2.20	71.680		71.040		.9298
	2050	2.20	72.726		71.958		.9418
	2447	2.22	74.169		73.317		.9596
	2923	2.20	76.508		75.451		.9875
	3551	2.20	80.210		78.936		1.0331
	4449	2.20	86.727		85.126		1.1142
	5423	2.20	95.366		93.421		1.2227
10°C.	0	9.95	59.598	59.321	59.452	59.177	1.0000
	293	9.95		58.158		57.917	.9787
	560	9.95		57.536		57.199	.9666
	837	9.95		57.223		56.812	.9600
	1124	9.95		57.326		56.830	.9603
	1385	9.97		57.526		57.993	.9631
	1722	9.95		58.201		57.542	.9724
	2038	9.95		58.986		58.248	.9843
	2441	9.95		60.275		59.440	1.0044
	3017	9.95		62.558		61.579	1.0406
	3831	9.95		66.469		65.273	1.1036
	4950	9.95		73.109		71.600	1.2099
	5946	9.95		80.156		78.312	1.3233
	7188	9.95	91.254		88.934		1.4959
20°C.	0	19.99	45.620	45.398	45.472	45.251	1.0000
	298	19.99		44.935		44.712	.9881
	705	19.99		44.832		44.512	.9837
	1102	19.91		45.051		44.555	.9846
	1582	19.99		45.864		45.363	1.0025
	2347	19.99		47.615		46.968	1.0373
	2944	19.99		49.518		48.755	1.0774
	4059	19.91		53.573		52.502	1.1602
	5315	19.99		59.394		58.163	1.2853
	6687	19.99		66.852		65.303	1.4431
	7940	19.99		75.080		73.189	1.6174
	8929	19.99		82.560		80.347	1.7755

Experimental results - Water.

	1. Press. kg/cm^2.	2. Temp. °C.	3. Mean fall time. sec. End 1.	4. Mean fall time. sec. Both ends.	5. Corrected fall time. sec. End 1.	6. Corrected fall time. sec. Both ends.	7. η_p/η_o
25°C.	0	24.92	40.867	40.667	40.622	40.424	1.0000
	229	24.92		40.547		40.262	.9960
	634	24.93		40.390		40.020	.9900
	1008	24.96		40.660		40.245	.9956
	1542	24.95		41.436		40.914	1.0121
	2787	24.93		44.331		43.571	1.0779
	3866	24.93		47.753		46.824	1.1583
	5043	24.92		52.564		51.393	1.2703
	6315	24.92		58.417		56.986	1.4095
	7315	24.92		64.277		62.602	1.5484
	8319	24.94	70.211		68.324		1.6818
	9298	24.94	76.794		74.604		1.8364
	0	25.03	40.964	40.760	40.824	40.621	1.0000
	3572	25.06		46.917		46.160	1.1364
	6004	25.13		56.708		55.616	1.3691
	8584	25.13	71.745		70.098		1.7171
	0	25.01		40.436		40.267	1.0000
	9561	24.98		77.672		75.517	1.8754
	0	24.98		40.297		40.102	1.0000
	4509	24.98		49.922		48.929	1.2201
	9954	25.01		80.312		78.074	1.9469
30°C.	0	29.93		12.034		11.532	1.0000
	2471	29.91		13.196		12.582	1.0783
	2761	29.93		12.278		12.739	1.1032
	3607	29.94		14.140		13.487	1.1665
	4686	29.94		15.347		14.656	1.2580
	5834	29.92		16.637		15.891	1.3730
	7083	29.94		18.556		17.749	1.5252
	8192	29.93		20.253		19.374	1.6720
	9243	29.93		22.164		21.221	1.8259
	10076	29.93		24.013		23.006	1.9824
	0	30.00		36.182		35.981	1.0000
	461	30.00		36.143		35.848	.9963
	922	30.00		36.536		36.161	1.0050
	1558	30.00		37.602		37.125	1.0318
	2403	30.00		39.304		38.708	1.0758
	3430	30.00		42.139		41.387	1.1500
	4570	30.00		45.971		45.030	1.2515

Experimental results - Water.

	1. Press. kg/cm^2.	2. Temp. °C.	3. Mean fall time. sec. End 1.	4. Mean fall time. sec. Both ends.	5. Corrected fall time. sec. End 1.	6. Corrected fall time. sec. Both ends.	7. η_p / η_o
30°C (cont).	0	30.01		36.265		36.069	1.0000
	251	29.98		36.288		36.022	.9987
	555	29.98		36.415		36.090	1.0006
	1118	29.99		36.961		36.549	1.0133
	0	29.96		36.246		36.013	1.0000
	2403	29.94		39.460		38.800	1.0774
	6155	29.93		51.896		50.613	1.4054
	9187	29.90		67.669		65.695	1.8242
	0	29.94		36.300		36.054	1.0000
	2596	29.93		39.867		39.216	1.0877
	5039	29.93		47.502		46.423	1.2876
35°C.	0	34.96		32.613		32.352	1.0000
	192	35.00		32.698		32.430	1.0024
	417	35.03		32.834		32.552	1.0062
	654	35.00		32.963		32.624	1.0084
	1414	35.03		34.032		33.604	1.0387
	2718	35.04		36.630		36.027	1.1136
	3789	35.04		39.345		38.602	1.1932
50°C.	0	49.98		24.937		24.630	1.0000
	345	49.96		25.280		24.923	1.0119
	2940	49.98		29.267		28.637	1.1627
	5145	49.98		34.154		33.361	1.3545
	7510	49.98		40.678		39.548	1.6057
	9816	49.99		48.809		46.999	1.9082
	0	49.94		24.912		24.588	1.0000
	463	49.98		25.398		25.038	1.0183
	870	49.98		25.965		25.559	1.0395
	1810	49.96		27.383		26.867	1.0927
	3132	49.95		29.802		29.135	1.1849
	4180	49.94		32.000		31.215	1.2695
	5336	49.96		34.643		33.739	1.3722
	6265	49.98		37.019		36.022	1.4650
	7394	50.04		40.197		39.106	1.5905
	8332	49.96		43.175		41.901	1.7041

Experimental results - Water.

	1. Press. kg/cm^2	2. Temp. °C.	3. Mean fall time. sec. End 1.	4. Mean fall time. sec. Both ends.	5. Corrected fall time. sec. End 1.	6. Corrected fall time. sec. Both ends.	7. η_p/η_o
75°C.	0	74.96	17.641	17.400	17.255	17.015	1.0000
	384	74.96		17.916		17.471	1.0268
	690	74.96		18.194		17.752	1.0433
	1111	74.96		18.672		18.198	1.0695
	1884	74.96		19.699		19.167	1.1265
	2755	74.96		21.041		20.450	1.2019
	3848	74.96		22.591		21.919	1.2882
	4893	74.96		24.297		23.547	1.3839
	5890	74.96		26.032		25.206	1.4814
	6816	74.96		27.751		26.850	1.5780
	8798	74.96	32.520		31.430		1.8215
	9816	74.96	34.768		33.577		1.9459
100°C.	0	99.88		13.041		12.569	1.0000
	452	99.89		13.564		13.071	1.0399
	1032	99.87		14.185		13.660	1.0868
	1888	99.85		15.131		14.566	1.1589
	2990	99.85		16.400		15.772	1.2548
	4194	99.88		17.805		17.120	1.3621
	4869	99.88		18.777		18.049	1.4360
	5814	99.87		19.996		19.210	1.5284
	7061	99.87		21.689		20.829	1.6572
	8275	99.86		23.398		22.449	1.7861
	9018	99.86		24.504		23.505	1.8701

(b). Heavy water.

The experimental results for D_2O are included in the specimen calculation in part (i) of this Appendix.

(c). Normal pentane:-

30°C.	0	29.88	9.359	9.307	8.677	8.629	1.0000
	514	29.86		14.278		13.737	1.5919
	1051	29.86		19.676		19.087	2.2119
	2096	29.86		32.012		31.201	3.6158
	3033	29.86		45.882		44.598	5.1684
	4036	29.86	65.007		63.417		7.3086
	5258	29.86	95.142		92.601		10.6719
	6258	29.86	127.480		123.834		14.2715
	7449	29.88	178.021		172.601		19.8917
	8574	29.90	241.733		234.063		26.9750
	9575	29.90	316.271		305.880		35.2517

All of the results, given in the preceding tables, refer to data obtained with the .004 inch clearance stainless steel sinker, except for the first set of figures for water at 30°C, which were obtained with a .006 inch clearance stainless steel sinker during preliminary trials on the viscometer.

The fall times for the atmospheric pressure condition are a mean of the fall time at the beginning and end of the experiment, where this is available. In the case of the three lowest isotherms on water, the water was frozen at high pressure, causing the rupture of the bursting disc, and for these experiments, the fall time at the end of the experiment could not be measured. Several of the fall times at atmospheric pressure at the end of an experiment were spoilt by leakage of petroleum ether into the viscometer on lowering the pressure of the system, as described in Chapter 3.

The difference between the atmospheric fall times in the first two and second two sets of results for water at 25°C, arises from dismantling of the sinker for cleaning. Also, the handling of water in the stainless steel seems to produce a film of corrosion products which is variable with exposure and cleaning. The dimensional changes required to produce a .1% change in fall time are very small indeed, and this, together with assembling the sinker in different planes within the tube, produces small random variations in fall time. However, the variations during an experiment are negligible.

(iii). Smoothed Viscosity Data.

(a). Water.

Press. kg/cm^2.	2.2°C. η_p/η_o	2.2°C. Viscosity cp.	10°C. η_p/η_o	10°C. Viscosity cp.	20°C. η_p/η_o	20°C. Viscosity cp.
0	1.0000	1.6617	1.0000	1.3077	1.0000	1.0050
250	.9672	1.6072	.9820	1.2842	.9903	.9953
500	.9455	1.5711	.9694	1.2677	.9852	.9901
750	.9327	1.5499	.9620	1.2580	.9827	.9876
1000	.9260	1.5387	.9569	1.2514	.9848	.9897
1250	.9252	1.5374	.9608	1.2564	.9890	.9939
1500	.9274	1,5411	.9655	1.2626	.9966	1.0016
1750	.9320	1.5487	.9732	1.2727	1.0072	1.0122
2000	.9398	1.5617	.9824	1.2847	1.0182	1.0233
2500	.9620	1.5986	1.0060	1.3155	1.0442	1.0494
3000	.9932	1.6504	1.0368	1.3558	1.0760	1.0814
4000	1.0718	1.7810	1.1185	1.4627	1.1570	1.1628
5000	1.1740	1.9508	1.2162	1.5904	1.2522	1.2585
6000	1.2965	2.1544	1.3298	1.7390	1.3605	1.3673
7000			1.4682	1.9200	1.4844	1.4918
8000					1.6212	1.6293
9000					1.7776	1.7865

	25°C.		30°C.		35°C.	
0	1.0000	.8937	1.0000	.8007	1.0000	.7225
250	.9940	.8883	.9972	.7984	1.0010	.7232
500	.9919	.8865	.9975	.7987	1.0040	.7254
750	.9922	.8867	1.0010	.8015	1.0110	.7304
1000	.9955	.8897	1.0080	.8071	1.0200	.7370
1250	1.0020	.8955	1.0172	.8145	1.0318	.7455
1500	1.0108	.9034	1.0275	.8227	1.0435	.7539
1750	1.0215	.9129	1.0392	.8321	1.0553	.7625
2000	1.0330	.9232	1.0527	.8429	1.0682	.7718
2500	1.0610	.9482	1.0802	.8649	1.0988	.7939
3000	1.0954	.9790	1.1158	.8934	1.1332	.8187
4000	1.1740	1.0492	1.1950	.9568	1.2127	.8762
5000	1.2660	1.1314	1.2842	1.0283		
6000	1.3724	1.2265	1.3860	1.1098		
7000	1.4934	1.3347	1.5070	1.2067		
8000	1.6310	1.4576	1.6420	1.3147		
9000	1.7850	1.5953	1.7912	1.4342		
10000	1.9534	1.7458	1.9500	1.5614		

Press. kg/cm^2.	η_p/η_o	Viscosity cp.	η_p/η_o	Viscosity cp.	η_p/η_o	Viscosity cp.
	50°C.		75°C.		100°C.	
0	1.0000	.5494	1.0000	.3799	1.0000	.2838
250	1.0100	.5549	1.0144	.3854	1.0223	.2901
500	1.0212	.5610	1.0295	.3911	1.0434	.2961
750	1.0330	.5675	1.0458	.3973	1.0638	.3019
1000	1.0455	.5744	1.0628	.4038	1.0850	.3079
1500	1.0738	.5899	1.0997	.4178	1.1270	.3198
2000	1.1042	.6066	1.1365	.4318	1.1695	.3319
2500	1.1372	.6248	1.1760	.4468	1.2134	.3444
3000	1.1740	.6450	1.2167	.4622	1.2565	.3566
4000	1.2535	.6887	1.3022	.4947	1.3492	.3829
5000	1.3418	.7372	1.3938	.5295	1.4452	.4101
6000	1.4392	.7907	1.4920	.5668	1.5464	.4389
7000	1.5463	.8495	1.5978	.6070	1.6495	.4682
8000	1.6635	.9139	1.7081	.6489	1.7575	.4988
9000	1.7930	.9851	1.8252	.6934	1.8700	.5307
10000	1.9358	1.0635	1.9476	.7399	1.9862	.5637

	η_p/η_o	Viscosity cp.
	0°C.	
0	1.0000	1.7921
500	.9375	1.6801
1000	.9140	1.6380
1500	.9120	1.6344
2000	.9250	1.6577
3000	.9755	1.7482
4000	1.0556	1.8917
5000	1.1555	2.0708
6000	1.2780	2.2903

(b). Heavy Water.

The following table includes the value of η_{D_2O}/η_{H_2O}.

25°C.

Press. kg/cm^2.	η_p/η_o	Viscosity D_2O. cp.	Viscosity H_2O. cp.	η_{D_2O}/η_{H_2O}
0	1.0000	1.1000	.8937	1.2312
250	.9912	1.0903	.8883	1.2278
500	.9863	1.0849	.8865	1.2242
750	.9860	1.0846	.8667	1.2238
1000	.9882	1.0870	.8897	1.2228
1250	.9932	1.0935	.8955	1.2203
1500	1.0003	1.1003	.9034	1.2183
1750	1.0095	1.1105	.9129	1.2167
2000	1.0208	1.1229	.9232	1.2166
2500	1.0468	1.1516	.9482	1.2146
3000	1.0780	1.1860	.9790	1.2115
4000	1.1525	1.2682	1.0492	1.2086
5000	1.2421	1.3670	1.1314	1.2079
6000	1.3472	1.4830	1.2265	1.2086
7000	1.4650	1.6129	1.3347	1.2077
8000	1.5998	1.7616	1.4576	1.2076
9000	1.7536	1.9312	1.5953	1.2094
10000	1.9230	2.1181	1.7458	1.2120

(c). Normal Pentane.

30°C.

Press. kg/cm^2.	log. (η_p/η_o).	η_p/η_o	η_p/η_o Bridgman.
0	0.0000	1.0000	1.000
500	.1930	1.5596	1.517
1000	.3280	2.1281	2.065
2000	.5350	3.4277	3.342
3000	.7025	5.0408	-
4000	.8522	7.1154	7.031
5000	.9886	9.7409	-
6000	1.1160	13.0620	12.91
7000	1.2382	17.3060	-
8000	1.3590	22.8560	22.91
9000	1.4795	30.1650	-
10000	1.5950	39.3550	40.27

(iv). Viscosity of Pressure Transmitting Fluid.

In the course of preliminary trials with the viscometer, the viscosity of the pressure transmitting fluid was determined approximately at 25°C. The data refer to a mixture of:-

100 - 120°C boiling range petroleum ether - 95% by volume.
DTD 585 hydraulic fluid - 5% by volume.

The results are summarised in Fig. 4.A4. The viscosity of the pressure transmitting fluid rises by a factor of almost 400 at 10,000 atmospheres, and as the initial viscosity is about .5cp., the viscosity under full pressure is 2 poise.

APPENDIX 5.

PRESSURE DEPENDENCE OF VISCOSITY.

In the Andrade [3] model of viscous flow, momentum transport by molecular convection is considered to be negligible, momentum being transferred by molecules in adjacent planes colliding at the extremities of their oscillations. The frequency of the vibrating molecules determines the rate of collision; hence, according to this model, the viscous drag, and the coefficient of viscosity is given by

$$\eta = 4\nu m/3a \qquad 1.A5.$$

where ν = frequency

m = molecular mass

a = intermolecular distance.

The model does not describe the temperature dependence of viscosity, but it is possible that the expression will give pressure dependence in that, as the volume decreases, ν must increase in order to maintain a constant energy, and in consequence, the viscosity rises.

From equation 1.A5, the pressure dependence of viscosity is given by

$$\left(\frac{\partial \eta}{\partial P}\right)_T = \frac{4m}{3}\left(1/a\left(\frac{\partial \nu}{\partial P}\right)_T + \nu\left(\frac{\partial 1/a}{\partial P}\right)_T\right)$$

then

$$1/\eta\left(\frac{\partial \eta}{\partial P}\right)_T = 1/\nu\left(\frac{\partial \nu}{\partial P}\right)_T - 1/a\left(\frac{\partial a}{\partial P}\right)_T$$

$$= \frac{V}{V\nu}\left(\frac{\partial \nu}{\partial V}\right)_T\left(\frac{\partial V}{\partial P}\right)_T - \frac{V}{Va}\left(\frac{\partial a}{\partial V}\right)_T\left(\frac{\partial V}{\partial P}\right)_T \qquad 2.A5.$$

where V is the molar volume.

Now the compressibility $\beta_T = -\frac{1}{V}\left(\frac{\partial V}{\partial P}\right)_T$

Then, from 2.A5,

$$\frac{1}{\eta}\left(\frac{\partial \eta}{\partial P}\right)_T = \beta_T\left(\frac{V}{a}\left(\frac{\partial a}{\partial V}\right)_T - \frac{V}{\nu}\left(\frac{\partial \nu}{\partial V}\right)_T\right) \qquad 3.A5.$$

Assuming a face centred cubic lattice structure in the liquid, the side of the cube $= a2^{\frac{1}{2}}$

the volume of the cube $= (a2^{\frac{1}{2}})^3$

which is the volume of 4 molecules.

Then volume of 1 molecule $v = \frac{(a2^{\frac{1}{2}})^3}{4} = \frac{V}{N}$

N = Avogadro's number

Then $a^3 = 2^{\frac{1}{2}}\frac{V}{N}$

i.e. $\left(\frac{\partial a}{\partial V}\right)_T = \frac{2^{\frac{1}{2}}}{3Na^2}$

or $\frac{V}{a}\left(\frac{\partial a}{\partial V}\right)_T = \frac{1}{3}$

From 3.A5,

$$\frac{1}{\eta}\left(\frac{\partial \eta}{\partial P}\right)_T = \beta_T\left(\frac{1}{3} - \frac{V}{\nu}\left(\frac{\partial \nu}{\partial V}\right)_T\right) \qquad 4.A5.$$

In order to determine the pressure dependence of viscosity, the dependence of frequency on volume must be evaluated. The evaluation follows the method of Horrocks & McLaughlin [65], in their determination of the temperature dependence of thermal conductivity.

Assuming the molecules in the liquid state to be vibrating harmonically about fixed lattice positions, and interacting with a Lennard-Jones 12:6 potential [81],

$$\phi(r) = 4\varepsilon\left(\left(\frac{\sigma}{r}\right)^{12} - \left(\frac{\sigma}{r}\right)^{6}\right)$$

the change in potential energy of a molecule when displaced a distance r from the centre of its own cell is given by

$$\psi_{(r)} - \psi_{(o)} = \frac{Z\varepsilon}{a^2}(L_1 v^{*4} - M_1 v^{*2})r^2 \qquad 5.A5.$$

where ε is the depth of the potential minimum.

σ is the molecular diameter.

Z is the co-ordination number (= 12 for f.c.c. lattice).

$v^* = v_o/v$, where $v_o = \sigma^3$

L_1 and M_1 are lattice summation constants of value 22.11 and 10.56

From equation 5.A5, the vibrational frequency may be derived as (115)

$$\nu = \frac{1}{2\pi m^{\frac{1}{2}}}\left\{\frac{2Z\varepsilon}{a^2}(L_1 v^{*4} - M_1 v^{*2})\right\}^{\frac{1}{2}}$$

Then $$\frac{V}{\nu}\left(\frac{\partial \nu}{\partial V}\right)_T = -\frac{1}{2}\left(\frac{103.18v^{*2} - 28.16}{22.11v^{*2} - 10.56}\right) \qquad 6.A5.$$

Substituting 6.A5 in 5.A5,

$$\frac{1}{\eta}\left(\frac{\partial \eta}{\partial P}\right)_T = \beta_T\left(\frac{1}{3} + \frac{1}{2}\left(\frac{103.18v^{*2} - 28.16}{22.11v^{*2} - 10.56}\right)\right)$$

This relationship suggests that the viscosity coefficient is a function of compressibility and volume only. The value of v^* is approximately 1, and does not change by more than about 25% up to 10,000kg/cm^2.

If $v^* = 1$, then $\frac{1}{\eta}\left(\frac{\partial \eta}{\partial P}\right)_T = 3.58\,\beta_T$.

If $v^* = 1.25$, then $\frac{1}{\eta}\left(\frac{\partial \eta}{\partial P}\right)_T = 3.1\,\beta_T$.

Thus, $\frac{1}{\eta}\left(\frac{\partial \eta}{\partial P}\right)_T \simeq C\beta_T$. 7.A5.

REFERENCES.

(1). Adams, L.H., Goranson,R.W. and Gibson, R.E.
Rev. Sci. Inst. 8. 1937. p.230.

(2). Andrade, E.N. da C. Nature 125. 1930. p.309 & 582.

(3). Andrade, E.N. da C. Phil. Mag. 17. 1934. 7th. Series. p.497 & 698.

(4). Arrhenius, S. Medd. K. Vetens Acad. Nobelinst. 3. 1916. p.20.

(5). A.S.M.E. Pressure Viscosity Report. 1953.

(6). Awbery, J.H. and Griffiths, E. Proc. Phys. Soc. 48. 1936. p.372.

(7). Babb, S.E. Rev. Sci. Inst. 31. 1960. p.219.

(8). Babo. Wied Ann. 17. 1882. p.390.

(9). Barlow, A.J., Harrison, C., Richter, J., Seguin, H. and Lamb, J.
Lab. Practice. 10. 1961. p.786.

(10). Batschinsky, A.J. Phys. Z. 13. 1912. p.1157.

(11). Bett, K.E. and Newitt, D.M.
Chemical Engineering Practice. Vol. 5. p.196.

(12). Bicher, L.B. Ind. Eng. Chem. 35. 1943. p.754.

(13). Bingham and Jackson. Bull. Bur. Stds. 14. 1918. p.75.

(14). Boelhouwer, J.W.M. and Toneman, Miss L.H.
Inst. Mech. Eng. Conference on Lubrication and Wear.
1st. - 3rd. October 1957.

(15). Boyd, J.H. Phys. Rev. 35. 1930. p.1284.

(16). Bradley, R.S. "High Pressure Physics and Chemistry", Vol. 1.
(Academic Press, London and N.Y.) 1963.

(17). Bridgman, P.W. Proc. Amer. Acad. 47. 1912. p.347.

(18). Bridgman, P.W. Proc. Amer. Acad. 58. 1923. p.166.

(19). Bridgman, P.W. Proc. Amer. Acad. 61. 1926. p.57.

(20). Bridgman, P.W. Proc. Amer. Acad. 62. 1927. p.187.

(21). Bridgman, P.W. J. Chem. Phys. 3. 1935. p.597.

(22). Bridgman, P.W. Rev. Modern Phys. 18. 1946. p.1.

(23). Bridgman, P.W. Proc. Amer. Acad. 77. 1949. p.117.

(24). Bridgman, P.W. "The Physics of High Pressure". (G. Bell and Sons, London). 1958.
(25). Carmichael, L.T. and Sage, B.H. Ind. Eng. Chem. 44. 1952. p.2728.
(26). Cohen, E. and Briuns, H.R. Z. Phys. Chem. 114. 1925. p.441.
(27). Cohen, R. Ann. Phys. 45. 1892. p.666.
(28). Comings, E.W. and Egly, R.S. Ind. Eng. Chem. 33. 1941. p.1224.
(29). Comings, E.W. Univ. Ill. Bull. 42. 1944. p.15.
(30). Comings, E.W. and Mayland, B.J. Chem. and Eng. 52. 1945. p.115.
(31). Cornish, R.H. and Ruoff, A.L. Rev. Sci. Inst. 32. 1961. p.639.
(32). Dadson, R.S. National Physical Laboratory. Private Communication.
(33). Dane, E.B. and Birch, G. J. Appl. Phys. 9. 1938. p.669.
(34). Daniel, S.G. J. Inst. Petroleum. 35. 1949. p.516.
(35). Daniels. Rev. Sci. Inst. 28. 1957. p.1058.
(36). Darling, H.E. and Newhall, D.H. Trans. A.S.M.E. 75. 1953. p.311.
(37). Dorsey, N.E. "Properties of Ordinary Water Substance". (Reinhold Publishing Corp. N.Y.). 1940. P.454.
(38). Dow, R.B. Physics. 6. 1935. p.71.
(39). Dow, R.B. and Fenske, M.R. Ind. Eng. Chem. 27. 1935. p.165.
(40). Dow, R.B. Phys. Rev. 54. 1938. p.312.
(41). Dow, R.B. Phil. Mag. 28. 1939, Series 7. ps.403 and 422.
(42). Dow, R.B. J. Inst. Petroleum. 27. 1941. p.301.
(43). Eakin, B.E. and Ellington, R.T. J. Petrol. Technol. 11. 1959.p.71.
(44). Eden, H.F. and Richardson, E.G. Acustica. 10. 1960. p.309.
(45). Faust, O. Z. Phys. Chem. 86. 1914. p.479.
(46). Fawcett. Engineering. 7th. March, 1958. p.314.
(47). Felsing, W.A. and Blankenship. Proc. Oklahoma Acad. Sc. 24. 1944. p.90.
(48). Flowers, A.E. Proc. Am. Soc. Test. Mat. 14. 1914. p.565.
(49). Frank, H.S. and Wen, W.Y. Discussions Faraday Soc. 24. 1957. p.133.
(50). Frank, H.S. Proc. Roy. Soc. 247A. 1958. p.481.
(51). Fritz, W. and Weber, W. Angew Chem. 196. 1947. p.123.

(52). Glasstone, S., Laidler, K.J. and Eyring, H.
"The theory of rate processes".
(McGraw-Hill Book, Inc. N.Y.). 1941.

(53). Gonikberg, M.G. and Vereshchagin, L.F.
Compt. Rend. Acad. Sci. USSR. 55. 1947. p.801.

(54). Griest, E.M., Webb, W. and Schiessler, R.W.
J. Chem. Phys. 29. 1958. p.711.

(55). de Guzman, J. An. Soc. esp. Fis. Quim. 11. 1913. p.353.

(56). Hardy and Cottingham. J. Res. Nat. Bur. Stand. 42. 1949. p.572.

(57). Hauser, L. Ann. Phys. 5. 1901. p.597.

(58). Hawkins, G.A., Solberg, H.L. and Potter, A.A.
Trans. A.S.M.E. 57. 1935. p.395.

(59). Heiks, J.R. and Orban, E. J. Phys. Chem. 60. 1956. p.1025.

(60). Hersey, M.D. J. Wash. Acad. Sc. 6. 1916. p.525.

(61). Hersey, M.D. and Shore, H. Mech. Eng. 50. 1928. p.221.

(62). Hersey, M.D. and Hopkins, R.F. A.S.M.E. Report, 1954.
"Viscosity of lubricants under pressure".

(63). Herzberg. "Infra Red and Raman Spectra".
(N.Y., Van Nostrad). 1956. p.488.

(64). Holton, G. J. Appl. Phys. 22. 1951. p.1407.

(65). Horrocks, J.K. and McLaughlin, E.
Trans. Faraday Soc. 59. 1963. p.1709.

(66). Hubbard, R.M. and Brown, G.G. Ind. Eng. Chem. 35. 1943. p.1276.

(67). Hughes. J. Opt. Soc. Am. 46. 1956. p.557.

(68). Hyde, J.H. Proc. Roy. Soc. 97. 1920. p.240.

(69). Jobling, A. and Lawrence, A.S.C. Proc. Roy. Soc. 206A. 1951. p.257.

(70). Johnson, D.P. and Newhall, D.H. Trans. A.S.M.E. 75. 1953. p.301.

(71). Katz, D.L. Ind. Eng. Chem. 35. 1943. p.754.

(72). Kleinschmidt, R.V. Mech. Eng. 50. 1928. p.682.

(73). Kuss, E. Naturwissenchaften. 33. 1946. p.312.

(74). Kuss, E. Erdöl. u. Kohle. 6. 1953. p.266.

(75). Kuss, E. Z. Angew. Phys. 7. 1955. p.327.

(76). Kuss, E. and Schultze, G.R. World Petrol. Congr. 4th. Rome. Proc. Sect. 5. 1955. p.101.

(77). Kuss, E. Z. Angew. Phys. 10. 1958. p.566.

(78). Lawaczeck, F. Z. Ver. Deut. Ing. 63. 1919. p.677.

(79). ~~Lawrence, E.O.~~ Brush, S.G. Chem. Rev. 62. 1962. p.513.

(80). Lawson. Rev. Sci. Inst. 25. 1954. p.1136.

(81). Lennard-Jones and Devonshire. Proc. Roy. Soc. 163A. 1937. p.53.

(82). Lisell, E. Upsala Universitets Arsskrift, Matematik och Naturvetenshap. No. 1. 1903.

(83). Litovtz, T.A. and Carnevale, E.H. J. App. Phys. 26. 1955. p.816.

(84). Lohrenz, J., Swift, G.W. and Kurata, F. A.I.Ch.E.J. 6. 1960. p.547.

(85). Lohrenz, J. and Kurata, F. A.I.Ch.E.J. 8. 1962. p.190.

(86). Longuet-Higgins. Nuovo Cimento, Supplemto al. 1. 1955. p.140.

(87). Lowitz, D.A., Webb, W. and Schiessler, R.W. Pres. to Chem. Phys. Div. Am. Phys. Soc. April 1955.

(88). Lowitz, D.A., Spencer,J.W., Webb, W. and Schiessler, R.W. J. Chem. Phys. 30. 1959. p.73.

(89). Lundberg, S. J. Inst. Petroleum. 40. 1954. p.104.

(90). Manning, W.R.D. Engineering. 169. 1950. ps.481, 509 and 562.

(91). Marchi, R.P. and Eyring, H. J. Phys. Chem. 68. 1964. p.221.

(92). Mason, D.M., Wilcox, O.W. and Sage, B.H. J. Phys. Chem. 56. 1952. p.1008.

(93). Mason, J.G. and Maass, O. Can. J. Res. 18B. 1940. p.128.

(94). Maxwell, B. and Jung, A. Mod. Plast. 35. 1957. p.174.

(95). Mayinger, F. Int. J. Mass Heat Transfer. 5. 1962. p.807.

(96). McLaughlin, E. Physica. 26. 1960. p.650.

(97). Metals Handbook. The American Society of Metals. 1948.

(98). Michels, A. and Gibson, R.O. Proc. Roy. Soc. 134. 1931. p.288.

(99). Miller, A.A. J. Chem. Phys. 38. 1963. p.568.

(100). Moore, W.J. "Physical Chemistry".
(Longmans, Green & Co., London. 1956). p.432.
(101). Morgan, J. and Warren, B.E. J. Chem. Phys. 6. 1938. p.666.
(102). Moszyinski, J.R. T.A.S.M.E. 83c. 1961. p.111.
(103). Naldrett, S.N. and Maass, O. Can. J. Res. 18B. 1940. p.112.
(104). Nassini, A.G. and Pastonesi, G. Politecnico. 80. 1932. p.191.
(105). Nassini, A.G. and Pastonesi, G. Gazz. Chim. Ital. 63. 1933. p.821.
(106). N.B.S. Report 5381. 1957.
(107). Nemethy, G. and Scheraga, H.A. J. Chem. Phys. 36. 1962. p.3382.
(108). Newhall, D.H., Abbot, L.H. and Dunn, R.A.
A.S.M.E. Paper no. 62-WA-283.
(109). Panchenkov, G.M. Compt. Rend. URSS. 51. 1946. ps.365 and 457.
(110). Parisot, P.E. and Johnson, E.F. J. Chem. Eng. Data. 6. 1961.
(111). Pauling, L. "The nature of the chemical bond". p.263.
(Cornell University Press, Ithaca, N.Y.). 1940.
2nd. ed. p.304.
(112). Phillips, P. Proc. Roy. Soc. 87A. 1912. p.48.
(113). Pople, J.A. Proc. Roy. Soc. 205A. 1951. p.163.
(114). Poulter. Phys. Rev. 39. 1932. p.816.
(115). Prigogine. "The Molecular Theory of Solutions". (N.H.P. Amster-
(116). Rankine, A.D. Proc. Roy. Soc. 83A. 1910. p.265. dam). 1957.
(117). Reamer, H.H., Cokelet, G. and Sage, B.H. Anal. Chem. 31. 1959.
(118). Reynolds, R.G. University of London Thesis, 1964. p.1422.
(119). Richardson, E.G. and Tait, R.I.
Phil. Mag. 8th. series. 2. 1957. p.441.
(120). Roentgen, W.C. Ann. Phy. 22. 1884. p.510.
(121). Sage, B.H. Ind. Eng. Chem. (Analytical Ed.). 5. 1933. p.261.
(122). Sage, B.H. and Lacey, W.N. Am. Inst. Min. Met. Eng., Tech. Publ.
(123). Sage, B.H., Lacey, W.N. and Yale, W.D. 845. 1937.
Ind. Eng. Chem. 31. 1939. p.223.
(124). Schroer, E. and Becker, G. Z. Phys. Chem. 173A. 1935. p.178.

(125). Scott, Miss R. PhD. Thesis 1959. University of London. "The viscosity of Argon".

(126). Shischenko, R.I. and Avanesova, A.M. Doklady Acad. Nauk. SSSR. 88. 1953. p.103.

(127). Shischenko, R.I. and Avanesova, A.M. Trudy Azerbaidzhan Nauch. Issledovatel Inst. po Dobyche Nefti. 2. 1955. p.48.

(128). Simon, I. Rev. Sci. Inst. 28. 1957. p.963.

(129). Smith, A.H. and Lawson, A.W. J. Chem. Phys. 22. 1954. p.351.

(130). Smith, A.S. and Brown, G.G. Ind. Eng. Chem. 35. 1943. p.705.

(131). Suge, Y. Sc. Papers Inst. Phys. Chem. Res. Tokio. No. 838. Vol. 34. 1937-38. p.1244.

(132). Swanson, J.C. and Hubbard, J.C. Phys. Rev. 45. 1934. p.291.

(133). Swearingen, J.S. and Redding, E.D. Ind. Eng. Chem. 34. 1942. p.1496.

(134). Tait, R.I. Acustica. 7. 1957. p.193.

(135). Thomas, B.W., Ham, W.R. and Dow, R.B. Ind. Eng. Chem. 31. 1939. p.1267.

(136). Train, D. Thesis, University of London, 1956.

(137). Wang, J.H., Robinson, C.V. and Edelman, I.S. J. Amer. Chem.Soc. 75. 1953. p.466.

(138). Warburg, E. and Sachs, J. Ann. Phys. 22. 1884. p.518.

(139). Webb, W., Griest, E.M. and Schiessler, R.W. Phys. Rev. 86. 1952. p.612.

(140). Webb, W., Spenser, J.W. and Schiessler, R.W. Phys. Rev. 94. 1954. p.753.

(141). Weber, W. Z. Angew Phys. 15. 1963. p.342.

(142). Whalley. J. Sci. Inst. 36. 1959. p.47.

(143). Van Wijk, W.R. and Van der Veen, J.H. Physica. 7. 1940. p.45.

(144). Wildhagen, M. Z. Angew Math. Mech. 3. 1923. p.181.

(145). Zhokhovskii, M.K. Izmeritel'naya Tekh. No.5. 1955. p.3.

(146). Zolotykh, E.V. Izmeritel'naya Tekh. No.3. 1955. p.42.

(147). Zolotykh, E.V. Komitet Standartov, Mer i Izmeritel'Nykh Proborov pri Sovete Ministrov SSSR. 46. 1960. p.62.

(148). Zolotykh, E.V. Trudy Inst. Komiteta Standartov, Mer i Izmerit Priborov pri Sov. Min. SSSR. 46. 1960. p.81.